THE UNIVERSITY *of* EDINBURGH

THE UNIVERSITY *of* EDINBURGH

Adsorption and Migration Mechanisms of Methane and Carbon Dioxide in Gas Shales at Pore Scale

A dissertation submitted to the School of Engineering in partial fulfilment of the requirements for the degree of Doctor of Philosophy

Karthikeyan Arunachalam

November 2020

1 Abstract

Storage and production mechanisms in gas shales are controlled by pore-scale adsorption and diffusion, respectively. Using a series of experimental and numerical techniques these processes that occur at a molecular level are investigated for their impact on field-scale technologies.

Type I adsorption isotherms were obtained for Lothian shale samples. Net sorption was found to contribute to the biggest errors in sorption characterization. Whilst the DR (Dubinin-Radushkevich) isotherm was found to provide the best fit, the Langmuir isotherm was thermodynamically consistent providing good fits to both adsorption and adsorption uptake, making it the best isotherm for shale reservoir characterization. Of three parameter isotherms, the Toth isotherm is preferred over the Sips isotherm given that it is more thermodynamically consistent. Using a series of numerical experiments, importance of adsorption and adsorption uptake on diffusion and gas production in shales are then investigated. Intrinsic permeability of shales decreased with increasing adsorption uptake. A dual porosity FEM (Finite Element Method) is solved to determine reserves. The decrease in effective diffusion with increasing adsorption was found to be quite significant and increasing amounts of sorbed gas in the reservoir counterintuitively results in decreased production for some reservoirs. However, it is possible to minimize this effect by good design of production technology. Smaller fracture spacing and higher fracture heights with very high fracture conductivity could be used to increase sorbed gas production from shale reservoirs.

Effect of geochemistry and pore structure on adsorption in Bowland shales is investigated using a series of experimental techniques. Pore characteristics are investigated under the SEM (Scanning Electron Microscopy, and mineral phases are identified using EDS (Energy Dispersive Spectroscopy). This provided good agreement with the shale's TOC (Total Organic Carbon) and XRD (X-Ray Diffraction) data. Using image analysis techniques, micropore volume was found to be predominantly located in the organic matter phase of gas shales. Clay minerals contribute to micropore volume, but to a lesser extent. Pore size distribution was analysed using N_2 isotherms with BET (Braunner-Emmett-Teller), BJH (Barrett-Joyner-Halenda), and DFT (Density Functional Theory) techniques. Most Bowland shales exhibit a bimodal pore size distribution with peaks in the micropore and mesopore range corresponding

to pores contributed by organic and clay minerals content, respectively. The BET theory corresponds to minimum energetic sorption in heterogeneous shales. For determination of pore size distribution, the DFT theory provides much better predictions compared to the BJH theory. High pressure adsorption and diffusion for methane and carbon dioxide in Bowland shales are determined using the manometric rig. A linear isotherm was obtained for sorption up to 60 bars. The second order kinetics based fit was found to better estimate diffusion than the first order based fit. Sorption and diffusion in shales was a strong function of organic matter, clay mineral content, surface area, and micropore volume.

Carbon dioxide sequestration in shales is investigated using a series of experimental and numerical techniques. Shales provide excellent carbon dioxide sequestration capabilities adsorbing nearly 1.25 times carbon dioxide as methane in laboratory experiments. High pressure methane and carbon dioxide adsorption isotherms are used as input parameters in a reservoir simulation using FEM (Finite Element Method) in COMSOL. 10 years of production was simulated to deplete the reservoir, followed by 10 years of carbon dioxide injection for carbon sequestration. A rapid dissipation of pressure was observed in the reservoir after carbon dioxide injection with nearly 10% of the total gas stored due to sorption. Sorbed carbon dioxide was also very stable even under methane production. However, there was no benefit to methane production under Huff-and-Puff carbon dioxide injection technology, which was conducted in a 5 year cycle. This is because high adsorption uptakes are expected to decrease the shale intrinsic permeability consistent with previous results. Also, longer injection times are required to store a similar amount of carbon dioxide in the reservoir for the same reason.

Adsorption characterization in methane was done at multiple temperatures to determine the temperature dependence and the heat of sorption. Governing equations of heat and mass balance are modified to include sorption and heat of sorption. These are solved using FEM in COMSOL. Thermal stimulation was found to provide strong benefits for methane production increasing ultimate recovery by 10%. Isosteric heat of sorption is an important parameter in the thermal stimulation of gas shales. Not including isosteric heat over predicted production by 13% compared to production with heat of sorption. Permeability, Langmuir volume, and Langmuir pressure are also significant parameters.

2 Lay Summary

Gas shales are becoming an increasingly important member of a 21st century low carbon energy portfolio. However, we do not understand how gases are stored and produced in these microporous substances where processes occur at a molecular scale. Molecules tend to get attracted to a surface when they are in its vicinity – this process is called adsorption; the movement of these molecules along the surface is called surface diffusion. Through experiments, we show that adsorption and diffusion in shales are controlled as a function of their chemical composition and pore structure. The shale's organic matter and clay mineral content are important as these contribute to most of the surface area needed for adsorption. Through experiments and computer simulations, we analyse how adsorption affects other aspects of reservoir characterization – permeability, resource estimation, and reserve estimation. Permeability is like diffusion coefficient but is also dependent on fluid properties unlike the intrinsic diffusion coefficient. Adsorption, the main topic of our thesis being a fluid property, was found to significantly decreases the shale's permeability. Adsorption contributed significantly to the shale's resource potential. However, since it was inversely proportional to permeability, it decreased the amount of resources that could be produced – which are known as reserves.

With a better understanding of how adsorption works in the micro pores of gas shales, we are able to analyse various production technologies that can be employed to increase recovery or even store carbon dioxide in the reservoir in place of methane. The carbon dioxide molecule being smaller than methane was adsorbed more readily adsorbed into the slit shaped pores of gas shales. This was reflected in computer simulations that studied carbon dioxide sequestration on a field scale. A key benefit of storing adsorbed carbon dioxide is the fact that it is a lot more stable compared to free carbon dioxide – it is less likely to leak out of the reservoir later or cause earthquakes due to overpressure. To improve the recovery of methane from the reservoir, we take advantage of the fact that adsorption is also controlled by temperature besides pressure. Increasing reservoir temperature increases gas recovery.

3 Acknowledgement

I would like to thank my supervisor Prof Xianfeng Fan. Without his support, I would not have been able to learn and connect ideas from different areas of science to which I had little exposure before starting my thesis. I count myself very lucky to have been able to work with a scientist of his calibre during my PhD.

I would like to thank my second supervisor Prof Ying Zheng for pointing me in the right direction at the beginning of my thesis.

I would like to thank my parents for their love and acceptance – my father for giving me the gift of education when he had no such handouts in his youth, and my mother for believing in me when I could not. I would also like to thank my sister for being my primary support system besides being my best friend.

I would like to thank other members and ex-members of the Institute of Materials and Processes, particularly Dr Francis Bougie for helping me become a better experimentalist and Dr Dimitri Mignard for his highly stimulating discussions and his mentorship.

I would like to thank the members of the mechanical workshop: particularly Mr Paul Aitken, for helping me put together the adsorption rig and fix it when it would not work. I would like to thank Mr Huw Clarke and Cuadrilla Resources for providing me with the Bowland shale samples, and Prof Stuart Haszeldine for helping me acquire Lothian shale samples. I would also like to thank Dr Ke Wang for teaching me PSD analysis, Dr Nicola Cayzer for teaching me SEM analysis, and Mr Fergus Dingwall for teaching me GC-FID.

I would like to thank other members of the teaching and support staff for their highly valued inputs over the last 4 years.

Table of Contents

List of Figures

List of Tables

List of Abbreviations

Symbol	Description
q_a	Absolute amount adsorbed
ρ_{ads}	Adsorbate molar density in adsorbed phase
ρ_a	Adsorbate molar density in bulk shale
ρ_{c0}	Average initial gas density
V_{bulk}	Bulk volume of sample
P_c	Charge pressure
α_g	Coefficient of thermal expansion
H	Enthalpy
S	Entropy
P_e	Equilibrium pressure
q_e	Excess amount adsorbed
a_1	Fitting Constant for Langmuir Volume
a_2	Fitting Constant for Langmuir Volume
F_R	Fractional gas uptake in the reference cell
k_F	Freundlich constant
z	Gas compressibility factor
Q_{if}	Gas flow into fracture
ρ_g	Gas molar density
K_C	Gas storage capacity ratio
μ	Gas viscosity
G	Gibbs Free Energy
V_{grain}	Grain volume of sample
Q_h	Heat input into reservoir
P_i	Initial pressure

H_i	Isosteric Heat of Sorption
c_g	Isothermal compressibility
q_L	Langmuir adsorption
b_L	Langmuir affinity constant
H_L	Langmuir Heat of Sorption
P_L	Langmuir Pressure
P_{L_∞}	Langmuir Pressure at infinite temperature
V_L	Langmuir Volume
n	Number of moles in the rig
k	Permeability
ϕ	Porosity
γ_g	Ratio of isothermal compressibility and coefficient of thermal expansion - c_g/α_g
V_r	Reference cell volume
V_s	Sample cell volume
b_s	Sips affinity constant
n_s	Sips constant
q_s	Sips maximum adsorption
V_{sp}	Specific volume of sample
b_T	Toth affinity constant
q_T	Toth maximum adsorption

4 Introduction

Natural gas has been identified as a bridge fuel to various fully carbon-neutral energy portfolios in the future (Mathieu, 2006). Occupying over two-thirds of the earth's strata (Garrels and Mackenzie, 1969), gas shales are an increasingly important energy source in the first half of the 21st century (King, 2010). Compared to other sources of natural gas, gas shales are characterised by extremely small micro-pores (Kuila and Prasad, 2013). Because of this, processes that govern storage and production mechanisms in gas shales occur at a molecular level. Nearly 20 - 80% of the total gas in shales is in the adsorbed state (Schettler Jr and Parmely, 1991). Production mechanisms are controlled by surface diffusion (Civan et al., 2013). However, there is still much that is not understood about these processes.

There is a wide discrepancy in the sorption and diffusion characteristics of gas shales reported by various laboratories (Klewiah et al., 2019; Merey, 2019; Pini, 2014). The most important reason for this is the inherent heterogeneities observed in gas shales on pore, core, and field scales (Garrels and Mackenzie, 1969). However, the complicated mathematical techniques required for these measurements also make a significant contribution to this lack of reproducibility (Civan et al., 2013). This is mainly because we do not yet understand the fundamental mechanisms that underlie these sorption and diffusion processes in shale micropores to make sufficient adjustments for them. This study will make contributions to further our understanding of these processes on the existing literature.

Sorption also plays a significant role in other areas of reservoir characterization. Whilst it is now common to account for sorption whilst characterizing a shale's permeability (Profice et al., 2012), it has still not been explored thoroughly in isolation. The impact of sorption on resource characterization is now well understood (Ambrose et al., 2012). However, it's effect on reserve estimation is still a matter of debate (Mengal and Wattenbarger, 2011; Yu et al., 2016). Further research in this area would be useful to the community. Production technologies such as carbon dioxide injection and thermal stimulation also need to account for sorption in their design (Guo et al., 2013; Liu et al., 2013). Shales have a significantly higher potential to adsorb carbon as compared to methane (Heller and Zoback, 2014). But we do not fully understand how this process translates into the potential for carbon dioxide

sequestration in the reservoir. Whilst the thermodynamics of sorption are well understood by the experimental community (Everett, 1964; Fianu et al., 2018), the thermal effects of sorption are largely ignored in the reservoir simulation community (Alafnan et al., 2020; Fianu et al., 2020). This effect is also explored in more detail.

To complete the project, 4 broad tasks were identified as shown in Figure 4-1. A manometric adsorption rig was fabricated in the workshop and assembled in the laboratory. The experiment, data acquisition, and data analysis were automated using LabVIEW and Python. Two sets of shale samples were acquired for this study. Lothian outcrop samples were obtained from the Straiton shale mine (ScottishShale, 2020). Bowland core samples were obtained from the operator Cuadrilla (Andrews, 2013). A wide range of samples representing different organic and mineral compositions were acquired.

High pressure methane and carbon dioxide adsorption isotherms were conducted in the laboratory. Different isotherm models that predict Type I isotherms – Langmuir, Freundlich, Dubinin-Radushkevich, Sips, and Toth – are fitted to the experimental data and analysed. From sorption characterization at multiple temperatures, the heat of sorption was calculated using the Clausius-Clapeyron equation. Multi-component adsorption measurement was conducted using manometric techniques, and elemental analysis using GC-FID (Gas Chromatography-Flame Ionisation Detector). The IAST (Ideal Adsorbed Solution Theory) and Extended Langmuir models are considered for multi-component adsorption. Diffusion characterization was performed using rate based and Fick's law based techniques wherever appropriate. Adsorption is included in the methodology for diffusion characterization in the manometric rig.

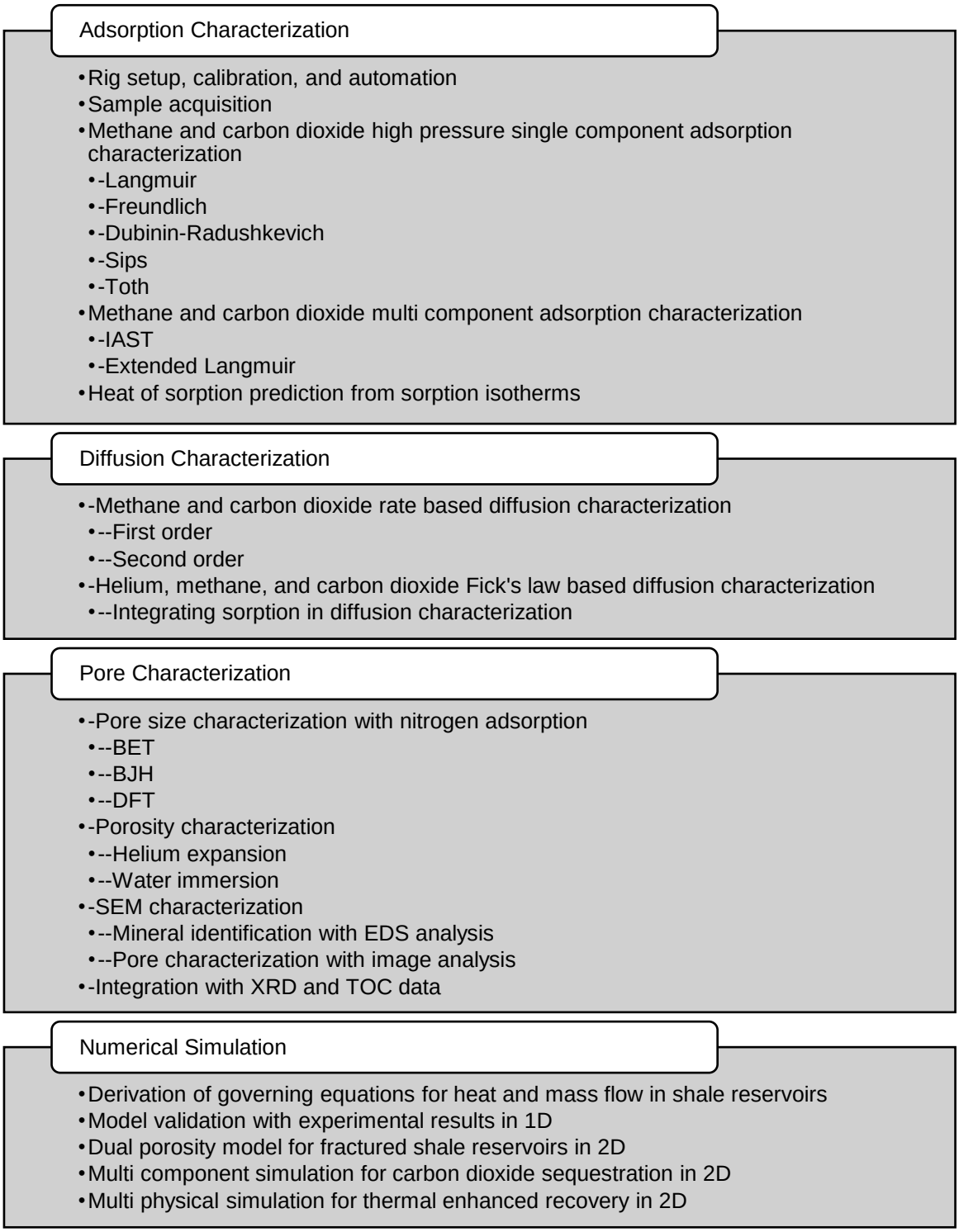

Figure 4-1 Research tasks identified

Pore size characterization was accomplished using nitrogen adsorption at 77 K. The BET (Braunner-Emmett-Teller), BJH (Barner-Joyner-Halenda), and DFT (Density Functional Theory) techniques are

used to determine pore sizes from experimental isotherms. Grain volume was measured using helium expansion, and bulk volume was measured using water immersion. Using SEM (Scanning Electron Microscopy) and EDS (Energy Dispersive Spectroscopy) analysis, further insights into the pore structure and mineral composition are obtained. A statistical analysis between shale sorption, pore structure, and geochemistry is presented.

Equations that govern heat and mass flow in shale reservoirs are derived. These equations are verified against experiments in 1 D. They are then used to derive insights into multiple areas of shale reservoir characterization – methane production, carbon dioxide sequestration, and thermal enhanced recovery.

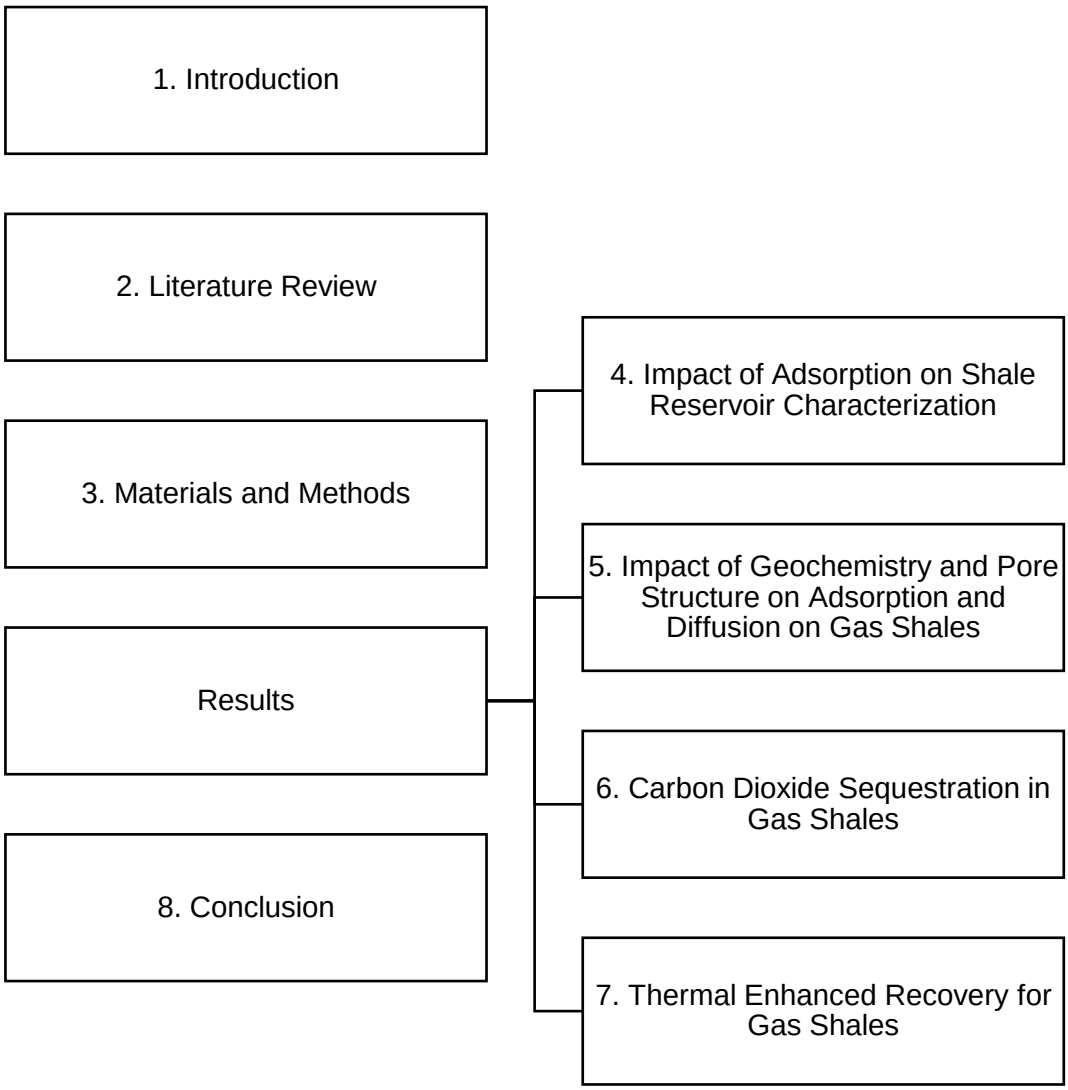

Figure 4-2 Thesis structure

The results from each research activity is combined with those from others to draw meaningful conclusions in the area of shale adsorption and diffusion as explained above. The thesis is organised into 4 main results chapters as shown in Figure 4-2.

The complete structure of the thesis is detailed below:

Chapter 1 provides a brief introduction to the problem and highlights the significance of this work. It then provides the structure of the research project and the thesis.

Chapter 2 discusses the current state of literature in gas shale adsorption. With a good understanding of the challenges associated with shale gas extraction, it then identifies key areas where this study could make contributions.

Chapter 3 outlines the shale materials used in this study and the experimental and computational methodologies used in this study.

Chapter 4 investigates the importance of adsorption on the shale gas reservoir characterization process. It makes recommendations on experimental technique for adsorption characterization in shales and investigates the impact of this processes on permeability characterization, resource characterization, and reserve estimation.

Chapter 5 builds on the results of the previous chapter. With a good understanding of the adsorption and diffusion experimental processes, the chapter investigates the importance of geochemistry and pore structure on adsorption and diffusion processes in shales. Pore size distributions, SEM images, shale compositions, adsorption characteristic, and diffusion characteristics are presented and analysed thoroughly.

Chapter 6 goes further in the application of adsorption to shale reservoir characterization. It connects the pore scale shale adsorption and diffusion characteristics and extends them to a field scale in the context of carbon dioxide sequestration and enhanced recovery. Experimentally acquired adsorption values are used in a reservoir simulation to analyse the impact of adsorption on carbon dioxide sequestration in the reservoir.

Chapter 7 builds on the previous results for the purpose of thermal enhanced recovery. Combining both the heat and mass transfer effects of adsorption measured at a pore scale, the chapter investigates thermal enhanced recovery on a field scale .

Chapter 8 presents the main findings of this research and highlights. It also presents the limitations of this work and identifies areas for future research.

Publication History:

Chapter 4: Impact of Adsorption on Shale Reservoir Characterization, was submitted to Journal of Petroleum Engineering. Chapter 5: Impact of Geochemistry and Pore Structure on Adsorption and Diffusion in Shales will be submitted to Journal of Petroleum Science and Engineering. Chapter 6: Carbon Dioxide Sequestration in Gas Shales was presented in COMSOL Europe Conference and published in conference proceedings. Chapter 7: Thermal Enhanced Recovery for Gas Shales was published in Journal of Natural Gas Science and Engineering.

4.1 References

Alafnan, S., Aljawad, M., Glatz, G., Sultan, A., Windiks, R., 2020. Sustainable Production from Shale Gas Resources through Heat-Assisted Depletion. Sustainability 12, 2145.

Ambrose, R.J., Hartman, R.C., Diaz-Campos, M., Akkutlu, I.Y., Sondergeld, C.H., 2012. Shale gas-in-place calculations part I: new pore-scale considerations. SPE J. 17, 219–229.

Andrews, I.J., 2013. The Carboniferous Bowland Shale gas study: geology and resource estimation. Br. Geol. Surv. Dep. Energy Clim. Chang. London, UK.

Civan, F., Devegowda, D., Sigal, R.F., 2013. Critical Evaluation and Improvement of Methods for Determination of Matrix Permeability of Shale, in: SPE Annual Technical Conference and Exhibition. Society of Petroleum Engineers.

Everett, D.H., 1964. Thermodynamics of adsorption from solution. Part 1.—Perfect systems. Trans. Faraday Soc. 60, 1803–1813.

Fianu, J., Gholinezhad, J., Hassan, M., 2020. Thermal simulation of shale gas recovery involving the use of microwave heating. J. Pet. Sci. Eng. 186, 106768.

Fianu, J., Gholinezhad, J., Hassan, M., 2018. Comparison of Temperature-Dependent Gas Adsorption Models and Their Application to Shale Gas Reservoirs.

Garrels, R.M., Mackenzie, F.T., 1969. Sedimentary rock types: relative proportions as a function of geological time. Science (80-.). 163, 570–571.

Guo, W., Xiong, W., Gao, S., Hu, Z., Liu, H., Yu, R., 2013. Impact of temperature on the isothermal adsorption/desorption of shale gas. Pet. Explor. Dev. 40, 514–519.

Heller, R., Zoback, M., 2014. Adsorption of methane and carbon dioxide on gas shale and pure mineral samples. J. Unconv. Oil Gas Resour. 8, 14–24.

King, G.E., 2010. Thirty years of gas shale fracturing: What have we learned?, in: SPE Annual Technical Conference and Exhibition. Society of Petroleum Engineers.

Klewiah, I., Berawala, D.S., Alexander Walker, H.C., Andersen, P.Ø., Nadeau, P.H., 2019. Review of Experimental Sorption Studies of CO2 and CH4 in Shales. J. Nat. Gas Sci. Eng. 103045.

Kuila, U., Prasad, M., 2013. Specific surface area and pore-size distribution in clays and shales, Geophysical Prospecting.

Liu, F., Ellett, K., Xiao, Y., Rupp, J.A., 2013. Assessing the feasibility of CO 2 storage in the New Albany Shale (Devonian–Mississippian) with potential enhanced gas recovery using reservoir simulation. Int. J. Greenh. Gas Control 17, 111–126.

Mathieu, P., 2006. The IPCC special report on carbon dioxide capture and storage, in: ECOS 2006 - Proceedings of the 19th International Conference on Efficiency, Cost, Optimization, Simulation and Environmental Impact of Energy Systems.

Mengal, S.A., Wattenbarger, R.A., 2011. Accounting For Adsorbed Gas in Shale Gas Reservoirs, in: SPE Middle East Oil and Gas Show and Conference. Society of Petroleum Engineers.

Merey, Ş., 2019. Analysis of the effect of experimental adsorption uncertainty on CH4 production and CO2 sequestration in Dadas shale gas reservoir by numerical simulations. J. Pet. Sci. Eng. 178, 1051–1066.

Pini, R., 2014. Interpretation of net and excess adsorption isotherms in microporous adsorbents. Microporous Mesoporous Mater. 187, 40–52.

Profice, S., Lasseux, D., Jannot, Y., Jebara, N., Hamon, G., 2012. Permeability, Porosity and Klinkenberg Coefficient Determination on Crushed Porous Media. Petrophysics 53.

Schettler Jr, P.D., Parmely, C.R., 1991. Contributions to total storage capacity in Devonian shales, in: SPE Eastern Regional Meeting. Society of Petroleum Engineers.

ScottishShale, 2020. Straiton Oil Works [WWW Document].

Yu, W., Sepehrnoori, K., Patzek, T.W., 2016. Modeling gas adsorption in Marcellus shale with Langmuir and bet isotherms. SPE J. 21, 589–600.

5 Literature Review

5.1 Introduction

Modern civilization has been made possible by the abundance of low priced energy contributed by hydrocarbon energy sources (Smil, 2019). Hydrocarbon energy sources are broadly classified into conventional and unconventional reservoirs. Amongst unconventional hydrocarbon reservoirs, shales have gained a lot of traction in the recent decades owing to it's abundance and relatively low carbon cost compared to other fossil fuels.

The storage and production mechanisms for gas shale reservoirs are heavily controlled by adsorption and diffusion processes (Civan et al., 2012; Yu et al., 2014b). The following sections seek to better understand the current literature, and the potential knowledge gaps for research focus. A background of gas shale geology is presented, followed by adsorption and diffusion literature. This is followed by a review of reservoir characterization techniques and production technologies. The current state of the literature pertinent to each of these areas are reviewed thoroughly in the appropriate sections. These are used to identify key challenges associated with shale reservoir characterization, identifying knowledge gaps that will be the focus of this thesis.

5.2 Gas Shale Reservoirs

Hydrocarbons are formed when marine or lacustrine algae and terrestrial plants with lipids, deposited as sediments on a suitable anoxic environment such as the seabed, over a slow process of burial over millions of years, are broken down and transformed with pressure, temperature, and bacterial decomposition. The hydrocarbons expelled due to overpressure from the source rock, migrate upwards through geologic faults and cracks owing to their lower densities compared to brine. Then on occasion,

they find a suitable stratum with sufficient porosity, such as sandstones or carbonates, termed as reservoirs. When the hydrocarbon reservoir, has on top of it, an impermeable sealing rock such as granite that constitutes a capillary force larger than the buoyancy force of migration, and these seals are of an appropriate geometry, the hydrocarbons are trapped in the reservoir rock, for later human exploitation. The aforementioned components – source, migration, reservoir, seal, and trap – colloquially termed as the five steps to heaven – constitute a conventional hydrocarbon play (Allen and Allen, 2005).

Resource depletion from conventional hydrocarbon reservoirs has given way to the industry seeking to produce from other hydrocarbon sources, which do not have one or more components that constitute the conventional hydrocarbon play. For example, in gas shales, the source rock is also the reservoir rock and the seal rock; in tight reservoirs, the reservoir rock is also the seal rock. The technique to produce these unconventional hydrocarbon reservoirs is different from the technique used to produce conventional hydrocarbons, and this usually makes it less economically attractive to produce unconventional hydrocarbons as compared to conventional hydrocarbons. For example, oil sands require heavy post-processing after extraction, and shale and tight gas requires hydraulic fracturing that improves the net reservoir permeability to allow gas flow.

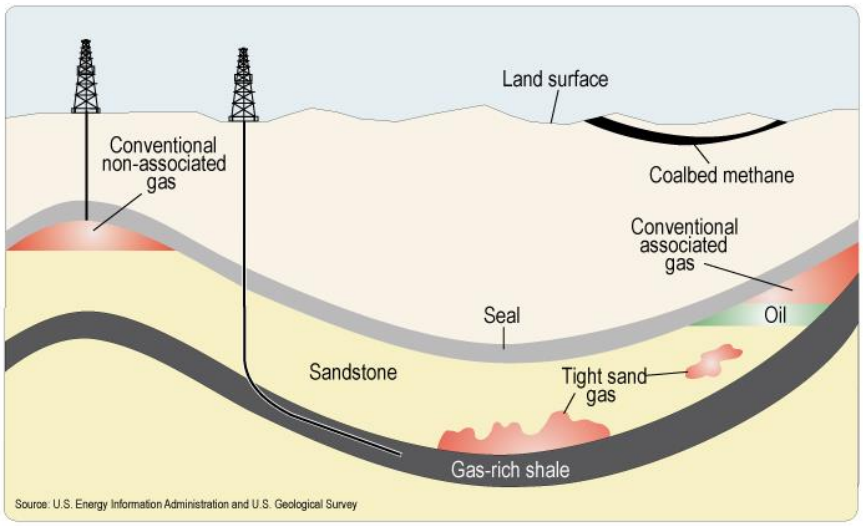

Figure 5-1 Geology of natural gas resources from (EIA, 2015a)

The technique to fracture shale and tight reservoirs to improve gas flow has been practised for over 40 years now (King, 2010). And hydrocarbons from shales have been utilized for over 200 years (Gallois, 1979). However, it is only recently that since the advent of hydraulic fracturing, that commercial production from gas shales have been possible (Mayerhofer et al., 1997). This has consequently led to a wide interest in gas shales from the research community, explored in the upcoming sections.

Shales are the largest stratigraphic constituent of our planet constituting to nearly two-thirds of the planets sedimentary stratigraphic record (Potter et al., 2005). Organic rich shales have always played a significant role in the formation of hydrocarbons which later migrated to highly porous sandstones and carbonate reservoir rocks (Allen and Allen, 2005). However, the research into these source rocks tended to focus mostly on the potential for the formation of hydrocarbons and their subsequent expulsion. For example, the industry standard for reservoir characterization by API (American Petroleum Institute) only has one section on adsorption characterization (RP40, 1998), which ignores the effects of net and excess adsorption (Brandani et al., 2017). It is common practice in the industry to still ignore these effects whilst reporting resources and reserves (Andrews, 2013; Clarke et al., 2018; Whitelaw et al., 2019). Whilst it is still important to understand the geochemical formation of these reservoirs, the increasing prevalence of gas shales as the reservoir rock has also increased the research community's interest in the storage and migration mechanisms of hydrocarbons within these shales itself.

5.3 Shale Geology

5.3.1 Depositional Environment and Hydrocarbon Formation

Shales have been widely classified based on their depositional environment into lacustrine, marine, and terrestrial basins (Allen and Allen, 2005). The depositional environment in which shales are formed has significance in a wide range of physical and chemical properties (Caineng et al., 2010). Phytoplankton's

are the world's biggest supply of primary organic matter constituting over 90% of the ocean's organic matter (Stockner, 1988). These are primarily found in continental shelves and lakes that have abundant sunlight and mineral resources from convection, that are necessary for photosynthesis. The most important land plant in terms of the carbon cycle is peat (Gorham, 1991). Marine organic matter is largely amorphous, whilst the terrestrial organic matter is mainly classified into vitrinite rich, inertinite rich, and exinite rich macerals, although other forms also exist (Allen and Allen, 2005). Alginite rich peats in Scotland play a major role in carbon sequestration owing to their high lipid content (Gorham, 1991).

Upon burial in an anoxic environment, the organic components form a substance known as kerogen, which defined as organic matter insoluble in organic solvents owing to their large molecular size. The presence of an anoxic environment is important as it prevents degradation of organic material by aerobic bacteria, and anaerobic decomposition of organic materials preserves the lipid content to a much greater extent (Allen and Allen, 2005). Over millions of years, the kerogen undergoes a phenomenon known as pyrolysis, in which hydrocarbons are expelled from lipids. Whilst other organic matters such as carbohydrates and proteins exist, their structures are not close enough to hydrocarbons to form hydrocarbons through pyrolysis (Allen and Allen, 2005). They kind of hydrocarbons formed depend both on the source of the kerogen, and on the burial environment. Increasing burial temperatures result in the formation of bitumen, which is subsequently transformed to liquid hydrocarbons at temperatures between 100 and 150 ^{o}C. Thermogenic gas is formed due to pyrolysis at temperatures between 150 and 200 ^{o}C, whilst biogenic gas is formed due to bacterial action at temperatures of 60 to 70 ^{o}C (Quigley and Mackenzie, 1988). It is also interesting to note that very high pressures and low temperatures could lead to the formation of methane hydrates (Vysniauskas and Bishnoi, 1983).

5.3.2 Geo-chemistry

Shales consists of 7 main mineralogical components (Daniel B. Shaw, 1965): quartz, feldspar, carbonates, Fe-oxides, clay minerals, other minerals, organic matter. Each of these individual components has significant implications for gas shale reservoir characterization. For example, a siliceous and calcareous mineral constituent is generally favourable for hydraulic fracturing, whereas clay minerals result in a more ductile response (Caineng et al., 2010). The brittleness of a gas shale could be defined based on its mineralogical composition as (Clarke et al., 2018): the shale's geochemistry has been linked to its depositional environment. In general, Lacustrine shales in general seem to have lower TOC contents compared to Marine or Terrestrial shales (Caineng et al., 2010). Lacustrine shales have also been found to exhibit a higher mineral content compared to Marine or Terrestrial shales (EIA, 2015b).

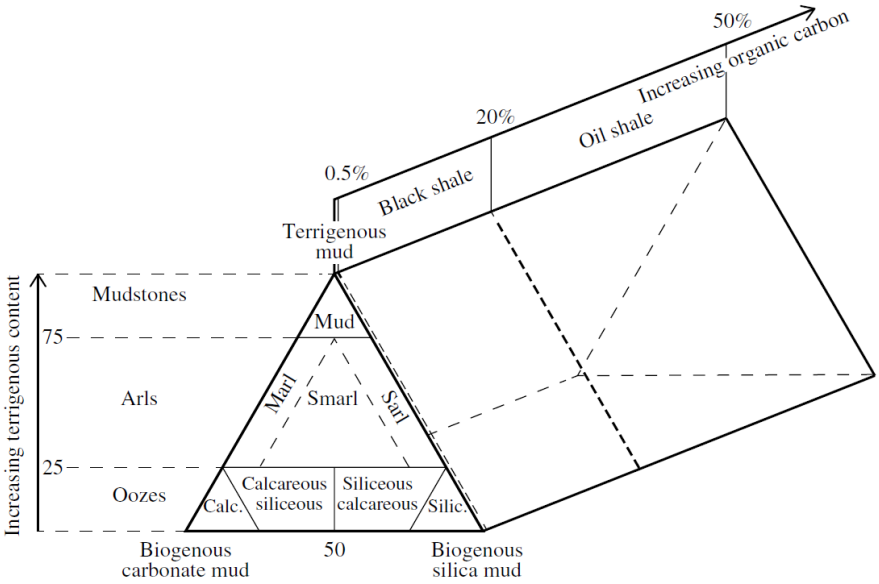

Figure 5-2 Classification of shales based on geochemistry from (Rezaee, 2015)

A common classification of shales based on their geochemistry is shown in Figure 5-2. Oil shales have a much higher organic carbon content compared to black shales. Black shales can be classified based on their mineral content as terrigenous or biogenous. Biogenous shales are classified into biogenous carbonate or biogenous silicate mud. Shales without a dominant component are termed as Smarls.

The amount and type of organic matter are particularly important as it is the source of hydrocarbon generation (Allen and Allen, 2005). A lower limit of 2% TOC is widely accepted as the cutoff point for commercial hydrocarbon generation in the United States (Rezaee, 2015). Both the quantity and the quality of organic matter are important parameters in gas shale reservoir characterization, as the amount of hydrocarbons that can be generated by kerogen is directly linked to its hydrogen content, which is a function of the original organic matter that forms the kerogen (Allen and Allen, 2005). Although there is a reduction in the amount of kerogen as hydrocarbons are generated, this reduction is often countered by the swelling of the kerogen with sorption thereby maintaining or increasing the kerogen volume with hydrocarbon generation (Loucks et al., 2009).

Other key petrophysical properties of a gas shale reservoir include porosity, permeability, stresses, maturity, and adsorption (RP40, 1998). A porosity value of over 5% is generally preferable for a commercial gas shale reservoir (Rezaee, 2015). In general, higher values for permeability and adsorption are preferable for more favourable resource characterizations. Geo-mechanical effects play a key role in the shale burial processes but are also in turn affected by the geochemistry of shales (Zoback and Kohli, 2019). A good understanding of the stress profile is necessary for the design of hydraulic fractures which are usually propagated perpendicular to the direction of maximum stress (Zoback and Kohli, 2019).

5.3.3 Pore Structure

Although there is no standard definition of microporous substances in the literature, one of the more widely accepted definitions is that they are substances having a pore diameter of less than 2 nm (Rouquerol et al., 2013). The pores in microporous substances are themselves classified into three types by IUPAC: micropores: < 2nm, mesopores: 2 - 50 nm, macropores: 50 - 100 nm (Rouquerol et al., 2013). This is convenient in the context of adsorption as different pore sizes exhibit different sorption

mechanisms – micropore filling, capillary condensation, and surface layering for micro, meso, and macropores respectively (Rouquerol et al., 1994).

Shales have been found to contain a significant amount of micropores contributed by organic matter (Al Hinai et al., 2014). Pore throat radii for shales from Australia were found to be around 6 nm (Al Hinai et al., 2014). Pore radii for south-eastern shales in China were found to be about 1.26 nm (Li et al., 2016). Shales from India are predominantly microporous (Rani et al., 2015). Micropores from clay minerals have shown that micropores are often associated with illite and smectite but not with kaolinite (Kuila and Prasad, 2013).

Pore characteristics also affect shale permeability (Al Hinai et al., 2014). Higher pore throat to pore body ratios (with larger pore throats compared to the pore volume) result in better-connected pores and is generally associated with higher permeability. Permeability is also dependent on the pore shape and tortuosity besides pore size. For example, upon diagenetic decomposition of clay minerals, through which illites are formed, reduces shale permeability from micro darcys to nano darcys, whilst maintaining the shale porosity (Nadeau, 2011).

5.4 Shale Basins in the UK

The UK consists of 3 main shale gas plays: 1) Carboniferous shales in the Midland Valley of Scotland, 2) Carboniferous shales of Bowland Hodder in central England, and 3) Jurassic Weald Basin in southern England (Andrews, 2013). All of these plays were formed under a Marine depositional environment (EIA, 2015b). Of these, the Bowland basin has received the most attention from the industry and academia due to its location and geology (Clarke et al., 2018, 2014; Fauchille et al., 2017). Permeability of Bowland shales was calculated to be about 1×10^{-24} m2; porosity was in the range of 4%; desorbed gas content was about 0.01 mol/kg (Clarke et al., 2018).

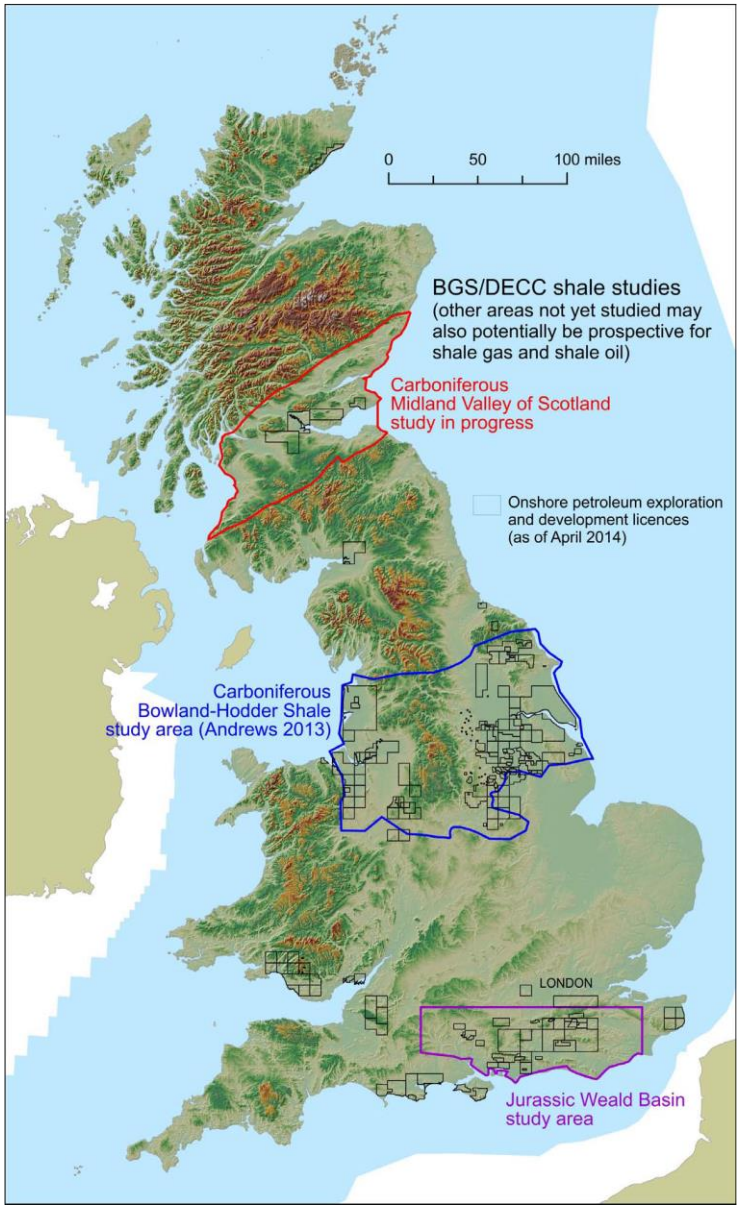

Figure 5-3 UK shale basins from (Andrews, 2013)

5.5 Storage and Production Mechanisms in Gas Shales

5.5.1 Adsorption

Adsorption is the tendency of fluid molecules to accumulate near the solid surface (Ruthven, 1984). Of the total gas stored in a gas shale reservoir, anywhere between 20 and 80% is stored in the adsorbed

state (Schettler Jr and Parmely, 1991). Although sorbed molecules in gas shales are not stationary, they have much lower mobility compared to the free gas phase (Riewchotisakul and Akkutlu, 2016). This results in a greatly reduced contribution to total production from adsorbed gas (Yu and Sepehrnoori, 2014a).

5.5.1.1 Adsorption Isotherms

Adsorption isotherms are classified into six types based on their shape (Thommes et al., 2015) as shown in Figure 5-4. Each of these isotherms could be expected to occur on substances with varying pore sizes (Do, 1998). For example, in predominantly macroporous substances, where monolayer adsorption occurs, there is an initial Henry region of linear increase with loading but no further adsorption uptake at higher pressures resulting in a Type I isotherm. When capillary condensation is observed in mesoporous substances a Type II isotherm is observed. Different pore size distributions and pore shapes result in different adsorption mechanisms as described in the literature (Rouquerol et al., 2013).

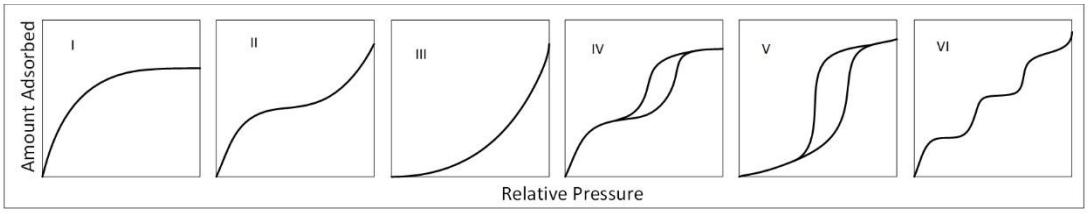

Figure 5-4 Adsorption isotherm types after (Sing, 1985)

Gas shales typically exhibit Type I isotherms up to reservoir pressures (Bae; and Bhatia, 2006; Wang et al., 2016a; Yuan et al., 2014; Zhang et al., 2012; Zhou et al., 2018). However, non-characteristic isotherms have also been reported from some shales (Krooss et al., 2002). Type II isotherms have also been reported in some shales (Yu et al., 2016). There was usually no hysteresis observed for methane isotherms but hysteresis was significant for carbon dioxide isotherms (Dutta et al., 2011; Rani et al.,

2019). Low-pressure moisture, nitrogen, and carbon dioxide isotherms in shales are usually Type II due to capillary condensation at saturation pressures (Brunauer et al., 1938; Wang and Zhang, 2020). Water isotherms have been usually fitted using the Guggenheim-Anderson-de Boer isotherm (Day et al., 2008; Do, 1998), whilst nitrogen and carbon dioxide isotherms are usually fitted using the BET isotherm.

Adsorption isotherms used to fit Type I isotherms are of 3 types: 1) based on the Gibbs adsorption theory; 2) based on the potential theory, and 3) Practical approaches such as the Langmuir isotherm and other empirical correlations. Most isotherms could be derived from the Gibbs isotherm equation through appropriate assumptions (Do, 1998):

$$\left(\frac{d\pi}{dlnP}\right)_T = \frac{n}{A}RT \quad (1)$$

Where π is the spreading pressure – the 2D equivalent of pressure, A is the surface area – the 2D equivalent of volume, P is gas pressure, T is temperature, n is the number of moles in the adsorbed phase, and R is the gas constant. Assumption of an ideal gas analogue to the 2D adsorbed phase provides the linear adsorption isotherm; accounting for finite atomic volume provides the Volmer isotherm; accounting for interatomic forces provides the Fowler-Guggenheim isotherm; accounting for both atomic volume and interatomic forces provides the Hill-deBoer isotherm (Do, 1998).

The potential theory has been proposed in the literature specifically to characterize sub-critical adsorption of vapours on microporous substances, where sorption is controlled by micropore filling (Bering et al., 1972; Dubinin, 1967). The D-R model is superior to the Langmuir model in modelling sub-critical adsorption in shales (Wang et al., 2016b). Variants of the DR model that has been empirically altered to provide a linear fit at low pressures have been proposed (Kapoor et al., 1989). However, they still lack a monolayer volume at high pressures.

Different variants of the Langmuir equation has been used in the literature. A bi-Langmuir / dual-site model has been used to account for sorption differently in kerogens and clay minerals (Lu et al., 1995; Tang et al., 2016; Wang et al., 2014). An Ono-Konodo monolayer model was used to account for further heterogeneities (Merey and Sinayuc, 2016). The Freundlich, Sips, and Toth isotherms have also been

used in the literature to fit Type I isotherms (Ahmadi and Shadizadeh, 2015; Bae; and Bhatia*, 2006; Do, 1998).

5.5.1.2 Multi-component adsorption

The IAST (Ideal Adsorbed Solution Theory) is one of the more rigorous techniques to multi-component adsorption (Myers and Prausnitz, 1965), and generally provides a much better fit to adsorption data as compared to other techniques (Clarkson and Bustin, 2000). The main assumptions of the Ideal Adsorbed Solution Theory are (Myers and Prausnitz, 1965): inert adsorbent without any change in internal energy, temperature invariant surface, equilibria could be described thermodynamically.

The IAST has several advantages over other model based prediction techniques: the accuracy is solely dependent on the accuracy of the single component isotherms and not on mixture properties. Multiple isotherms can be applied although the IAST runs into numerical complications with certain micropore filling based isotherms (Laskar and Hashisho, 2020). Researchers have proposed novel numerical schemes to overcome these complexities (Santori et al., 2014). However, it is generally more preferable to use either a Langmuir based isotherm or an interpolation isotherm for quick and accurate convergence (Simon et al., 2016). The IAST also has several drawbacks. The main drawback for shale gas reservoir characterization is that a simple model based differential relationship to adsorption cannot be derived for this isotherm as these are highly useful in several areas of gas shale reservoir characterization (Civan et al., 2012). Also, neglecting mixture properties, it does not account for real gas behaviour. Real Adsorption Solution Theory has been proposed to overcome this drawback (Erto et al., 2012). The Vacancy Solution Theory (VST) assumes that the adsorption system consists of vacancies with 2 different solutions – gas phase and the adsorbed phase with both solutions having different properties (Laskar and Hashisho, 2020). The Multi Component Potential Theory of Adsorption builds on the potential theory for multiple components (Tun and Chen, 2020). However, these methods are not

broadly adopted, due to the wide availability of existing tools and numerical techniques to solve the IAST more readily (Simon et al., 2016).

Variants of the Langmuir model based on first principles have also been proposed for multi-component adsorption (Berawala and Østebø Andersen, 2019). The ZGR (Zhou-Gasem-Robinson Equation of State) and the LRC (Loading Ratio Correlation) models based on pure component sorption were found to give good fits for multi-component sorption in shales (Fitzgerald et al., 2005). The primary advantage of these model based empirical approaches over thermodynamic approaches is their simplicity resulting in a much simpler integration with other techniques for gas shale reservoir characterization (Liu et al., 2013). However, they also suffer from serious drawbacks in terms of their accuracy and the ability of the model to model varying adsorptive selectivity over the adsorption range (Laskar and Hashisho, 2020).

5.5.1.3 Thermodynamics of Adsorption

Whilst adsorption usually increases with increasing pressure, it decreases with increasing temperature (Zou et al., 2017). Adsorption thermodynamics is widely characterised using isosteric heats of sorption – standard enthalpy at fixed loading (Sircar et al., 1999). Methods to predict the isosteric heat of adsorption from specific adsorption isotherms have been proposed in the literature (Bakhtyari et al., 2019). The Clausius-Clapeyron equation is widely used for this purpose (Guo et al., 2013).

The second technique to estimate sorption for microporous substances is through the application of characteristic curves (Dubinin, 1960). When a substance exhibits characteristic curves, it is usually possible to obtain temperature invariant characteristic curves of amount adsorbed against adsorption potential (Clarkson et al., 1997; Do, 1998). Other studies have indicated that it was not possible to obtain a characteristic curve based on the potential theory for gas shales (Chen et al., 2011).

However, methodologies proposed to account for the temperature dependence of sorption are largely empirical, in the context of numerical studies. Although the Langmuir volume does not change with

temperature theoretically, shales have significantly altered adsorption capacities to temperature (Guo et al., 2013; Lu et al., 1995). Whilst some have proposed an exponential relationship (Gasparik et al., 2014), others have proposed a linear relationship between Langmuir volume and temperature (Rexer et al., 2013). The following is a summary of empirical techniques used to account for Langmuir adsorption characteristics (Do, 1998; Fianu et al., 2018; Gasparik et al., 2014):

$$V_L = a_1 + \frac{a_2}{T} \tag{2}$$

$$V_L = q_1 \exp\left(-\frac{q_1}{T}\right) \tag{3}$$

$$P_L = P_{L_\infty} \exp\left(-\frac{H_L}{RT}\right) \tag{4}$$

Where V_L and P_L are Langmuir volume and pressure. T is temperature, a_1, and a_2 are fitting constants for Langmuir volume; P_{L_∞}, H_L,are theoretical Langmuir pressure at infinite temperature, and Langmuir heat of sorption used to fit temperature depended.

5.5.1.4 Adsorption Characterization in Shales

It is common to obtain adsorption isotherms from canister tests, where the core samples are left in a sealed container as soon as they are retrieved, and sorption is calculated from the amount of gas displaced from the core sample (Clarke et al., 2018; RP40, 1998; Shtepani et al., 2010). Other novel techniques have been explored for adsorption measurement in gas shales such as the dielectric method (Bose et al., 1987), the NMR technique (Li et al., 2019; Liu et al., 2017), and the continuous flow method (Nelsen and Eggertsen, 1958). The manometric method is by far the most commonly used technique to characterize sorption in gas shales (Krooss et al., 2002; Lu et al., 1995). In the manometric technique for adsorption characterization, the adsorptive is isolated in a pressure vessel coupled with a pressure sensor, a known amount of the adsorptive is injected and the amount adsorbed is calculated through a mass balance (Rouquerol et al., 2013). Variants of the manometric method have also been proposed for multi-component sorption measurement and sorption measurement in the presence of

moisture (Do, 1998; Jahediesfanjani and Civan, 2007; Talu, 1998). Adsorption isotherms obtained from any of the above techniques could then be integrated into an OGIP estimate (Mengal and Wattenbarger, 2011), or a reservoir simulation to estimate reserves (Yu and Sepehrnoori, 2014a).

5.5.2 Diffusion

Material transfer in shales is controlled by both bulk convection and surface diffusion. Surface diffusion plays an increasingly important role at smaller pore sizes where the pore diameter approaches the mean free path of the molecule (K. Wu et al., 2015; Yang et al., 2020). This is shown in Figure 5-5. Based on the shale's Knudsen number, the flow regimes are classified into 4 broad types: Darcy flow with basic Darcy permeability, slip flow with the Klinkenberg correction, transition flow with the Knudsen correction, and surface diffusion where the Knudsen effect dominates. In the continuum region, the no-slip condition usually assumed in models is sufficient. However, with smaller pore sizes, more effects come into play and the permeability value needs to be altered to reflect this. That said, for most used cases in the slip flow or transition flow region, it is usually possible to account for surface diffusion effects using a modified value for permeability that includes this effect (Wu and Di, 2014; Yu and Sepehrnoori, 2018). This method is generally preferred in the literature.

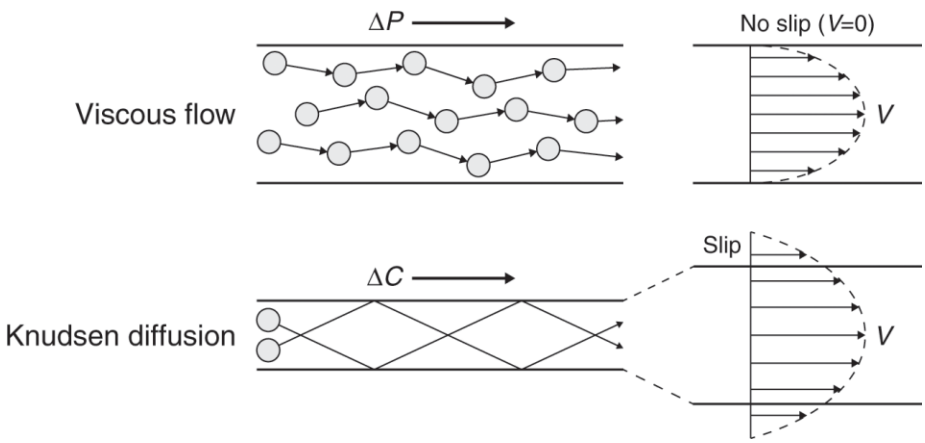

Figure 5-5 Continuum flow vs Surface Diffusion from (Zoback and Kohli, 2019)

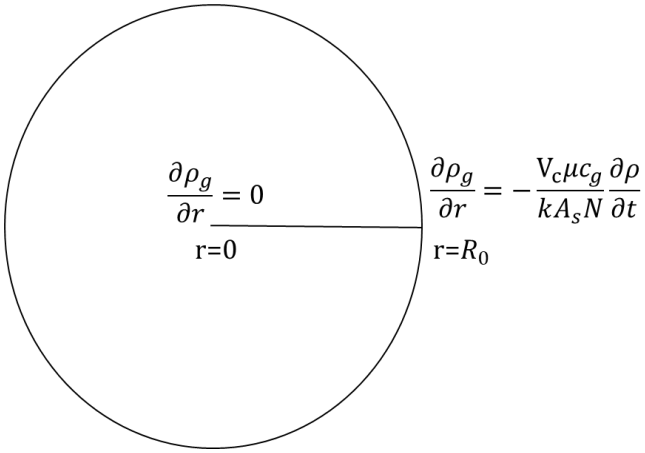

Figure 5-6 Diffusion in gas shales in 1D

It is also important to distinguish between a shale's intrinsic diffusivity and apparent permeability that could be measured in the laboratory. As apparent permeability depends on shale, fluid, and adsorption properties, it is usually different from the intrinsic permeability (Civan et al., 2013). Consider a crushed shale sample shown in Figure 5-6 (Civan et al., 2013; Cui et al., 2009). The governing equation is given in Equation (5).

$$\phi \frac{\partial \rho_g}{\partial t} + (1-\phi) \frac{\partial \rho_a}{\partial t} = \frac{k}{\mu c_g} \frac{1}{r^2} \frac{\partial}{\partial r} \left(r^2 \frac{\partial \rho_g}{\partial r} \right) \tag{5}$$

Where ϕ is porosity; ρ_g is gas density, t is time, ρ_a is adsorbed phase density, k is permeability, μ is viscosity, c_g is compressibility factor, The governing equation can be rearranged in a more canonical form to better understand the effects of adsorption on diffusion coefficient.

$$\frac{\partial \rho_g}{\partial t} = K \frac{\partial}{\partial r} \left(r^2 \frac{\partial \rho_g}{\partial r} \right) \tag{6}$$

Where K is the diffusion coefficient. It is now easy to see how permeability and sorption affect diffusion in shales.

$$K = \frac{k}{\mu c_g (\phi + (1-\phi)\, K_a)} \tag{7}$$

Where adsorption uptake, K_a, is given as:

$$K_a = \rho_{sb} \frac{\partial \rho_a}{\partial \rho_g} \tag{8}$$

From Equation (7), diffusion in shales is directly proportional to its permeability but inversely proportional to its viscosity and adsorption uptake. Diffusion in the presence of sorption is a function of pressure and temperature and decreases with increased pressure and increases with increased temperature (Charrière et al., 2010). Carbon dioxide diffusion was found to be faster than methane (Busch et al., 2008; Pone et al., 2009). The Arrhenius law was found to provide a good fit to the temperature effect on diffusion coefficients (Charrière et al., 2010).

Two approaches could be used to characterize diffusion in general (Cussler, 2012): 1) Rate based methods, which characterize the rate of mass transfer based on the average concentration in the system, modelling concentration only as a function of time (Fan et al., 2003). 2) Fick's equations, which characterize mass transfer with an approach analogous to heat and momentum transfer, and models concentration both in time and space (Cui et al., 2009).

The first and second-order rate equations are widely used to characterize diffusion (Fan et al., 2003). Other models such as the linear driving force model and the Elovich model have also been proposed in the literature for more complex fits (Do, 1998). When characterizing diffusion across space, variants of the Fick's model have been adopted. The unipore and bidisperse model has been popular in the experimental community (Crosdale et al., 1998). Effects of Knudsen diffusion and Klinkenberg effect are also widely explored (Profice et al., 2012).

5.5.3 Mass Transfer Controls in Gas Shales

Adsorption in shales has been demonstrated to be a strong function of its organic matter (Chalmers and Bustin, 2007; Ross and Marc Bustin, 2009; Wang et al., 2013, 2016b). The type of organic matter also played a part in adsorption capacity. Vitrinite rich coals exhibited greater sorption capacities compared to inertinite rich coals (Crosdale et al., 1998). Mineralogy was also demonstrated to hold a strong control

on gas sorption in shales (Gasparik et al., 2014; Ross and Bustin, 2008), however, it was not as important as the shale's organic content (Liang et al., 2016). In general, clay mineral content strongly correlated with micropore volume and adsorption capacities (Ji et al., 2012).

Amongst clay minerals, adsorption capacities of illite were greater than chlorite (Liang et al., 2016). However, adsorption is expected to occur preferentially on the organic matter due to having higher surface areas and stronger adsorption energies (Ji et al., 2012). Increases in carbonates resulted in a decrease in porosity and gas capacity (Ross and Bustin, 2008). Since carbon dioxide is a foreign component to the shale reservoir, carbon dioxide sorption could often be accompanied by other effects such as mineralization. The mechanisms of mineral trapping of carbon dioxide in dawsonite and ankerite have been studied in the literature (Xu et al., 2005). Other studies have noted that carbonate minerals are particularly susceptible to CO_2-brine dissolution (Lu et al., 2016). Pyrite showed slight alteration on exposure to super critical carbon dioxide, whilst quartz and feldspar minerals remained largely intact (Lu et al., 2016).

Adsorption affinity seemed to decrease as a function of pore size using a GCMC simulation (Zhou et al., 2016), whilst adsorption capacity has been found to increase as a function of both pore size and surface area (Gasparik et al., 2014; Rexer et al., 2014; Wang et al., 2016a). On multi-component adsorption, it was not possible to determine a relationship between carbon dioxide selectivity and geochemistry (Clarkson and Bustin, 2000).

Swelling due to sorption is a well-observed phenomenon in kerogen and clays, but never studied rigorously (Heller and Zoback, 2014; Zhao et al., 2019). The amount of swelling to loading is still not well understood. Some authors have proposed a linear relationship (Heller and Zoback, 2014) whilst others have proposed a more characteristic relationship. For example, the swelling has been observed to increase to loading for high pressures up to a certain point, but decrease after that (Pan and Connell, 2007). Sorption was also found to decrease with increase in effective stress suggesting that reservoir gas in place might be smaller by a factor of about 5-50% (Hol et al., 2011; Pone et al., 2009).

Impact of moisture on adsorption in gas shales has generally been investigated on moisture equilibrated samples (ASTM, 2000). Many studies have observed that moisture decreased the potential for methane adsorption in shales (Crosdale et al., 2008; Day et al., 2008; Krooss et al., 2002; Liang et al., 2016; Merkel et al., 2015; Ross and Marc Bustin, 2009; Wang and Zhang, 2020). Some studies have also observed a decrease in amount adsorbed with increasing moisture content (Chalmers and Bustin, 2007). Moisture has also been found to increase the hysteresis in dry shales as the desorbed water molecules block the pore throats for the larger methane molecules (Wang and Zhang, 2020). Moisture effect is expected to be more significant for adsorption on clay minerals over organic content (Ji et al., 2012). The relationship between moisture and methane adsorption in shales is not linear (Crosdale et al., 2008). It must be noted that sorption determination on moisture equilibrated samples does not reflect the reality in the reservoir. Other methods have been proposed to properly account for water content in gas shale reservoirs but are not widely practised (Jahediesfanjani and Civan, 2007).

5.6 Reservoir Characterization in Gas Shales

5.6.1 Geochemical Characterization

The kerogen type is usually identified by elemental analysis of five components – carbon, hydrogen, oxygen, nitrogen, and sulphur (Allen and Allen, 2005). Several techniques have been widely used to assess the geochemical characteristics of shales in the literature (RP40, 1998). The Total Organic Carbon has widely used benchmark different shales based on their hydrocarbon generation potential (Schumacher, 2002). Bitumen content is also strongly correlated with oil content (Allen and Allen, 2005). The standard technique for the analysis of organic content in source rocks is known as Rock-Eval pyrolysis (RP40, 1998). The gas samples from the rock sample being combusted in an inert atmosphere are analysed as a function of time in a GC-FID. The peaks corresponding to bitumen, hydrocarbon, and gas formation are then analysed. Visual analysis is also common. These make use of

the translucent organic matter in shales and measure the reflected light to classify shales in the order of increasing reflectance as exinite, vitrinite, and inertinite rich shales (Allen and Allen, 2005). X-Ray Diffraction could be used to study the non-organic composition of shales.

5.6.2 Adsorption Characterization

Adsorption measurement techniques are broadly classified into manometric, gravimetric, and gas flow techniques. Gravimetric adsorption techniques could provide very high accuracy with small sample sizes. However manometric techniques are generally preferred for adsorption characterization in shales due to their ability to accommodate large sample sizes, which partly counteracts shale heterogeneities (Heller and Zoback, 2014). Also, adsorption determination in the presence of gas flow introduces a further unknown into the equation which is already fairly complicated due to the heterogeneous nature of shale permeabilities (Civan et al., 2012). Therefore, it is generally not practised widely the shale gas literature.

Sorption of gases in microporous substances at high pressures is complicated by two issues: 1) A certain amount of the adsorptive is distributed in the adsorbed phase at the start of the experiment. Since the experimental rig measures the signal difference between the distribution of adsorptive molecules during adsorption, the experimentally measured excess sorption needs to include a correction term (Rouquerol et al., 2016). 2) The concept of adsorption space itself becomes complicated for highly fractal microporous shales. This further complicates the measurement of changes in adsorptive distribution across the gas phase and the adsorbed phase (Pini, 2014).

Both of these complications are addressed by adopting the Gibbs approach to adsorption measurement (Rouquerol et al., 2013). This involves an arbitrary definition for the adsorbed phase using a Gibbs exclusion volume, as shown in Figure 5-7. This arbitrary definition simplifies the sorption

characterization and inter-laboratory comparison (Brandani et al., 2017, 2016; Pini, 2014; Rouquerol et al., 2016).

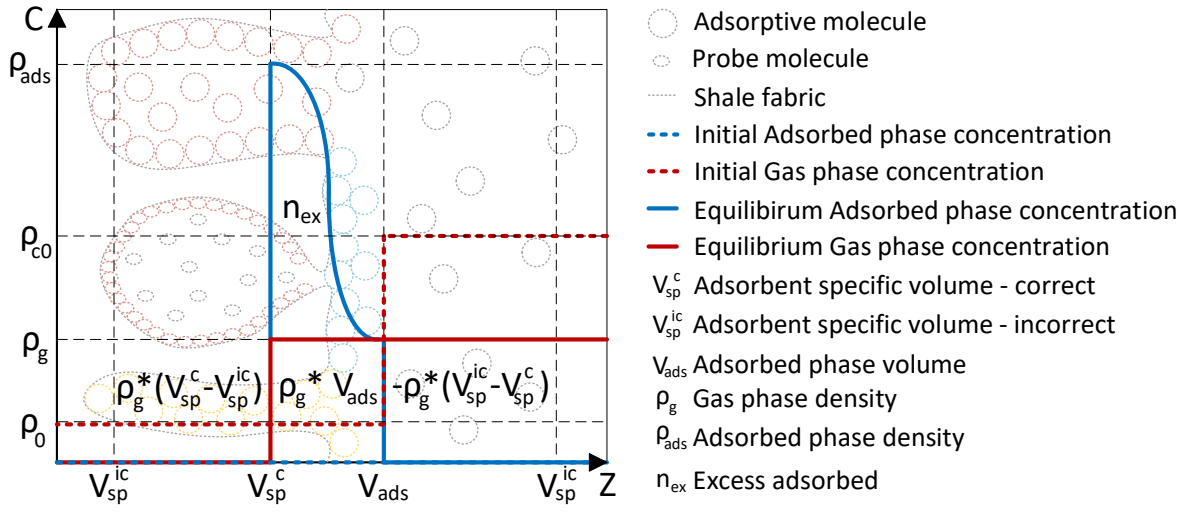

Figure 5-7 Gibbs approach to adsorption characterization after (Rouquerol et al., 2013)

Using the Gibbs approach for adsorption characterization, three metrics are commonly used in the literature to report adsorption results on different samples. 1) Net adsorption is obtained by assuming an arbitrary value for the Gibbs exclusion volume. This removes the uncertainty in the estimation of the grain density of gas shale (Pini, 2014). 2) Excess adsorption is obtained by measuring the difference between the initial distribution of adsorptive molecules in the adsorption (Rouquerol et al., 2016). 3) Absolute adsorption includes correction terms for both the Gibbs exclusion volume and the initially distributed molecules in the adsorbed phase (Do, 1998).

The method from the net to highly relevant for gas shales, as the potential for organic matter and clay minerals to swell with sorption is well documented (Pan and Connell, 2007; Siemons and Busch, 2007). Correction of excess adsorption isotherms to absolute adsorption isotherms can be done in one of the following two ways: 1) assuming a surface coverage mechanism, and 2) assuming a micropore filling mechanism (Brandani et al., 2016). Both methods require appropriate assumptions. Assuming a surface coverage mechanism to convert from excess to absolute isotherms, require the adsorbed phase density

to be measured accurately. Whilst it is possible to measure this from the slope of the excess isotherms at high pressures (Do, 1998; Fitzgerald et al., 2005; Zhou et al., 2018), it is most commonly assumed to be equal to the liquid density of the adsorbent (Krooss et al., 2002). Assuming a micropore filling mechanism require the pore volume to be measured accurately, which is very complicated for heterogeneous microporous substances (Weidenthaler, 2011). A technique to account for sorbed phase volume whilst estimate original gas in place has been proposed in the literature (Ambrose et al., 2012). Also, the dominant mechanism could be different for different shales, and there is currently no clear understanding of this in the literature. Incorrect or improperly applied methods to correct between different kinds of sorption could lead to erroneous values. Negative adsorption isotherms have been observed in the literature for certain shales and other microporous substances (Andreas Busch et al., 2007; Do et al., 2010).

As discussed previously, adsorbed phase density is a very important parameter when correcting excess adsorbed values to absolute adsorbed values, and this deserves further discussion. Although it is most commonly assumed to be the liquid density of the adsorbent at boiling point, or equal to the co-volume van der Waals constant (Do, 1998; Zhou et al., 2018), it can also be determined experimentally from the slope of the adsorption isotherm at high pressures (Pini, 2014) or through the potential theory of adsorption (Zhou et al., 2018). As the sorption mechanisms in shales are not well understood, experimentally determined sorbed phase density values have often provided very different results to thermodynamic assumptions (Zhou et al., 2018). This is an area of active research for shale gas reservoir characterization (Pini, 2014).

Multi-component adsorption isotherms are usually obtained by coupling elemental analysis with another adsorption measurement technique (Talu, 1998). This technique is fairly involved, in usually the Ideal Adsorbed Solution Theory is preferred to predict multi-component isotherms in the literature (Simon et al., 2016). Experimentally measured excesses sorption isotherms are converted to absolute sorption in a similar way to single-component isotherms (Brandani et al., 2017).

Calorimetric methods are associated with a means of adsorption characterization. In general, there are 4 types of adsorption calorimeters: adiabatic calorimeters where the sample temperature is followed by

the surrounding temperature, diathermal-conduction calorimeters where the sample temperature follows surrounding temperature by conduction, diathermal-compensation calorimeters where the sample temperature follows surrounding temperature using power compensation, and isoperibol calorimeters where there is no connection between sample temperature and surrounding temperature (Rouquerol et al., 2013). However, it is also possible to estimate the heat of sorption from adsorption isotherms measured at different temperatures using the Clausius-Clapeyron equation (and and Kaneko*, 2001).

5.6.3 Permeability Characterization

Permeability characterization based on the diffusion equation methods are broad of two types (Cui et al., 2009): 1) steady-state methods which require extremely long equilibrium times for gas shales (Cao et al., 2016), and 2) unsteady-state methods which require more complex data analysis. The impact of sorption on permeability characterization in gas shales has been considered in the literature (Cao et al., 2016; Civan et al., 2013; Zhao et al., 2019). The impact of non-Darcy flow has also been explored (Profice et al., 2012). Knudsen diffusion was found to be increasingly important at smaller pore sizes (Kim et al., 2015). This suggests that different flow regimes should be considered when characterizing diffusion in gas shales. Impact of sorption on permeability has also been measured in the literature (Zhao et al., 2019).

Diffusion characterization based on unsteady-state methods is usually performed on crushed samples (Cui et al., 2009). There is some evidence in the literature to suggest that crushed shale samples do not have significantly different permeabilities to core samples (Guidry et al., 1996). But other studies have reported that transient analysis on crushed samples is unreliable due to the highly complex nature of mathematical techniques required to measure them (Fisher et al., 2017)

5.6.4 Pore Characterization

To study the pore sizes, different techniques are available in the literature depending on the range of pores that need to be studied as summarised by Figure 5-8. In the literature, SEM (Scanning Electron Microscopy), MICP (Mercury Induced Porosimetry, N_2 adsorption, Helium expansion, and water immersion have been very commonly used for shale pore characterization (Al Hinai et al., 2014; Ji et al., 2017; Kuila et al., 2014; Kuila and Prasad, 2013; Rani et al., 2019).

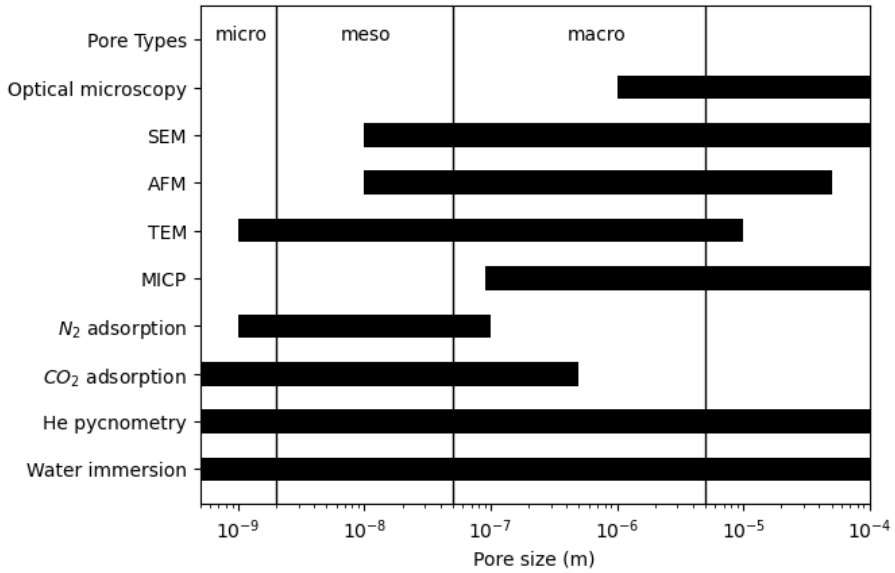

Figure 5-8 Pore Characterization Techniques for Different Pore Sizes after (Anovitz and Cole, 2015)

Scanning Electron Microscopy, Transmission Electron Microscopy, and Atomic Force Microscopy have been used in the literature to study nano-scale structures of shale rocks (Wu and Aguilera, 2012). Different techniques and magnifications have different applications. Larger magnifications are usually used to relate pore sizes and shapes with the shale geochemical components, whilst smaller magnification are used to study the pore size distribution and pore connectivity. It is possible to apply image segmentation algorithms to analyse the shale pore structure (Gostick et al., 2019). This is done using a series of clustering algorithms, first in terms of the pixel density of different phases of the shale

matrix, and then in terms of the pore distribution along these phases. However these techniques don't tend to be very accurate in characterizing pore size distributions and are interpreted along with other pore characterization techniques to derive useful results (Gostick et al., 2019). The mercury porosimetry technique uses the Washburn equation to calculate a pore size associated with a specific saturation of mercury on the gas shale.

$$q = -\frac{\pi r^2 k(\Delta P - P_c)}{\mu L} \tag{9}$$

Where q is volume flux, r is pore radius, k is permeability, ΔP is the pressure difference between nodes, P_c is capillary pressure in the tube, μ is viscosity, L is the length. From equation (9), as the pore radius decreases, higher pressure differences are required to measure a comparable amount of pre volume. The pressures required for gas pore characterization in gas shales could be as high as 420 MPa, which renders in unsuitable for pore characterization in shales (Kuila and Prasad, 2013). Also, it can be derived from Figure 5-8, that MICP is better suited for macropore analysis, whilst most shales have been noted to have meso or micro pores (Clarke et al., 2018; Ji et al., 2017).

Adsorption techniques are usually used to characterize extremely small pores from 2 to 50 nm (Sweatman and Quirke, 2001). The Kelvin equation forms the basis for adsorption pore analysis in the mesopore region (Everett and Powl, 1976) as shown in Equation (10).

$$\frac{P}{P_0} = \exp\left(-\frac{2\sigma v_M}{RT}\frac{1}{r_m}\right) \tag{10}$$

Where P is system pressure, P_0 is saturation pressure, σ is surface tension, v_m is liquid molar volume, r_m is the mean radius of the curvature. Canonical methods based on the BET isotherm are not to be applied to microporous shales blindly as they do not reflect the more complicated sorption characteristics of shales (Llewellyn et al., 2007). However, there is some evidence that the BET monolayer volume corresponds to energetically minimum adsorption, which could be a useful metric to track for heterogeneous substances (Llewellyn et al., 2007). Other techniques such as the t-plot and α_s plot could potentially be used for microporous substances if an appropriate reference material is

used. (Rouquerol et al., 1994). The BJH technique is also based on the capillary condensation phenomenon in the mesopore region (Barrett et al., 1951).

The DFT technique has been used to study the pore structure of shales in the literature (Li et al., 2016). This takes a completely different approach and minimizes the grand potential of the adsorbent adsorbate system by using appropriate Lennard Jones interaction parameters. However, the choice of interaction parameters is extremely important for the accuracy of this technique. In general, the Steele equation has been widely used to model adsorption interactions on carbonaceous substances (Landers et al., 2013).

Helium expansion and water immersion are standard techniques for measuring grain volume and bulk volume respectively (Kuila et al., 2014). Although, some authors prefer to use mercury induction for the determination of bulk volumes (Ross and Marc Bustin, 2009), water immersion is more accurate as it's least count is determined by the mass balance used instead of a volumetric measurement. It is also non-destructive allowing to conserve more valuable shale core samples whilst mercury induction destroys the shale pores (Anovitz and Cole, 2015).

5.6.5 Resource Characterization Methodologies

To better account for uncertainties associated with resource estimation, 4 resource categories have been proposed in the literature (EIA, 2015b). The OGIP (Original Gas in Place), estimated based on a volumetric assessment of the reservoir and the adsorption capacity, is the most uncertain resource category albeit the largest. Technically Recoverable Resources (TRR) include the portion of the OGIP that could be produced with current technology. Economically Recoverable Resources (ERR) are TRRs that could be produced under current economic conditions. Proven Reserves are ERRs that could be produced with the infrastructure that is already present. This is the smallest resource category, but the most certain. This study will mostly be concerned with the impact of sorption on both OGIP and TRR.

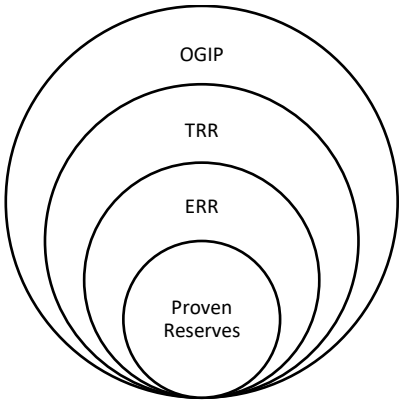

Figure 5-9 Resource categories (EIA, 2015a)

5.6.6 Reserve Estimation through Reservoir Simulation

Inclusion of adsorption in resource estimate has the potential to increase total OGIP from anywhere between 20 and 80% (Schettler Jr and Parmely, 1991). However, the impact of sorption on reserve estimates is less well understood. In some studies, adsorption has been demonstrated to have a significant effect on gas flow in shales at the reservoir scale (Zhao et al., 2020). However, other studies have demonstrated that adsorption could decrease the net recovery from Barnett shales (Mengal and Wattenbarger, 2011). A method to fit field production data using a simple least-squares algorithm to predict desorption from the reservoir has also been explored (Lane et al., 1989).

Several techniques exist to study gas flow in shales. The Lattice Boltzmann method has been explored to study gas transport in shales (Yang et al., 2020). Molecular Dynamics simulations are typically performed to study sorption and diffusion characteristics in shale nanopores (H. Wu et al., 2015; Zhai et al., 2014), whilst Grand canonical Monte Carlo simulations provide further insights on sorption characteristics (Zhou et al., 2016). Markov chains have also been used to provide preliminary estimates of reserves (Kass et al., 1997). However, the most accepted technique for reserve estimation is a field-scale simulation of the gas flow in shale reservoirs.

The governing equations that describe heat and mass transfer in gas shales are highly non-linear (Wu and Di, 2014). Therefore, it is not a simple task to derive analytical solutions for most use-cases

(Thambynayagam, 2011). Although semi-analytical methods have been proposed for certain cases in the literature (Yu et al., 2014a), numerical methods are necessary to study the behaviour of gas flow in shales for most applications. Numerical methods for solving PDEs could either be based on the Taylor series – Finite Differences and Finite Volume or based on test functions – Finite Elements. The Finite Element technique is preferred for this study due to its ability to work more stably with complex shale geometries (Reddy, 2010).

5.7 Production Technologies for Shale Gas Recovery

5.7.1 Reservoir Fracturing

Hydraulic fracturing is often undertaken in stages as it is not possible to maintain sufficient pressure to stimulate the entire well (Rezaee, 2015). The Expected Ultimate Recovery of a conventional well is about 750 times higher than that of a gas shale well (Rezaee, 2015). This has consequently resulted in a massive discrepancy between Original Gas in Place and the Technically Recovery Resources of many shale reservoirs.

5.7.2 Thermal Stimulation

Sorption is significantly affected by the system temperature (Lu et al., 1995). Increasing reservoir temperature has been demonstrated to increase sorbed gas recovery from shales in the literature (Liu et al., 2018; Teng et al., 2019; Wang et al., 2014; Zhu et al., 2016). Thermal stimulation also has benefits in terms of increased diffusivity in the shale matrix (Liu et al., 2018).

Formation heat capacity did not have a significant impact on thermal enhanced recovery (Wang et al., 2014). However, heat conductivity showed a negative correlation with the potential for thermal enhanced recovery (Wang et al., 2014). Langmuir volume was positively correlated with the potential for thermal enhanced recovery, whilst Langmuir pressure was negatively correlated (Teng et al., 2019; Wang et al., 2014).

Specific thermal stimulation technologies have also been investigated. Microwave heating was found to be an effective technology for thermal stimulation in gas shale reservoirs using a multi-physical model that accounts for Electromagnetic effects in addition to thermal and mass transfer effects (Liu et al., 2018). Electrical heating technology has also been investigated to provide a significant benefit (Wang et al., 2017). This suggests that any choice of heating technology can be expected to provide significant benefit to the total production.

5.7.3 Carbon Dioxide Injection / Sequestration

Carbon dioxide has a higher adsorption capacity in shales in general (Heller and Zoback, 2014). Carbon dioxide can displace methane in the shale nanopores with a relatively slow breakthrough (Liu et al., 2017; H. Wu et al., 2015). Carbon dioxide diffusivity was found to decrease with increasing concentration indicating better sealing mechanisms for shales for carbon dioxide sequestration (Busch et al., 2008). Carbon dioxide could also be trapped in a mineral form in certain clay minerals at high pressures (Liu et al., 2020; Xu et al., 2005). However, this form of trapping may require several years to trap carbon dioxide effectively (Xu et al., 2005).

Field studies have demonstrated the potential for enhanced methane recovery through carbon dioxide injection (Mavor et al., 2004; van Bergen et al., 2006; Wong et al., 2007; Yost, 1994; Yost et al., 1993). Other gases injection technologies such as nitrogen have also been explored in the literature (Puri and Yee, 1990). The potential for a carbon-dioxide-based fracturing fluid with a sand-based proppant has also demonstrated on the field (Lillies and King, 1982). Using carbon dioxide as the fracturing fluid has

the advantage of rapid clean up and evaluation following the stimulation (Lillies and King, 1982). Studies have also demonstrated that water creates thermal barriers on kerogen surface inhibiting recovery; replacing hydraulic fracturing with carbon dioxide, eliminates this barrier with potential for more efficient and clean recovery (Lee et al., 2016). Most of the gas injected is instantaneously stored in the form of adsorbed gas (Liu et al., 2013). However, carbon dioxide injection did not lead to a substantial increase in the recovery rate (Liu et al., 2013). The possibility to inject hot flue gas into the reservoir has also been investigated, thus coupling heating effect with carbon dioxide injection (Mu et al., 2019). However, it any study for gas injection must be balanced against the cost for gas purification that would be required downstream (Mu et al., 2019).

5.8 Challenges Associated with Shale Resource Extraction

5.8.1 Challenges Associated with Water Management

The biggest challenge to gas shale extraction in the 21st century is considered to be the implications of the hydraulic fracturing technology on the local freshwater resources (Gregory et al., 2011; Rahm and Riha, 2014; Wang and Li, 2016). Shale prospects in China often lack access to freshwater resources needed for hydraulic fracturing (Rezaee, 2015). Wastewater disposal from hydraulic fracturing has also been known to cause earthquakes if not managed properly owing to further build up of pore pressure after fracturing (Ellsworth, 2013). Because of this, any research into techniques to increase recovery from shale reservoirs besides hydraulic fracturing is highly topical. Carbon dioxide and nitrogen based fracturing fluids were of broad interest before the advent of hydraulic fracturing (Lillies and King, 1982). Owing to the challenges associated with hydraulic fracturing, these are seeing renewed interest from the community (Zhou et al., 2020). Besides solving issues with water management, they also offer better clean up and production due to competitive adsorption (Zhou et al., 2020). However, a lot more research is needed to further optimize this technology so it can be cost-effective. Further information

on adsorption mechanisms of methane and carbon dioxide is very important in this regard. With a better understanding of single and multi-component adsorption and diffusion behaviour at reservoir conditions, we should be able to optimize this technology further.

The problem being addressed here is sharp decline curves from gas shale reservoirs which make continued production uneconomic without frequent refracturing (Yu and Sepehrnoori, 2014b).

Another technique proposed in the literature is thermal stimulation (Mu et al., 2019). This takes advantage of the fact that both sorption and diffusion in shales is temperature-dependent, and there is some evidence that this can counterbalance the need to for frequent hydraulic fracturing by maintaining higher production rates (Teng et al., 2016). However studies so far have tended to ignore the thermal effects of

5.8.2 Challenges Associated with Carbon Management

Natural gas is a carbon-based energy source emits carbon dioxide upon combustion. This is important as the world is moving away from carbon-based fuels to combat climate change, we must do all we can to expedite the transition towards renewable energy sources. Fugitive methane emissions are another major concern as methane has a much higher global warming potential compared to carbon dioxide (Wang and Li, 2016).

However, the amount of carbon emitted from natural gas is much lower than other carbon-based fuels – only a third of the carbon dioxide emitted by coal for similar energy output. There is also some evidence that the low carbon natural gas could displace high carbon coal for energy consumption as shown in Figure 5-10.

Carbon dioxide sequestration has been identified as an important technology to meet emission targets in the IPCC roadmap (Mathieu, 2006). The interesting thing about shale is the mechanism in which the

gas is stored in the micropores – adsorption. Whilst conventional reservoirs store carbon dioxide through capillary forces and a solution mechanism, it will never be possible for conventional reservoirs to be carbon negative as the atomic carbon density of hydrocarbons is always going to be higher than the atomic carbon density of carbon dioxide. However, in shales, you also have adsorption as a potential carbon sequestration mechanism. Since shales have a much higher affinity towards carbon dioxide, shales have the potential to be a carbon-negative energy source when carbon dioxide is injected back into the reservoir. Therefore, further research on this topic is very important.

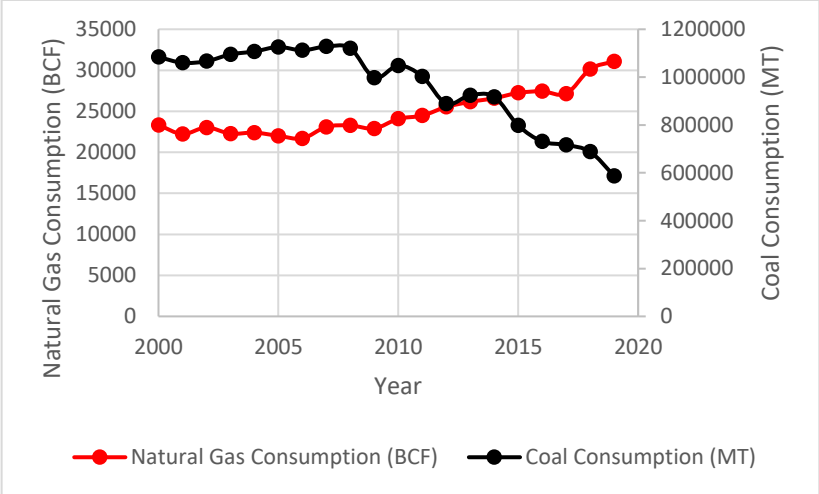

Figure 5-10 US primary energy consumption after (U.S. Energy Information Agency, 2019)

5.8.3 Challenges Associated with Resource Extraction

The recovery rates for most shale plays around the world is still below 5% (Yu et al., 2016). This is partly due to the extremely low permeabilities of gas shale reservoirs, and partly due to gas desorption. When gas is produced in a shale reservoir, the rate controlling step is the desorption and diffusion in nanopores. Since gas shales are governed by Type I isotherms, much of the gas is left behind in the reservoir. Whilst this makes sense intuitively, and there has been a lot of research on the impact of adsorption along with other parameters (Merey, 2019; Richardson and Yu, 2018), there is, as of today,

no studies on the fundamental aspects that govern this phenomenon. Further research into the adsorption and migration mechanisms of shales based on first principles is, therefore, highly topical. With an improved understanding of how gases are stored and transported in shale reservoirs, we will be better equipped to design more efficient production technologies.

5.9 References

Ahmadi, M.A., Shadizadeh, S.R., 2015. Experimental investigation of a natural surfactant adsorption on shale-sandstone reservoir rocks: Static and dynamic conditions. Fuel 159, 15–26.

Al Hinai, A., Rezaee, R., Esteban, L., Labani, M., Al, A., Rezaee, R., Esteban, L., Labani, M., 2014. Comparisons of pore size distribution: A case from the Western Australian gas shale formations. J. Unconv. Oil Gas Resour. 8, 1–13.

Allen, J.R., Allen, P. a, 2005. Basin Analysis.pdf. J. Opt. Soc. Am.

Ambrose, R.J., Hartman, R.C., Diaz-Campos, M., Akkutlu, I.Y., Sondergeld, C.H., 2012. Shale gas-in-place calculations part I: new pore-scale considerations. SPE J. 17, 219–229.

and, K.M., Kaneko*, K., 2001. The General Equation of Supercritical Gas Adsorption Isotherm.

Andreas Busch, *, Yves Gensterblum, and, Krooss, B.M., 2007. High-Pressure Sorption of Nitrogen, Carbon Dioxide, and their Mixtures on Argonne Premium Coals.

Andrews, I.J., 2013. The Carboniferous Bowland Shale gas study: geology and resource estimation. Br. Geol. Surv. Dep. Energy Clim. Chang. London, UK.

Anovitz, L.M., Cole, D.R., 2015. Characterization and analysis of porosity and pore structures. Rev. Mineral. Geochemistry.

ASTM, D., 2000. 1412-99 standard test method for equilibrium moisture of coal at 96 to 97 percent relative humidity and 30 C, vol. 05.06. West Conshohocken, PA Am. Soc. Test. Mater. 99–102.

Bae;, J.-S., Bhatia, S.K., 2006. High-Pressure Adsorption of Methane and Carbon Dioxide on Coal.

Bakhtyari, A., Mofarahi, M., Bakhtyari alibakhtyari, A., 2019. A New Approach in Predicting Gas Adsorption Isotherms and Isosteric Heats Based on Two-Dimensional Equations of State. Arab. J. Sci. Eng. 44, 5513–5526.s

Barrett, E.P., Joyner, L.G., Halenda, P.P., 1951. The determination of pore volume and area distributions in porous substances. I. Computations from nitrogen isotherms. J. Am. Chem. Soc. 73, 373–380.

Berawala, D.S., Østebø Andersen, P., 2019. Evaluation of Multicomponent Adsorption Kinetics for CO2 Enhanced Gas Recovery from Tight Shales, in: SPE Europec Featured at 81st EAGE Conference and Exhibition. Society of Petroleum Engineers.

Bering, B.P., Dubinin, M.M., Serpinsky, V. V, 1972. On thermodynamics of adsorption in micropores. J. Colloid Interface Sci. 38, 185–194.

Bose, T.K., Chahine, R., Marchildon, L., St-Arnaud, J.M., 1987. New dielectric method for the measurement of physical adsorption of gases at high pressure. Rev. Sci. Instrum. 58, 2279–2283.

Brandani, S., Mangano, E., Luberti, M., 2017. Net, excess and absolute adsorption in mixed gas adsorption. Adsorption 23, 569–576.

Brandani, S., Mangano, E., Sarkisov, L., 2016. Net, excess and absolute adsorption and adsorption of helium. Adsorption 22, 261–276.

Brunauer, S., Emmett, P.H., Teller, E., 1938. Adsorption of gases in multimolecular layers. J. Am. Chem. Soc. 60, 309–319.

Busch, A., Alles, S., Gensterblum, Y., Prinz, D., Dewhurst, D.N., Raven, M.D., Stanjek, H., Krooss, B.M., 2008. Carbon dioxide storage potential of shales. Int. J. Greenh. Gas Control 2, 297–308.

Caineng, Z., Dazhong, D., Shejiao, W., Jianzhong, L., Xinjing, L., Yuman, W., Denghua, L., Keming, C., 2010. Geological characteristics and resource potential of shale gas in China.

Cao, C., Li, T., Shi, J., Zhang, L., Fu, S., Wang, B., Wang, H., 2016. A new approach for measuring the permeability of shale featuring adsorption and ultra-low permeability. J. Nat. Gas Sci. Eng. 30, 548–556.

Chalmers, G.R.L., Bustin, R.M., 2007. The organic matter distribution and methane capacity of the Lower Cretaceous strata of Northeastern British Columbia, Canada. Int. J. Coal Geol. 70, 223–239.

Charrière, D., Pokryszka, Z., Behra, P., 2010. Effect of pressure and temperature on diffusion of CO 2 and CH 4 into coal from the Lorraine basin (France). Int. J. Coal Geol. 81, 373–380.

Chen, S., Jin, L., Chen, X., 2011. The effect and prediction of temperature on adsorption capability of coal/CH4. Procedia Eng. 26, 126–131.

Civan, F., Devegowda, D., Sigal, R.F., 2013. Critical Evaluation and Improvement of Methods for Determination of Matrix Permeability of Shale, in: SPE Annual Technical Conference and Exhibition. Society of Petroleum Engineers.

Civan, F., Rai, C.S., Sondergeld, C.H., 2012. Determining Shale Permeability to Gas by Simultaneous Analysis of Various Pressure Tests. SPE J. 17, 717–726.

Clarke, H., Bustin, M., Turner, P., 2014. Unlocking the Resource Potential of the Bowland Basin, NW England, in: SPE/EAGE European Unconventional Resources Conference and Exhibition.

Clarke, H., Turner, P., Bustin, R.M., Riley, N., Besly, B., 2018. Shale gas resources of the Bowland Basin, NW England: a holistic study. Pet. Geosci. 24, 287–322.

Clarkson, C.R., Bustin, R.M., 2000. Binary gas adsorption/desorption isotherms: effect of moisture and coal composition upon carbon dioxide selectivity over methane. Int. J. Coal Geol. 42, 241–271.

Clarkson, C.R., Bustin, R.M., Levy, J.H., 1997. Application of the mono/multilayer and adsorption potential theories to coal methane adsorption isotherms at elevated temperature and pressure. Carbon N. Y. 35, 1689–1705.

Crosdale, P.J., Beamish, B.B., Valix, M., 1998. Coalbed methane sorption related to coal composition. Int. J. Coal Geol. 35, 147–158.

Crosdale, P.J., Moore, T.A., Mares, T.E., 2008. Influence of moisture content and temperature on methane adsorption isotherm analysis for coals from a low-rank, biogenically-sourced gas reservoir. Int. J. Coal Geol. 76, 166–174.

Cui, X., Bustin, A.M.M., Bustin, R.M., 2009. Measurements of gas permeability and diffusivity of tight reservoir rocks: Different approaches and their applications. Geofluids 9, 208–223.

Cussler, E.L., 2012. Fundamentals of Mass Transfer. Part III- Mass Transf.

Daniel B. Shaw, C.E.W., 1965. The Mineralogical Composition of Shales. SEPM J. Sediment. Res. Vol. 35, 213–222.

Day, S., Sakurovs, R., Weir, S., 2008. Supercritical gas sorption on moist coals. Int. J. Coal Geol. 74, 203–214.

Do, D.D., 1998. Adsorption Analysis: Equilibria And Kinetics: (With CD Containing Computer Matlab Programs).

Do, D.D., Do, H.D., Fan, C., Nicholson, D., 2010. On the existence of negative excess isotherms for argon adsorption on graphite surfaces and in graphitic pores under supercritical conditions at pressures up to 10,000 atm. Langmuir 26, 4796–4806.

Dubinin, M.M., 1967. Adsorption in Micropores. J. Colloid Interface Sci. 23, 487–499.

Dubinin, M.M., 1960. Theory of the physical adsorption of gases and vapors and adsorption properties of adsorbents of various natures and porous structures. Bull. Acad. Sci. USSR Div. Chem. Sci. 9, 1072–1078.

Dutta, P., Bhowmik, S., Das, S., 2011. Methane and carbon dioxide sorption on a set of coals from India. Int. J. Coal Geol. 85, 289–299.

EIA, 2015a. Technically Recoverable Shale Oil and Shale Gas Resources:

EIA, 2015b. World Shale Resource Assessments, Eia.

Ellsworth, W.L., 2013. Injection-Induced Earthquakes. Science (80-.). 341, 1225942.

Erto, A., Lancia, A., Musmarra, D., 2012. A Real Adsorbed Solution Theory model for competitive multicomponent liquid adsorption onto granular activated carbon. Microporous Mesoporous Mater. 154, 45–50.

Everett, D.H., Powl, J.C., 1976. Adsorption in slit-like and cylindrical micropores in the henry's law region. A model for the microporosity of carbons. J. Chem. Soc. Faraday Trans. 1.

Fan, X., Parker, D.J., Smith, M.D., 2003. Adsorption kinetics of fluoride on low cost materials. Water Res. 37, 4929–4937.

Fauchille, A.L., Ma, L., Rutter, E., Chandler, M., Lee, P.D., Taylor, K.G., 2017. An enhanced understanding of the Basinal Bowland shale in Lancashire (UK), through microtextural and mineralogical observations. Mar. Pet. Geol.

Fianu, J., Gholinezhad, J., Hassan, M., 2018. Comparison of Temperature-Dependent Gas Adsorption Models and Their Application to Shale Gas Reservoirs.

Fisher, Q., Lorinczi, P., Grattoni, C., Rybalcenko, K., Crook, A.J., Allshorn, S., Burns, A.D., Shafagh, I., 2017. Laboratory characterization of the porosity and permeability of gas shales using the crushed shale method: Insights from experiments and numerical modelling. Mar. Pet. Geol. 86, 95–110.

Fitzgerald, J.E., Pan, Z., Sudibandriyo, M., Robinson Jr, R.L., Gasem, K.A.M., Reeves, S., 2005. Adsorption of methane, nitrogen, carbon dioxide and their mixtures on wet Tiffany coal. Fuel 84, 2351–2363.

Gallois, R.W., 1979. Oil shale resources in Great Britain. Inst. Geol. Sci. Open File Rep.

Gasparik, M., Bertier, P., Gensterblum, Y., Ghanizadeh, A., Krooss, B.M., Littke, R., 2014. Geological controls on the methane storage capacity in organic-rich shales. Int. J. Coal Geol. 123, 34–51.

Gorham, E., 1991. Northern peatlands: role in the carbon cycle and probable responses to climatic warming. Ecol. Appl.

Gostick, J., Khan, Z., Tranter, T., Kok, M., Agnaou, M., Sadeghi, M., Jervis, R., 2019. PoreSpy: A Python Toolkit for Quantitative Analysis of Porous Media Images. J. Open Source Softw.

Gregory, K.B., Vidic, R.D., Dzombak, D.A., 2011. Water Management Challenges Associated with the Production of Shale Gas by Hydraulic Fracturing. Elements 7, 181–186.

Guidry, K., Luffel, D., Curtis, J., 1996. Development of laboratory and petrophysical techniques for evaluating shale reservoirs. Final technical report, October 1986-September 1993. ResTech Houston, Inc., TX (United States).

Guo, W., Xiong, W., Gao, S., Hu, Z., Liu, H., Yu, R., 2013. Impact of temperature on the isothermal adsorption/desorption of shale gas. Pet. Explor. Dev. 40, 514–519.

Heller, R., Zoback, M., 2014. Adsorption of methane and carbon dioxide on gas shale and pure mineral samples. J. Unconv. Oil Gas Resour. 8, 14–24.

Hol, S., Peach, C.J., Spiers, C.J., 2011. Applied stress reduces the CO 2 sorption capacity of coal. Int. J. Coal Geol. 85, 128–142.

Jahediesfanjani, H., Civan, F., 2007. Determination of multi-component gas and water equilibrium and non-equilibrium sorption isotherms in carbonaceous solids from early-time measurements. Fuel 86, 1601–1613.

Ji, L., Zhang, T., Milliken, K.L., Qu, J., Zhang, X., 2012. Experimental investigation of main controls to methane adsorption in clay-rich rocks. Appl. Geochemistry 27, 2533–2545.

Ji, W., Song, Y., Rui, Z., Meng, M., Huang, H., 2017. Pore characterization of isolated organic matter from high matured gas shale reservoir. Int. J. Coal Geol. 174, 31–40.

Kapoor, A., Ritter, J.A., Yang, R.T., 1989. On the Dubinin-Radushkevich equation for adsorption in microporous solids in the Henry's law region. Langmuir 5, 1118–1121.

Kass, R.E., Gilks, W.R., Richardson, S., Spiegelhalter, D.J., 1997. Markov Chain Monte Carlo in Practice. J. Am. Stat. Assoc.

Kim, C., Jang, H., Lee, J., 2015. Experimental investigation on the characteristics of gas diffusion in shale gas reservoir using porosity and permeability of nanopore scale. J. Pet. Sci. Eng. 133, 226–237.

King, G.E., 2010. Thirty years of gas shale fracturing: What have we learned?, in: SPE Annual Technical Conference and Exhibition. Society of Petroleum Engineers.

Krooss, B.. M. v, van Bergen, F., Gensterblum, Y., Siemons, N., Pagnier, H.J.. J.M., David, P., 2002. High-pressure methane and carbon dioxide adsorption on dry and moisture-equilibrated Pennsylvanian coals. Int. J. Coal Geol. 51, 69–92.

Kuila, U., McCarty, D.K., Derkowski, A., Fischer, T.B., Prasad, M., 2014. Total porosity measurement in gas shales by the water immersion porosimetry (WIP) method. Fuel 117, 1115–1129.

Kuila, U., Prasad, M., 2013. Specific surface area and pore-size distribution in clays and shales, Geophysical Prospecting.

Landers, J., Gor, G.Y., Neimark, A. V., 2013. Density functional theory methods for characterization of porous materials. Colloids Surfaces A Physicochem. Eng. Asp. 437, 3–32.

Lane, H.S., Watson, A.T., Lancaster, D.E., 1989. Identifying and estimating desorption from Devonian shale gas production data, in: SPE Annual Technical Conference and Exhibition. Society of Petroleum Engineers.

Laskar, I.I., Hashisho, Z., 2020. Insights into modeling adsorption equilibria of single and multicomponent systems of organic and water vapors. Sep. Purif. Technol.

Lee, T., Bocquet, L., Coasne, B., 2016. Activated desorption at heterogeneous interfaces and long-time kinetics of hydrocarbon recovery from nanoporous media. Nat. Commun. 7.

Li, L., Li, C., Kang, T., 2019. Adsorption/desorption Behavior of CH4 on Shale during CO2 Huff-and-Puff Process. Energy & Fuels acs.energyfuels.9b00920.

Li, T., Tian, H., Chen, J., Cheng, L., 2016. Application of low pressure gas adsorption to the characterization of pore size distribution of shales: An example from Southeastern Chongqing area, China. J. Nat. Gas Geosci. 1, 221–230.

Liang, L., Luo, D., Liu, X., Xiong, J., 2016. Experimental study on the wettability and adsorption characteristics of Longmaxi Formation shale in the Sichuan Basin, China. J. Nat. Gas Sci. Eng. 33, 1107–1118.

Lillies, A.T., King, S.R., 1982. Sand fracturing with liquid carbon dioxide, in: SPE Production Technology Symposium. Society of Petroleum Engineers.

Liu, C., Sang, S., Fan, X., Zhang, K., Song, F., Cui, X., Wang, H., 2020. Influences of pressures and temperatures on pore structures of different rank coals during CO2 geological storage process. Fuel 259, 116273.

Liu, F., Ellett, K., Xiao, Y., Rupp, J.A., 2013. Assessing the feasibility of CO 2 storage in the New Albany Shale (Devonian–Mississippian) with potential enhanced gas recovery using reservoir simulation. Int. J. Greenh. Gas Control 17, 111–126.

Liu, J., Wang, J., Leung, C., Gao, F., Liu, J., Wang, J., Leung, C., Gao, F., 2018. A Fully Coupled Numerical Model for Microwave Heating Enhanced Shale Gas Recovery. Energies 11, 1608.

Liu, J., Yao, Y., Liu, D., Elsworth, D., 2017. Experimental evaluation of CO2 enhanced recovery of adsorbed-gas from shale. Int. J. Coal Geol. 179, 211–218.

Llewellyn, P.L., Rodriquez-Reinoso, F., Rouqerol, J., Seaton, N., 2007. Is the BET equation applicable to microporous adsorbents? Stud. Surf. Sci. Catal. 160, 49.

Loucks, R.G., Reed, R.M., Ruppel, S.C., Jarvie, D.M., 2009. Morphology, genesis, and distribution of nanometer-scale pores in siliceous mudstones of the mississippian barnett shale. J. Sediment. Res. 79, 848–861.

Lu, J., Nicot, J.-P., Mickler, P.J., Ribeiro, L.H., Darvari, R., 2016. Alteration of Bakken reservoir rock during CO 2-based fracturing—An autoclave reaction experiment. J. Unconv. Oil Gas Resour. 14, 72–85.

Lu, X.-C., Li, F.-C., Watson, A.T., 1995. Adsorption measurements in Devonian shales. Fuel 74, 599–603.

Mathieu, P., 2006. The IPCC special report on carbon dioxide capture and storage, in: ECOS 2006 - Proceedings of the 19th International Conference on Efficiency, Cost, Optimization, Simulation and Environmental Impact of Energy Systems.

Mavor, M.J., Gunter, W.D., Robinson, J.R., 2004. Alberta multiwell micro-pilot testing for CBM properties, enhanced methane recovery and CO2 storage potential, in: SPE Annual Technical Conference and Exhibition. Society of Petroleum Engineers.

Mayerhofer, M.J., Richardson, M.F., Walker, R.N., Meehan, D.N., Oehler, M.W., Browning, R.R., 1997. Proppants? We don't need no proppants. Proc. - SPE Annu. Tech. Conf. Exhib.

Mengal, S.A., Wattenbarger, R.A., 2011. Accounting For Adsorbed Gas in Shale Gas Reservoirs, in: SPE Middle East Oil and Gas Show and Conference. Society of Petroleum Engineers.

Merey, Ş., 2019. Analysis of the effect of experimental adsorption uncertainty on CH4 production and CO2 sequestration in Dadas shale gas reservoir by numerical simulations. J. Pet. Sci. Eng. 178, 1051–1066.

Merey, S., Sinayuc, C., 2016. Analysis of carbon dioxide sequestration in shale gas reservoirs by using experimental adsorption data and adsorption models. J. Nat. Gas Sci. Eng. 36, 1087–1105.

Merkel, A., Fink, R., Littke, R., 2015. The role of pre-adsorbed water on methane sorption capacity of Bossier and Haynesville shales. Int. J. Coal Geol. 147, 1–8.

Mu, Y., Fan, Y., Wang, J., Fan, N., 2019. Numerical study on injection of flue gas as a heat carrier into coal reservoir to enhance CBM recovery. J. Nat. Gas Sci. Eng. 72, 103017.

Myers, A.L., Prausnitz, J.M., 1965. Thermodynamics of mixed-gas adsorption. AIChE J. 11, 121–127.

Nadeau, P.H., 2011. Earth's energy "Golden Zone": a synthesis from mineralogical research. Clay Miner.

Nelsen, F.M., Eggertsen, F.T., 1958. Determination of surface area. Adsorption measurements by continuous flow method. Anal. Chem. 30, 1387–1390.

Pan, Z., Connell, L.D., 2007. A theoretical model for gas adsorption-induced coal swelling. Int. J. Coal Geol. 69, 243–252.

Pini, R., 2014. Interpretation of net and excess adsorption isotherms in microporous adsorbents. Microporous Mesoporous Mater. 187, 40–52.

Pone, J.D.N., Halleck, P.M., Mathews, J.P., 2009. Sorption capacity and sorption kinetic measurements of CO2 and CH4 in confined and unconfined bituminous coal. Energy & Fuels 23, 4688–4695.

Potter, P.E., Maynard, J.B., Depetris, P.J., 2005. Mud and mudstones: Introduction and overview. Springer Science & Business Media.

Profice, S., Lasseux, D., Jannot, Y., Jebara, N., Hamon, G., 2012. Permeability, Porosity and Klinkenberg Coefficient Determination on Crushed Porous Media. Petrophysics 53.

Puri, R., Yee, D., 1990. Enhanced coalbed methane recovery, in: SPE Annual Technical Conference and Exhibition. Society of Petroleum Engineers.

Quigley, T.M., Mackenzie, A.S., 1988. The temperatures of oil and gas formation in the sub-surface. Nature.

Rahm, B.G., Riha, S.J., 2014. Evolving shale gas management: water resource risks, impacts, and lessons learned. Environ. Sci. Process. Impacts 16, 1400–1412.

Rani, S., Padmanabhan, E., Prusty, B.K., 2019. Review of gas adsorption in shales for enhanced methane recovery and CO2 storage. J. Pet. Sci. Eng.

Rani, S., Prusty, B.K., Pal, S.K., 2015. Methane adsorption and pore characterization of Indian shale samples. J. Unconv. Oil Gas Resour. 11, 1–10.

Reddy, J.N., 2010. An Introduction to Nonlinear Finite Element Analysis, An Introduction to Nonlinear Finite Element Analysis.

Rexer, T.F., Mathia, E.J., Aplin, A.C., Thomas, K.M., 2014. High-pressure methane adsorption and characterization of pores in Posidonia shales and isolated kerogens. Energy & Fuels 28, 2886–2901.

Rexer, T.F.T., Benham, M.J., Aplin, A.C., Thomas, K.M., 2013. Methane adsorption on shale under simulated geological temperature and pressure conditions. Energy & Fuels 27, 3099–3109.

Rezaee, R., 2015. Fundamentals of gas shale reservoirs. John Wiley & Sons.

Richardson, J., Yu, W., 2018. Calculation of Estimated Ultimate Recovery and Recovery Factors of Shale-Gas Wells Using a Probabilistic Model of Original Gas in Place.

Riewchotisakul, S., Akkutlu, I.Y., 2016. Adsorption-Enhanced Transport of Hydrocarbons in Organic Nanopores. SPE J.

Ross, D.J.K., Bustin, R.M., 2008. Characterizing the shale gas resource potential of Devonian–Mississippian strata in the Western Canada sedimentary basin: Application of an integrated formation evaluation. Am. Assoc. Pet. Geol. Bull. 92, 87–125.

Ross, D.J.K., Marc Bustin, R., 2009. The importance of shale composition and pore structure upon gas storage potential of shale gas reservoirs. Mar. Pet. Geol. 26, 916–927.

Rouquerol, J., Avnir, D., Fairbridge, C.W., Everett, D.H., Haynes, J.M., Pernicone, N., Ramsay, J.D.F., Sing, K.S.W., Unger, K.K., 1994. Recommendations for the characterization of porous solids (Technical Report). Pure Appl. Chem. 66, 1739–1758.

Rouquerol, J., Rouquerol, F., Llewellyn, P., Denoyel, R., 2016. Surface excess amounts in high-pressure gas adsorption: Issues and benefits. Colloids Surfaces A Physicochem. Eng. Asp. 496, 3–12.

Rouquerol, J., Rouquerol, F., Llewellyn, P., Maurin, G., Sing, K.S.W., 2013. Adsorption by powders and porous solids: principles, methodology and applications. Academic press.

RP40, A., 1998. Recommended practices for core analysis. Feb.

Ruthven, D.M., 1984. Principles of adsorption and adsorption processes. Chem. Eng. Process. Process Intensif.

Santori, G., Luberti, M., Ahn, H., 2014. Ideal adsorbed solution theory solved with direct search minimisation. Comput. Chem. Eng. 71, 235–240.

Schettler Jr, P.D., Parmely, C.R., 1991. Contributions to total storage capacity in Devonian shales, in: SPE Eastern Regional Meeting. Society of Petroleum Engineers.

Schumacher, B. a, 2002. Methods for the Determination of Total Organic Carbon in Soils and Sediments. Carbon N. Y.

Shtepani, E., Noll, L.A., Elrod, L.W., Jacobs, P.M., 2010. A new regression-based method for accurate measurement of coal and shale gas content. SPE Reserv. Eval. Eng. 13, 359–364.

Siemons, N., Busch, A., 2007. Measurement and interpretation of supercritical CO 2 sorption on various coals. Int. J. Coal Geol. 69, 229–242.

Simon, C.M., Smit, B., Haranczyk, M., 2016. pyIAST: Ideal adsorbed solution theory (IAST) Python package. Comput. Phys. Commun. 200, 364–380.

Sing, K.S.W., 1985. Reporting physisorption data for gas/solid systems with special reference to the determination of surface area and porosity (Recommendations 1984). Pure Appl. Chem. 57, 603–619.

Sircar, S., Mohr, R., Ristic, C., Rao, M.B., 1999. Isosteric Heat of Adsorption: Theory and Experiment. J. Phys. Chem. B 103, 6539–6546.

Smil, V., 2019. Energy in world history, Energy in World History.

Stockner, J.G., 1988. Phototrophic picoplankton: An overview from marine and freshwater ecosystems. Limnol. Oceanogr.

Sweatman, M.B., Quirke, N., 2001. Characterization of porous materials by gas adsorption: comparison of nitrogen at 77 K and carbon dioxide at 298 K for activated carbon. Langmuir 17, 5011–5020.

Talu, O., 1998. Needs, status, techniques and problems with binary gas adsorption experiments. Adv. Colloid Interface Sci. 76–77, 227–269.

Tang, X., Ripepi, N., Stadie, N.P., Yu, L., Hall, M.R., 2016. A dual-site Langmuir equation for accurate estimation of high pressure deep shale gas resources. Fuel 185, 10–17.

Teng, T., Wang, J.G., Gao, F., Ju, Y., 2016. Complex thermal coal-gas interactions in heat injection enhanced CBM recovery. J. Nat. Gas Sci. Eng. 34, 1174–1190.

Teng, T., Xue, Y., Cun, Z., 2019. Modeling and simulation on heat-injection enhanced coal seam gas recovery with experimentally validated non-Darcy gas flow. J. Pet. Sci. Eng.

Thambynayagam, R.K.M., 2011. The diffusion handbook : applied solutions for engineers. New York. N.Y. , New York. [N.Y.] .

Thommes, M., Kaneko, K., Neimark, A. V, Olivier, J.P., Rodriguez-Reinoso, F., Rouquerol, J., Sing, K.S.W., 2015. Physisorption of gases, with special reference to the evaluation of surface area and pore size distribution (IUPAC Technical Report). Pure Appl. Chem. 87, 1051–1069.

Tun, H., Chen, C., 2020. Prediction of <scp>mixed-gas</scp> adsorption equilibria from pure component adsorption isotherms. AIChE J. 66, e16243.

U.S. Energy Information Agency, 2019. Annual Energy Outlook 2019 with projections to 2050. Annu. Energy Outlook 2019 with Proj. to 2050.

van Bergen, F., Pagnier, H., Krzystolik, P., 2006. Field experiment of enhanced coalbed methane-CO2 in the upper Silesian basin of Poland. Environ. Geosci. 13, 201–224.

Vysniauskas, A., Bishnoi, P.R., 1983. A kinetic study of methane hydrate formation. Chem. Eng. Sci.

Wang, H.Y., Ajao, O., Economides, M.J., 2014. Conceptual study of thermal stimulation in shale gas formations. J. Nat. Gas Sci. Eng.

Wang, M., Zhang, D., 2020. Influences of moisture on adsorption and desorption of methane on gas shales. Energy Sources, Part A Recover. Util. Environ. Eff.

Wang, Q., Li, R., 2016. Natural gas from shale formation: A research profile. Renew. Sustain. Energy Rev. 57, 1–6.

Wang, S., Song, Z., Cao, T., Song, X., 2013. The methane sorption capacity of Paleozoic shales from the Sichuan Basin, China. Mar. Pet. Geol. 44, 112–119.

Wang, Y., Wang, X., Xing, Y., Xue, J., Wang, D., 2017. Three-dimensional numerical simulation of enhancing shale gas desorption by electrical heating with horizontal wells. J. Nat. Gas Sci. Eng. 38, 94–106.

Wang, Y., Zhu, Y., Liu, S., Zhang, R., 2016a. Pore characterization and its impact on methane adsorption capacity for organic-rich marine shales. Fuel 181, 227–237.

Wang, Y., Zhu, Y., Liu, S., Zhang, R., 2016b. Methane adsorption measurements and modeling for organic-rich marine shale samples. Fuel 172, 301–309.

Weidenthaler, C., 2011. Pitfalls in the characterization of nanoporous and nanosized materials. Nanoscale.

Whitelaw, P., Uguna, C.N., Stevens, L.A., Meredith, W., Snape, C.E., Vane, C.H., Moss-Hayes, V., Carr, A.D., 2019. Shale gas reserve evaluation by laboratory pyrolysis and gas holding capacity consistent with field data. Nat. Commun. 10, 3659.

Wong, S., Law, D., Deng, X., Robinson, J., Kadatz, B., Gunter, W.D., Jianping, Y., Sanli, F., Zhiqiang, F., 2007. Enhanced coalbed methane and CO 2 storage in anthracitic coals—Micro-pilot test at South Qinshui, Shanxi, China. Int. J. Greenh. Gas Control 1, 215–222.

Wu, H., Chen, J., Liu, H., 2015. Molecular dynamics simulations about adsorption and displacement of methane in carbon nanochannels. J. Phys. Chem. C 119, 13652–13657.

Wu, K., Li, X., Wang, C., Yu, W., Chen, Z., 2015. Model for surface diffusion of adsorbed gas in nanopores of shale gas reservoirs. Ind. Eng. Chem. Res. 54, 3225–3236.

Wu, P., Aguilera, R., 2012. Investigation of Gas Shales at Nanoscale Using Scan Electron Microscopy, Transmission Electron Microscopy and Atomic Force Microscopy, in: SPE Annual Technical Conference and Exhibition. Society of Petroleum Engineers.

Wu, Y.-S., Di, Y., 2014. A Generalized Framework Model for the Simulation of Gas Production in Unconventional Gas Reservoirs.

Xu, T., Apps, J.A., Pruess, K., 2005. Mineral sequestration of carbon dioxide in a sandstone–shale system. Chem. Geol. 217, 295–318.

Yang, X., Zhou, W., Liu, X., Yan, Y., 2020. A multiscale approach for simulation of shale gas transport in organic nanopores. Energy.

Yost, A.B., 1994. Analysis of production response to CO2/sand fracturing: A case study, in: SPE Eastern Regional Meeting. Society of Petroleum Engineers.

Yost, A.B., Mazza, R.L., Gehr, J.B., 1993. CO2/Sand fracturing in devonian shales, in: SPE Eastern Regional Meeting. Society of Petroleum Engineers.

Yu, W., Huang, S., Wu, K., Sepehrnoori, K., Zhou, W., 2014a. Development of a Semi-Analytical Model for Simulation of Gas Production in Shale Gas Reservoirs. Unconv. Resour. Technol. Conf.

Yu, W., Sepehrnoori, K., 2018. Shale gas and tight oil reservoir simulation.

Yu, W., Sepehrnoori, K., 2014a. Simulation of gas desorption and geomechanics effects for unconventional gas reservoirs. Fuel 116, 455–464.

Yu, W., Sepehrnoori, K., 2014b. An efficient reservoir-simulation approach to design and optimize unconventional gas production. J. Can. Pet. Technol. 53, 109–121.

Yu, W., Sepehrnoori, K., Patzek, T.W., 2016. Modeling gas adsorption in Marcellus shale with Langmuir and bet isotherms. SPE J. 21, 589–600.

Yu, W., Sepehrnoori, K., Patzek, T.W., 2014b. Evaluation of gas adsorption in Marcellus Shale, in: SPE Annual Technical Conference and Exhibition. Society of Petroleum Engineers.

Yuan, W., Pan, Z., Li, X., Yang, Y., Zhao, C., Connell, L.D., Li, S., He, J., 2014. Experimental study and modelling of methane adsorption and diffusion in shale. Fuel 117, 509–519.

Zhai, Z., Wang, X., Jin, X., Sun, L., Li, J., Cao, D., 2014. Adsorption and diffusion of shale gas reservoirs in modeled clay minerals at different geological depths. Energy & Fuels 28, 7467–7473.

Zhang, T., Ellis, G.S., Ruppel, S.C., Milliken, K., Yang, R., 2012. Effect of organic-matter type and thermal maturity on methane adsorption in shale-gas systems. Org. Geochem. 47, 120–131.

Zhao, Y., Lu, G., Zhang, L., Wei, Y., Guo, J., Chang, C., 2020. Numerical simulation of shale gas reservoirs considering discrete fracture network using a coupled multiple transport mechanisms and geomechanics model. J. Pet. Sci. Eng.

Zhao, Y., Wang, C., Zhang, Y., Liu, Q., 2019. Experimental Study of Adsorption Effects on Shale Permeability. Nat. Resour. Res. 28, 1575–1586.

Zhou, B., Xu, R., Jiang, P., 2016. Novel molecular simulation process design of adsorption in realistic shale kerogen spherical pores. Fuel 180, 718–726.

Zhou, S., Xue, H., Ning, Y., Guo, W., Zhang, Q., 2018. Experimental study of supercritical methane adsorption in Longmaxi shale: Insights into the density of adsorbed methane. Fuel 211, 140–148.

Zhou, Y., Ni, H., Shen, Z., Wang, M., 2020. Study on Proppant Transport in Fractures of Supercritical Carbon Dioxide Fracturing. Energy and Fuels 34, 6186–6196.

Zhu, G., Yao, J., Sun, H., Zhang, M., Xie, M., Sun, Z., Lu, T., 2016. The numerical simulation of thermal recovery based on hydraulic fracture heating technology in shale gas reservoir. J. Nat. Gas Sci. Eng. 28, 305–316.

Zoback, M.D., Kohli, A.H., 2019. Unconventional Reservoir Geomechanics, Unconventional Reservoir Geomechanics.

Zou, J., Rezaee, R., Liu, K., 2017. Effect of Temperature on Methane Adsorption in Shale Gas Reservoirs.

6 Materials and Methodology

6.1 Sample Description

Two sets of samples are considered for this study – outcrops from Straiton, Lothian, and core samples from the Bowland formation. These samples are chosen due to their availability and their topical nature in current UK energy landscape. Whilst there is a lot of heterogeneities associated with gas shale characterization, samples in the UK tend to fall in the middle for most parameters (Rezaee, 2015).

6.1.1 Lothian Shale Outcrops

Shale outcrop samples from Straiton, Lothian were acquired for the study. The location of the sample is shown in Figure 6-1. The shales occur in lower Carboniferous strata of a predominantly lacustrine depositional condition (Cameron and McAdam, 1978; Jones, 2005). Total organic content has been found to vary between 2% and 12% and was found to be predominantly Type III kerogen (Follows and Tyson, 1998). To account for this heterogeneity, a large amount of sample (>30 g) was used for analysis. This counters pore scale heterogeneities well, but field scale heterogeneities are addressed using sample statistics. Upon receival, the samples were washed with water and with Toluene to remove entrenched water, salts, and oil. They were then crushed to appropriate sieve sizes using a geological hammer. After this, the samples were stored in airtight containers until the start of outgassing.

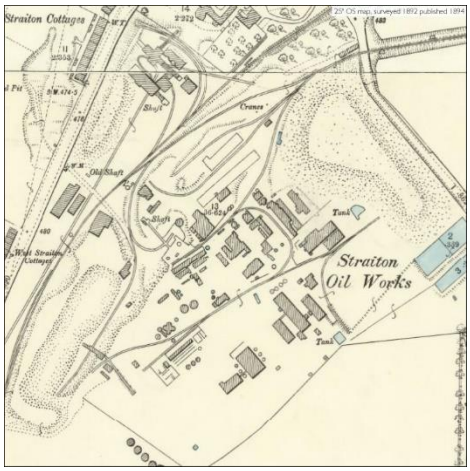

Figure 6-1 Shale mine in Straiton from (ScottishShale, 2020)

6.1.2 Bowland Shales

Bowland shales are one of the three shale plays in the UK (Andrews, 2013). The other two plays are the Wald Basin and the Midland Valley in Scotland. However, these have not been considered for active geologic exploration and are therefore not considered in this study. The Bowland contain several strata of organic-rich shales that are interesting for petroleum exploration (Clarke et al., 2018). These include the upper Milstone Grit, Lower Milstone Grit, Upper Bowland Shale, Lower Bowland Shale, and the Hodder Mudstone Units. Table 6-1 and Table 6-2 represent the stratigraphic units and sample compositions provided by Cuadrilla. A wide range of samples from every stratum in the Bowland basin was chosen for analysis.

Table 6-1 Sample Description

Sample	Depth (ft)	Stratigraphic unit
B53	5269	Upper Milstone Grit
AT1	5889.71	Lower Milstone Grit
AT9	6837.8	Upper Bowland Shale

A153	7803.5	Hodder Mudstone
AA94	8160.63	Upper Bowland Shale
AA114	8510.38	Lower Bowland Shale
AA83A	8895.21	Lower Bowland Shale

From Table 6-2 Sample Composition, the range of TOC considered in this study is between 0.77% and 7.04%. The maximum reported TOC in the literature is 7.55% (Gross et al., 2015). The depth of the samples ranged from 5000 feet to 9000 feet. Also, a large amount of sample (>30 g) was considered. This is essential given the pore, core, and field-scale heterogeneities associated with gas shales (Rezaee, 2015). Sample preparation was carried out similar to Lothian shales. The samples were washed with water, and then with Toluene. Subsequently, they were crushed to specific sieve sizes and stored in airtight containers until the start of the experiment (RP40, 1998).

Table 6-2 Sample Composition (weight percentage)

Sample	Quartz	Feldspar	Calcite	Dolomite	Ferroan carbonate	Illite/mica	Chlorite	Kaolinite	Pyrite	Apatite	TOC
B53	39.2	4.6	0	0	0	37.6	2.6	11.6	1.4	0	1.02
AT1	12	4.9	0	0	0	38.6	3.2	41.3	0	0	5.99
AT9	34.6	2.6	2.2	0	2	21.8	0	2.4	4.3	30.1	4.73
A153	30.4	3.3	2.7	1.9	1.1	31.8	5.6	21.1	2.1	0	1.6
AA94	20.6	0.4	58.4	0	19.6	1.1	0	0	0	0	0.36
AA114	54.5	4.9	2.8	0	3.9	22.1	0	7.5	4.3	0	7.04
AA83A	5.1	0	13.8	57.9	16.1	5.4	0	0.9	0.8	0	0.77

6.1.3 Sample Preparation

The samples were crushed to a sieve size of 350 - 1000 μm as shown in Figure 6-2 to characterize them in a reasonable amount of time. However, there is evidence in the literature that sorption and diffusion characteristics of crushed shale samples are comparable to bulk shale samples (Luffel and Guidry, 1992). Before the start of the adsorption and permeability experiment, the samples are placed in the rig, flushed with Helium several times and outgassed at 80 ^{0}C 100 Torr for 8 hours. A sample pressure profile of the rig during outgassing is shown in Figure 6-3. Nearly 15 hours are necessary to outgas the sample completely. Performing outgassing in situ allowed us to make sure there is no moisture adsorption or physisorption of any other species in the air before the start of the experiment. This was necessary as sorption on the surface of shales is nearly instantaneous, and outgassing in an autoclave before the experiment could lead to erroneous values for sorption and diffusion. Also, knowing when outgassing has reached equilibrium allowed starting the experiment immediately after outgassing increasing sample turnover.

Figure 6-2 Crushed shale sample for sorption and permeability experiments

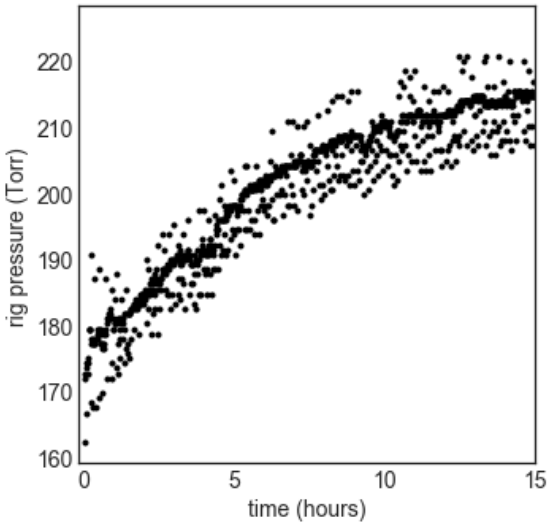

Figure 6-3 Outgassing pressure profile

For SEM and EDS experiments, the crushed samples were mounted on to a glass holder, polished, and coated with carbon through thermal evaporation as shown in Figure 6-4. Fine carbon layers are transparent to the electron beam but are conductive. This allowed using a higher operating voltage, corresponding to high-resolution images.

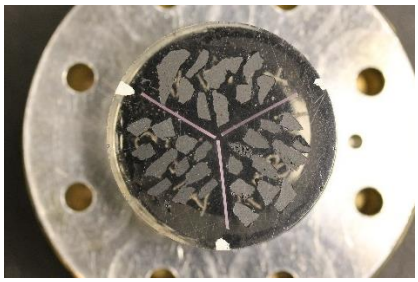

Figure 6-4 Carbon coated samples for SEM and EDS experiments

6.2 Scanning Electron Microscopy / Energy Dispersive Spectroscopy

Scanning Electron Microscopy shown in Figure 6-5, produces images of a sample by scanning the surface with a focussed beam of electrons. This allows for extremely high magnification limits

(Weidenthaler, 2011). Through an analysis of the backscattered electrons, it is also possible to perform elemental analysis in the same experiment using Energy Dispersive X-Ray Spectroscopy. Different atomic structures provide unique peaks on its electromagnetic emission spectrum, which allows us to predict the elemental composition of the sample using Mosley's law, which states that the square root of the frequency of the emitted x-ray is approximately proportional to the atomic number (Moseley, 1913).

The Carl Zeiss SIGMA HD VP Field Emission SEM with Oxford Aztec ED X-ray analysis and Electron Backscatter Diffraction system was used in this study. The samples were mounted on to the holder and placed in the rig. The rig was evacuated to 2.5×10^{-6} Torr. After the evacuation, a Schottky thermal field emitter was used as an electron source with an operating voltage of 15.kV. An aperture-size of 30 microns, a working distance of 7 mm, and a scan speed of 9 were used. A magnification of about 10 μm was achieved. Backscatter Electron imaging was used to perform compositional analysis of the sample.

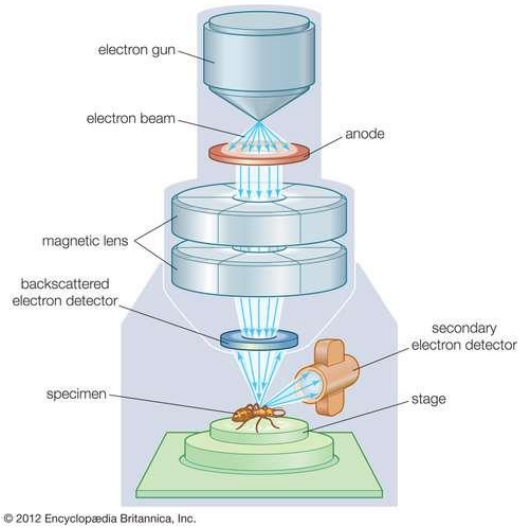

Figure 6-5 Scanning Electron Microscopy from (Ford, 2020)

6.3 Helium Porosimetry

Grain volume of the shale sample was characterized using Helium expansion in the rig shown in Figure 6-6. This is because helium adsorption on shales is negligible (Luffel and Guidry, 1992). Outgassed samples are isolated in the sample cell. The reference cell is charged with Helium, and after thermal equilibrium is reached, the valve connecting reference and sample cells is opened. Shale specific volume is calculated as shown in (11) using the volumetric law.

$$\frac{P_i}{z_i}\left(V_S - V_{sp} \times w_s\right) + \frac{P_c}{z_c}(V_R) = \frac{P_E}{z_E}(V_R + V_S - V_{sp} \times w_s) \tag{11}$$

Where P is pressure, V is volume, w is weight, and z is the non-ideality factor. Subscripts i, c, and e represent initial, charge, and equilibrium parameters, respectively.

6.4 Water Immersion

Bulk volume of the shale sample was characterized using water immersion. Shale samples were saturated under distilled water for 2 days. This allowed water to be completely absorbed in the grain volume of the shale sample. They were then suspended over a beaker with distilled water on a high precision balance with an accuracy of ± 0.0001 g. Bulk volume was calculated from Equation (12). This method provides a much higher accuracy compared to mercury porosimetry also commonly used in the literature to calculate the shale bulk volume (RP40, 1998),

$$V_{b,sp} = \frac{w_{water\ displaced}}{998.203 \times w_{sh}} \tag{12}$$

6.5 Nitrogen Adsorption

Pore size distribution was calculated from Nitrogen adsorption at 77 K. The QuantaChrome Autosorb iQ rig was used for analysis. Samples were heated in an autoclave at $100\ ^0$C for 8 hours. The samples were then weighed loaded on the rig and outgassed again at $80\ ^0C$. N_2 adsorption and desorption characterization were performed automatically in about 12 - 16 hours. Longer equilibrium times were required for characterizing lower pressure steps. The analysis was carried out in the rig using the BET,

BJH, and DFT methods. The linear form of the BET isotherm is used for surface area analysis as shown in Equation (13) (Brunauer et al., 1938):

$$\frac{1}{\left[V_a\left(\frac{P_0}{P}-1\right)\right]}=\frac{C-1}{V_mC}\frac{P}{P_0}+\frac{1}{V_mC} \tag{13}$$

Where V_a is the standard volume of gas adsorbed at STP, P_0 is the saturation pressure, V_m is monolayer volume, C is a dimensionless constant. V_m is calculated from the slope and the intercept. To calculate the BET SSA from V_m, Equation (14) is used.

$$SSA_{BET}=\frac{V_mN_a}{22400\,w_s} \tag{14}$$

Where N_a is the Avogadro's constant, w_s is the sample weight. The Barret-Joyner-Halenda scheme is based on Equation (15) (Barrett et al., 1951).

$$V_{ads}(x_k)=\sum_{i=1}^{k}\Delta V_i\left(r_i\le r_c(x_k)\right)+\sum_{i=k+1}^{n}\Delta S_i t_i\left(r_i>r_c(x_k)\right) \tag{15}$$

Where $V_{ads}(x_k)$ is the volume of the liquid adsorbate at relative pressure x_k. V and S are pore volume and surface area, respectively.

The NLDFT method involves the minimization of the grand potential of the fluid based on the NLDFT theory (Landers et al., 2013) as shown in Equation (16).

$$\Omega_f\left[\rho_{f(r)}\right]=F_f\left[\rho_f(r)\right]-\int dr\rho_f(r)\left[\mu_f-U_{ext}(r)\right] \tag{16}$$

Where r is a position vector inside the pore, $\rho_{f(r)}$ is the fluid density, F_f is the Helmholtz free energy. The calculated theoretical isotherms are then matched against the experimental isotherm. The BJH and DFT Analysis were carried out using the Autosorb iQ software. Using multiple methods for pore characterization allows accounting for the complex nature of micropores, whilst also maintaining comparability with other studies in the literature.

6.6 Manometric Adsorption Characterization

The samples are weighed and loaded on to the experimental rig shown in Figure 6-6. The rig is flushed with Helium several times and evacuated to about ≈ 150 Torr. Outgassing is performed at 80 ^{0}C for 8 hours. Performing outgassing in situ removes exposure to moisture and other species in the atmosphere that could be adsorbed on the sample. The system is evacuated to ≈ 150 Torr again and allowed to reach thermal equilibrium at the experimental temperature. The data analysis pipeline is automated in LabView. Residual Helium present in the rig after outgassing is given as:

$$n_{is}(He) = EOS(\mathrm{P}, V_v, T) \tag{17}$$

Where EOS is the chosen Equation of State used to calculate the number of moles, P is the rig pressure, V_v is the sample cell void volume, and T is the rig temperature. Different techniques are available to account for non-ideality of the gas phase. The CoolProp library is an open-source alternative to the well known RefProp library (Bell et al., 2014). Other equations of state such as the Peng Robinson equation of state, Redlich Kwong equation of state are also included in the LabView software. However, since these are not easily applied to multi-component gas behaviour, the CoolProp library is preferred in this study. The sample cell is isolated from the rig, and a known amount of the adsorptive is injected into the reference cell:

$$n_{ir} = EOS(P_{r,f}, V_r, T) - EOS(P_{r,i}, V_r, T) \tag{18}$$

Where, n_{ir} is the number of moles injected into the reference cell, $P_{r,f}$ is the final pressure of the reference cell, and $P_{r,i}$ is initial pressure of the reference cell.

moles present in the rig at any given instance is calculated as:

$$n_c = EOS(P_s, V_v, T_s) \tag{19}$$

Excess adsorbed # moles for the nth pressure step is calculated as:

$$n_a = n_{ir}(1) + n_{ir}(2) + \cdots + n_{ir}(n) + n_{is} - n_c \tag{20}$$

Where, $n_{ir}(n)$ is the number of moles injected at nth pressure step. Excess adsorbed is the adsorbed moles over sample weight:

$$q_e = \frac{n_a}{M} \tag{21}$$

Correction from net sorption to excess sorption could be accomplished using the following equation:

$$q^c = q^{ic} + \rho_g(V_{sp}^c - V_{sp}^{ic}) \tag{22}$$

Where the superscripts ^{c} and ^{ic} denote correct and incorrect values for amount adsorbed and shale specific volume, respectively. Correction from excess sorption to absolute sorption may be accomplished using one of two methods:

1. Assuming a constant adsorbed phase density, which occurs when the adsorptive molecules accumulate on the surface of the adsorbent on subsequent layers of the same density – a surface layering mechanism (Heller et al., 2014).

$$q_a = \frac{q_e}{1 - \frac{\rho_g}{\rho_{ads}}} \tag{23}$$

2. Assuming a constant adsorbed phase volume, which occurs when the adsorptive molecules fill a given space becoming denser over time – a micropore filling mechanism (Pini, 2014).

$$q_a = q_e + \rho_g \times V_{ads} \tag{24}$$

To perform multi-component analysis, the same approach was used, but the material balance was carried out through GC-FID. Samples were acquired before and after the experiment to determine the mole fractions of individual components.

6.6.1.1 Gas Chromatography Flame Ionisation Detection

GC-FID is used to quantify the amount of methane in the gas phase. After the mixtures are separated in a chromatographic column, they are passed through a flame ionisation detector and the ions formed during the combustion of organic compounds in hydrogen flame are measured. A method developed with shincarbon packed column was used for separation and the flame ionisation detection was used for quantification (Wang et al., 2019). Spool temperature was 473 K with pressure at 230 kPa. The column

temperature was 303 K. FID temperature was 553 K. Calibration was performed against a known gas composition, and these are compared with gas compositions in the rig during the experiment.

To prepare standard gas compositions, methane is injected into the adsorbent cell to pressure P_m. After equilibrium is reached, the cell is isolated, and carbon dioxide is injected into the sample cell to pressure P_c. The number of moles of methane and carbon dioxide in the rig is given as:

$$n_m = EOS(P_m, V_s, T); n_c = EOS(P_c, V_R, T) \tag{25}$$

Mole fractions are given as:

$$x_m = \frac{n_m}{n_m + n_c}; x_c = \frac{n_c}{n_m + n_c} \tag{26}$$

Amount of methane and carbon dioxide injected during the experiment is calculated during the experiment as:

$$n_{ir,m} = n_{ir} * x_m; n_{ir,c} = n_{ir} * x_c \tag{27}$$

Amount of methane and carbon dioxide at equilibrium is given as:

$$n_{c,m} = n_{ir} * x_m; n_{ir,c} = n_{ir} * x_c \tag{28}$$

The calculation for adsorption is similar to single component methodology (Brandani et al., 2017).

6.6.2 Adsorption Isotherms

Adsorption isotherms characterize sorption at a given temperature and provide a convenient way of integrating sorption into other aspects of gas shale reservoir characterization. The simplest isotherm in the literature is the linear isotherm with just one parameter (Do, 1998).

$$q_a = k_l \rho_g \tag{29}$$

Where q_a is the amount adsorbed, k_l is the Henry's constant, ρ_g is the gas phase concentration. The first derivative of the linear isotherm is simply its Henry's constant.

$$\frac{\partial q_a}{\partial \rho_g} = k_l \tag{30}$$

The Langmuir isotherm has been widely used to characterize sorption in gas shales (Li et al., 2016; Merey and Sinayuc, 2016; Rani et al., 2015; Wang et al., 2016; Yu and Sepehrnoori, 2014a; Zhang et al., 2012).

$$q_a = q_L \frac{b_L \rho_g}{1 + b_L \rho_g} \tag{31}$$

Where, q_L is the Langmuir monolayer sorption capacity in mol/kg and b_L is the Langmuir affinity constant in m^3/mol. The first derivative of the Langmuir model to pressure is given as:

$$\frac{\partial q_a}{\partial \rho_g} = q_L \frac{b_L}{\left(b_L \rho_g + 1\right)^2} \tag{32}$$

The Freundlich isotherm, although not widely used in the gas shale literature, is very common in the general adsorption literature for Type I isotherm characterization (Do, 1998; Fan et al., 2003).

$$q_a = k_F \rho_g^{\frac{1}{n_F}} \tag{33}$$

Where k_F and n_F are fitting constants. The first derivative of the Freundlich isotherm is given as:

$$\frac{\partial q_a}{\partial \rho_g} = k_F \frac{\rho_g^{\frac{1}{n}-1}}{n} \tag{34}$$

However, the Freundlich isotherm does not have the proper thermodynamic behaviour at low and high pressures, with the adsorption uptake approaching infinity as pressure approaches 0, and with no monolayer sorption at high pressures (Do, 1998).

The DR equation is based on the potential theory of adsorption and is commonly applied to sub-critical adsorption in microporous substances (Bering et al., 1966; Clarkson et al., 1997). The DR equation does not have the correct thermodynamic behaviour at low and high pressures.

$$q_a = q_0 \exp\left[-\frac{R^2 T^2}{E}\left(ln\left(\frac{\rho_g}{\rho_{gs}}\right)\right)^2\right] \tag{35}$$

Where q_o is maximum sorption, E is characteristic energy of the adsorbent-adsorbate pair. Whilst using isotherms that are based on the potential theory of adsorption, the pseudo-vapour pressure of the adsorbent needs to be estimated. Several methods have been proposed for this purpose (Amankwah and Schwarz, 1995; Kapoor et al., 1989). Equations (36), (37), and (38) can be used to calculate the

pseudo vapour pressures based on the Dubinin, Amankwah, and Reduced-Kirchoff equations, respectively:

$$P_s = P_c \left(\frac{T}{T_c}\right)^2 \tag{36}$$

$$P_s = P_c \left(\frac{T}{T_c}\right)^k \tag{37}$$

$$P_s = P_c \exp\left(\frac{T_{nbp}}{T_c}\left(\frac{\ln P_c}{1 - T_{nbp}/T_c}\right)\left(1 - \frac{T_c}{T}\right)\right) \tag{38}$$

Where P_s is pseudo saturation pressure, P_c is critical pressure, T_c is critical temperature, T is temperature, T_{nbp} is the temperature at normal boiling point. The first derivative of the DR equation to loading is given as:

$$\frac{\partial q_a}{\partial \rho_g} = -\left(\frac{2q_a}{\rho_g}\right)\left(\frac{(RT)^2}{E}\right)\left(ln\left(\frac{\rho_{gs}}{\rho_g}\right)\right)\left(exp\left(-\left(\frac{(RT)^2}{E}\right)\left(ln\left(\frac{\rho_{gs}}{\rho_g}\right)\right)^2\right)\right) \tag{39}$$

The Sips isotherm has the correct thermodynamic behaviour at high pressures with a monolayer volume, but adsorption uptakes approach 0 at very low pressures. Another drawback of the Sips isotherm is that it has three parameters.

$$q_a = q_S \frac{\left(b_S \rho_g\right)^{\frac{1}{n_S}}}{1 + \left(b_S \rho_g\right)^{\frac{1}{n_S}}} \tag{40}$$

The first derivative of the Sips isotherm is given as:

$$\frac{\partial q_a}{\partial \rho_g} = q_s \frac{\left(b_S \rho_g\right)^{\frac{1}{n_S}}}{n_S \rho_g \left(1 + \left(b_S \rho_g\right)^{\frac{1}{n_S}}\right)^2} \tag{41}$$

The Toth isotherm has both Henry's law region at low surface coverages and a monolayer capacity at sufficiently high surface coverages (Do, 1998).

$$q_a = q_T \frac{b_T \rho_g}{\left(1 + \left(b_T \rho_g\right)^t\right)^{\frac{1}{t}}} \tag{42}$$

The first derivative of the Toth isotherm is given as:

$$\frac{\partial q_a}{\partial \rho_g} = q_T b_T \left(1 + \left(b_T \rho_g\right)^t\right)^{-\frac{1}{t}-1} \tag{43}$$

The Dubinin Ashtakov isotherm is a variant of the Dubinin Radushkevich isotherm with potential for heterogeneous surfaces through an additional parameter (Do, 1998). It is theoretically applicable for subcritical adsorption in micropores but can be empirically used for other applications.

$$q_a = q_0 \exp\left[-\frac{R^2T^2}{E}\left(ln\left(\frac{\rho_g}{\rho_{gs}}\right)\right)^n\right] \tag{44}$$

The first derivative of the DA isotherm is given as:

$$\frac{\partial q_a}{\partial \rho_g} = -\left(\frac{nq_a}{\rho_g}\right)\left(\frac{(RT)^2}{E}\right)\left(ln\left(\frac{\rho_{gs}}{\rho_g}\right)\right)^{n-1}\left(exp\left(-\left(\frac{(RT)^2}{E}\right)\left(ln\left(\frac{\rho_{gs}}{\rho_g}\right)\right)^n\right)\right) \tag{45}$$

6.6.3 Temperature Dependence and Isosteric Heat Determination

The isosteric heats of sorption were calculated using the Clausius-Clapeyron equation (Guo et al., 2013):

$$H_i = -RT^2\left(\frac{\partial lnP}{\partial T}\right)_{q_a} \tag{46}$$

Where H_i is isosteric heat of sorption. When only two isotherms are measured, it could be simplified as follows:

$$\ln\left(\frac{P_1}{P_2}\right) = -\frac{\mathrm{H_i}}{R}\left(\frac{1}{T_2} - \frac{1}{T_1}\right) \tag{47}$$

Temperature dependence of sorption was calculated based on an empirical form of the pressure-based Langmuir equation (Arunachalam and Fan, 2020). Temperature dependence relations are given as:

$$P_L = P_{L\infty} \exp\left(-\frac{H_L}{RT}\right) \tag{48}$$

$$V_L = \left(a_1 + \frac{a_2}{T}\right) \tag{49}$$

$$q_a = \frac{\left(a_1 + \frac{a_2}{T}\right)P}{P_{L\infty} \exp\left(-\frac{H_L}{RT}\right) + P} \tag{50}$$

Where a_1, a_2, P_{L_∞}, and H_L are fitting parameters. Differentiating Equation (50) to T:

$$\left(\frac{\partial q_a}{\partial T}\right)_P = P\frac{\frac{d\left[\frac{a_2}{T}+a_1\right]}{dT}.\left(P_{L_\infty}\exp\left(-\frac{H_L}{RT}\right)+P\right)-\left(\frac{a_2}{T}+a_2\right).\frac{d\left[P_{L_\infty}\exp\left(-\frac{H_L}{RT}\right)+P\right]}{dT}}{\left(P_{L\infty}\exp\left(-\frac{H_L}{RT}\right)+P\right)^2} \quad (51)$$

$$\left(\frac{\partial q_a}{\partial T}\right)_P = P\frac{-\frac{a_2}{T^2}.\left(P_{L_\infty}\exp\left(-\frac{H_L}{RT}\right)+P\right)-\left(\frac{a_2}{T}+a_2\right).\frac{H_L P_{L_\infty}\exp\left(-\frac{H_L}{RT}\right)}{RT^2}}{\left(P_{L\infty}\exp\left(-\frac{H_L}{RT}\right)+P\right)^2} \quad (52)$$

$$\left(\frac{\partial q}{\partial T}\right)_P = -\frac{a_2 P}{T^2\left(P_{L\infty}\exp\left(-\frac{H_L}{RT}\right)+P\right)}-\frac{P\,P_{L\infty}\exp\left(-\frac{H_L}{RT}\right)\left(\frac{a_2}{T}+a_2\right)H_L}{RT^2\left(P_{L\infty}\exp\left(-\frac{H_L}{RT}\right)+P\right)^2} \quad (53)$$

Simplifying, we get:

$$\left(\frac{\partial q}{\partial T}\right)_P = -\frac{a_2 P}{T^2(P_L+P)}-\frac{P\,P_L V_L H_L}{RT^2(P_L+P)^2} \quad (54)$$

6.6.4 Multi-Component Adsorption Prediction

Multi-component adsorption isotherms could be modelled either using the Extended Langmuir isotherm or using the Ideal Adsorbed Solution Theory (Do, 1998).

As the Langmuir theory assumes that the monolayer volume is constant for all species, it has been modified empirically to be able to fit adsorption isotherms on microporous substances (Yang et al., 2019). However, it also assumes that the selectivity of the two species remains constant for all concentrations, but this is not true for real systems where an increasing selectivity towards the more strongly adsorbed component is observed with decreasing concentration of that component (Myers and

Prausnitz, 1965). In the Extended Langmuir model, the pure component isotherm values are used to fit multi-component adsorption values (Ruthven, 1984).

$$q_{a,i} = q_{L,i} \frac{b_{L,i}\rho_{g,i}}{1 + \Sigma b_{L,i}\rho_{g,i}} \tag{55}$$

Where, $q_{L,i}$ is the pure component Langmuir monolayer sorption capacity of component i in mol/kg and b_L is the pure component Langmuir affinity constant of component I in m^3/mol. The first derivative of the Langmuir model to the pressure of a single component remains the same as for pure component isotherm:

$$\frac{\partial q_{a,i}}{\partial \rho_{g,i}} = q_{L,i} \frac{b_{L,i}}{\left(b_{L,i}\rho_{g,i} + 1\right)^2} \tag{56}$$

Using the Ideal Adsorbed Solution Theory, multi-component sorption behaviour can be simulated based on single-component isotherms using the Gibbs-Duhem equation (Simon et al., 2016):

$$\pi_i\left(p_i^0\right) = \frac{RT}{A} \int_0^{p_i^0} \frac{n_i^0(P)}{P} dP \tag{57}$$

The individual sorbed phase concentrations could be calculated based on the 2D analogue of the Raoult's law:

$$p_i = x_i p_i^0(\pi, T) \tag{58}$$

$$\pi = \pi_1(p_1^0) = \cdots = \pi\_N(p_N^0) \tag{59}$$

The total amount adsorbed is calculated using Equation (20). The PyIAST package is used for the calculation of multi-component isotherms (Simon et al., 2016)

$$\frac{1}{n_T} = \sum_{i=1}^{N} \frac{x_i}{n_i^0(p_i^0)} \tag{60}$$

However, there is currently no methodology to calculate adsorption uptakes using the IAST. This makes it unsuitable for many reservoir characterization applications.

6.7 Diffusion Characterization

The manometric rig as described in Figure 6-6 is used to characterize permeability in crushed shale samples. Once the samples are loaded on to the rig, the rig is flushed with Helium several times evacuated to near-vacuum pressure and outgassed at 80 °C to remove physisorbed species. The reference cell is then charged with Helium and allowed to reach thermal equilibrium. The valve connecting the reference and sample cells is opened, and the system pressure is monitored over time.

6.7.1 Rate-Based Characterization

First-order kinetics is given as (Fan et al., 2003):

$$-\frac{dq}{dt} = k_1 q \tag{61}$$

Integrating between initial conditions at $t = 0$, $q = q_i$ and operating conditions at $t = t$, $q = q_t$.

$$q_t = q_i \exp(-k_1 t) \tag{62}$$

Second-order kinetics is given as (Fan et al., 2003):

$$-\frac{dq}{dt} = k_1^2 q \tag{63}$$

Integrating between initial conditions at $t = 0$, $q = q_i$ and operating conditions at $t = t$, $q = q_t$.

$$q_t = \frac{1}{\frac{1}{q_i} + k_2 t} \tag{64}$$

6.7.2 Late Time Diffusion Characterization

It is assumed that diffusion in the void space of the reference and sample volume is instantaneous. Initial conditions are assumed to be a time where Helium concentration across the reference and sample cells is uniform after the valve connecting reference and sample cells is opened.

$$\rho = \rho_0 \; for \; 0 \leq r < a \; at \; t = 0 \tag{65}$$

$$\rho = \rho_{c_0} \; for \; r = R_0 \; at \; t = 0$$

The gas-phase concentration at the initial condition is therefore given as:

$$\rho_{c_0} = \frac{\rho_g V_R + \rho_g V_S}{V_R + V_S} \tag{66}$$

During the experiment, the adsorptive slowly diffuses into the shale pores where it is adsorbed. Boundary condition at R_0 is given as:

$$\frac{\partial \rho_g}{\partial r} = -\frac{V_c \mu c_g}{k A_s N} \frac{\partial \rho}{\partial t} \tag{67}$$

Due to symmetry, there is no diffusion at R_0:

$$\frac{\partial \rho_g}{\partial r} = 0 \tag{68}$$

This problem is well described in the literature. The analytical solution is given as (Carslaw and Jaeger, 1959):

$$\rho_g = \rho_{c_0} - \frac{\rho_{c_0}}{1} + 6K_C(\rho_{c_0} - \rho_0) \sum_{n=1}^{\infty} \exp\left(-\frac{K\alpha_n^2 t}{R_a^2}\right) \frac{1}{K_C^2 \alpha_n^2 + 9(K_C + 1)} \tag{69}$$

Where K_c is the ratio of gas storage capacities of the rig's void volume and the sample's pore volume:

$$K_C = \frac{V_C}{M V_{sb}(\phi + (1-\phi)K_a)} \tag{70}$$

6.8 Construction and Automation of Manometric Rig

A generic manometric adsorption measurement rig was constructed as shown in Figure 6-6. A pressure transducer with an accuracy of ± 0.001 barg up to 60 bar and a temperature bath with an accuracy of ± 0.01 °C is included with the rig. Let-lok fittings of 1/8 inch were used to connect different cells. The pressure transducer was connected using 1/4 inch ISO fittings along with a Dowty seal. The adsorbent cell was designed specifically with a fine mesh to prevent shale samples from leaking into the rig. They were designed and fabricated to withstand pressures of up to 300 bars, and provided with a single Viton o ring seal with a groove size of 2 mm, accommodating ISO 27 O-rings. A spring-loaded pressure safety valve was also included and calibrated to release gas at 70 bars. This was connected to the rig using 1/4 let-lok fittings and to the vent using silicone fittings. The outlet was connected to the vent to Nedderman

Local Extraction Vents. A provision to collect samples is also provided. It is also possible to connect this outlet to vacuum pumps to remove gas before the start of the experiment. A vacuum pump able to create a vacuum of up to 140 Torrs was available on stand by and connected to the rig as required.

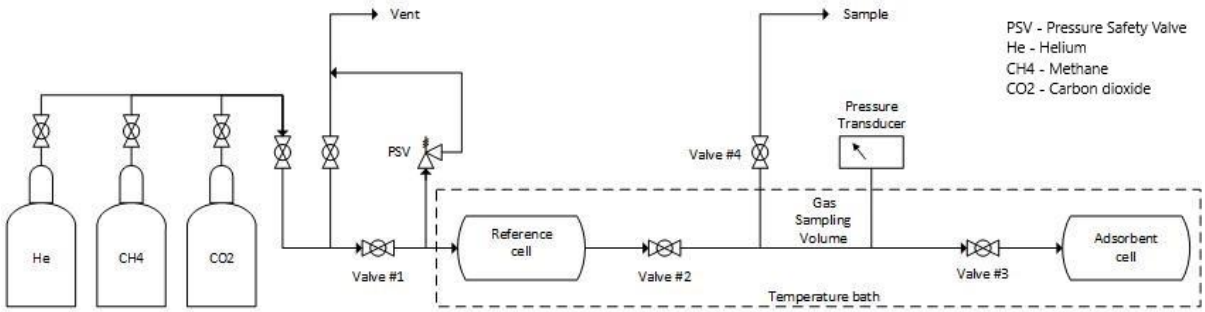

Figure 6-6 Manometric Adsorption Measurement Rig

6.8.1 Rig Calibration

To calibrate rig volumes, a volume expansion experiment with a standard known volume was used. The first run is done without any standard volume. The reference cell is charged to the charge pressure and allowed to reach equilibrium. In the second run, a standard volume is inserted into the sample cell and the process is repeated. With this method, the least count of the volume depends on the accuracy of the standard volume and the accuracy of the pressure transducer. Therefore it is possible to achieve a higher resolution compared to using water volume or using manufacturer volumes, which excludes the volume of pipes and other peripherals.

$$\left(\frac{P_c}{z_c}-\frac{P_e}{z_e}\right)V_R+\left(\frac{P_i}{z_i}-\frac{P_e}{z_e}\right)V_S+\left(\frac{P_e}{z_e}-\frac{P_i}{z_i}\right)V_{std}=0 \tag{71}$$

With 2 runs, it should be possible to determine the reference and sample cell volumes as shown in Figure 6-7. The process was automated in LabVIEW as shown in Figure 6-12.

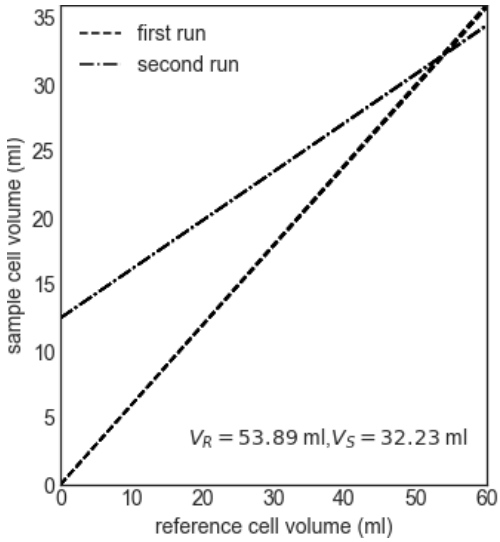

Figure 6-7 Rig volume calibration

Although leaks were minimized during adsorption characterization, in some cases they were unavoidable. The programme accounts for leaks by modelling it as a flow-through an orifice using the Poiseulle's equation (Bomelburg, 1977).

$$Q = \frac{\pi R^4 |P_1^2 - P_2^2|}{16 \eta l P_2} \tag{72}$$

Where Q is the volumetric flow of the outlet side pressure (atmospheric pressure), P_1 is the rig pressure, P_2 is atmospheric pressure, R is the radius of opening, l is the length of the opening, η is the viscosity of the fluid. Hence it's sufficient to measure leak resistance at one sufficiently high pressure, to be able to account for leaks for the whole experiment. It is noted that although this functionality was added to the LabVIEW programme, experiments were repeated when a leak was found and was therefore not used in the final results. Nevertheless, it was included as a useful option for salvaging data when necessary.

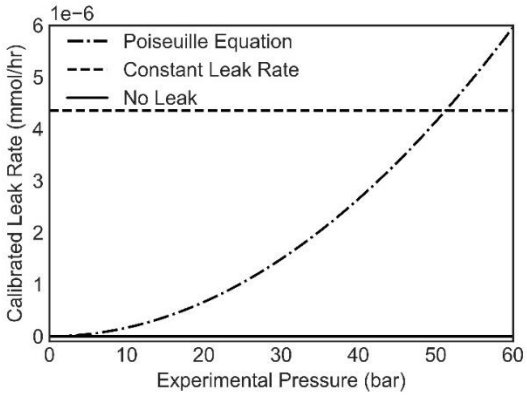

Figure 6-8 Rig leak calibration

6.8.2 Rig Automation

Rig automation was performed in LabVIEW as shown in Figure 6-9, Figure 6-10, Figure 6-11, and Figure 6-12. For permeability analysis, the values were post-processed in Python as the data analysis was too complex to automate graphically. An analytical solution to the diffusion equation used for this purpose. The first 20 terms in Equation (69) are used. The LabVIEW programme is capable of dynamically adjusting to various adsorptive and adsorbents through appropriate equations of states and calibration files.

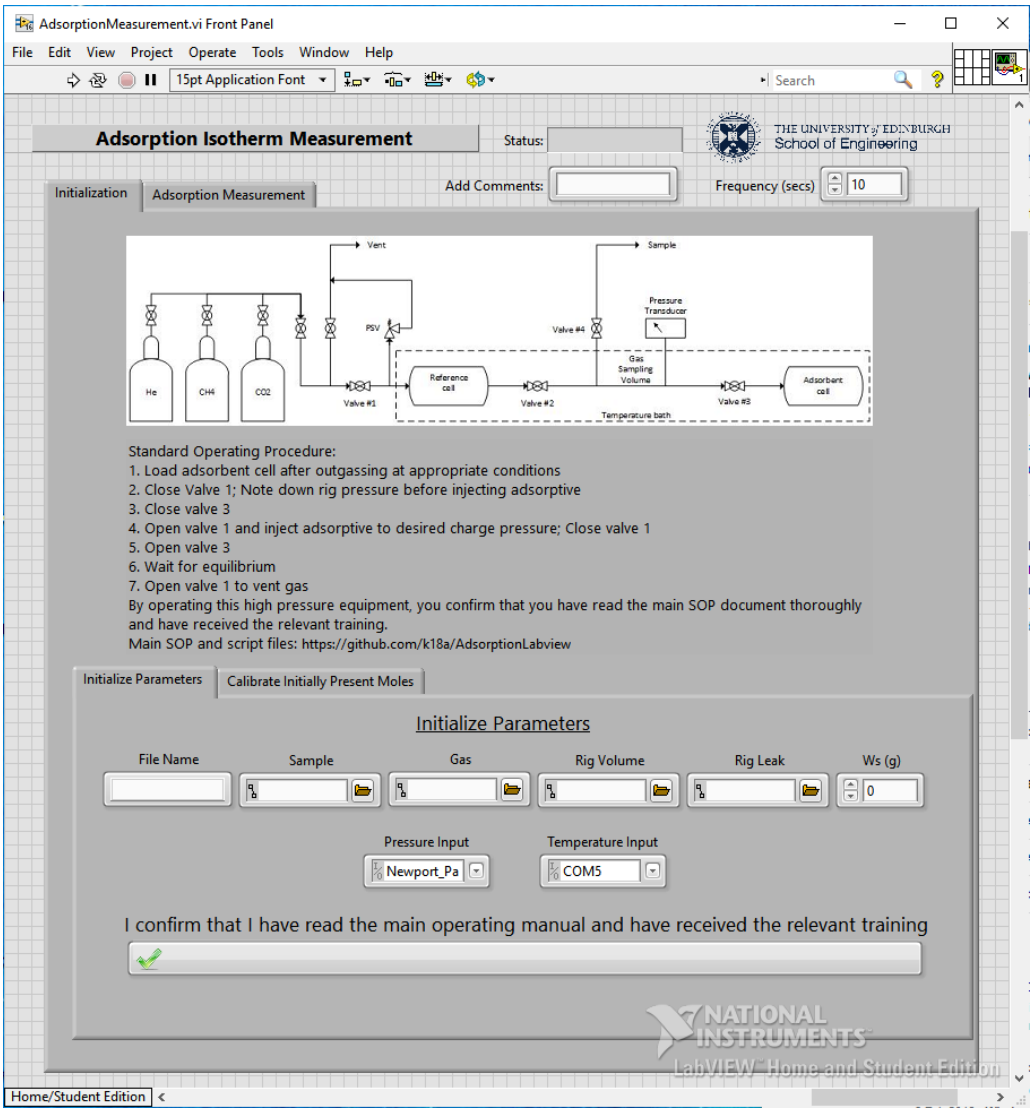

Figure 6-9 LabVIEW adsorption programme a

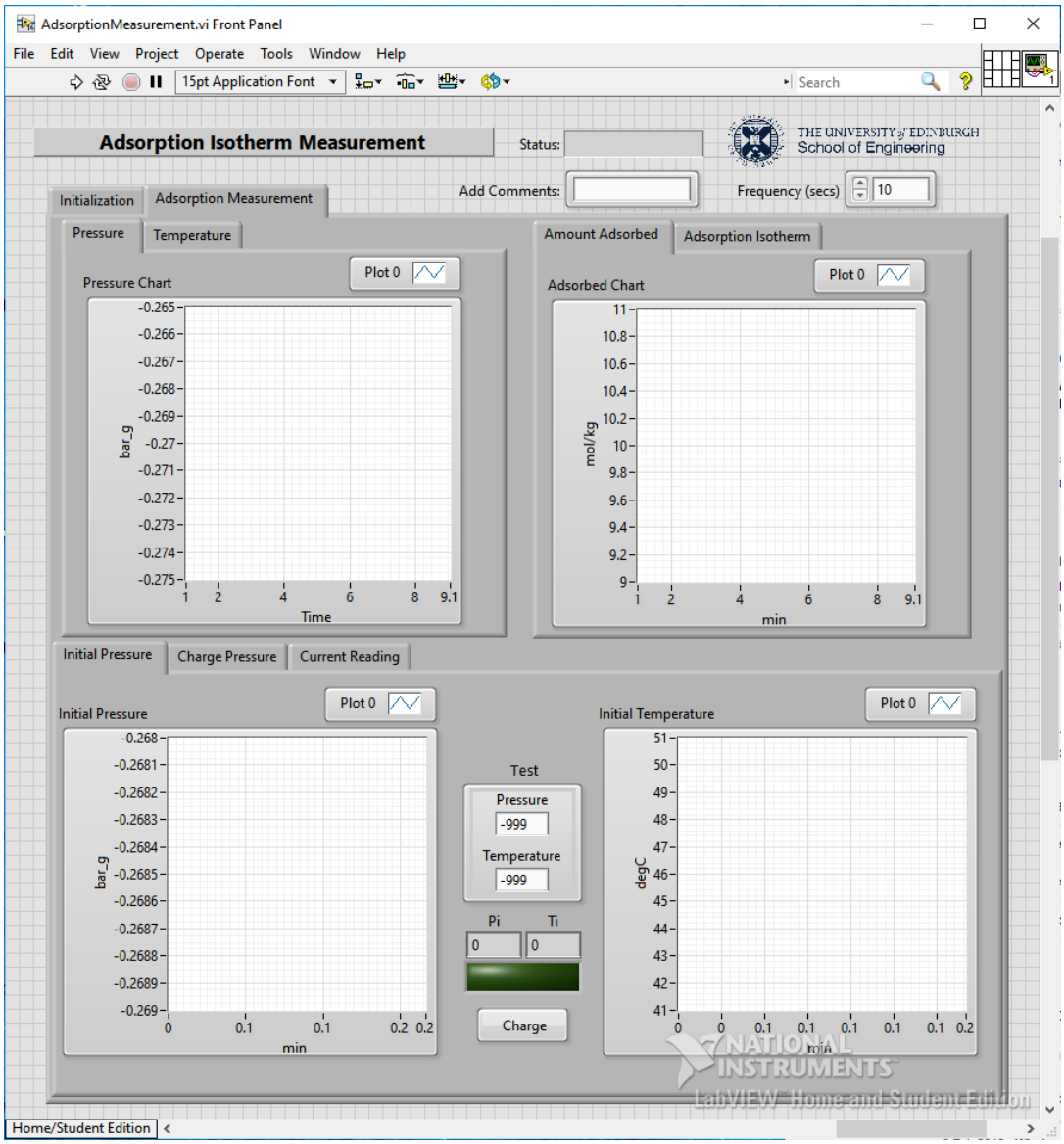

Figure 6-10 LabVIEW adsorption programme b

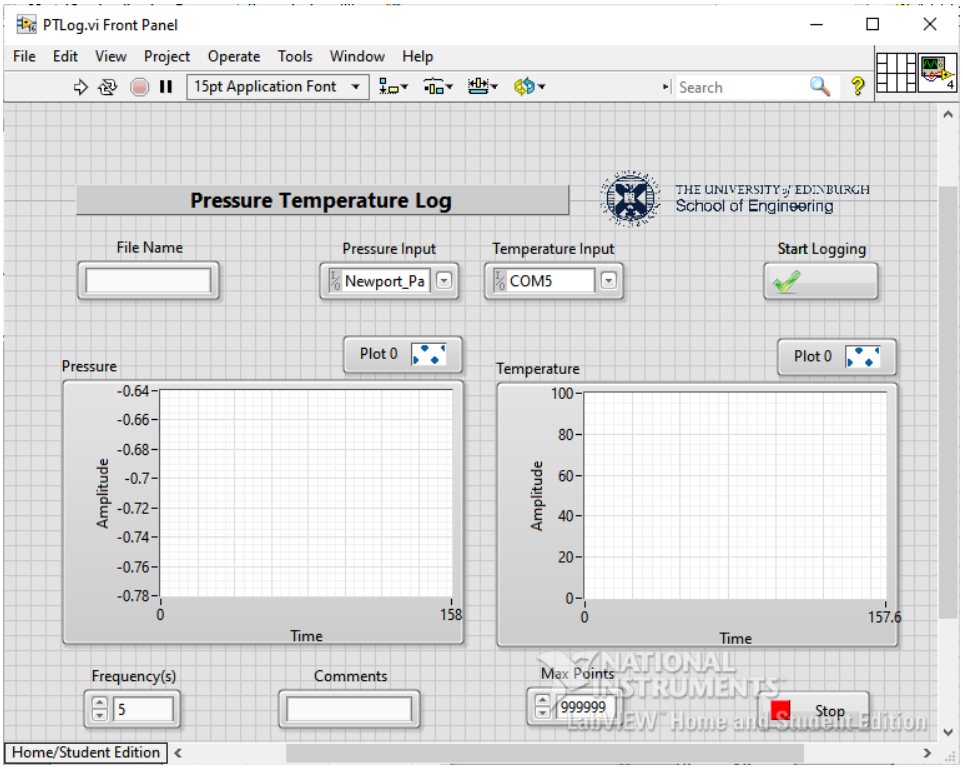

Figure 6-11 LabVIEW permeability programme

Before calibration, the programme collects the appropriate calibration files and files for the equation of state as shown in Figure 6-9. Adsorption measurement is carried out sequentially. Before each pressure step, the programme monitors the pressure profile until equilibrium is reached and gas is injected into the reference cell. The programme then automatically calculates and records the amount of adsorptive in the rig and subsequently, the excess adsorbed at any given instance as shown in Figure 6-10. It is capable of converting experimentally measured excess adsorption to absolute adsorption by assuming a constant adsorbed phase density or a constant adsorbed phase volume.

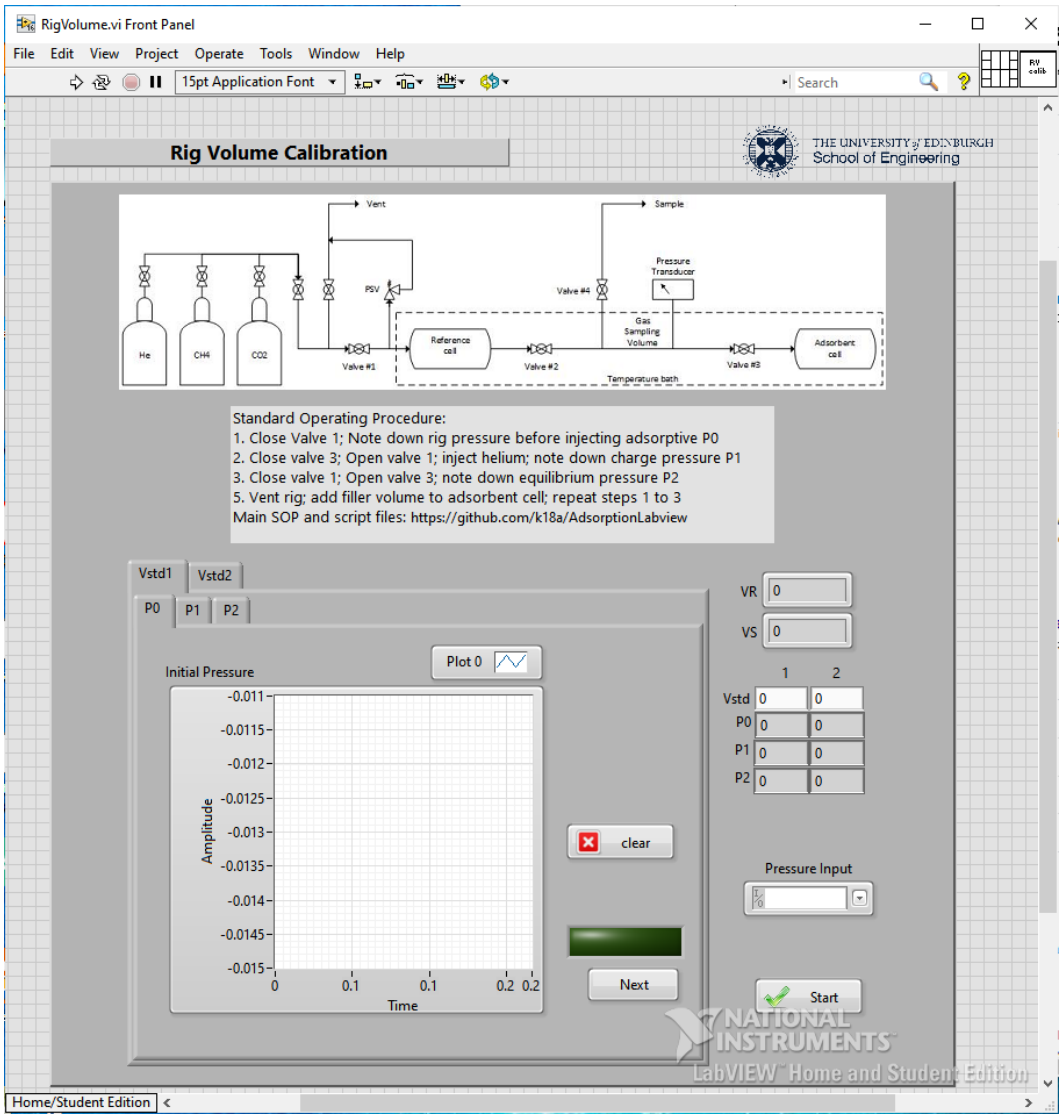

Figure 6-12 LabVIEW volume calibration programme

6.9 Reservoir Model

The reservoir model shown in Figure 6-13 is considered. The well is represented using a blue line and fractures orthogonal to the well are represented using red lines. It is then recognised that the model is symmetric along the wellbore and also along the fractures. It is therefore possible to derive insights on the whole reservoir by studying the gas behaviour in the Simulated Reservoir Volume. Alternatively, a dual-porosity model could also be considered (Warren and Root, 1963), this considers the whole reservoir volume by assuming separate governing equations for matrix and fracture flows. However,

due to advancements in numerical techniques and meshing software, the former approach is more widely practiced (Yu et al., 2014). The fracture was assumed to be at the same temperature as well with a Dirichlet boundary condition (Wang et al., 2014). Symmetry boundary conditions are imposed in other places (Yu and Sepehrnoori, 2014b).

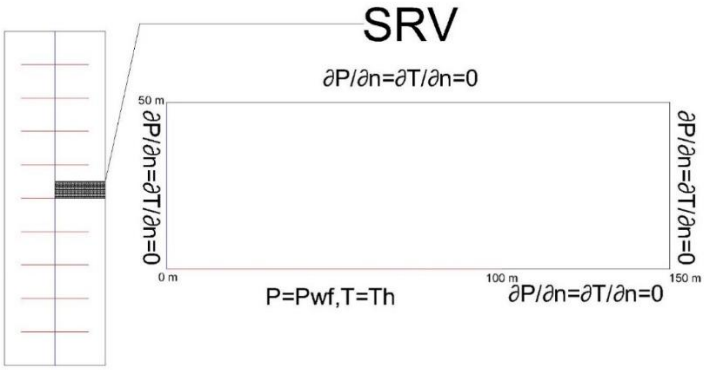

Figure 6-13 Shale reservoir model

6.9.1 Resource Estimation

Total gas in the reservoir includes both the free gas and the sorbed gas content. This is calculated as:

$$Total\ Resource\ in\ Place = \phi \frac{P_r V_r}{zRT_r} + (1-\phi) V_r \rho_s n_{ads} \tag{73}$$

6.9.2 Governing Equations for Reserve Estimation

Mass balance for gas flow in shales is given as:

$$\begin{gathered} mass\ accumulation\ from\ free\ gas \\ +mass\ accumulation\ from\ adsorbed\ gas \\ +gas\ flow \\ = source/sink \end{gathered} \tag{74}$$

$$\phi \frac{\partial \boldsymbol{\rho_g}}{\partial t} + (1-\phi)\frac{\partial \boldsymbol{\rho_a}}{\partial t} + \nabla(\boldsymbol{\rho_g}\phi\vec{\boldsymbol{v}}) = \dot{Q_{if}} \tag{75}$$

Where $\boldsymbol{\rho_g}$ gas density matrix, $\boldsymbol{\rho_a}$ is adsorbed phase density matrix, $\boldsymbol{\phi}$ is porosity, t is time, $\vec{\boldsymbol{v}}$ is velocity vector, Q_{if} is source/sink.

Where isothermal compressibility and coefficient of thermal expansion are given as

$$c_g = \frac{1}{\rho_g}\left(\frac{\partial \rho_g}{\partial P}\right)_T \tag{76}$$

$$\alpha_g = \frac{1}{\rho_g}\left(\frac{\partial \rho_g}{\partial T}\right)_P \tag{77}$$

$$\gamma_g = \frac{c_g}{\alpha_g} \tag{78}$$

Gas non ideality is given in the literature (Mahmoud, 2013):

$$z = (0.702exp(-2.5T_{pr}))(P_{pr}^2) - (5.24exp(-2.5T_{pr}))(P_{pr}) + (0.044T_{pr}^2 - 0.164T_{pr} + 1.15) \tag{79}$$

Darcy law is given as:

$$\vec{\boldsymbol{v}} = \frac{k}{\mu\phi}\nabla \boldsymbol{P} \tag{80}$$

The above equations can be simplified to give mass flow equation in gas shale reservoir

$$\begin{aligned}&\left[\phi \boldsymbol{c_g}\boldsymbol{\rho_g} + (1-\phi)\rho_s\left[\left(\frac{\partial \boldsymbol{q_a}}{\partial \boldsymbol{P}}\right)_T + \gamma_g\left(\frac{\partial \boldsymbol{q_a}}{\partial \boldsymbol{T}}\right)_P\right]\right]\frac{\partial \boldsymbol{P}}{\partial t}\\ &+\left[\phi \boldsymbol{\alpha_g}\boldsymbol{\rho_g} - (1-\phi)\rho_s\left[\left(\frac{\partial \boldsymbol{q_a}}{\partial \boldsymbol{T}}\right) + \frac{1}{\gamma_g}\left(\frac{\partial \boldsymbol{q_a}}{\partial \boldsymbol{P}}\right)_T\right]\right]\frac{\partial \boldsymbol{T}}{\partial t}\\ &+\nabla\left(\frac{\boldsymbol{\rho_g} k}{\boldsymbol{\mu}}.\nabla \boldsymbol{P}\right) = -Q_{if}\end{aligned} \tag{81}$$

At constant temperature, this simplifies to:

$$\left[\phi \boldsymbol{c_g}\boldsymbol{\rho_g} + (1-\phi)\rho_s c_g\left(\frac{\partial \boldsymbol{q_a}}{\partial \boldsymbol{P}}\right)_T\right]\frac{\partial \boldsymbol{P}}{\partial t} + \nabla\left(\frac{\boldsymbol{\rho_g} k}{\boldsymbol{\mu}}.\nabla \boldsymbol{P}\right) = -Q_{if} \tag{82}$$

General energy balance for porous media is given as:

$$
\begin{aligned}
&energy\ accumulation\ from\ bulk\ shale \\
&+ energy\ accumulation\ from\ free\ gas \\
&+ energy\ accumulation\ from\ adsorbed\ gas \\
&+ energy\ flow\ from\ conduction \\
&+ energy\ flow\ from\ convection \\
&= source/sink
\end{aligned}
\tag{83}
$$

In terms of pressure and temperature:

$$
\begin{aligned}
&-\left[(1-\phi)\rho_s H_i\left(\frac{\partial \boldsymbol{q_a}}{\partial \boldsymbol{P}}\right)_T\right]\left(\frac{\partial \boldsymbol{P}}{\partial t}\right) \\
&+\left[\phi\rho_g MW\ Cp_g + (1-\phi)\rho_s\left(Cp_s - H_i\left(\frac{\partial \boldsymbol{q_a}}{\partial \boldsymbol{T}}\right)_P\right)\right]\frac{\partial \boldsymbol{T}}{\partial t} \\
&-\nabla\cdot\left(\phi\lambda_g + (1-\phi)\lambda_s\right)\nabla \boldsymbol{T} \\
&+\rho_g MWCp_g\left(\frac{k_m \nabla \boldsymbol{P}}{\mu}\right)\cdot\nabla \boldsymbol{T} \\
&= Q_h
\end{aligned}
\tag{84}
$$

The governing equations were solved using a Finite Element Scheme in MATLAB and COMSOL. MATLAB was preferred over COMSOL for easier access due to limitations of COMSOL licenses. However, it was not possible to achieve convergence for convection and multi-component diffusion in MATLAB. Therefore COMSOL was used for these applications. The mesh size was reduced until a stable solution after 30 days of production was achieved. A timestep of 1 day was used, Higher timesteps were also used without any change in production after 30 days. An implicit method was used for the time differential whilst the space differential was handled using the Finite Element Technique. Specific solvers used in the software are discussed in appropriate sections.

6.10 References

Amankwah, K.A.G., Schwarz, J.A., 1995. A modified approach for estimating pseudo-vapor pressures in the application of the Dubinin-Astakhov equation. Carbon N. Y. 33, 1313–1319.

Andrews, I.J., 2013. The Carboniferous Bowland Shale gas study: geology and resource estimation. Br. Geol. Surv. Dep. Energy Clim. Chang. London, UK.

Arunachalam, K., Fan, X., 2020. Impact of heat of sorption on thermal enhanced recovery of sorbed gas from gas shale reservoirs – An experimental and simulation study. J. Nat. Gas Sci. Eng. 79.

Barrett, E.P., Joyner, L.G., Halenda, P.P., 1951. The determination of pore volume and area distributions in porous substances. I. Computations from nitrogen isotherms. J. Am. Chem. Soc. 73, 373–380.

Bell, I.H., Wronski, J., Quoilin, S., Lemort, V., 2014. Pure and Pseudo-pure Fluid Thermophysical Property Evaluation and the Open-Source Thermophysical Property Library CoolProp. Ind. Eng. Chem. Res. 53, 2498–2508.

Bering, B.P., Dubinin, M.M., Serpinsky, V. V, 1966. Theory of volume filling for vapor adsorption. J. Colloid Interface Sci. 21, 378–393.

Bomelburg, H.J., 1977. Estimation of Gas Leak Rates Through Very Small Orifices and Channels.

Brandani, S., Mangano, E., Luberti, M., 2017. Net, excess and absolute adsorption in mixed gas adsorption. Adsorption 23, 569–576.

Brunauer, S., Emmett, P.H., Teller, E., 1938. Adsorption of gases in multimolecular layers. J. Am. Chem. Soc. 60, 309–319.

Cameron, I.B., McAdam, A.D., 1978. Oil-shales of the Lothians, Scotland: present resources and former workings. Inst. Gas Technol., Chicago, Res. Bull.; (United States) 78/28.

Carslaw, H.S., Jaeger, J.C., 1959. Conduction of heat in solids. Oxford Clarendon Press. 1959, 2nd ed.

Clarke, H., Turner, P., Bustin, R.M., Riley, N., Besly, B., 2018. Shale gas resources of the Bowland Basin, NW England: a holistic study. Pet. Geosci. 24, 287–322.

Clarkson, C.R., Bustin, R.M., Levy, J.H., 1997. Application of the mono/multilayer and adsorption potential theories to coal methane adsorption isotherms at elevated temperature and pressure. Carbon N. Y. 35, 1689–1705.

Do, D.D., 1998. Adsorption Analysis: Equilibria And Kinetics: (With CD Containing Computer Matlab Programs).

Fan, X., Parker, D.J., Smith, M.D., 2003. Adsorption kinetics of fluoride on low cost materials. Water Res. 37, 4929–4937.

Follows, B., Tyson, R. V., 1998. Organic facies of the Asbian (early Carboniferous) Queensferry Beds, Lower Oil Shale Group, South Queensferry, Scotland, and a brief comparison with other Carboniferous North Atlantic oil shale deposits. Org. Geochem. 29, 821–844.

Ford, B.J., 2020. Scanning electron microscope [WWW Document].

Gross, D., Sachsenhofer, R.F., Bechtel, A., Pytlak, L., Rupprecht, B., Wegerer, E., 2015. Organic geochemistry of Mississippian shales (Bowland Shale Formation) in central Britain: Implications for depositional environment, source rock and gas shale potential. Mar. Pet. Geol. 59, 1–21.

Guo, W., Xiong, W., Gao, S., Hu, Z., Liu, H., Yu, R., 2013. Impact of temperature on the isothermal adsorption/desorption of shale gas. Pet. Explor. Dev. 40, 514–519.

Heller, R., Vermylen, J., Zoback, M., 2014. Experimental investigation of matrix permeability of gas shales. Am. Assoc. Pet. Geol. Bull. 98, 975–995.

Jones, N.S., 2005. The West Lothian oil-shale formation : results of a sedimentological study.

Kapoor, A., Ritter, J.A., Yang, R.T., 1989. On the Dubinin-Radushkevich equation for adsorption in microporous solids in the Henry's law region. Langmuir 5, 1118–1121.

Landers, J., Gor, G.Y., Neimark, A. V, Yu Gor, G., Neimark, A. V, 2013. Density functional theory methods for characterization of porous materials. Aspects 437, 3–32.

Li, P., Jiang, Z., Zheng, M., Bi, H., Chen, L., 2016. Estimation of shale gas adsorption capacity of the Longmaxi Formation in the Upper Yangtze Platform, China. J. Nat. Gas Sci. Eng. 34, 1034–1043.

Luffel, D.L., Guidry, F.K., 1992. New core analysis methods for measuring reservoir rock properties of Devonian shale. J. Pet. Technol. 44, 1–184.

Mahmoud, M.A., 2013. Development of a New Correlation of Gas Compressibility Factor (Z-Factor) for High Pressure Gas Reservoir. North Africa Tech. Conf. Exhib.

Merey, S., Sinayuc, C., 2016. Analysis of carbon dioxide sequestration in shale gas reservoirs by using experimental adsorption data and adsorption models. J. Nat. Gas Sci. Eng. 36, 1087–1105.

Moseley, H.G.J., 1913. XCIII. The high-frequency spectra of the elements . London, Edinburgh, Dublin Philos. Mag. J. Sci.

Myers, A.L., Prausnitz, J.M., 1965. Thermodynamics of mixed-gas adsorption. AIChE J. 11, 121–127.

Pini, R., 2014. Interpretation of net and excess adsorption isotherms in microporous adsorbents. Microporous Mesoporous Mater. 187, 40–52.

Rani, S., Prusty, B.K., Pal, S.K., 2015. Methane adsorption and pore characterization of Indian shale samples. J. Unconv. Oil Gas Resour. 11, 1–10.

Rezaee, R., 2015. Fundamentals of gas shale reservoirs. John Wiley & Sons.

RP40, A., 1998. Recommended practices for core analysis. Feb.

Ruthven, D.M., 1984. Principles of adsorption and adsorption processes. Chem. Eng. Process. Process Intensif.

ScottishShale, 2020. Straiton Oil Works [WWW Document].

Simon, C.M., Smit, B., Haranczyk, M., 2016. pyIAST: Ideal adsorbed solution theory (IAST) Python package. Comput. Phys. Commun. 200, 364–380.

Wang, H.Y., Ajao, O., Economides, M.J., 2014. Conceptual study of thermal stimulation in shale gas formations. J. Nat. Gas Sci. Eng.

Wang, K., Fu, J., Zheng, Y., 2019. Insights into photocatalytic CO2 reduction on C3N4: Strategy of simultaneous B, K co-doping and enhancement by N vacancies. Appl. Catal. B Environ. 254, 270–282.

Wang, Y., Zhu, Y., Liu, S., Zhang, R., 2016. Pore characterization and its impact on methane adsorption capacity for organic-rich marine shales. Fuel 181, 227–237.

Warren, J.E., Root, P.J., 1963. The Behavior of Naturally Fractured Reservoirs. Soc. Pet. Eng. J. 3, 245–255.

Weidenthaler, C., 2011. Pitfalls in the characterization of nanoporous and nanosized materials. Nanoscale.

Yang, S., Wu, K., Xu, J., Li, J., Chen, Z., 2019. Roles of multicomponent adsorption and geomechanics in the development of an Eagle Ford shale condensate reservoir. Fuel 242, 710–718.

Yu, W., Huang, S., Wu, K., Sepehrnoori, K., Zhou, W., 2014. Development of a Semi-Analytical Model for Simulation of Gas Production in Shale Gas Reservoirs. Unconv. Resour. Technol. Conf.

Yu, W., Sepehrnoori, K., 2014a. Simulation of gas desorption and geomechanics effects for unconventional gas reservoirs. Fuel 116, 455–464.

Yu, W., Sepehrnoori, K., 2014b. An efficient reservoir-simulation approach to design and optimize unconventional gas production. J. Can. Pet. Technol. 53, 109–121.

Zhang, T., Ellis, G.S., Ruppel, S.C., Milliken, K., Yang, R., 2012. Effect of organic-matter type and thermal maturity on methane adsorption in shale-gas systems. Org. Geochem. 47, 120–131.

7 Impact of Adsorption on Shale Reservoir Characterization

7.1 Introduction

Sorbed gas contributes to about 20 to 80% of the total methane storage capacity of gas shales (Schettler Jr and Parmely, 1991). It can subsequently be expected to have a significant effect on several aspects of gas shale reservoir characterization. However, these effects have not been fully explored in the literature.

Since adsorption occurs primarily due to interatomic forces that are present in shale micropores (Zhang et al., 2016), physisorption in shales is largely a function of its pore size (Do, 1998). Smaller pores entail larger surface area which consequently results in higher adsorption. However, the shale's pore size is a function of several other factors such as geochemistry and geomechanics (Ji et al., 2017; Kuila and Prasad, 2013).

The manometric methodology is widely used to characterize sorption in gas shales (Rouquerol et al., 1994). The procedure for adsorption characterization in a manometric rig is complicated for microporous gas shales by two issues: 1) incorrect characterization of the shale's grain density – net sorption, 2) incorrect characterization of the initially distributed gas in the sorption space – excess sorption (Brandani et al., 2016). Absolute sorption values are obtained after correcting for both. Further, there are two commonly used methods to correct for excess sorption – assuming surface coverage and assuming micro-pore filling (Pini, 2014; Wang et al., 2016a). The relative importance of all these assumptions is unclear. Other parameters are often assumed whilst designing an adsorption experiment such as the particle size and equilibrium conditions. These conditions have never been analysed thoroughly, and are usually not even reported (Psarras et al., 2017; Rani et al., 2015; Talu, 1998; Wang et al., 2016b).

In order to address these issues, this study measures the grain volume using Helium expansion at 80 °C 150 Torr pressure. This minimizes any errors due to adsorption on the sample. To correct excess

adsorption measurements, both techniques are explored, and the appropriate technique is chosen based on the shale's pore size distribution based on N_2 adsorption.

Given that sorption significantly influences reservoir characterization, it is effects on permeability characterization, resource estimation, and reserve estimation is also explored. Highly complicated techniques used in individual laboratories have made inter-laboratory comparison very difficult (Civan et al., 2013). This is especially true for permeability characterization, where highly non-linear equations need to be solved, which vary widely based on pore and sorption characteristics (Profice et al., 2012). The impact of sorption on resource characterization is much clearer given that it is straight forward to estimate based on a volumetric method (Ambrose et al., 2010). That said, it is important to recognize that although sorbed gas contributes to a significant portion of the shale's total resource in place, not all of it is produced. Typically 90% of the sorbed gas is left behind in the reservoir (Yu and Sepehrnoori, 2014). The metric actual amount that could be produced known as reserve becomes a lot more important. For reserve estimation, the adsorption uptake – differential of sorption to loading – is more important than the absolute sorption itself. This value is dependent on the choice of isotherm used to model adsorption (Do, 1998). However, this has never been addressed in the literature. Adsorption isotherms in gas shales are of Type I (Rouquerol et al., 2013). This implies that they have a linear Henry's law region at low pressures and relatively constant adsorption at higher pressures. The importance of these regions on adsorption uptake and subsequently, gas shale reservoir characterization is unclear. The abovementioned uncertainties have caused significant roadblocks in gas shale reservoir characterization and need to be addressed before proceeding further.

This study covers the entire pipeline of sorption in gas shale reservoir characterization. It starts with a thorough analysis of the shale's pore size distribution which is the primary control on its sorption. After this, the manometric methodology used to characterize sorption in shales is investigated critically with a focus on reservoir characterization. Since the oil shale considered for this study did not exhibit much visual field scale heterogeneities (ScottishShale, 2020), only one sample was considered. In order to address pore scale heterogeneities, a much larger sample size of 30 g was considered (Pini, 2014). Resulting sorption isotherms are fit with adsorption isotherm models – Linear, Langmuir, Freundlich,

Dubinin-Radushkevich, Sips, and Toth (Ruthven, 1984). The impact of each of these isotherms on reservoir characterization is explored. Adsorption uptake is demonstrated to be an extremely important property – more than adsorption for shale reservoir characterization. The study then investigates the effects of sorption on permeability characterization through experimental characterization and modelling. Simplifying techniques are proposed to facilitate permeability characterization in shales. These results facilitate inter-laboratory comparison of highly complicated models used to characterize sorption and permeability in shales. Finally, the impact of sorption on resource and reserve estimation is explored. The volumetric method is used for resource characterization, whilst a Finite Element Model of the reservoir is used to characterize reserves. Adsorption is demonstrated to be highly significant in all areas of shale reservoir characterization setting the stage for the rest of the thesis.

7.2 Pore Characterization

To characterize the shale's pore characteristics, three methods were used. The bulk volume of the crushed shale outcrop was measured using water immersion of samples previously saturated with water as 0.37 cc/g. The grain volume was measured using He expansion as 0.35 cc/g. The porosity was calculated as 0.05. The pore size distribution was characterized using low-pressure N_2 sorption using the DFT method. An outline is provided below; detailed methods are given in Chapter 3.

To characterize the grain density, helium gas was used as a probe. This is because helium gas adsorption in shales is negligible compared to methane and carbon dioxide adsorption (RP40, 1998). The characterization itself was done at about 180 Torrs. This further minimizes any adsorption effect that could potentially make measurements unreliable. The bulk density was characterized using water immersion over a high accuracy mass balance. This allowed a higher accuracy compared to methods that use volumetric methods (Kuila and Prasad, 2013). Before bulk volume characterization, shales were immersed in water for 24 hours. This is because dry samples would adsorb water upon immersion.

Making sure that the shale sample was previously saturated with water makes sure that the measurements are accurate (Kuila and Prasad, 2013).

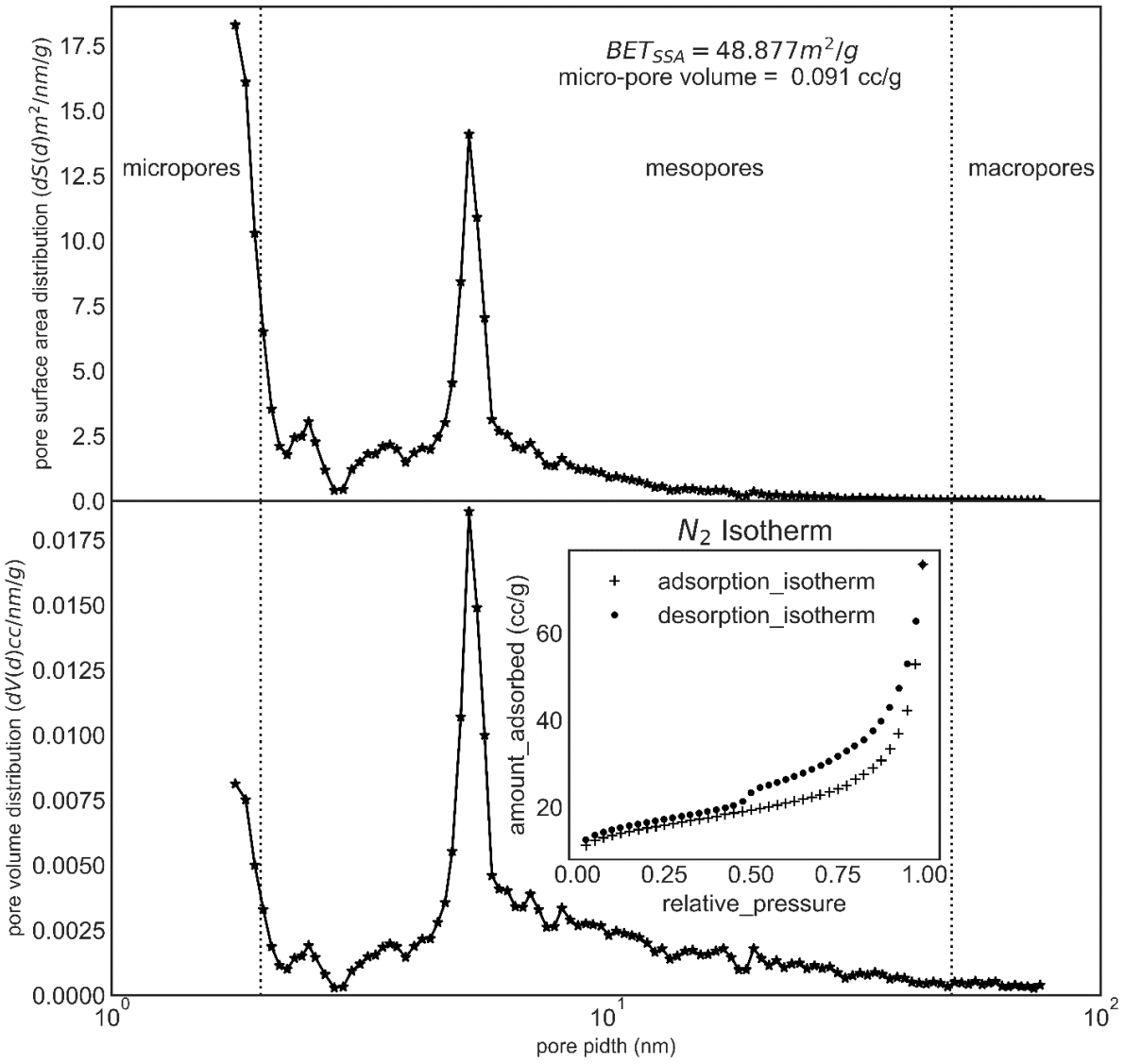

Figure 7-1 N_2 Sorption and Pore Size Distribution of Lothian Gas Shales

To measure the pore size distribution, N_2 sorption was used. Since the shales were expected to consist of a significant amount of micro-pores, it was necessary to use gas sorption for characterizing pore size distribution (Kuila and Prasad, 2013; Weidenthaler, 2011). Before N_2 sorption the samples were outgassed in an autoclave and then in the rig to remove entrenched moisture. An outgassing parameter

of 80 °C and 80 Torr pressure were used for 8 hours. The Quantachrome Autosorb iQ apparatus was used to characterize N_2 sorption at 77 K. The resulting isotherm was analysed in the rig using the and DFT method. The BET and BJH methods based on the Kelvin equation does not provide sufficient information on the micropore region (Llewellyn et al., 2007). Therefore the DFT method that models condensation in micropores is used. This fits standard isotherms that could be expected for a given pore size distribution to the experimentally obtained isotherm. Performing analysis in the rig, ensured high accuracy of the resulting analysis. Further details on pore size analysis using N_2 isotherms will be presented in Chapter 5.

As shown in Figure 7-1, there is minimal N_2 sorption at low relative pressures at 77 K. This implies that the Lothian shales are predominantly non-porous / macro-porous compared to activated carbons (Sing, 1985). These results are in agreement with data in the literature presented for other shales (Kuila and Prasad, 2013; Rani et al., 2015). The micropore volume calculated using the DFT method was 0.091 cc/g. Even though the BET method is not strictly applicable to microporous substances, it is still widely used to serve as a benchmark to compare adsorbents of different types (Weidenthaler, 2011). The BET specific surface area was calculated from the monolayer point as 48.877 m^2/g (Do, 1998). For comparison, the specific surface area of a typical activated carbon is around 1200 m^2/g. This suggests that shales would exhibit a much smaller adsorption capacity compared to activated carbons. Since the force fields surrounding various pores sizes are different, condensation occurs slightly differently in different pore sizes. Hysteresis in the relative pressure region between 0.35 and 1 suggests the presence of mesopores where condensation follows the Kelvin equation (Do, 1998). It is also possible to predict the shape of the pores using the hysteresis curve. Given that the hysteresis arms are horizontal rather than vertical, the presence of slit-shaped pores is more likely compared to cylindrical pores (Sing, 1985). This is expected as shales are sedimentary rocks formed by the subsequent layering of organic and mineral matter. Over time, these are compacted to form very thin layers (Garrels and Mackenzie, 1969). From the DFT pore size distribution, a bimodal trend could be observed, with peaks at 1.8 nm, and 8 nm.

7.3 High-Pressure Methane and Carbon Dioxide Adsorption Measurement

High-pressure methane and carbon dioxide adsorption isotherms were measured in a manometric adsorption rig using a stepwise procedure. Whilst there are other methods to measure sorption such as the gravimetric method (Rouquerol et al., 2013), the manometric method is the most widely used technique in the reservoir engineering community (RP40, 1998). The main advantage of using manometric methods for shale gas adsorption measurement is the relative simplicity of setting up the experiment using readily available fittings. It also allows using higher sample volumes compared to gravimetric methods, which needs to balance sample weights with the least count of the balance. This addresses pore scale heterogeneities (Pini, 2014). Using a stepwise procedure allows the adsorption characterization in a reasonable timeframe and also conserves expensive adsorptive gas. Accurate calibration of the manometric rig is important for sorption characterization (Talu, 1998). This was carried out using helium expansion. The reference cell was charged with Helium and the valve connecting reference and sample cells was opened. The same procedure was repeated after inserting a standard volume into the sample cell. Using the gas law, we can derive two equations for each run which are then solved to calibrate the cell volumes. Reference cell volume was calibrated as 70.95 ml; sample cell volume was calibrated as 41.28 ml.

Before the experiment, the samples were crushed manually using a geologic hammer to pass through various sieve sizes. After sieve analysis, samples between 0.5 mm and 2 mm were chosen for adsorption characterization. Crushed samples are necessary for sorption characterization in shales as core samples would need prohibitively long equilibrium times in the order of several months (Luffel and Guidry, 1992). Before sorption characterization, the samples were washed with water and Toluene (RP40, 1998). Whilst water removes any entrenched salts and dirt that is present in the sample, it does not sufficiently remove entrenched oil which could significantly affect sorption measurements. For this reason, extraction with Toluene was also performed.

Prepared samples are then outgassed in the manometric rig. During experimentation, it was observed that a significant amount of sorption occurred in the first few seconds. Therefore, performing outgassing

outside the experimental rig would result in significant moisture adsorption from the atmosphere that could impact methane and carbon dioxide adsorption. For this reason, the rig was evacuated to about 140 Torr pressure and 80 °C for about 15 hours until a constant pressure profile was obtained. About 15 hours were required for the pressure to stabilize. After outgassing, the rig is flushed with helium and evacuated back to about 140 Torr and allowed to reach thermal equilibrium at the experimental temperature.

After thermal equilibrium was reached, the reference cell is injected with the adsorptive and allowed to reach thermal equilibrium before equalizing reference and sample cell pressures. The process is repeated for higher pressure steps. About 8 hours were required to reach equilibrium for each pressure step. The excess sorption was calculated based on a simple volumetric mass balance. However, this only measures the difference in the distribution of adsorptive molecules from the initial and final states. Since a certain amount of the adsorptive molecule was distributed in the adsorption space at the start of the experiment, these excess sorption values need to be corrected to absolute sorption values. To do this two methods are explored assuming surface coverage and micropore filling mechanisms. To obtain absolute sorption values assuming a surface coverage mechanism, the adsorbate density was assumed to be equal to the liquid density of the adsorptive. This is a fair assumption, although the reality is a little more complicated. Varying adsorptive densities have been observed in the literature – this is an area of active research (Pini, 2014). To obtain absolute sorption values assuming a micropore filling mechanism, the micropore volume calculated from the N_2 sorption was used. This is accompanied by its uncertainties associated with the characterization of micropore volumes (Weidenthaler, 2011). Both of these results are plotted in Figure 7-2. However, the biggest source of error in sorption occurs in the characterization of shale grain volume through helium expansion. To remove this error some people have proposed using net sorption values which assume a standard density for shales. It is common to assume a standard density of 0.5 g/cc for different adsorbents (Brandani et al., 2016). These results are also plotted for reference.

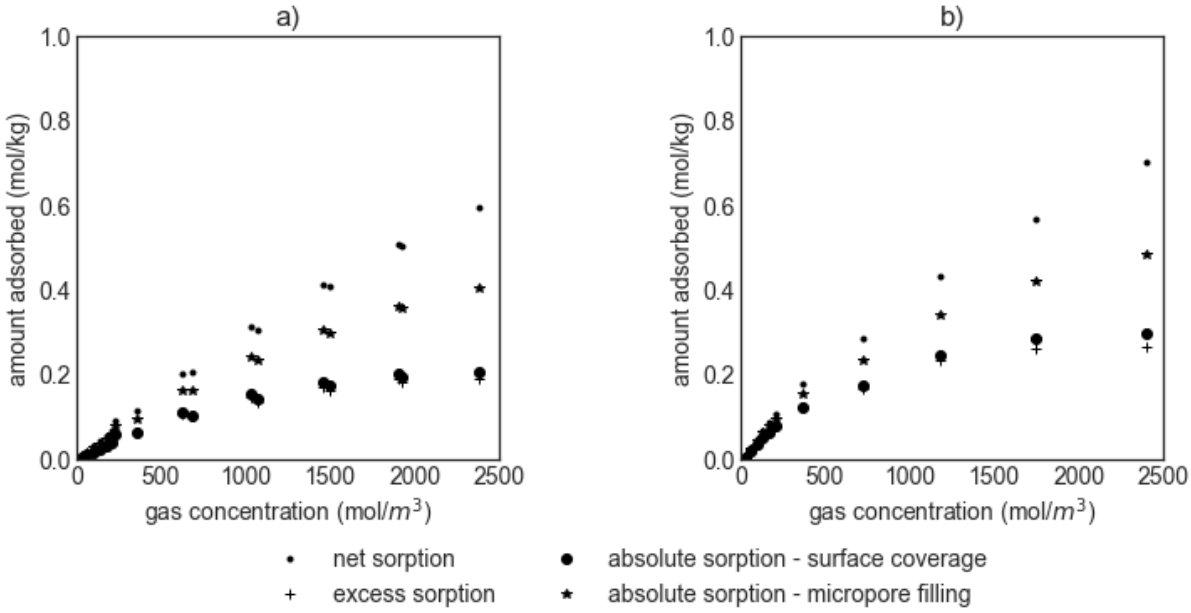

Figure 7-2 Net, Excess, and Absolute sorption on Lothian shale outcrops. Sub-figure 2a represents methane sorption values, and Sub-figure 2b represents carbon dioxide sorption

From Figure 7-2, reporting net sorption instead of absolute sorption results in an error of almost 200% for methane sorption, and by 150% for carbon dioxide sorption. There is also a significant difference in the calculated absolute sorption values depending on the method used to correct for initially present gas in the adsorbed phase. Absolute sorption values calculated assuming a micro-pore filling adsorption mechanism overpredicts sorption by almost 100% as compared to values calculated assuming a surface coverage mechanism. It is therefore essential to report the methodology used to calculate absolute sorption values along with the results. The whole experiment was repeated again with less than 5% errors for absolute adsorption at 60 bars.

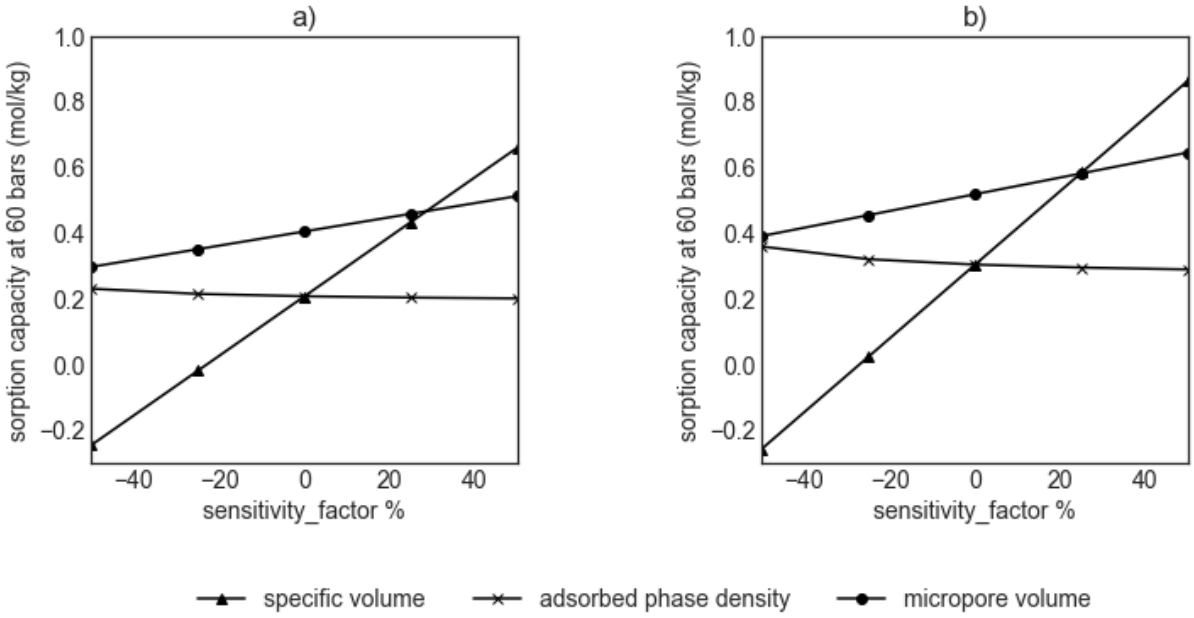

Figure 7-3 Sensitivity of experimental assumptions on resulting isotherms. Sub-figure 3a represents methane sorption values, and Sub-figure 3b represents carbon dioxide sorption

To further understand the importance of these assumptions a sensitivity analysis is performed. Figure 7-3 analyses the sensitivity of different experimental assumptions on resulting absolute sorption values. As discussed previously, it is evident that shale's density has the strongest correlation to the calculated sorption values. The micropore volume used to calculate sorption has a positive correlation, whilst the adsorbed phase density used has a negative correlation to calculated absolute sorption values. This can be explained as with increasing micropore volume, more molecules of the adsorptive are initially distributed in the adsorbed phase, and with decreasing adsorbed phase density, the difference in the densities of the sorbed phase and gas phase increases for higher pressures.

It must also be noted that both shales exhibit a Type I isotherm at experimental pressures. This is explained as the shales exhibit a significant amount of micropores through DFT analysis. Although there seem to be a significant amount of mesopores in the PSD analysis, no capillary condensation phenomenon was observed at experimental pressures, with the adsorption and desorption arms on top

of each other. However, it might be possible for this shale to exhibit hysteresis due to capillary condensation at high pressures beyond what is considered in this study (Yu et al., 2016).

Carbon dioxide adsorption capacity is significantly higher than that of methane. However, a higher variability is also observed for carbon dioxide sorption from Figure 7-3 compared to methane. But the trends are similar. Net sorption contributes to the biggest error, whilst the method of correction from excess to absolute being significant. This provides further evidence that these findings would apply to other adsorbent-adsorbate combinations as well.

Given that the shales were found to be predominantly macro-porous in the previous section, the absolute sorption isotherm obtained by assuming a surface coverage mechanism (constant adsorbed phase density) is considered for further analysis in this chapter.

7.4 Adsorption Modelling

The measured sorption values are considered for adsorption modelling in Figure 7-4. Given that the isotherms are of Type I, the Langmuir, Freundlich, Dubinin-Radushkevich, Sips, Toth, and Dubinin-Ashtakov isotherm models are considered. The linear isotherm model is also considered for low pressures. Both the amount adsorbed and the adsorption uptakes are considered for analysis.

As for all Type I isotherms, the linear model provides a very good fit for sorption at low pressures (up to 5 bars). However, it severely underpredicts sorption at high pressures, where monolayer adsorption is achieved after a certain experimental pressure. Therefore, a single parameter is not sufficient to characterize sorption in shales.

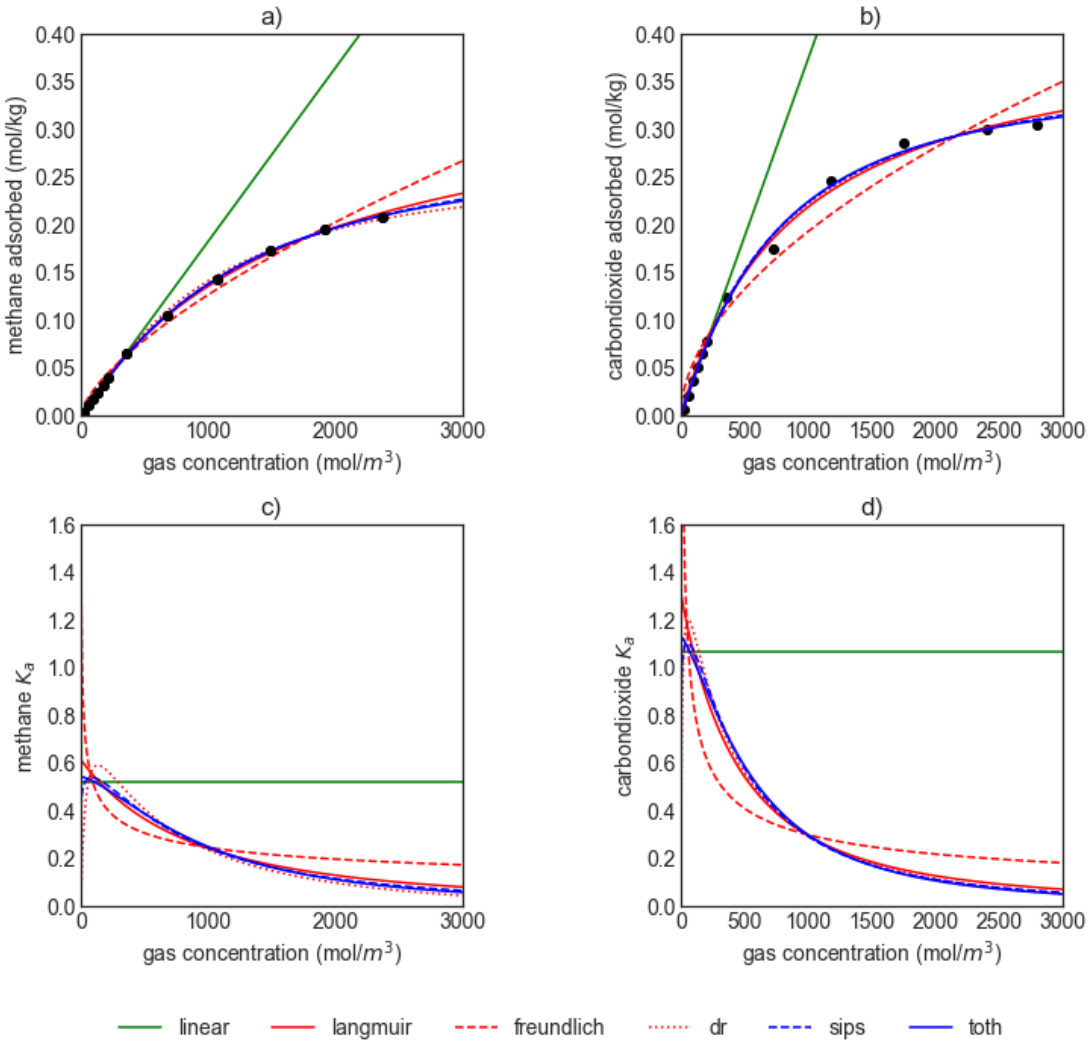

Figure 7-4 Adsorption modelling on Lothian shale outcrops

The Langmuir model proposed for adsorption based on a surface coverage mechanism and the ideal adsorbed surface is used empirically to fit adsorption values. It provides an excellent fit at both low and high pressures. It is the only two-parameter model used that has consistent thermodynamic behaviour throughout the experimental pressure range. However, it slightly over-predicts the Henry's constant at very low pressures. At high pressures, the adsorption uptake approaches 0 which is thermodynamically consistent for Type I isotherms (Do, 1998). The Freundlich model which is derived assuming a heterogenous surface does poorly on the experimental data. It can be seen that the adsorption uptake values approach infinity as loading approaches 0. This would cause serious numerical instabilities in

shale reservoir characterization. It also does not have a monolayer capacity at high pressure with the adsorption uptakes approaching 0 at a much slower rate. Both of these defects are serious, and therefore render the Freundlich isotherm ill-suited for shale reservoir characterization.

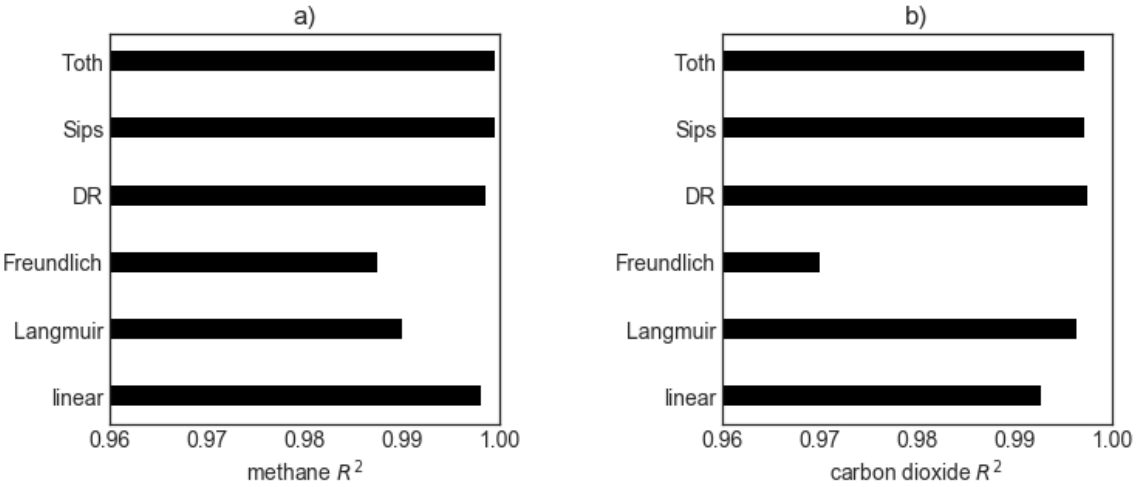

Figure 7-5 Goodness of fit metrics for isotherm models

The DR isotherm is also considered. This was originally proposed to model subcritical adsorption in microporous substances but has been popular in the shale gas literature (Clarkson et al., 1997). It could be empirically used for super-critical adsorption by assuming a pseudo vapour pressure as described in Chapter 3. The Dubinin equation was used to calculate the pseudo vapour pressure in this study (Everett and Powl, 1976). It provides a much better fit to the experimental data compared to both the Langmuir and the Freundlich isotherm. However, it does not have the correct thermodynamic behaviour at low and high pressures. The adsorption uptake approaches 0 at low pressures, and the DR isotherm generally does not have a monolayer adsorption capacity (Do, 1998). Both of these limitations are significant in gas shale reservoir characterization, despite providing an excellent fit to experimental data as shown in Figure 7-5. It is however noted here that the linear isotherm only has a good fit at low pressures < 5 bars.

Three parameter models are also considered in this study. Whilst they both provide an excellent fit to the experimental data, the Sips isotherm does not have consistent thermodynamic behaviour at low pressures with the adsorption uptake approaching 0 at very low loading. However, it does have consistent thermodynamic behaviour at high pressures. The Toth isotherm excels in all areas providing consistent thermodynamic behaviour at all pressures, whilst also providing an excellent fit to the experimental data. It also predicts a more accurate Henry's constant compared to the Langmuir isotherm. The only drawback is that it has three parameters instead of two.

Given that the Langmuir isotherm provides an excellent fit to the experimental data with only 2 parameters and has consistent thermodynamic behaviour at both low and high pressures, it is considered for further analysis in this chapter. To manage the scope of this chapter, only the methane isotherm is considered in this chapter. However, given that the underlying phenomena that govern sorption measurement such as assumptions during sorption measurement and modelling are common, these results are also applicable to other adsorbates on gas shales. Implications of carbon dioxide sorption mechanisms on carbon dioxide sequestration are considered in Chapter 6.

7.5 Permeability Characterization

Diffusion in shales can be characterized using the transient pressure data obtained during adsorption experiments (Profice et al., 2012). Here, it is important to differentiate between the shale's intrinsic diffusivity and the measured permeability. Whilst the intrinsic diffusion coefficient is only dependent on the shale's pore characteristics – pore size and connectedness, the measured permeability is dependent on both the shale pore characteristics and fluid characteristics. Fluid characteristics that affect measured permeability include viscosity, surface diffusion effect, adsorption, etc. To completely analyse the effects of adsorption on the shale's permeability, we will be ignoring other fluid effects such as Klinkenberg effect and Knudsen diffusion (Profice et al., 2012). However, viscosity effects will be included in this study.

The manometric rig is used for permeability characterization as well. The system is isolated and allowed to reach thermal equilibrium. The sample cell is then isolated and the reference cell is charged with the probe molecule – helium or methane. Once thermal equilibrium is achieved, the valve containing reference and sample cell is opened, and the pressure is monitored over time. This pressure profile could be analysed using the analytical solution proposed in the literature (Carslaw and Jaeger, 1959). The first 20 roots of the analytical solution were included as including further roots did not change the calculated pressure profile significantly.

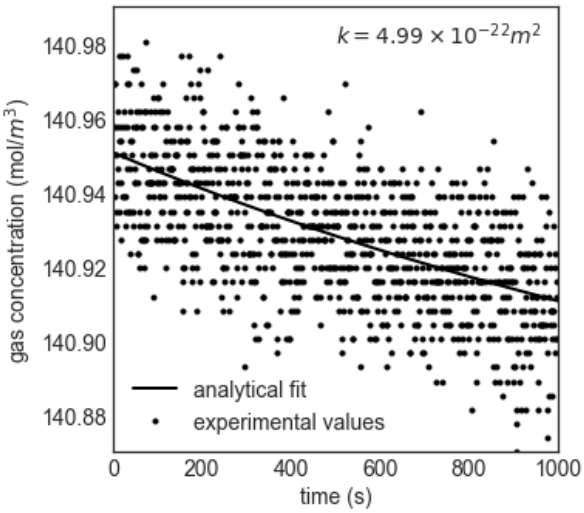

Figure 7-6 Helium Permeability of Lothian shale outcrops

Shales with extremely low permeability have an initial linear transient region during permeability measurement experiments. The complete procedure is explained in Chapter 3. Fitted permeability to He expansion at 5 bars was calculated as 4.99×10^{-2} m^2 as shown in Figure 7-6. This value is much lower compared to other shales around the world (Cui et al., 2009), and longer equilibrium times may be necessary to complete gas sorption experiments. However, it is still in the range of permeabilities for shales (Manger and 1902-, 1963).

Since the isotherm was found to exhibit sufficient linear behaviour up to 5 bars, the linear, Langmuir, and Toth isotherms were used to model methane diffusion in shales at 5 bars. Other isotherms models were demonstrated to have inconsistent thermodynamic behaviour with adsorption uptakes approaching 0 or infinity at low pressures. This can cause numerical instabilities during optimization. The linear, Langmuir, and Toth isotherms give a sufficient fit to the experimental data as shown in Figure 7-7. Since the derivative of linear isotherm to loading is simply its Henry's constant, the use of linear isotherm simplifies permeability measurement greatly at low pressures. The adsorption uptake for Langmuir isotherm leads to a non-linear analytical solution that complicates permeability characterization. A permeability value of 4.99×10^{-2} m^2 was found to provide a sufficient fit to both the Helium and Methane experimental data.

A series of numerical experiments were performed to assess the impact of isotherm shape on diffusion. Results are plotted in Figure 7-8. At low pressures, where the Langmuir isotherm approaches the linear isotherm, it was possible to model diffusion using the linear isotherm in place of the Langmuir isotherm. At high pressures, where the adsorption uptake of the Langmuir isotherm approaches 0, it was possible to ignore adsorption all together whilst characterizing permeability. However, at intermediate pressures, it becomes necessary to use the appropriate isotherm to characterize permeability. Figure 7-10 shows that the errors due to the assumption of linear isotherm increases with increasing pressure and decreases with increasing Langmuir pressure. Therefore, for shales with high Langmuir pressure, the linear isotherm may be used to fit the diffusion phenomenon in shales at low pressures.

Figure 7-11 shows that the no sorption assumption leads to highly erroneous permeability values at low pressures. However, the errors of no sorption assumption are much smaller at higher pressures and lower Langmuir pressures Therefore for shales with low Langmuir pressures, no sorption assumption may be used to estimate permeability at very high pressures. Using the principle of Occam's Razor, we must not include additional parameters in our model when it could be sufficiently and accurately described using a smaller number of parameters. Therefore, the linear isotherm is recommended for permeability characterization at low pressures, and the no sorption assumption is recommended for

permeability characterization at high pressures. However, the Langmuir model needs to be used for intermediate pressure ranges.

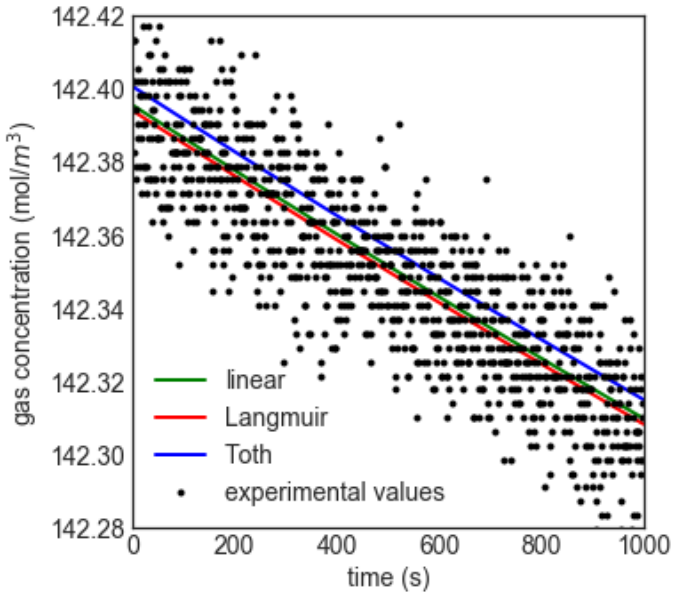

Figure 7-7 Permeability fits for Methane – Lothian shale outcrops

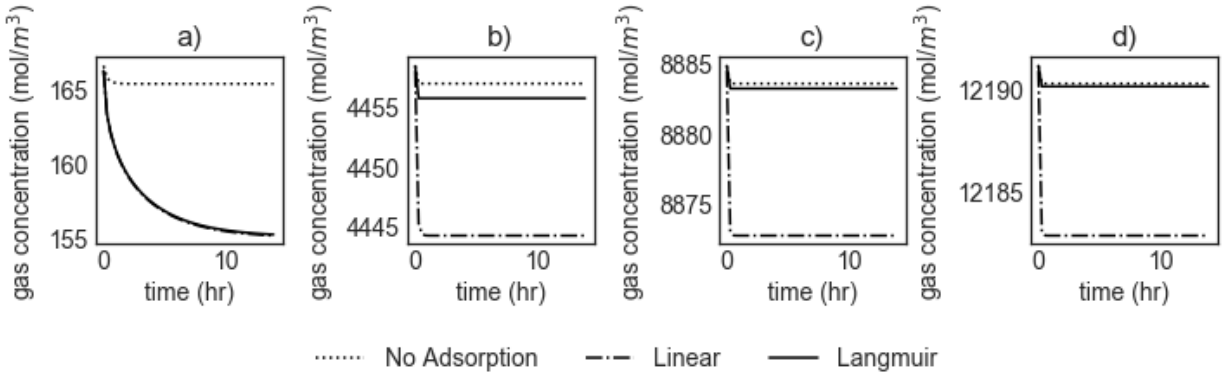

Figure 7-8 Gas diffusion in shales Figure 8a, 8b, 8c, and 8d represent modelled diffusion at 5, 105, 205, and 305 bars respectively.

Figure 7-9 plots the sensitivities of different experimental parameters on diffusion in gas shales. The particle size seems to hold the strongest correlation with equilibrium times, whilst permeability is also important. Therefore, for shales with very low permeability, using a smaller particle size would allow adsorption characterization in a reasonable amount of time. Also, the increase in equilibrium time required with decreasing permeability is not a linear function. Therefore, these experiments must be repeated in the vicinity of the particle size and shale permeability considered for an experiment. Doing so will ensure that the experiment was designed accurately for the given sample. Figure 7-9 also shows that longer equilibrium times are needed with increasing adsorption uptake. This implies that lower pressure steps where adsorption uptake approaches linear isotherm will need more time to reach equilibrium as compared to higher pressure steps where adsorption uptake approaches 0. Also, carbon dioxide isotherm with higher adsorption uptakes will need longer equilibrium times compared to methane isotherms with lower adsorption uptakes. However, there is no predicted difference in equilibrium times required for adsorption and desorption isotherms in this numerical study in this numerical study.

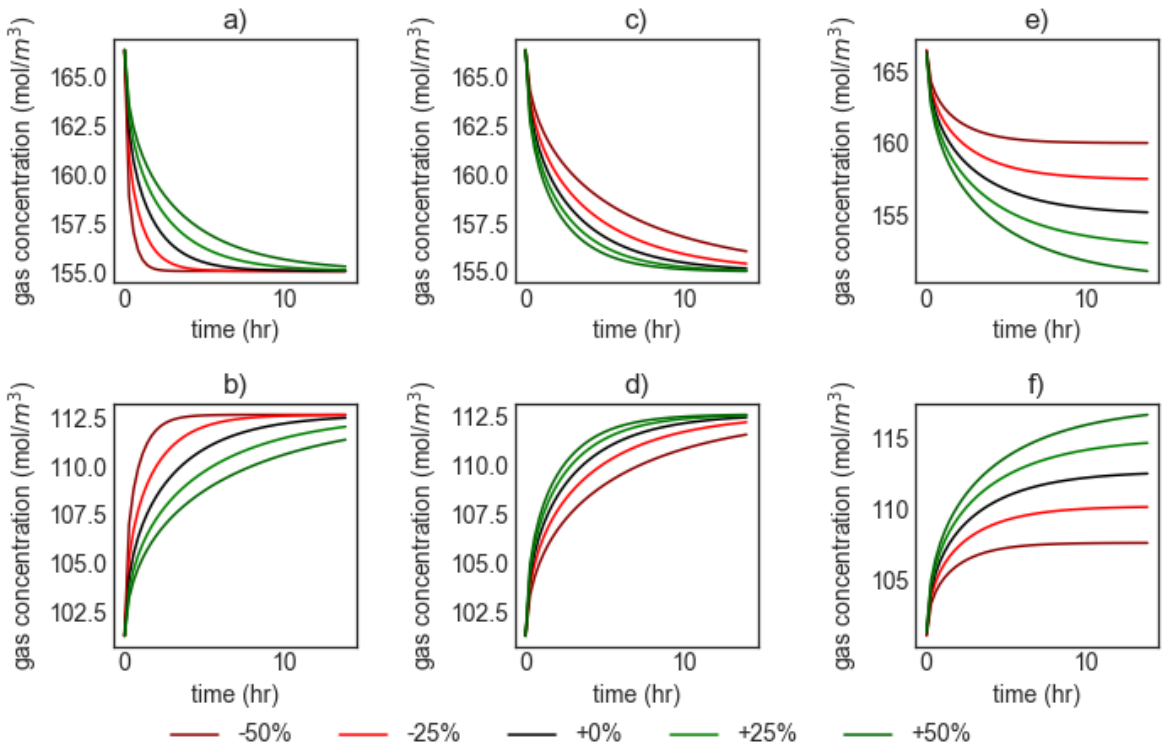

Figure 7-9 Sensitivity of experimental parameters on gas diffusion in shales. Figure 11a and 11b model adsorption and desorption diffusion for different particle sizes. Figures 11c and 11d model adsorption and diffusion for different permeability values. Figures 11e and 11f model adsorption and diffusion for different adsorption uptakes.

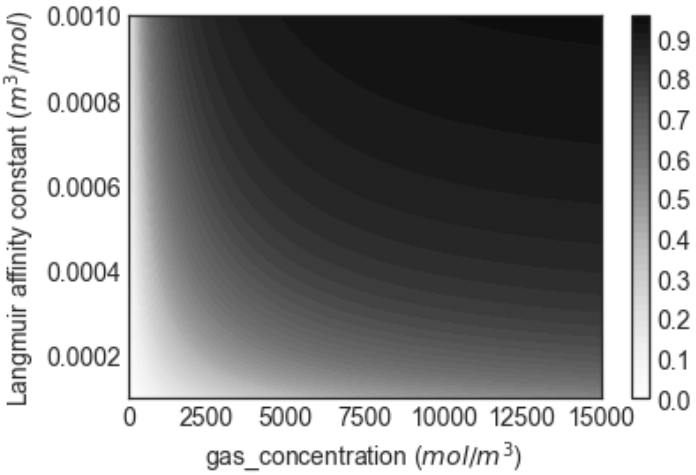

Figure 7-10 Percentage Errors in Permeability Measurement due to the Assumption of a Linear Isotherm

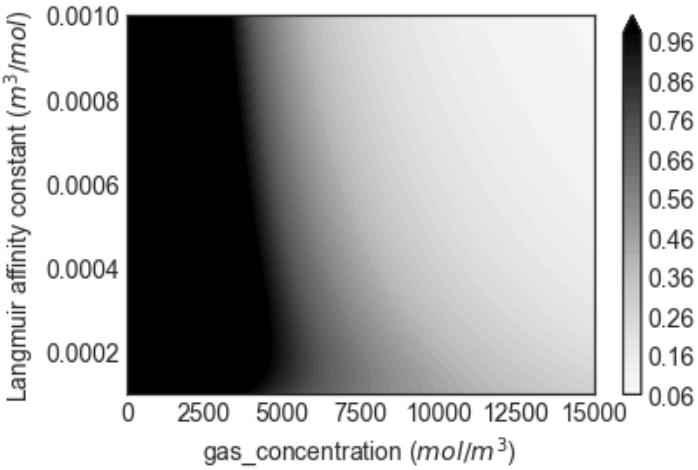

Figure 7-11 Percentage Errors in Permeability Measurement due to the Assumption of No Sorption

7.6 Resource Estimation

The total gas present in the reservoir is the sum of free gas in the shale pores and adsorbed gas in the bulk shale. The amount of free gas could be calculated using an equation of state, whilst the amount of sorbed gas could be calculated from an adsorption isotherm:

Table 7-1 Assumed Reservoir Parameters

Parameter	Symbol	Value	Units
Matrix porosity	ϕ_m	0.05	-
Shale density	ρ_s	2.7 $\times 10^3$	kg/m^3
Matrix permeability	k_m	4.99 $\times 10^{-22}$	m^2
Fracture porosity	ϕ_f	1	
Fracture permeability	k_m	1 $\times 10^{-14}$	m^2
Fracture spacing	l_x	20	m
Well radius	r_w	0.05	m
Reservoir height		300	m
Fracture height		200	m
Fracture width		0.01	m
Equivalent radius	r_e	100	m
Reservoir temperature	T	333.15	K
Well flowing pressure	P_{wf}	35	bar

7.7 Reserve Estimation

Mass balance in matrix and fracture regions are given as (Yu et al., 2014):

$$[\phi_m + (1-\phi_m)K_a]c_g\rho_g\frac{\partial P}{\partial t} + \nabla\left(\frac{\rho_g k_m}{\mu}.\nabla P\right) = -Q_{if} \quad (85)$$

$$\phi_m c_g\rho_g\frac{\partial P}{\partial t} + \nabla\left(\frac{\rho_g k_f}{\mu}.\nabla P\right) = Q_{if} - Q_p \quad (86)$$

Interporosity flow was calculated as follows (Warren and Root, 1963):

$$Q_{if} = \frac{\lambda k_m \rho_g}{\mu}\left(P_m - P_f\right) \tag{87}$$

Where, $\lambda = \frac{12}{l_x{}^2}$.

Gas production was calculated using the following equation (Guo et al., 2014):

$$Q_p = \frac{k_f \rho_f}{\mu}\frac{\theta(\bar{p}_f - p_{wf})}{ln(r_e/r_w)} \tag{88}$$

Single component equation outlined in Equations (*85*), (*86*), *(87)*, and (*88)* are solved in the domain represented by Figure 7-12. The complete derivation of these equations is presented in Chapter 3. Simulation parameters are summarised in Table 7-1. The domain represents the shale matrix and fracture, with the wellbore represented by the horizontal boundary in the middle, and the fractures represented by the vertical boundaries. The complete details are provided in Chapter 3. A mesh independence study was conducted to calculate production after 30 days, with the results plotted in Figure 7-14. It can be seen that convergence was achieved for the given number of mesh elements. The physics has also been validated in 1D from Figure 7-6 and Figure 7-7.

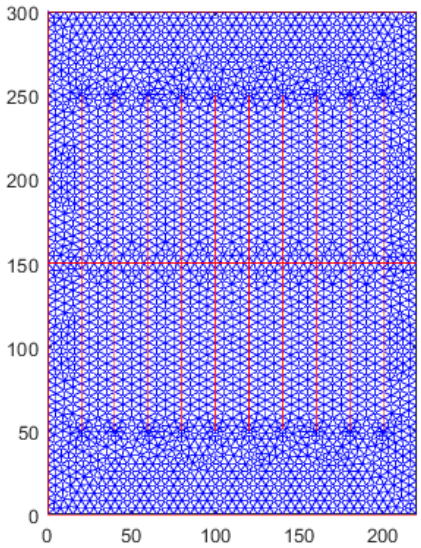

Figure 7-12 Finite Element Meshing for Shale Reservoir Model

From Figure 7-15, the total recovery rate after 10 years was about 6%, and the sorbed gas recovery rate was about 3%. This suggests that further production technologies besides hydraulic fracturing are required to increase the recovery rate from shale reservoirs. Figure 7-13 shows that production occurs primarily along with the fractures. However, most of the gas in the reservoir is left behind.

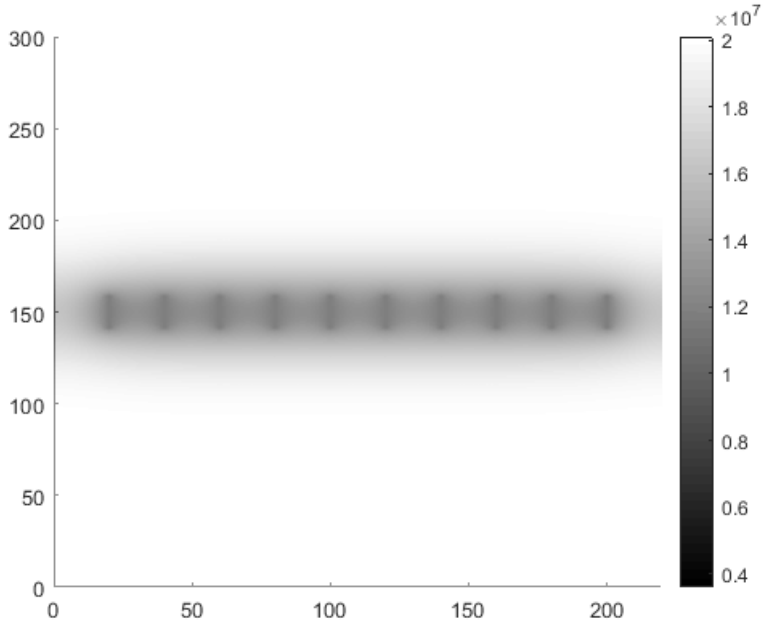

Figure 7-13 Reservoir gas distribution after 10 years

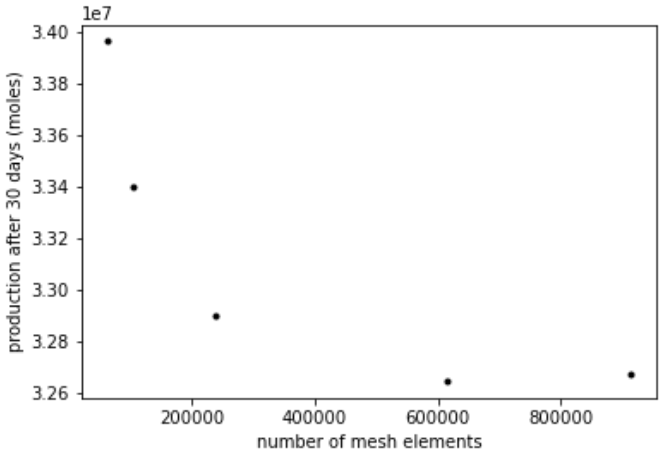

Figure 7-14 Mesh Independence Study

Figure 7-16 shows the sensitivities of different model parameters on production. Matrix permeability has the strongest correlation with production. Langmuir volume has a negative correlation, and Langmuir affinity has a positive correlation. This behaviour is expected from the results of the previous section, where we observed that longer equilibrium times were required to achieve a similar amount of mass transfer for higher adsorption uptakes. And since we know that adsorption uptake is directly correlated with Langmuir volume and inversely correlated with Langmuir affinity, the seemingly unusual result of total production decreasing with increasing Langmuir volume is completely expected. Since fracture permeability was assumed to be extremely high, it did not influence the production.

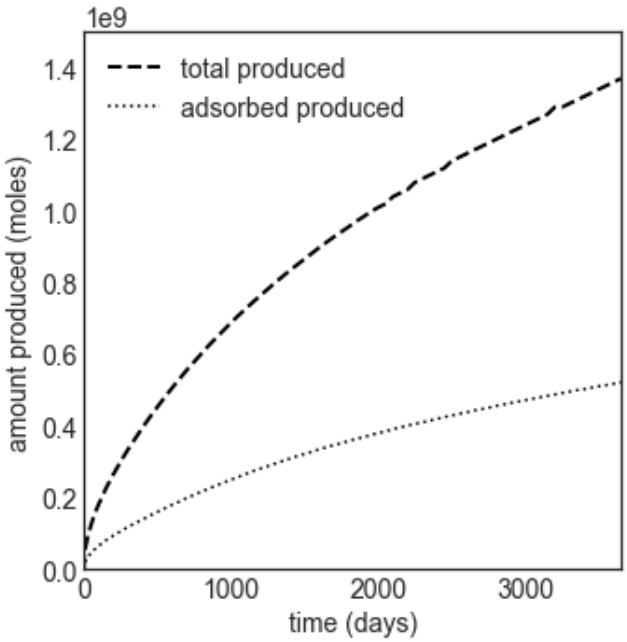

Figure 7-15 Production from Reservoir

It can be noted that with increasing Langmuir volume, the total production after 10 years decreases, whilst the recovery rate decreases even more significantly as most of the sorbed gas is left behind in the reservoir. The first trend can be explained given that adsorption uptake is directly proportional to Langmuir volume and inversely proportional to Langmuir affinity constant. We know that increasing amounts of adsorption uptake decreases the amount of mass transfer that occurs in a fixed amount of time, although the total mass transfer that occurs is higher - increasing adsorption uptake could decrease the amount of gas that could be produced during the primary recovery period. However, this trend has not been observed consistently in the literature, suggesting that this phenomenon is more complex than what is observed here. Whilst some authors have noted an increase in reserve estimates with increasing sorption (Teng et al., 2019), some have noted no change in reserve estimates due to sorption (Yu et al., 2016), and others have noted a net decrease in reserves with increasing sorption (Mengal and Wattenbarger, 2011). A more complete analysis of different parameters would be of interest to the research community.

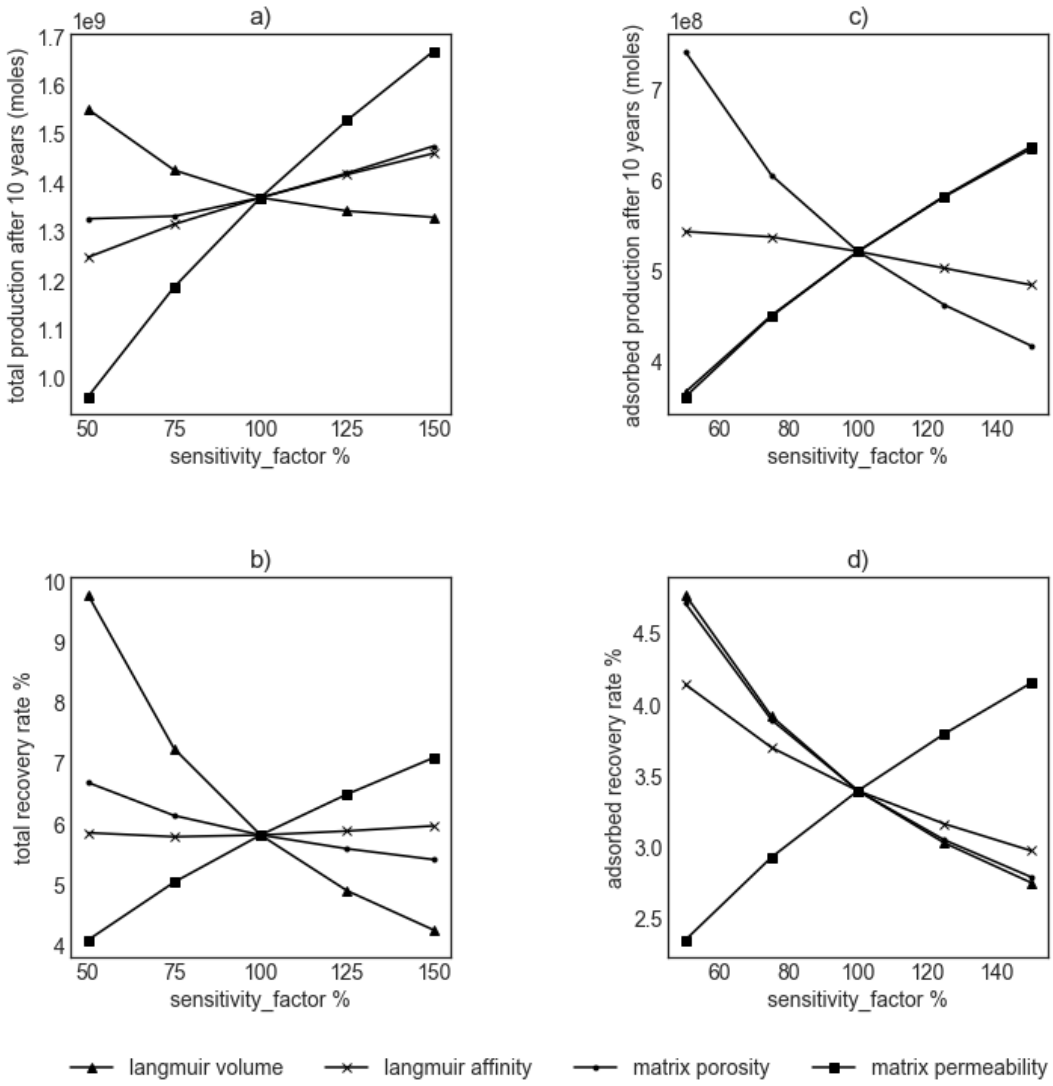

Figure 7-16 Total production sensitivity to model parameters

Figure 7-17 analyses the sensitivity of fracture parameters on total recovery. By design, both the fracture permeability and fracture width do not have any effect on production. This is because a very high fracture conductivity corresponding to a perfect hydraulic fracturing was assumed in this study (Guo et al., 2014). However, both fracture height and fracture spacing are significant in the processes of reserve estimation. Recovery rate increases with taller fractures that are more closely spaced as expected.

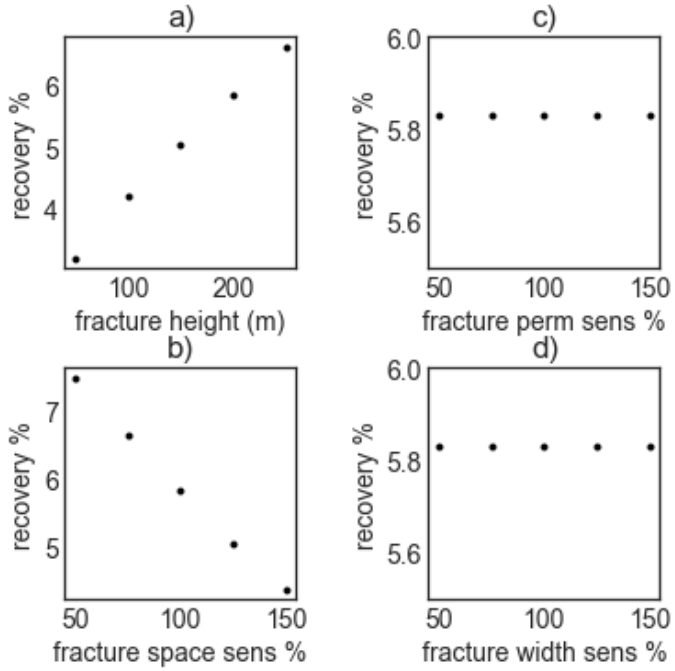

Figure 7-17 Sensitivity of fracture parameters on total recovery

To further understand the impact of sorption on reserve estimation for different shale operation parameters, more numerical experiments were carried out as shown in Figure 7-18. To allow this study to be useful for coal bed methane extraction as well, a higher adsorption limit of 1 mol/kg was assumed. The results suggest that the impact of sorption on shale reserve estimation is not straight forward, and strongly dependent on the operating parameter for the shale in question. Whilst, sorption tends to result in a net increase in the reserve potential at higher permeabilities, it seems to decrease the reserve potential at lower permeabilities. Fracture design is also very important for releasing sorbed gas, with the number of fractures parameter being more significant than the fracture height. The implications of these for field planning are significant. Phenomena such as clay swelling and caking, that decrease permeability (Pan and Connell, 2007) could seriously diminish the producibility of a low permeability reservoir compared to a reservoir with slightly higher permeability. These limitations could be overcome to a certain extent using acid fractures and hydraulic fracturing (King, 2010). However, enhanced recovery technologies that target sorbed gas are extremely important whilst designing production technologies for gas shale reservoirs.

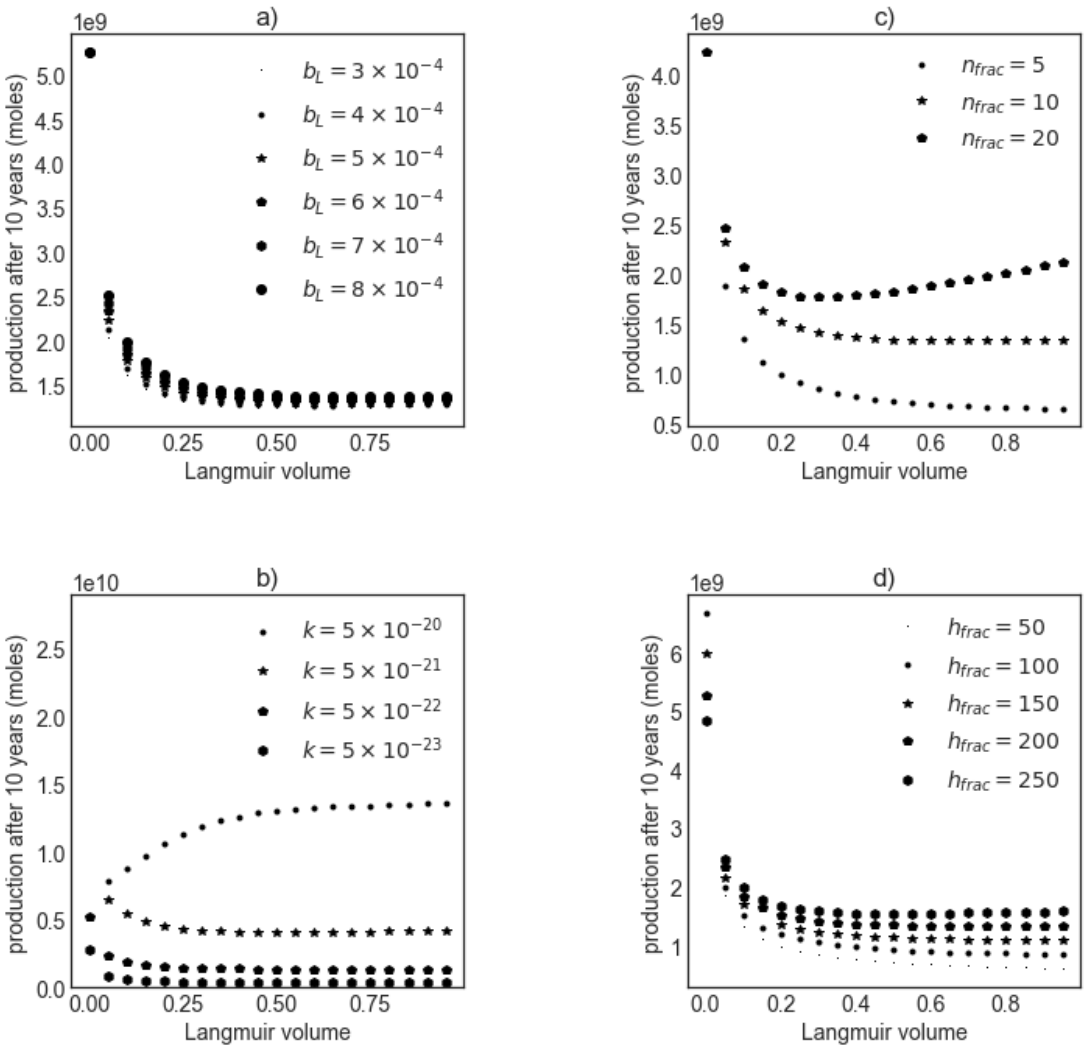

Figure 7-18 Impact of sorption on shale reservoir estimation. Subfigure a analyses the impact of maximum sorption for different adsorption affinities, subfigure b considers different permeabilities, subfigure c considers a different number of fractures, and subfigure d considers different fracture heights.

7.8 Conclusion

High-pressure methane and carbon dioxide isotherms were measured on Lothian shale outcrops, along with their pore characteristics. Largest errors in sorption characterization stem from the incorrect characterization of shale density. Sorption mechanism plays a significant role in the correction of excess

sorption to absolute sorption values. Therefore, further research into different sorption mechanisms in shales is necessary.

Sorption plays a significant role in the permeability characterization as well as production estimation. Linear isotherm simplifies permeability characterization at low pressures and no sorption assumption simplifies permeability characterization at high pressures. Equilibrium times required for sorption characterization are strongly correlated with particle size and adsorption uptake and negatively correlated with permeability.

Estimated recovery rates after 10 years are only 6%, with recovery from sorbed gas being only 3%. Recovery is strongly correlated with matrix permeability and negatively correlated with Langmuir volume and Langmuir pressure.

7.9 References

Ambrose, R.J., Hartman, R.C., Diaz Campos, M., Akkutlu, I.Y., Sondergeld, C., 2010. New pore-scale considerations for shale gas in place calculations, in: SPE Unconventional Gas Conference. Society of Petroleum Engineers.

Brandani, S., Mangano, E., Sarkisov, L., 2016. Net, excess and absolute adsorption and adsorption of helium. Adsorption 22, 261–276.

Carslaw, H.S., Jaeger, J.C., 1959. Conduction of heat in solids. Oxford Clarendon Press. 1959, 2nd ed.

Civan, F., Devegowda, D., Sigal, R.F., 2013. Critical Evaluation and Improvement of Methods for Determination of Matrix Permeability of Shale, in: SPE Annual Technical Conference and Exhibition. Society of Petroleum Engineers.

Clarkson, C.R., Bustin, R.M., Levy, J.H., 1997. Application of the mono/multilayer and adsorption potential theories to coal methane adsorption isotherms at elevated temperature and pressure. Carbon N. Y. 35, 1689–1705.

Cui, X., Bustin, A.M.M., Bustin, R.M., 2009. Measurements of gas permeability and diffusivity of tight reservoir rocks: Different approaches and their applications. Geofluids 9, 208–223.

Do, D.D., 1998. Adsorption Analysis: Equilibria And Kinetics: (With CD Containing Computer Matlab Programs).

Everett, D.H., Powl, J.C., 1976. Adsorption in slit-like and cylindrical micropores in the henry's law region. A model for the microporosity of carbons. J. Chem. Soc. Faraday Trans. 1.

Garrels, R.M., Mackenzie, F.T., 1969. Sedimentary rock types: relative proportions as a function of geological time. Science (80-.). 163, 570–571.

Guo, C., Wei, M., Chen, H., He, X., Bai, B., 2014. Improved Numerical Simulation for Shale Gas Reservoirs, in: Offshore Technology Conference-Asia. Offshore Technology Conference.

Ji, W., Song, Y., Rui, Z., Meng, M., Huang, H., 2017. Pore characterization of isolated organic matter from high matured gas shale reservoir. Int. J. Coal Geol. 174, 31–40.

King, G.E., 2010. Thirty years of gas shale fracturing: What have we learned?, in: SPE Annual Technical Conference and Exhibition. Society of Petroleum Engineers.

Kuila, U., Prasad, M., 2013. Specific surface area and pore-size distribution in clays and shales, Geophysical Prospecting.

Llewellyn, P.L., Rodriquez-Reinoso, F., Rouqerol, J., Seaton, N., 2007. Is the BET equation applicable to microporous adsorbents? Stud. Surf. Sci. Catal. 160, 49.

Luffel, D.L., Guidry, F.K., 1992. New core analysis methods for measuring reservoir rock properties of Devonian shale. J. Pet. Technol. 44, 1–184.

Manger, G.E. (George E., 1902-, 1963. Porosity and bulk density of sedimentary rocks.

Mengal, S.A., Wattenbarger, R.A., 2011. Accounting For Adsorbed Gas in Shale Gas Reservoirs, in: SPE Middle East Oil and Gas Show and Conference. Society of Petroleum Engineers.

Pan, Z., Connell, L.D., 2007. A theoretical model for gas adsorption-induced coal swelling. Int. J. Coal

Geol. 69, 243–252.

Pini, R., 2014. Interpretation of net and excess adsorption isotherms in microporous adsorbents. Microporous Mesoporous Mater. 187, 40–52.

Profice, S., Lasseux, D., Jannot, Y., Jebara, N., Hamon, G., 2012. Permeability, Porosity and Klinkenberg Coefficient Determination on Crushed Porous Media. Petrophysics 53.

Psarras, P., Holmes, R., Vishal, V., Wilcox, J., 2017. Methane and CO2 Adsorption Capacities of Kerogen in the Eagle Ford Shale from Molecular Simulation. Acc. Chem. Res. 50, 1818–1828.

Rani, S., Prusty, B.K., Pal, S.K., 2015. Methane adsorption and pore characterization of Indian shale samples. J. Unconv. Oil Gas Resour. 11, 1–10.

Rouquerol, J., Avnir, D., Fairbridge, C.W., Everett, D.H., Haynes, J.M., Pernicone, N., Ramsay, J.D.F., Sing, K.S.W., Unger, K.K., 1994. Recommendations for the characterization of porous solids (Technical Report). Pure Appl. Chem. 66, 1739–1758.

Rouquerol, J., Rouquerol, F., Llewellyn, P., Maurin, G., Sing, K.S.W., 2013. Adsorption by powders and porous solids: principles, methodology and applications. Academic press.

RP40, A., 1998. Recommended practices for core analysis. Feb.

Ruthven, D.M., 1984. Principles of adsorption and adsorption processes. Chem. Eng. Process. Process Intensif.

Schettler Jr, P.D., Parmely, C.R., 1991. Contributions to total storage capacity in Devonian shales, in: SPE Eastern Regional Meeting. Society of Petroleum Engineers.

ScottishShale, 2020. Straiton Oil Works [WWW Document].

Sing, K.S.W., 1985. Reporting physisorption data for gas/solid systems with special reference to the determination of surface area and porosity (Recommendations 1984). Pure Appl. Chem. 57, 603–619.

Talu, O., 1998. Needs, status, techniques and problems with binary gas adsorption experiments. Adv.

Colloid Interface Sci. 76–77, 227–269.

Teng, T., Xue, Y., Cun, Z., 2019. Modeling and simulation on heat-injection enhanced coal seam gas recovery with experimentally validated non-Darcy gas flow. J. Pet. Sci. Eng.

Wang, Y., Zhu, Y., Liu, S., Zhang, R., 2016a. Pore characterization and its impact on methane adsorption capacity for organic-rich marine shales. Fuel 181, 227–237.

Wang, Y., Zhu, Y., Liu, S., Zhang, R., 2016b. Methane adsorption measurements and modeling for organic-rich marine shale samples. Fuel 172, 301–309.

Warren, J.E., Root, P.J., 1963. The Behavior of Naturally Fractured Reservoirs. Soc. Pet. Eng. J. 3, 245–255.

Weidenthaler, C., 2011. Pitfalls in the characterization of nanoporous and nanosized materials. Nanoscale.

Yu, W., Sepehrnoori, K., 2014. Simulation of gas desorption and geomechanics effects for unconventional gas reservoirs. Fuel 116, 455–464.

Yu, W., Sepehrnoori, K., Patzek, T.W., 2016. Modeling gas adsorption in Marcellus shale with Langmuir and bet isotherms. SPE J. 21, 589–600.

Yu, W., Sepehrnoori, K., Patzek, T.W., 2014. Evaluation of gas adsorption in Marcellus Shale, in: SPE Annual Technical Conference and Exhibition. Society of Petroleum Engineers.

Zhang, Y., Shao, D., Yan, J., Jia, X., Li, Y., Yu, P., Zhang, T., 2016. The pore size distribution and its relationship with shale gas capacity in organic-rich mudstone of Wufeng-Longmaxi Formations, Sichuan Basin, China. J. Nat. Gas Geosci. 1, 213–220.

8 Impact of Geochemistry and Pore Structure on Adsorption and Diffusion on Gas Shales

8.1 Introduction

Adsorption, one of the primary storage mechanisms in gas shales, is generally considered to be a physical phenomenon (Heller and Zoback, 2014). It is, therefore, a strong function of the shale's pore size distribution (Do, 1998). The shale's pore size distribution is, in turn, a strong function of its geochemistry, with pores from different components in shales exhibiting different characteristics. This suggests that further research on sorption and diffusion characteristics in the context of the shale's geochemistry and pore structure would be highly useful for the research community.

Shale geochemistry could be classified into 3 broad types – quartz, feldspar, carbonates, clay minerals, and organic matter (Rezaee, 2015). Whilst kerogen and clay minerals are highly microporous and contribute to the surface area required for adsorption, quartz, and feldspar are generally nonporous (Ross and Marc Bustin, 2009). Further different kinds of kerogen and clay minerals could be expected to contribute to different pore shapes and sizes. Although there has been some work on the importance of pore structure and geochemistry on methane sorption in the literature (Ross and Marc Bustin, 2009), research into this domain is limited by the highly heterogeneous nature of gas shales, on the pore, core, and field scales. This is especially important as carbon dioxide being a foreign substance could be expected to react differently with in situ shale minerals as compared to methane (Liu et al., 2020). Further, the effects of other minerals such as carbonates, pyrites, and apatites on sorption mechanisms in shales are still unknown.

This study involves a geochemical analysis of 7 different shale samples from the Bowland play. The geochemical analyses are coupled with low-pressure N_2 sorption and analysis of pore size distribution. Then 3 samples with different compositions are selected further analysis with SEM, and high-pressure adsorption and diffusion analysis. High-pressure methane and carbon dioxide isotherms are presented

along with the first and second-order diffusion characteristics of methane and carbon dioxide on gas shales.

The resulting isotherms are analysed along with the insights from the previous chapter. This is possible because the results from the previous chapter, though based on a different sample, are based on first principles, and are therefore fundamental in nature. So although the results might not be comparable, the concepts could be applied from one study to another. The Bowland shale samples are chosen for this study over the Lothian shale samples as they offer a greater deviation in their composition and pore structure allowing us to derive insights on their respective effects.

8.2 X-Ray Diffraction and Total Organic Carbon

Figure 8-1 shows the XRD composition of all samples considered. This data was provided by Cuadrilla and integrated with other data obtained from the laboratory. The samples considered have a wide range of geochemical composition and are obtained from a wide range of formations – samples AT9 and AA94 from upper Bowland shales at depts of about 2500 meters, samples AA114 and AA83A from lower Bowland shales at about 3000 meters, samples B53, and AT1 from the Millstone Grit formation at 2000 meters, and A153 from the Hodder Mudstone formation at 2500 meters. They have all the main constituents of a gas shale – quartz, feldspar, carbonates, minerals and organic matter as shown in Figure 8-1 (Daniel B. Shaw, 1965).

Sample AA114 has the highest quartz content, whilst the sample AA83A has the lowest. However, sample AA83A has a very high dolomite concentration. Significant amounts of illite were also found in samples AA114, A153, AT9, AT1, and B53. Kaolinite was found in samples B53, AT1, A153, and AA114. Trace amounts of pyrite were found in samples A153, AT9, B52, and AA114. Figure 8-2 shows the TOC content of different shale samples considered. Samples with a wide range of organic content from under 1% to about 7% have been acquired. It is interesting to note that whilst shale plays with

TOC content less than 2% is usually considered unsuitable for commercial exploration, plays with over 5% TOC content are generally viewed as particularly favourable.

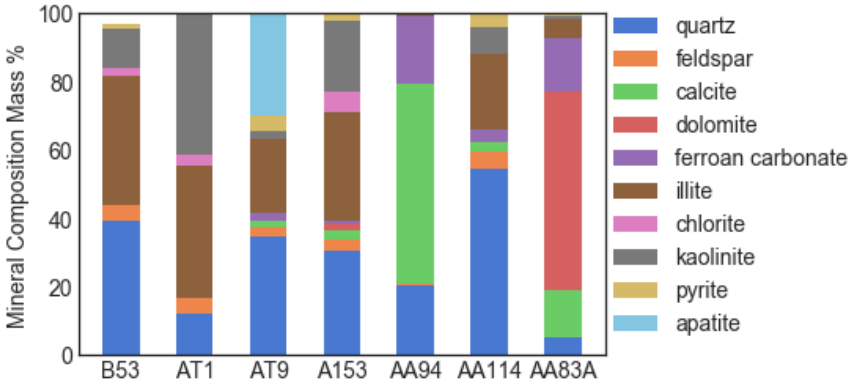

Figure 8-1 XRD Composition of Shale Samples

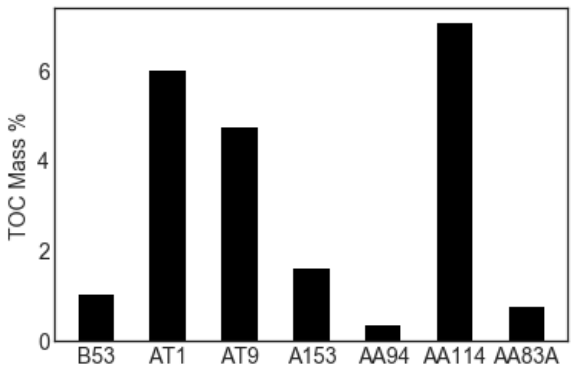

Figure 8-2 TOC Content of Bowland Shale Samples

For comparison, plays in the Longmaxi formation have been found to have a wide range of TOC values from 0.4% to 18% (Dai et al., 2014). Woodford shale samples have TOC values between 5% and 15% (Romero and Philp, 2012). Australian shales have been found to contain average TOC contents between 2% and 6% (Rezaee, 2015). Polish shales also seem to exhibit lower average TOC contents at about 2% to 6% (Rezaee, 2015). Whilst the UK shales have been found to exhibit lower TOC contents compared

to some other plays in other different of the world, it has a significant amount of thickness making it worth exploring (Rezaee, 2015).

Geochemical constituents play an important role in shale reservoir characterization. For example, shales with high quartz contents are easier to hydraulically fracture (Caineng et al., 2010). Whilst mineral sequestration of carbon dioxide for long term sequestration has also been explored in the literature (Romanov et al., 2015). That said, in the context of adsorption, samples AA114, AT1, and AT9 with both high organic content and high clay mineral content can be expected to exhibit high adsorption, whilst samples AA94 and AA83A with low organic carbon and low mineral content can be expected to exhibit low adsorption.

8.3 Scanning Electron Microscopy and Energy Dispersive Spectrometry

To gain further insights on the shale's structure and geochemistry SEM and EDS analysis were performed on samples AA114, A153, and AA83A. These samples were chosen because of being sufficiently different from each other in terms of mineral composition and organic content. Whilst samples AA114 is rich in both organic content and mineral content, sample A153 is rich in only clay mineral content. Sample AA83A, although not rich in organic carbon or clay minerals, is rich in carbonates, which is also very interesting to study.

SEM and EDS analysis were performed on Carl Zeiss SIGMA HD and Oxford Aztec ED systems. A magnification of 4.3×10^{-3} was achieved providing excellent images for further analysis. Through the analysis of backscattered electrons, a qualitative elemental analysis was performed as shown in Figure 8-4. The EDS spectra at individual points are compared with standard spectra for minerals found in the literature to identify different chemical phases found in Figure 8-3 (Kenneth P. Severin, 2004). Larger EDS spectra corresponding to the whole SEM region is also shown in Figure 8-4 for comparison. Despite shales being highly heterogeneous, a good correlation with the XRD data supplied by Cuadrilla was achieved for the most part.

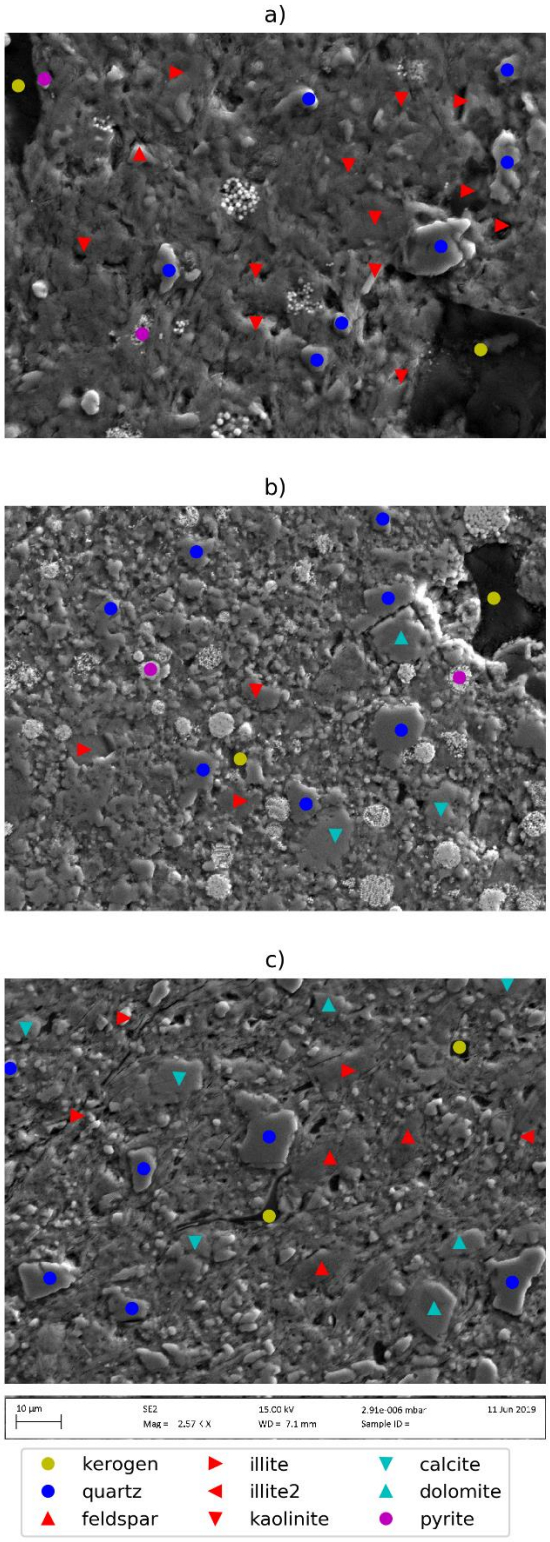

Figure 8-3 EDS Images of Bowland Shale Samples. Sub-figures a, b, and c are images of samples AA114, A153, and AA83A.

Several phases of clay minerals were identified in all three samples. Large amounts of organic matter are also present along with quartz phases and characteristic pyrite crystals. Significant pore volumes are locked in the organic region and the clay mineral region. However, very low porosities were observed in phases constituted by quartz and carbonates.

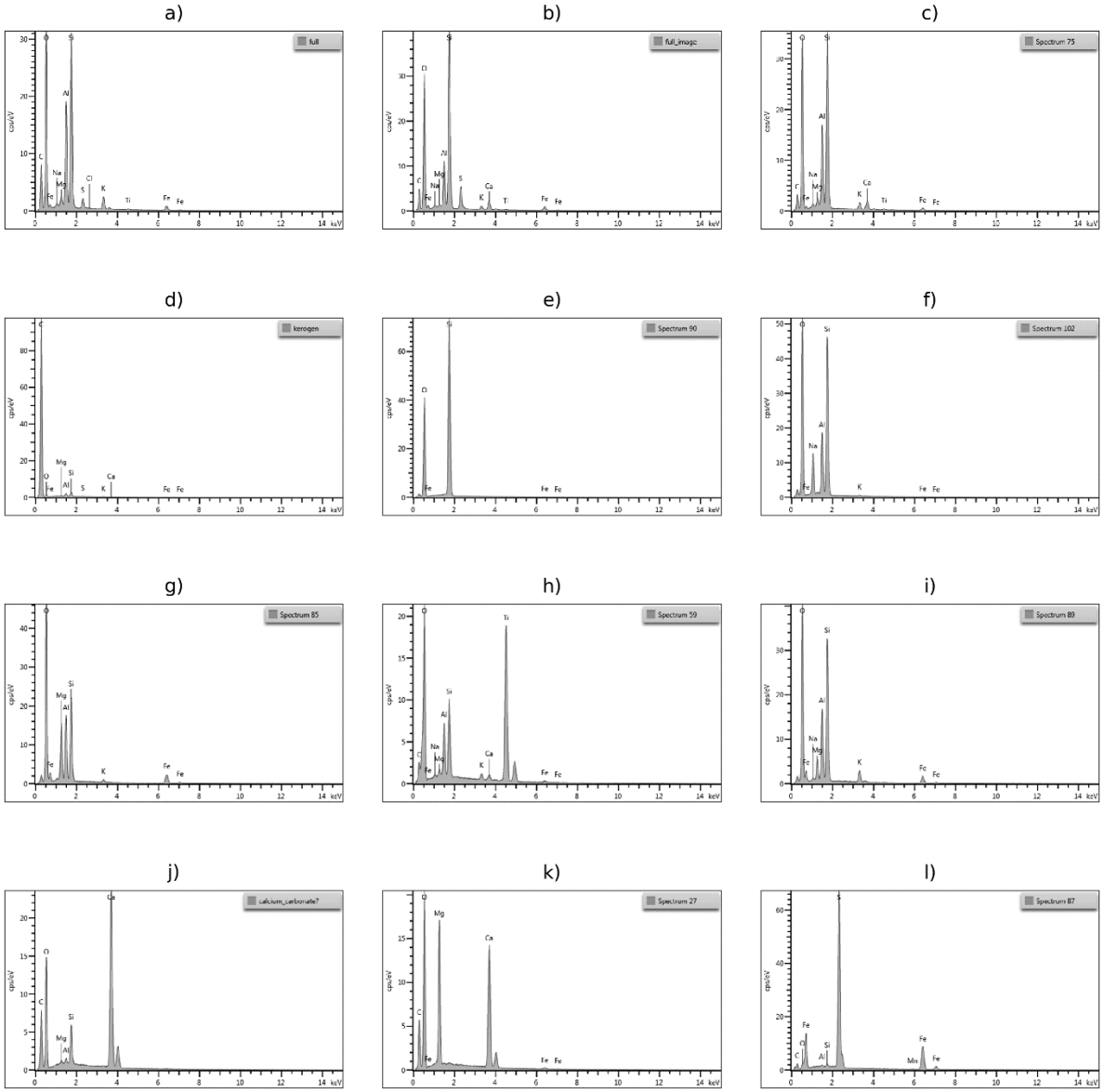

Figure 8-4 EDS Spectra for different chemicals. Subfigures a, b, and c show the full EDS spectra of samples AA114, A153, and AA83A respectively. Subfigures c, d, e, f, g, h, i, j, k, and l show the point EDS spectra for organic matter, quartz, feldspar, illite, illite2, kaolinite, calcite, dolomite, and pyrite, respectively.

Some notable differences from the XRD data were also observed. A single phase of dolomite was identified in sample A153, which was not revealed in the XRD analysis. It was not possible to identify any chlorite phases, despite these being present in the XRD analysis. Another interesting EDS spectra corresponding to Titanium was found in a clay mineral phase – identified as Illite2 in Figure 8-3 and Figure 8-4. Titanium substituted forms have been known to be interspersed in several clay mineral samples (Dolcater et al., 1970). However, this was also not detected in the XRD analysis due to sample heterogenities. Moreover, these individual point discrepancies are also not significant in the EDS spectra obtained for the whole of the SEM image shown in Figure 8-4 - a, b, and c. This suggests that they are relatively minor, constituted by shale heterogeneities at pore scales.

These minor anomalies are not unexpected as the amount of sample considered in SEM analysis is several orders of magnitude smaller than that considered in XRD analysis, which is already relatively small. It is therefore unrealistic to expect perfect agreement on highly heterogeneous shale geochemical characteristics with a relatively small sample set.

8.4 Nitrogen Adsorption

N_2 sorption experiments were carried out on all samples at 77 K using Quantachorme Autosorb iQ. Before characterization, samples were outgassed in-situ at 80 ^oC under vacuum and the grain volume was characterized use He expansion. Results are plotted in Figure 8-5a. They are all predominantly Type II isotherms (Sing, 1985), and exhibit several regions of interest where different pore characteristics could be studied. Type II isotherms are achieved here as the saturation pressure of nitrogen has been achieved during the experiment resulting in complete condensation. For methane isotherms, under supercritical conditions, a similar phenomenon does not exist resulting in Type I isotherms. Sorption at very low partial pressures is controlled by a micropore filling mechanism (Polanyi, 1963), and high initial sorption typically tends to correspond to high micropore volume as monolayer sorption is not sufficient to account for this (Rouquerol et al., 2013). After this comes the

multilayer region where subsequent layers of the adsorbate are deposited on the first. This is modelled using the BET theory (Brunauer et al., 1938). Then comes the capillary condensation region, where mesopores are filled using a capillary condensation mechanism governed by the Kelvin equation (Do, 1998). Mesopore shapes and sizes could be studied by studying the adsorption and hysteresis characteristics in this region (Barrett et al., 1951). Finally, at a relative pressure of 1, complete condensation occurs.

Different levels of initial sorption are observed for different sorbents. The highest monolayer volume is found in the AA114 sample which also has the highest organic content. The lowest monolayer volume is found in sample AA83A with the second-lowest organic content. To quantify the monolayer volume, we need to look further into the multilayer region. For this purpose datapoints between partial pressures of 0.025 and 0.3 are chosen as the multilayering mechanism modelled by the BET theory occurs in this area (Brunauer et al., 1938). Beyond this region, capillary condensation renders the BET theory invalid. In this linear region, however, it is possible to find the fitting constants V_m, corresponding to the monolayer volume, and C, corresponding to the sorption energies. Higher V_m results in larger monolayer sorption, and higher C results in the monolayer capacity being achieved at lower relative pressures (Do, 1998). Good fits are obtained for all samples except AT9 and AA83A, both of which exhibit very low sorption in the multilayer region considered. However, for the sake of reproducibility, the same linear region is used to find the BET surface area for all samples. From the calculated V_m, it was possible to find out the specific surface area by assuming the cross-sectional area of a nitrogen molecule 0.162 nm^2, the Avogadro's number 6.023×10^{23}, and the standard molar volume of an ideal gas 22414 ml.

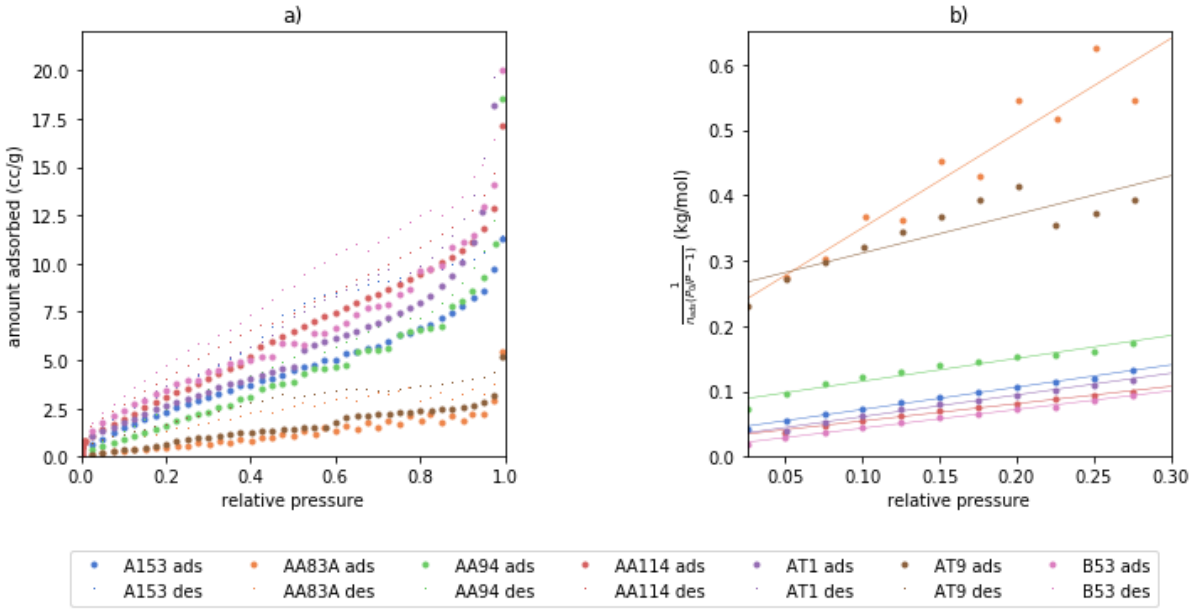

Figure 8-5 N_2 Sorption Isotherms. Subfigure a shows adsorption and desorption isotherms. Subfigure b shows linear fits for the BET isotherm in the multilayer region

Here it is important to acknowledge the limitations of the BET isotherm, which was proposed for a multilayer sorption mechanism for homogeneous solids with energetically identical adsorption sites. The theory further assumes that the heat of sorption remains constant for all subsequent layers beyond the first, which is unrealistic. Whilst it is acknowledged that the BET theory has little physical significance when applied to microporous substances (Weidenthaler, 2011), it is still a widely used yardstick to compare different adsorbent materials objectively (Clarkson and Bustin, 1999; Do, 1998; Llewellyn et al., 2007). This is important as the mathematical complexities and assumptions associated with more complex pore analysis techniques make them less reproducible in different laboratories (Weidenthaler, 2011), and reproducibility is extremely important for heterogeneous shale reservoir characterization (Rezaee, 2015). It has also been shown in the literature that the BET monolayer capacity corresponds to energetically strong retention exhibited by heterogeneous microporous substances (Llewellyn et al., 2007), and is, therefore, an important and reproducible physical yardstick that can be used for comparison. The resulting monolayer volumes obtained from the BET equation are plotted in Figure 8-8 along with other techniques. They are discussed in more detail in the next section.

The shape of the sorption curves beyond the multilayer region is also very interesting. Significant hysteresis is observed for all samples indicating the presence of some mesopores. It is also noted that the shape of the hysteresis curve is horizontal rather than vertical, which suggests that the phenomenon is happening in a slit-shaped pore where higher energies required for the gradual desorption of adsorbed molecules, as compared to cylindrical or bottle-shaped pores, where the entire adsorbate is desorbed once a certain threshold value is reached, leading to a vertical hysteresis region (Sing, 1985). This pore shape is perfectly expected for gas shales which are formed by the geological deposition of mud and organic matter and subsequent compression (Daniel B. Shaw, 1965).

8.5 Pore Characterization

In the previous sections, we looked at the general pore structure and geochemical composition of Bowland shales using XRD, TOC, SEM, EDS, and N_2 adsorption techniques. In this section, all of this data is collated to provide a more complete understanding of the shale pore structure along with the entire pore size distribution and thereby derive summary statistics that are relevant for shale adsorption.

SEM images obtained from the Carl Zeiss Sigma HD are shown in Figure 8-6. These are passed through the watershed image segmentation algorithm to derive a binary image. A threshold value of 70 pixels on a scale of 256 pixels was found to provide a good resolution whilst also sufficiently preserving pore volumes. The opensource image analysis programme OpenCV in Python was used for this purpose (OpenCv, 2014). The resulting images from the watershed algorithm are passed through another segmentation algorithm that plots the prevalence of different pore sizes in the region of interest. Pores are segmented based on their sizes and the resulting prevalence histogram is plotted in 2D in Figure 8-6. The scale of this figure is the same as that of Figure 8-3This was subsequently passed through a counting programme to calculate the pore size distribution from SEM images. The python package PoreSpy, which provides a common interface for several pore network modelling techniques is used for

this purpose (Gostick et al., 2019). However, due to the scale of the SEM images, it was not possible to measure the PSD of these samples.

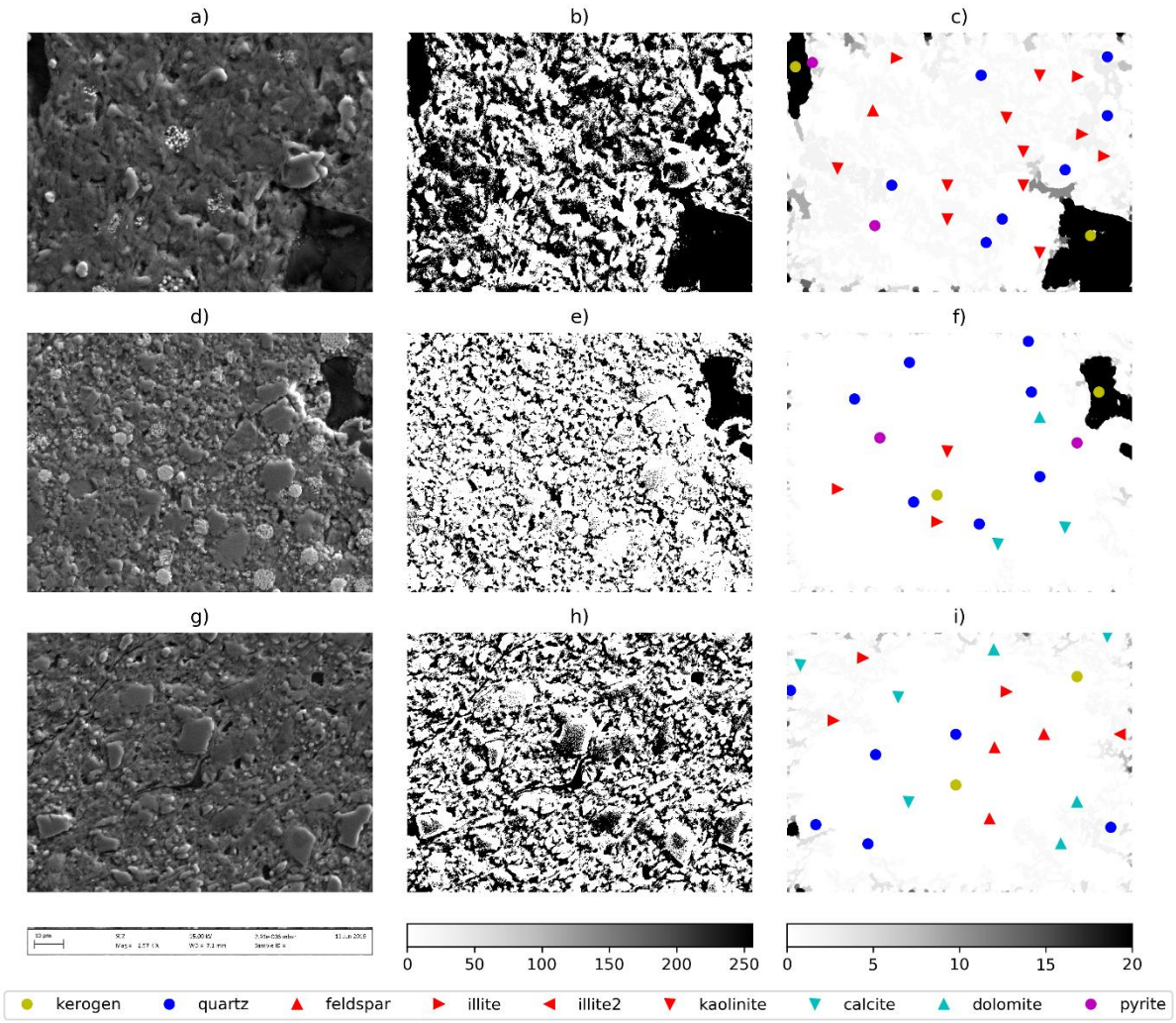

Figure 8-6 SEM Images and pore characteristics. Subfigures a, d, and g show the SEM images of samples AA114, A153, and AA83A respectively. Subfigures b, e, and h, show the segmented images from the watershed algorithm. Subfigures c, f, and i, show the prevalence of various pores in various regions along with the identified mineral phases from EDS analysis.

The results from the above analysis are highly interesting when combined with the EDS data obtained from Oxford Aztec AD and the pore size distribution obtained from Quantachrome Autosorb iQ. It is possible to see that most of the micropores are concentrated in the organic matter region, constituted by kerogens in Figure 8-6. Clay minerals also contribute to the micropores, but not to the same extent as

organic matter. Other chemical phases such as Quartz, Pyrites, Apatities, Calcites, and Dolomites do not contribute to the pore volume. These results are consistent with those observed in the literature (Clarkson and Bustin, 1999; Daniel B. Shaw, 1965; Gross et al., 2015). Nevertheless, it is still interesting to see how significantly organic matter contributes to the surface area available for adsorption in shales through the combination of different experimental techniques.

The N_2 isotherms shown in Figure 8-5 were analysed using BJH and DFT methods to derive insights on pore characteristics. This was done in the Autosorb iQ software provided with the rig. Performing analysis in the rig improved reproducibility as the pore size distribution algorithms, especially the DFT theory, are highly complex.

To derive pore characteristics from the BJH, the desorption arm of the isotherm is used. The data points between relative pressures 0.4-0.967 are considered. The equation describing capillary condensation phenomenon in slit-shaped mesopores is minimized iteratively and pore sizes are calculated. The results are plotted in Figure 8-7. Based on BJH analysis, the shales were predicted to be predominantly microporous. However, this is not in line with the hysteresis phenomena observed in N_2 isotherms. The tendency of the BJH method to underpredict mesopores for microporous substances has been discussed in the literature (Weidenthaler, 2011). Others have attributed the limitations of the BJH method for microporous substances to its inabilities to address various physical effects associated with physisorption such as tensile strength, pore network effects etc. (Bardestani et al., 2019). Also, owing to limitations in the physics of capillary condensation, the BJH method does not consider pore sizes above 60 nm (Barrett et al., 1951). This also partly explains the observed underprediction of mesopores.

Based on the pore size distribution calculated, the specific surface area and the micropore volume were also estimated using the BJH method. These are plotted in Figure 8-8. In general, higher surface area and pore volume were estimated compared to the BET method and severely overpredicts both parameters compared to the DFT method.

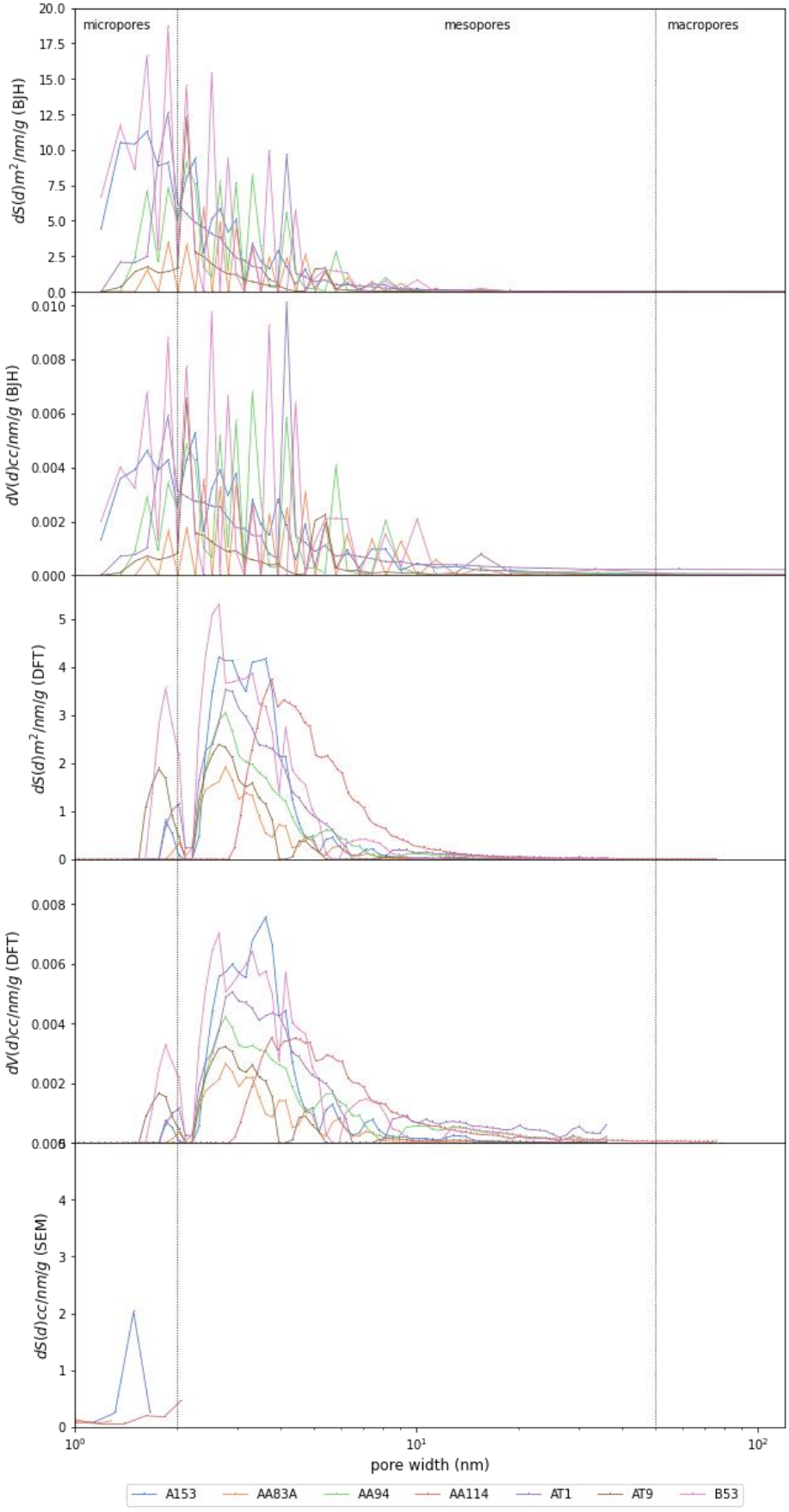

Figure 8-7 PSD of Bowland shales calculated from different techniques.

The DFT method is generally recommended for the pore size analysis of mesoporous substances (Bardestani et al., 2019; Landers et al., 2013; Seaton et al., 1989; Weidenthaler, 2011). This technique minimizes the grand potential of the fluid in the adsorption space using the Non-Linear Density Functional Theory (Landers et al., 2013). However, the accuracy of this technique is highly dependent on the adsorbent-adsorbate interactions assumed (Bardestani et al., 2019). Thankfully, the Autosorb iQ software is well equipped with the Steele equation to deal with slit-shaped carbonaceous pores of gas shales (Bardestani et al., 2019; Steele, 1973).

Here it is also important to note that there exists a more sophisticated form of the Density Function Theory that accounts for surface heterogeneities known as the Quenched Solid Density Function Theory (Neimark et al., 2009). However, in the interest of balancing reproducibility and accuracy, the Non-Linear Density Functional Theory is preferred in this study.

The pore size distribution estimated using the NLDFT theory is plotted in Figure 8-7. The summary pore characteristics are plotted in Figure 8-8 along with other techniques. The surface area of the Bowland shales are much lower compared to other microporous substances, but are comparable or even higher than many other shale plays (Do, 1998; Kuila and Prasad, 2013). For comparison, the shales considered in this study exhibited a median surface area of about 12 m^2/g for sample A153. The calculated BET surface area for activated carbons is about 1200 m^2/g (Do, 1998). And the specific surface area of Woodford shales in the literature is about 2 m^2/g, and that of North Sea shales which are also from a geologic extension of the play as considered here is about 9 m^2/g (Kuila and Prasad, 2013). Whilst the median micropore volume reported in this study is about 0.02 cc/g, the micropore volumes of activated carbons are in the range of 0.45 cc/g (Do, 1998); the micropore volume of Woodford shales is much lower than those of Bowland shales (Kuila and Prasad, 2013). This provides further corroboration to the accuracy of these results for further analysis in subsequent sections.

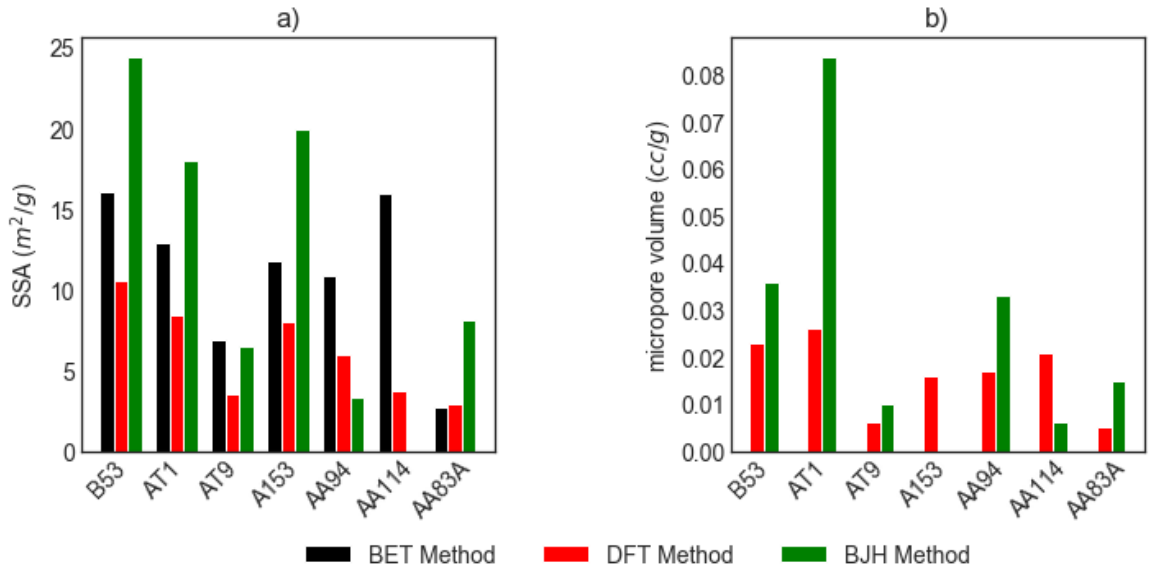

Figure 8-8 Pore Characteristics of Bowland Shale Samples. Subfigure a represents the surface area and Subfigure b represents the micropore volume

It is noted that that pore size distribution of shales was also calculated using an image analysis technique from SEM images. However, this did not provide a good correlation with the far better pore characterization techniques from adsorption, partly due to the extremely small sample size and partly due to the limitation of the image segmentation algorithm itself. However, it is still useful to visualize the pore characteristics to the shale geochemical composition and therefore included in this study in Figure 8-7.

A good correlation between the shale geochemical characteristics and the pore characteristics is also observed. Sample A153 seems to exhibit a significant amount of micropore and mesopore volume based on both DFT and BJH analyses. Sample B53 also exhibits a significant pore volume possibly contribute to by clay minerals. Sample AA83A exhibit pore surface area and pore volumes on the lower end of the spectrum in both DFT and BJH analyses. This is expected given that it has a very low TOC content. Sample AA114 with a TOC over 6% seems to have a very high SSA. However, the BET method also predicted a very high SSA for B53 which has a low TOC. In general, a higher TOC corresponds to a higher SSA and micropore volume except for Sample B53.

8.6 Methane and Carbon Dioxide Adsorption

High-pressure methane and carbon dioxide isotherms were measured on Bowland shale samples. The detailed experimental technique for this was already discussed in the previous chapter. However, certain changes were made during the characterization of Bowland shales. A smaller sample size was used to achieve faster equilibrium. Samples were crushed to a sieve size of between 120 and 300 μm. This allowed equilibrium to be reached in less than 2 hours for a single pressure step. But on the flip side, the signal from late time analysis was not sufficient to measure gas permeability.

After crushing, the samples were prepared similarly as in the previous chapter, with treatment with Toluene and water. They were then outgassed in situ at about 80 °C and 140 Torr pressure overnight. Grain volumes were calculated based on He expansion as 0.46 ml/g, 0.5 ml/g, and 0.4 ml/g, for samples A153, AA83A, and AA114, respectively. Methane and carbon dioxide adsorption isotherms were calculated using a step-wise procedure. Experimentally measured excess sorption was converted into absolute sorption assuming a surface coverage mechanism. Adsorbed phase density was assumed as 2630 mol/m^{3}for methane and 2110 mol/m^3 for carbon dioxide, respectively (Pini, 2014). Results are displayed in Figure 8-9. Isotherms up to 60 bars are mostly linear. These values are also within the range of methane adsorption values on Bowland shales reported in the literature (Clarke et al., 2018). Although monolayer sorption was not achieved for any of these samples, it is possible to see some bending of datapoints at higher pressures suggesting that monolayer adsorption might be achieved at higher pressures as reported in recent literature (Whitelaw et al., 2019). All three samples exhibit significantly higher adsorption capacity for carbon dioxide as compared to methane. Adsorption capacities for AA114 were found to be the highest, given that it has the highest TOC. AA83A exhibited the lowest sorption capacity.

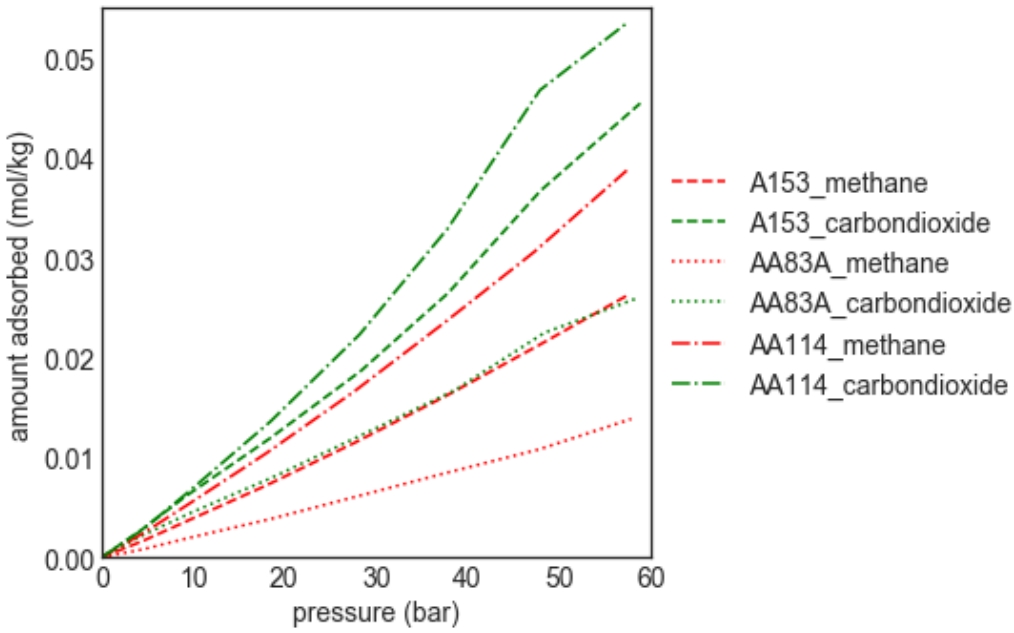

Figure 8-9 Methane and Carbon dioxide Adsorption Isotherms on Bowland Shale Samples

It is interesting to note that there are other mechanisms besides sorption, solution, and capillary force by which carbon dioxide is stored in shales (Liu et al., 2020). Mineralization of various shale geochemical components in the presence of carbon dioxide is an area of active research (Romanov et al., 2015). However, these reactions typically occur at supercritical conditions (Liu et al., 2020). But this was not achieved in the current study. Some studies have also reported the existence of negative sorption isotherms for carbon dioxide at supercritical conditions (Krooss et al., 2002). However, in this study it was possible to achieve repeatable adsorption isotherms for carbon dioxide and methane, suggesting that mineral storage did not occur at experimental conditions. Nevertheless, it is an important enough phenomenon to deserve mention here.

8.7 Methane and Carbon Dioxide Diffusion

Rate based diffusion characterization methods are preferred over Fick's law-based methods in this study. This is because, here we are trying to characterize the overall diffusion to geochemistry, and

therefore are not interested in the concentration profile of the adsorbate within the shale micropores. Further, as smaller sieve sizes were used for adsorption characterization, it was not possible to achieve a good enough signal for late time characterization using methods based on Fick's laws (Profice et al., 2012).

Figure 8-10 plots the amount adsorbed vs time for sample different isotherms. Equilibrium was achieved within 1-2 hours for most pressure steps. In general, second-order fits provided a better fit to first-order fits except for a few pressure steps for sample AA114. It is also possible to see the pressure transducer effect in the first few seconds of every pressure step. However, from Figure 8-11, it was not possible to derive any trends from the first and second-order rate constants fit experimental data at different pressures. It is noted that no relation could be observed between pressure and kinetics. This is in line with the results from the previous chapter where we noted that adsorption is dependent on adsorption uptake and not adsorption. Since the isotherms here are linear, it is expected that there would be no relation between loading and kinetics. The high variance is attributed to the variation in sample size. Since the amount of samples available for Bowland shales were much smaller, the variation in sieve size was larger, subsequently affecting adsorption kinetics. Impact of geochemistry and pore structure on rate based diffusion constants is discussed in the next section.

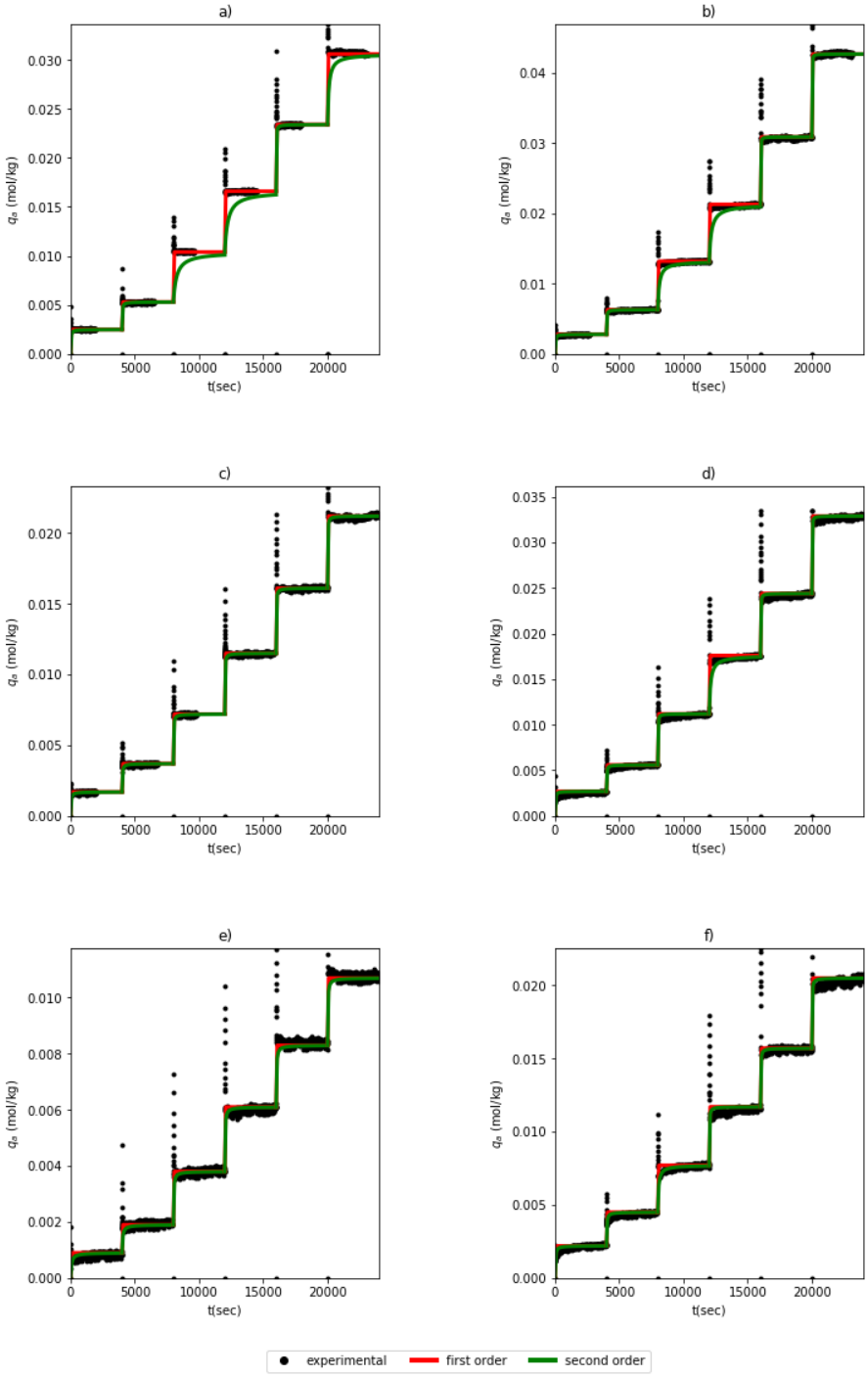

Figure 8-10 Diffusion fits for different isotherms. Subfigures a, c, and e represent methane isotherms for samples AA114, A153, and AA83A. Subfigures b, d, and f represent carbon dioxide isotherms for samples AA114, A153, and AA83A.

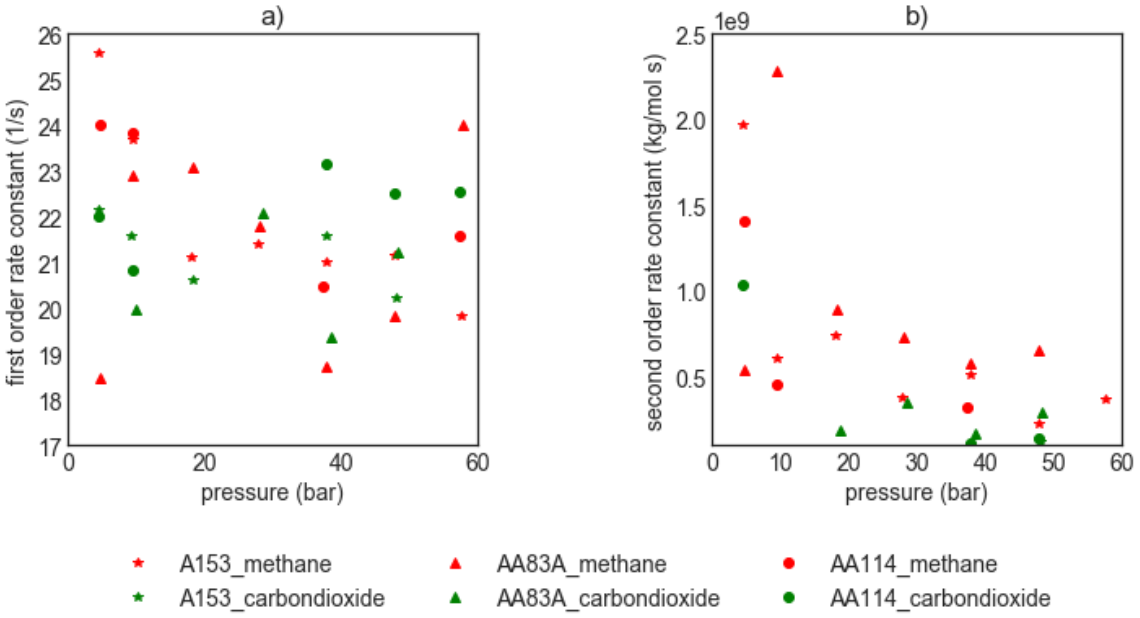

Figure 8-11 First and second-order rate constants for adsorption in Bowland shale samples.

8.8 Discussion

The correlation matrices for pore characteristics of various shales and their geochemical concentration is shown in Figure 8-12. Despite the relatively small sample size, it is possible to see that pore characteristics are in general positively correlated with TOC and clay mineral content, and negatively correlated with carbonates and other minerals. This is in line with the data available in the literature (Clarkson and Bustin, 1999), and also with the results derived in the previous section of this study. These results suggest that shales with high amounts of TOC and Clay mineral content could be good candidates for both methane extraction and carbon dioxide sequestration. However, carbonate minerals and other minerals have a negative correlation with surface area and micropore volume. This can be compared to Figure 8-6 where it was noted visually that both surface area and micropore volume were highly correlated with kerogen and clay mineral content.

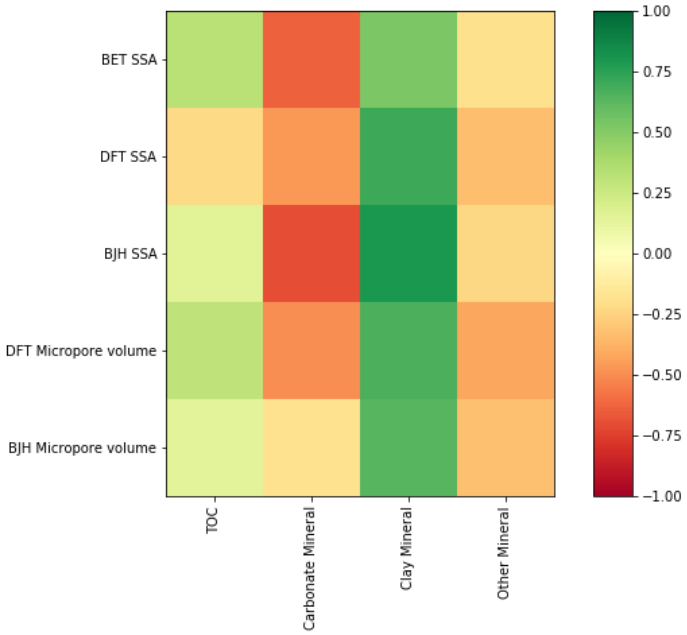

Figure 8-12 Correlation matrix for shale pore characteristics and composition

The correlation between adsorption and diffusion characteristics, and the shale's pore and geochemical characteristics were also calculated using linear regression. The mean diffusion characteristics for both first-order and second-order kinetics are considered. Also, the linear regression coefficient obtained from fitting the sorption points is used as the adsorption fit. These are plotted in Figure 8-13. It is possible to see that good correlation are obtained between a shale's sorption and diffusion metrics, and it's TOC, clay mineral, surface area, and micropore volume. It is also interesting to note that kerogens contribute to adsorption and diffusion in shales more than clay minerals. However, there are some unexpected results largely due to the small sample size considered in this study. For example, a strong positive correlation between (other minerals) pyrite and sorption capacity is observed. However, this is mostly because pyrites content seems to correlate with TOC content for the small sample set considered here. In our literature search, it was not possible to find any correlations between a shale's pyrite content and TOC content. Therefore, this trend is not expected to be valid for a larger sample set, although further research is necessary in this regard. It can also be seen that negative correlations are obtained for the pore metrics obtained by the BJH method, due to its tendency to overpredict surface area and micropore volume.

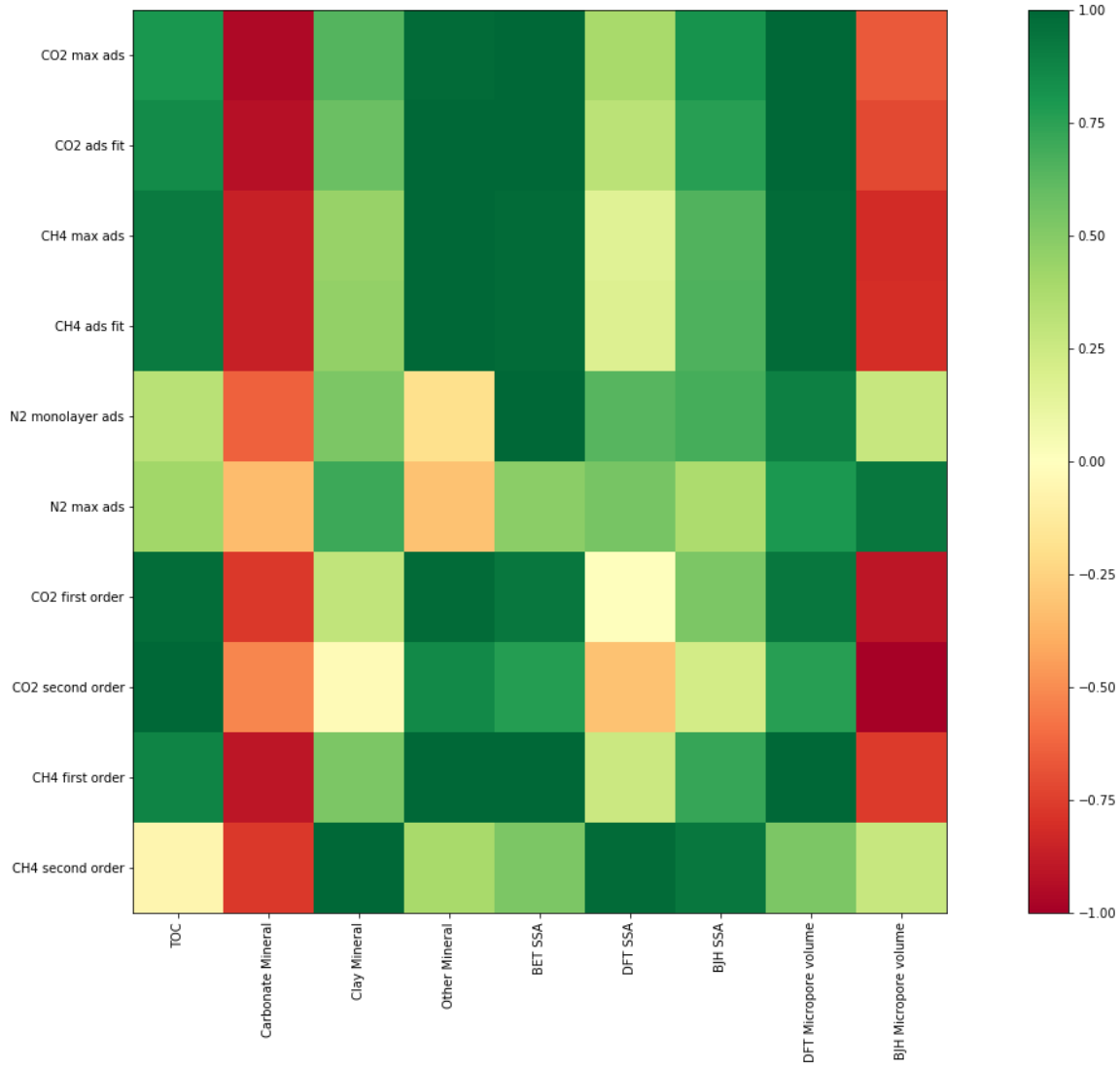

Figure 8-13 Geochemistry and pore structure sensitivity on adsorption

It is further interesting to note that kerogen and clay minerals contribute to adsorption differently in shales. Whilst kerogen sorption is largely contributed by van der Waals forces and its large surface area (Psarras et al., 2017), sorption on clay minerals is also dependent on its interlayer cations which react differently to different adsorbents (Zhang et al., 2016). That said, we also need to keep in mind that high sorption content need not necessarily translate into higher reserves as shown in Chapter 3, due to sorption decreasing the effective diffusivity of shales. It is also interesting to note that no correlation could be established between the shale's mineralogical content and it's formation. This is because shales are highly heterogeneous on the pore, core, and field scales (Rezaee, 2015).

8.9 Conclusion

Shale geochemistry and pore structure play a very important role in their sorption and diffusion characteristics. These trends were demonstrated using a variety of experimental techniques that focus on elemental analysis, pore characterization, and adsorption characterization.

For further research, it would be very useful to extract individual elements from a gas shale to characterize sorption on each of those. Also, whilst the effects of kerogen and clay minerals on methane and carbon dioxide storage mechanism in shales has been widely researched, there is still very little data on the importance of other minerals such as pyrite and apatite on gas storage mechanisms in shales. Given that these minerals only occur in smaller amounts, their role can only be studied accurately in isolation.

8.10 References

Bardestani, R., Patience, G.S., Kaliaguine, S., 2019. Experimental methods in chemical engineering: specific surface area and pore size distribution measurements—BET, BJH, and DFT. Can. J. Chem. Eng.

Barrett, E.P., Joyner, L.G., Halenda, P.P., 1951. The determination of pore volume and area distributions in porous substances. I. Computations from nitrogen isotherms. J. Am. Chem. Soc. 73, 373–380.

Brunauer, S., Emmett, P.H., Teller, E., 1938. Adsorption of gases in multimolecular layers. J. Am. Chem. Soc. 60, 309–319.

Caineng, Z., Dazhong, D., Shejiao, W., Jianzhong, L., Xinjing, L., Yuman, W., Denghua, L., Keming, C., 2010. Geological characteristics and resource potential of shale gas in China.

Clarke, H., Turner, P., Bustin, R.M., Riley, N., Besly, B., 2018. Shale gas resources of the Bowland Basin, NW England: a holistic study. Pet. Geosci. 24, 287–322.

Clarkson, C.R., Bustin, R.M., 1999. The effect of pore structure and gas pressure upon the transport properties of coal: a laboratory and modeling study. 1. Isotherms and pore volume distributions. Fuel 78, 1333–1344.

Dai, J., Zou, C., Liao, S., Dong, D., Ni, Y., Huang, J., Wu, W., Gong, D., Huang, S., Hu, G., 2014. Geochemistry of the extremely high thermal maturity Longmaxi shale gas, southern Sichuan Basin. Org. Geochem. 74, 3–12.

Daniel B. Shaw, C.E.W., 1965. The Mineralogical Composition of Shales. SEPM J. Sediment. Res. Vol. 35, 213–222.

Do, D.D., 1998. Adsorption Analysis: Equilibria And Kinetics: (With CD Containing Computer Matlab Programs).

Dolcater, D.L., Syers, J.K., Jackson, M.L., 1970. Titanium as free oxide and substituted forms in kaolinites and other soil minerals. Clays Clay Miner.

Gostick, J., Khan, Z., Tranter, T., Kok, M., Agnaou, M., Sadeghi, M., Jervis, R., 2019. PoreSpy: A Python Toolkit for Quantitative Analysis of Porous Media Images. J. Open Source Softw.

Gross, D., Sachsenhofer, R.F., Bechtel, A., Pytlak, L., Rupprecht, B., Wegerer, E., 2015. Organic geochemistry of Mississippian shales (Bowland Shale Formation) in central Britain: Implications for depositional environment, source rock and gas shale potential. Mar. Pet. Geol. 59, 1–21.

Heller, R., Zoback, M., 2014. Adsorption of methane and carbon dioxide on gas shale and pure mineral samples. J. Unconv. Oil Gas Resour. 8, 14–24.

Kenneth P. Severin, 2004. Energy Dispersive Spectrometry of Common Rock Forming Minerals, Energy Dispersive Spectrometry of Common Rock Forming Minerals.

Krooss, B.. M. v, van Bergen, F., Gensterblum, Y., Siemons, N., Pagnier, H.J.. J.M., David, P., 2002. High-pressure methane and carbon dioxide adsorption on dry and moisture-equilibrated Pennsylvanian coals. Int. J. Coal Geol. 51, 69–92.

Kuila, U., Prasad, M., 2013. Specific surface area and pore-size distribution in clays and shales, Geophysical Prospecting.

Landers, J., Gor, G.Y., Neimark, A. V, Yu Gor, G., Neimark, A. V, 2013. Density functional theory methods for characterization of porous materials. Aspects 437, 3–32.

Liu, C., Sang, S., Fan, X., Zhang, K., Song, F., Cui, X., Wang, H., 2020. Influences of pressures and temperatures on pore structures of different rank coals during CO2 geological storage process. Fuel 259, 116273.

Llewellyn, P.L., Rodriquez-Reinoso, F., Rouqerol, J., Seaton, N., 2007. Is the BET equation applicable to microporous adsorbents? Stud. Surf. Sci. Catal. 160, 49.

Neimark, A. V., Lin, Y., Ravikovitch, P.I., Thommes, M., 2009. Quenched solid density functional theory and pore size analysis of micro-mesoporous carbons. Carbon N. Y.

OpenCv, 2014. OpenCV Library. OpenCV Website.

Pini, R., 2014. Interpretation of net and excess adsorption isotherms in microporous adsorbents. Microporous Mesoporous Mater. 187, 40–52.

Polanyi, M., 1963. The potential theory of adsorption. Science (80-.). 141, 1010–1013.

Profice, S., Lasseux, D., Jannot, Y., Jebara, N., Hamon, G., 2012. Permeability, Porosity and Klinkenberg Coefficient Determination on Crushed Porous Media. Petrophysics 53.

Psarras, P., Holmes, R., Vishal, V., Wilcox, J., 2017. Methane and CO2 Adsorption Capacities of Kerogen in the Eagle Ford Shale from Molecular Simulation. Acc. Chem. Res. 50, 1818–1828.

Rezaee, R., 2015. Fundamentals of gas shale reservoirs. John Wiley & Sons.

Romanov, V., Soong, Y., Carney, C., Rush, G.E., Nielsen, B., O'Connor, W., 2015. Mineralization of Carbon Dioxide: A Literature Review. ChemBioEng Rev. 2, 231–256.

Romero, A.M., Philp, R.P., 2012. Organic geochemistry of the Woodford Shale, southeastern Oklahoma: How variable can shales be? Am. Assoc. Pet. Geol. Bull. 96, 493–517.

Ross, D.J.K., Marc Bustin, R., 2009. The importance of shale composition and pore structure upon gas storage potential of shale gas reservoirs. Mar. Pet. Geol. 26, 916–927.

Rouquerol, J., Rouquerol, F., Llewellyn, P., Maurin, G., Sing, K.S.W., 2013. Adsorption by powders and porous solids: principles, methodology and applications. Academic press.

Seaton, N.A., Walton, J.P.R.B., quirke, N., 1989. A new analysis method for the determination of the pore size distribution of porous carbons from nitrogen adsorption measurements. Carbon N. Y.

Sing, K.S.W., 1985. Reporting physisorption data for gas/solid systems with special reference to the determination of surface area and porosity (Recommendations 1984). Pure Appl. Chem. 57, 603–619.

Steele, W.A., 1973. The physical interaction of gases with crystalline solids. I. Gas-solid energies and properties of isolated adsorbed atoms. Surf. Sci.

Weidenthaler, C., 2011. Pitfalls in the characterization of nanoporous and nanosized materials. Nanoscale.

Whitelaw, P., Uguna, C.N., Stevens, L.A., Meredith, W., Snape, C.E., Vane, C.H., Moss-Hayes, V., Carr, A.D., 2019. Shale gas reserve evaluation by laboratory pyrolysis and gas holding capacity consistent with field data. Nat. Commun. 10, 3659.

Zhang, J., Clennell, M.B., Liu, K., Pervukhina, M., Chen, G., Dewhurst, D.N., 2016. Methane and Carbon Dioxide Adsorption on Illite. Energy and Fuels 30, 10643–10652.

9 Carbon Dioxide Sequestration and in Gas Shales

9.1 Introduction

Several pathways for limiting global warming have been identified to include Carbon Capture and Storage (Mathieu, 2006). Shales typically exhibit a much higher adsorption capacity towards carbon dioxide as compared to Methane (Busch et al., 2008). This suggests that shales could also be considered as a potential reservoir for carbon sequestration. However, gas shales are capable of trapping carbon dioxide through adsorption in addition to the solution and capillary traps (Liu et al., 2013; Nuttall et al., 2005). This phenomenon is still not well understood and deserves further investigation.

It is now well understood that most of the sorbed gas is left behind in the reservoir after primary recovery (Yu et al., 2014). This is explained by the shape of the adsorption isotherms in gas shales which typically follows Type I isotherms (Heller and Zoback, 2014; Rouquerol et al., 2016). That said, this phenomenon could assist in the storage of carbon dioxide trapping larger amounts of sorbed carbon dioxide at lower partial pressures, significantly contributing to the shale's carbon sequestration potential. However, given the importance of this phenomenon, further study is warranted in the context of how sorption affects actual carbon dioxide sequestration mechanisms in the reservoir. Impact of carbon dioxide injection on enhanced recovery has also been investigated with mixed results (Lillies and King, 1982; Liu et al., 2013). This phenomenon also warrants further investigation.

This study presents methane and carbon dioxide isotherms on Lothian shales at 45 ^{o}C. The study then measures multi-component adsorption and uses the Ideal Adsorbed Solution Theory to predict multi-component isotherms at different pressures and concentrations. The adsorption data is then integrated into a Finite Element reservoir simulation in COMSOL that allows us to study the behaviour of these fluids in a 2D system, with particular emphasis on the impact of sorption for carbon dioxide sequestration and enhanced hydrocarbon recovery. The choice of units in this chapter and in other

chapters reflect the choice of units currently used in the shale adsorption literature for easy comparability (Pini, 2014; Rouquerol et al., 1994).

9.2 Adsorption Characterization

Adsorption measurements were carried out in the manometric rig shown in Chapter 3. The Lothian sample was also preferred in this study. This was preferred over the Bowland sample as having a smaller Langmuir pressure, it achieved monolayer volume at lower loading, allowing us to derive further insights on the importance of sorption on gas shale reservoir characterization. However, smaller particle size was used in this study – of sieve size 300 μm. This allowed faster equilibrium times. The same manometric adsorption measurement methodology was used for both methane and carbon dioxide adsorption measurement. For multi-component adsorption, elemental analysis using GC-FID was combined with manometric adsorption results to predict methane and carbon dioxide isotherms. The Langmuir isotherm found to provide a good fit for both sorption and sorption uptake is used for pure component isotherms. Multi-component isotherms are predicted using the Ideal Adsorbed Solution Theory. Gas-phase density was calculated using the open-source CoolProp library which is comparable to the NIST's RefProp library (Bell et al., 2014). Adsorbed phase density was assumed to be equal to the liquid density at the critical point (Pini, 2014). This is a fair assumption in the absence of experimentally measured adsorbed phase densities at extremely high pressures (Do et al., 2010).

Figure 9-1 plots experimental pressures observed during the characterization of methane and carbon dioxide isotherms in the adsorption measurement rig. Carbon dioxide adsorption isotherms required longer equilibrium times as compared to methane isotherms. Other researchers have also observed a similar phenomenon (Heller and Zoback, 2014), and this phenomenon is following insights derived from Chapter 4. Carbon dioxide with higher adsorption uptakes needed longer equilibrium times. Since smaller particle sizes were used in this study, nearly 1 to 2 hours were required for equilibrium for each pressure step on average, with the entire isotherm requiring nearly a day as shown in Figure 9-1. The

adsorbed phase density of methane and carbon dioxide were assumed to be 26300 mol/m^3 and 21100 mol/m^3 respectively (Pini, 2014). The complete methodology used to measure adsorption in manometric rigs is outlined in Chapter 3.

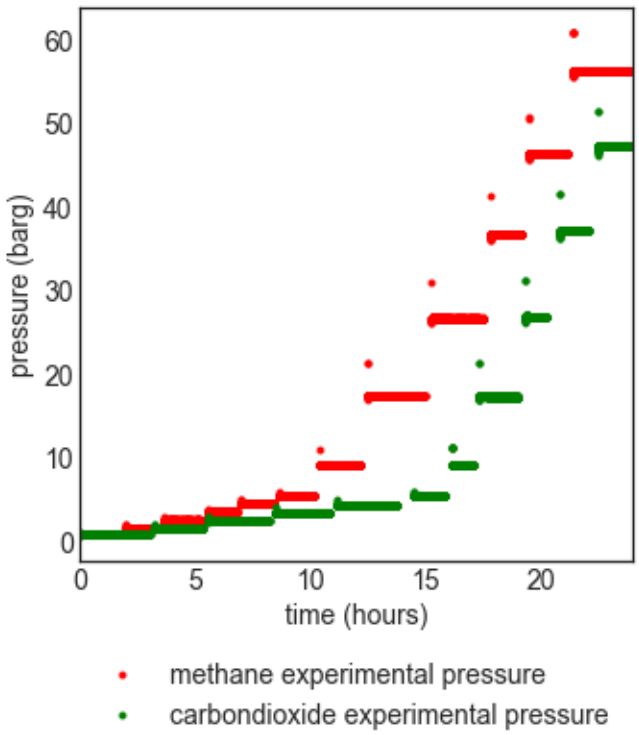

Figure 9-1 Experimental pressures

From pressure profiles recorded over time, it is possible to calculate the number of moles of the adsorptive that has been injected into the rig, and also the number of moles of the adsorptive that is currently present in the gas phase. This gives the difference in the distribution of the adsorptive molecules between the gas phase and the adsorbed phase at any given point. This was corrected to absolute adsorption by assuming a constant adsorbed phase density. By accounting for the adsorptive molecules that are initially present in the adsorbed phase, and therefore not measured by the rig, we obtain the absolute adsorption of the system. Resulting isotherms are plotted in Figure 9-2. The experiment was repeated twice without any change in the calculated adsorption. Carbon dioxide has a significantly higher adsorption capacity with a Langmuir volume of 0.41 mol/kg. Methane isotherm had a Langmuir volume of 0.36 mol/kg. Langmuir affinity constants for carbon dioxide and methane

were found to be 1.11 × 10^{-3} m^3/mol and 5.91 × 10^{-4} m^3/mol. The Langmuir isotherm provides an excellent fit to the experimental data up to 60 bars.

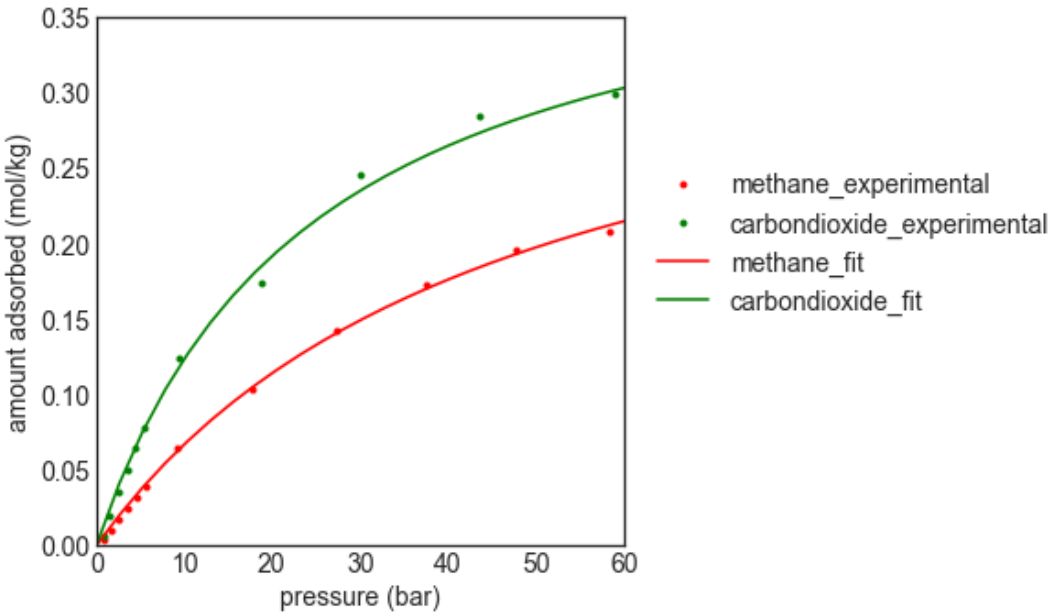

Figure 9-2 High-pressure single component adsorption isotherms

To measure multi-component adsorption, it was necessary to combine manometric adsorption measurement with an elemental analysis of the gas phase (Talu, 1998). As the gas phase had to be sampled before and after each pressure step, it was not possible to measure adsorption sequentially, and each pressure step was carried out as an individual experiment. To make up gases accurately, first methane was injected into the sample cell and allowed to reach equilibrium. Subsequently, carbon dioxide was injected into the reference cell and the valve connecting cells is opened.

GC-FID calibration was performed using standard gas samples made up in the laboratory. A column of length 250 m and 0.47 mm ID was packed with Shincarbon is known to provide excellent separation for hydrocarbons (Wang et al., 2019). The characterization time was about 16 minutes as shown in Figure 9-3. The spool temperature was maintained at 200 °C with a split injection mode. The helium carrier gas was used with pressure control at 230 kPa. The column was maintained at 30 °C with a max

temperature of 270 °C. The FID detector was maintained at 280 °C with a sampling rate of 40 msec. Nitrogen was used as a makeup gas with a flow of 30 ml/min, H2 flow was maintained at 30 ml/min, and airflow was maintained at 400 ml/min. Methane peaks were obtained at around 2 minutes. The area under the curve was calculated to find out the methane content of the mixture. Carbon dioxide content was then calculated using mass balance. The resulting calibration curve is plotted in Figure 9-4.

For adsorption experiments, the gas was made up using the same procedure and sampled. Then the sample is inserted into the reference cell, and another sample is collected after equilibrium. Using the pressure data and the elemental composition obtained from GC-FID measurements, it was possible to calculate multicomponent adsorption isotherms shown in Figure 9-5.

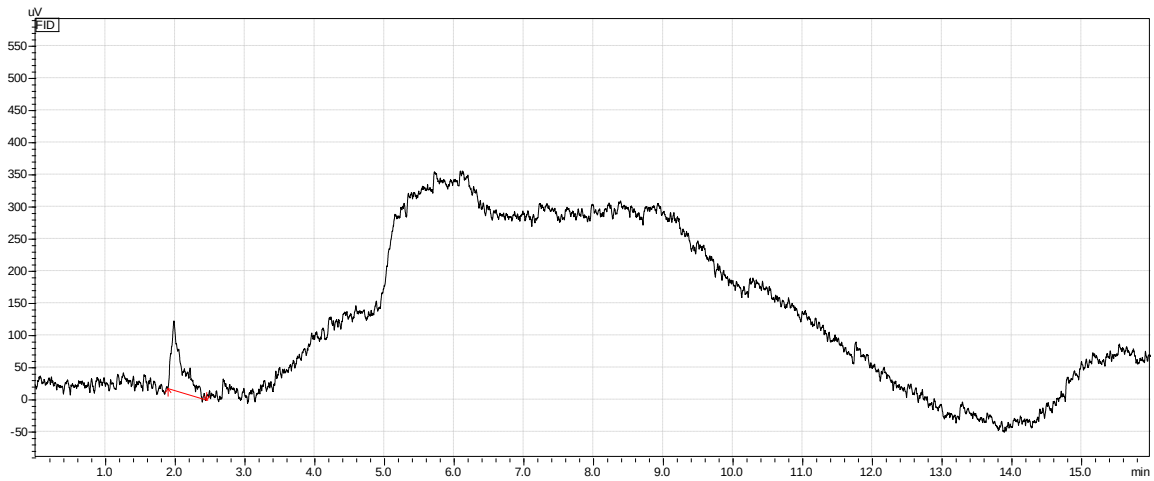

Figure 9-3 Sample GC-FID curve μV vs time (min)

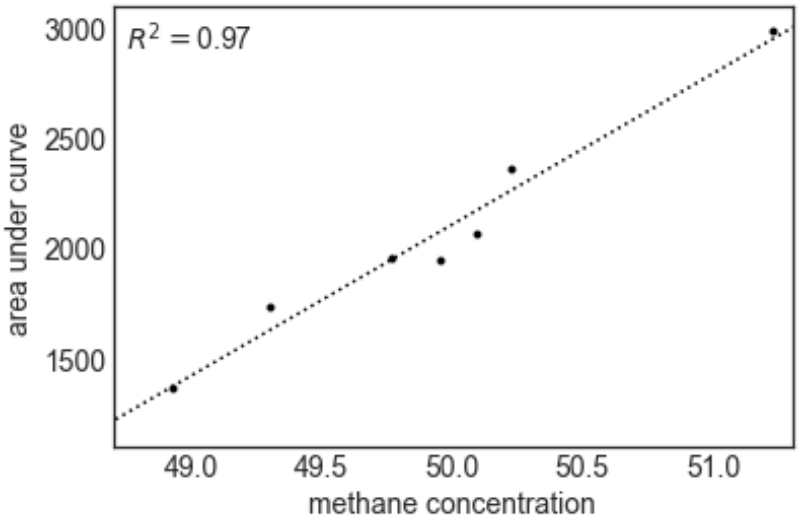

Figure 9-4 GC FID calibration curve

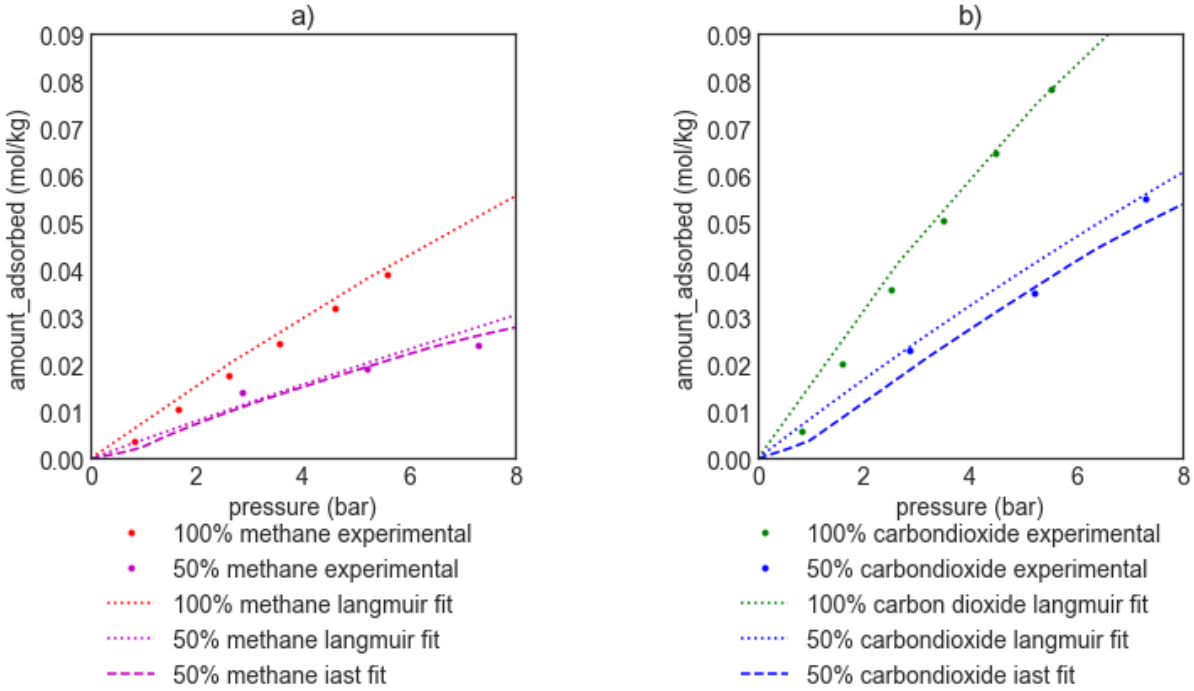

Figure 9-5 Langmuir and IAST Fits experimental measurements

Although it was not possible to repeat these experiments owing to time constraints to provide further verification on reproducibility and accuracy, both the IAST and Extended Langmuir isotherms provide

a good fit to the experimental data at pressures below 6 bars. This is in line with the observed trend in the literature suggesting that these measurements are fairly accurate (Walton and Sholl, 2015). Whilst fitting IAST models, an interpolation isotherm was preferred over the Langmuir isotherm as this has been shown to provide more accurate results for systems with many data points for pure component isotherms (Simon et al., 2016). Due to long periods required for experimental setup and sample analysis, it was not possible to provide more data points for multi-component isotherms. However, the IAST has routinely be used in the literature to predict multi-component isotherms in the absence of experimental results (Simon et al., 2016). That said, it is important here to mention the limitations of IAST. The IAST does not consider the mixture properties of the adsorptive molecules (Laskar and Hashisho, 2020). When considered along with the numerical complications associated with the model make the Extended Langmuir model the preferred choice to account for sorption in this study despite it's limitations. It must also be noted that the Extended Langmuir equation predicts a constant selectivity across the entire concentration range and is therefore not thermodynamically consistent (Myers and Prausnitz, 1965). Whilst the Ideal Adsorbed Solution Theory has consistent thermodynamic selectivity, it does not have a provision for calculating adsorption uptakes (Do, 1998). Therefore it is not suitable for several aspects of shale reservoir characterization where it is essential to model sorption uptake (Profice et al., 2012).

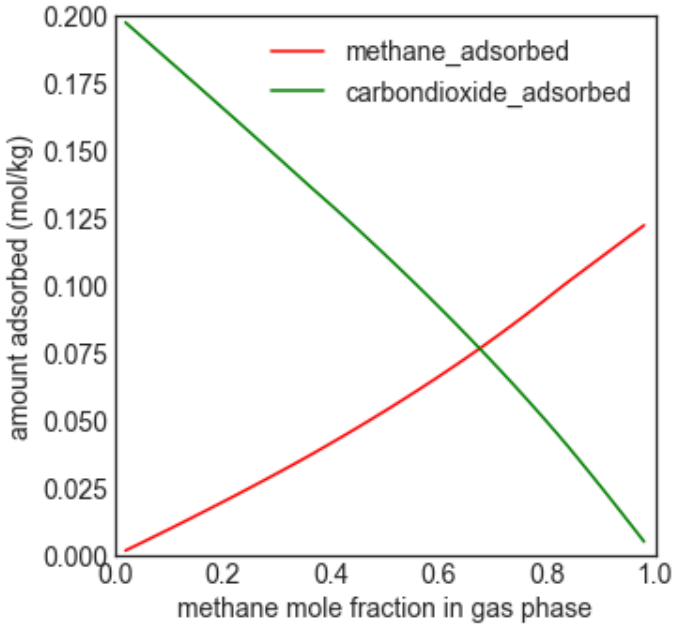

Figure 9-6 Predicted IAST isobars at 23 bars for different concentrations

Multi-component adsorption behaviour predicted using the IAST in Python is plotted in Figure 9-7. As there are significant numerical challenges associated with implementing certain isotherms in IAST, multi-component isotherms were calculated using interpolation isotherms as recommended in the literature (Simon et al., 2016). This reduces any model uncertainties used for single component isotherms. Multi-component adsorption closely resembles single component adsorption behaviour. It can also be seen from Figure 9-6 that carbon dioxide sorption is predicted to increase at a much higher rate with for lower carbon dioxide concentrations as compared to methane. This nonlinear behaviour of adsorptive selectivity is well documented in the literature (Myers and Prausnitz, 1965). However, the literature for gas shale reservoir characterization usually prefers the Extended Langmuir equation for sorption characterization due to its ability to model adsorption uptakes (Heller and Zoback, 2014; Liu et al., 2013). This has significant implications particularly for carbon dioxide sequestration and enhanced recovery where carbon dioxide mole fraction is expected to be much lower than the native methane. Predicting a constant selectivity in this scenario would underpredict the carbon dioxide sequestration potential of the reservoir.

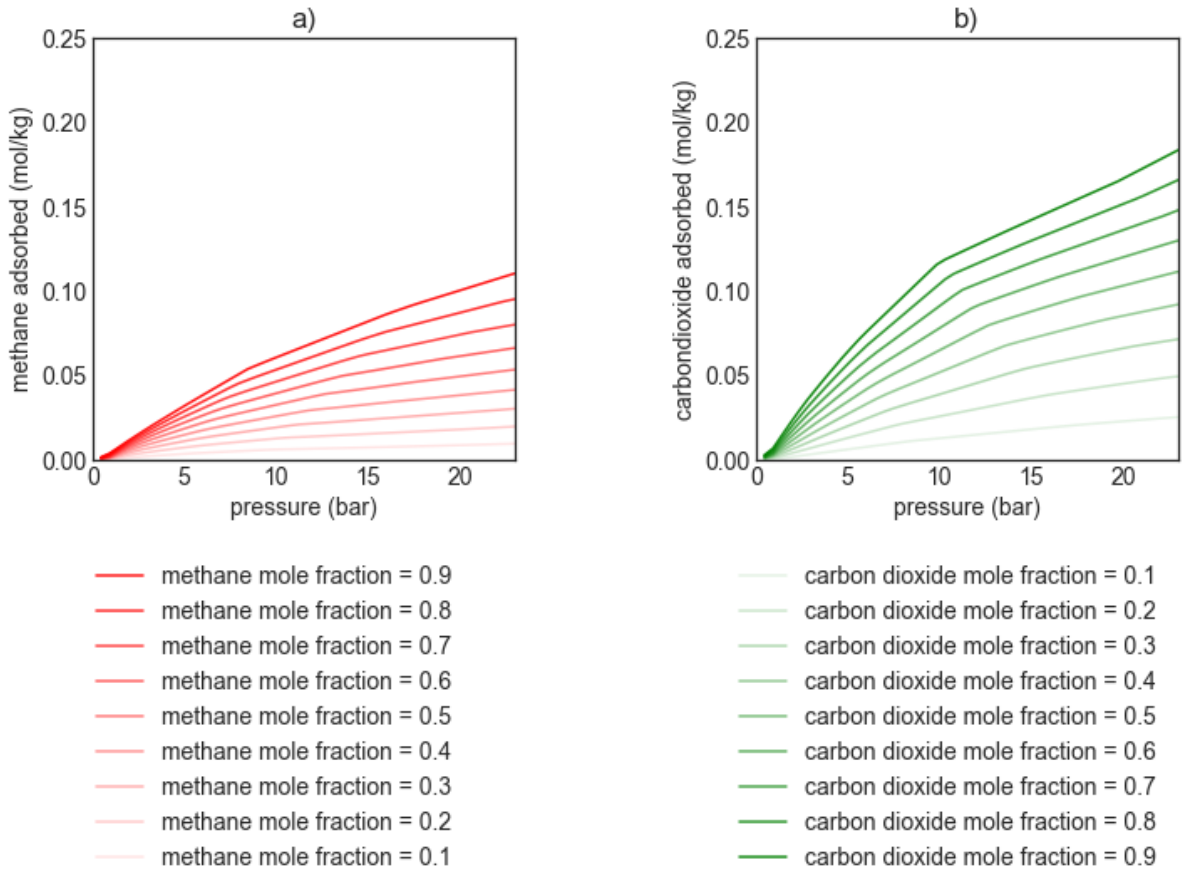

Figure 9-7 Predicted IAST isotherms at different concentrations

9.3 Reservoir Simulation

To understand the implications of sorption behaviour on gas shale's ability to sequester carbon dioxide and the potential for carbon dioxide enhanced recovery, a series of numerical simulations were performed in COMSOL using the Finite Element Method. The general diffusion equation was modified to include adsorption as described in equation (89). Since we are solving mass diffusion for both methane and carbon dioxide, two parallel equations were solved separately. The Transport of Diluted Species module in COMSOL is used for this purpose. As the Ideal Adsorbed Solution Theory does not provide estimates for adsorption uptakes, the Extended Langmuir equation was used in this study to model adsorption uptakes in the diffusion equation. This is especially convenient as the adsorption

uptakes predicted by the extended Langmuir equation is the same as those predicted by the Langmuir equation for pure components.

It was noted in Chapter 3 that the reservoir is symmetrical along the wellbore and along with the fractures. Therefore it is possible to study gas flow behaviour in the reservoir by considering the SRV domain represented in Figure 9-8. Due to symmetry, boundary conditions for the simulated reservoir volume are no-flow boundary conditions except for the fracture, which is modelled using a constant pressure boundary condition. This assumption is valid when we assume that the fracture is ideal with infinite fracture conductivities (Yu and Sepehrnoori, 2018). This geometry has also been previously used in the literature to simplify the computational complexities of fracture modelling (Zhu et al., 2016). Model parameters are summarised in Table 9-1. The matrix porosity was previously measured in the lab using He expansion and water immersion. The matrix permeability was measured using late time analysis. Fluid parameters were acquired using Lee's correlation (Lee et al., 1966). An initial reservoir pressure of 200 bar is assumed, which is within the pressure range of several major shale plays (King, 2010). A well-flowing pressure of 30 bar and an injection pressure of 200 bar were also assumed. The finer mesh size in COMSOL was used to discretize the solution in the domain. A time step of 1 day was used. Smaller mesh size and time step were also tried without any change in the result. The MUMPS solver was used in COMSOL to perform the simulation. This solver uses Finite Elements to discretize the space dimension and an implicit formulation to discretize the time dimension. An implicit formulation allows the solution to be accurate for longer time steps as compared to an explicit formulation.

Since carbon dioxide sequestration is usually carried out in depleted reservoirs, the simulation was carried out in 2 parts. The first part involved 10 years of methane production resulting in a depleted reservoir, and the second part involved 10 years of carbon dioxide injection to study the implications of sorption on the shale's potential to sequester carbon dioxide. In a second simulation scenario, methane production and carbon dioxide were alternated for 5 years to assess the potential for Huff-and-Puff carbon dioxide enhanced recovery for shales. Gas present at any given point is calculated by integrating the domain of simulation with an appropriate gas law and adsorption isotherm equation. The

amount produced/injected is then calculated by mass balance. The whole processes were automated in COMSOL.

$$\phi \frac{\partial \boldsymbol{\rho_g}}{\partial t} + (1-\phi)\frac{\partial \boldsymbol{\rho_a}}{\partial t} + \nabla\left(\frac{\boldsymbol{\rho_g k}}{\boldsymbol{\mu}}.\nabla \boldsymbol{P}\right) = Q \tag{89}$$

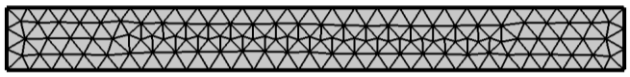

Figure 9-8 FEM Meshing

Table 9-1 Summary of Model Parameters

Parameter	Symbol	Value	Units
Matrix porosity	ϕ_m	0.05	-
Matrix permeability	k	4.99×10^{-22}	m^2
Methane viscosity	μ_m	11.71×10^{-6}	$Pa\ s$
Carbon dioxide viscosity	μ_c	15.9×10^{-6}	$Pa\ s$
Shale density	ρ_s	2870	kg/m^3
Reservoir height		100	m
Reservoir width		10	m
Fracture height		80	m
Initial reservoir pressure		200	bar
Reservoir temperature		45	^0C
Well flowing pressure		30	bar
Injection pressure		200	bar

The results of the simulation are plotted in Figure 9-9. Even though there appears to be a sudden change in production when boundary conditions are altered, we would like to clarify that these changes occur over a period of 30 days. This kind of behaviour is typical for gas shales (Yu and Sepehrnoori, 2014). About 1.2×10^{9} moles of methane are produced at the end of 10 years without carbon dioxide injection. However, only 0.8×10^{9} moles of methane are produced with carbon dioxide injection. This can be explained due to decreased convection of free methane in the presence of carbon dioxide, and the overall reduction in the effective permeability of the reservoir due to increased adsorption uptake. These results are consistent with those previously reported in the literature (Liu et al., 2013). This suggests that huff-and-puff carbon dioxide injection might not be a good way to increase methane recovery from gas shale reservoirs under these operating parameters. However, we also previously saw that gas flow in shales is highly complex dependent on several non-linear factors besides adsorption. Therefore studies must be conducted for individual formations before ruling out carbon dioxide injection as a potential enhanced recovery mechanism.

It can also be seen that after 10 years of injection, the amount of carbon dioxide injected was only about 70% of the total methane injected. This result is explained given that carbon dioxide uptake on shales is much higher than methane uptake, and that the rate of mass transfer decreases with increasing adsorption uptake although the overall mass transfer is higher. This effect was explored in more detail in Chapter 3. Because of this behaviour, longer injection times would be required inject the same amount of carbon into the reservoir as was originally produced. However, after 10 years of injection, it was possible to reduce the carbon footprint of these shales significantly. However breaking up the injection period into two parts – each of 5 years decreased the total amount injected by about 10%. Form Figure 9-9 b, the proportion of sorbed gas contributing to carbon dioxide storage is nearly 5 times that of methane production. This suggests that negative emissions could potentially be achieved on continued injection, although further research is necessary in this regard.

From Figure 9-10 and Figure 9-11, the contribution of adsorbed methane to total production is much lower than the contribution of adsorbed carbon dioxide to total gas sequestered in Figure 9-12 and Figure 9-13. This is because adsorption uptake for carbon dioxide at lower carbon dioxide partial pressures is nearly 300 times the adsorption uptake of methane at high methane partial pressures. Consequently, the carbon dioxide stored in the adsorbed state is a lot more stable and is less susceptible to leaks as compared to other carbon sequestration technologies (Celia et al., 2015). This is reflected in Figure 9-9b. Even though there is a bit of production from free carbon dioxide in scenario 2 from years 10 to 15, the amount of sorbed carbon dioxide remains stable. This is due to the shape of the adsorption curve, where high adsorption uptakes are observed at low loadings, and low adsorption uptakes are observed at high loading. Since the partial pressure of carbon dioxide in the reservoir initially is 0, carbon dioxide sequestration occurs in the high adsorption uptake region whilst methane production occurs in the low adsorption uptake region. Consequently, where it was difficult to produce adsorbed methane, it is now much easier to sequester adsorbed carbon dioxide. This makes gas shales a very attractive sink for storing carbon dioxide in the sorbed state.

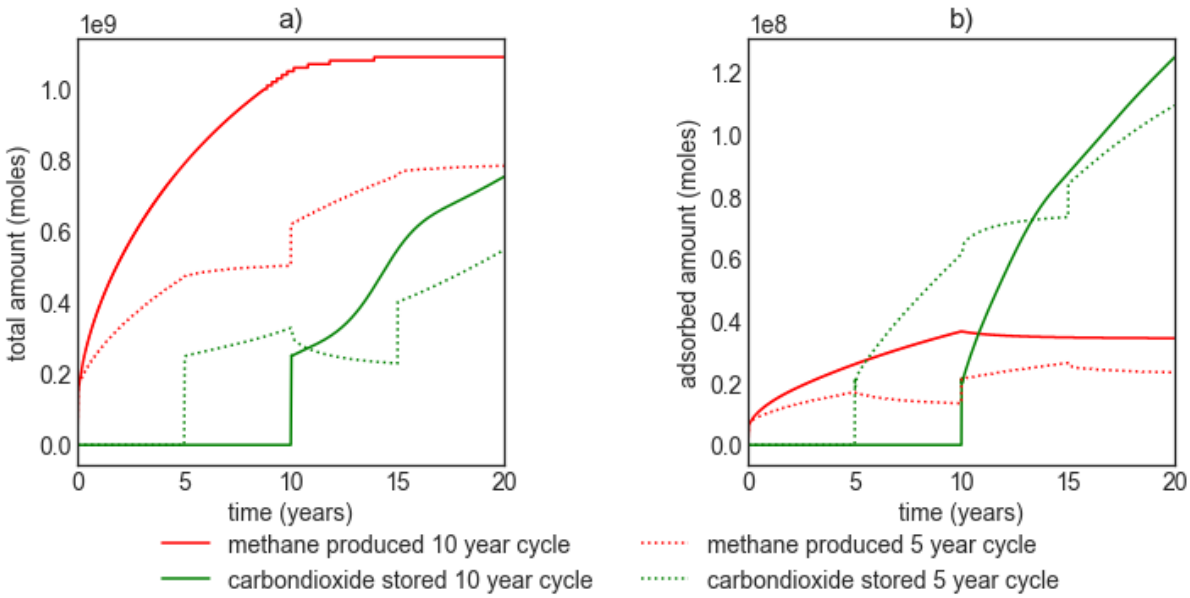

Figure 9-9 Production and Sequestration Estimates. Subfigure a represents total production and sequestration. Subfigure b represents adsorbed production and sequestration

To further understand the implications of sorption on carbon sequestration in gas shales, the internal distribution of the components in the reservoir is analysed over simulation time for scenario 1. In Figure 9-10, we can see that most of the methane is left behind in the reservoir after 10 years of production, as production is limited by the low permeability of the formation. There seems to be some redistribution of molecules during carbon dioxide injection, but we previously noted that this is not sufficient to increase methane recovery for our reservoir parameters. From Figure 9-11, we note that this phenomenon is even more pronounced for sorbed methane. As methane production occurs in the monolayer region of the adsorption isotherm, there is very little production from the sorbed methane in the reservoir. These phenomena are reversed for carbon dioxide sequestration which occurs in the linear region of the reservoir. Total carbon dioxide stored is limited by the low permeability of the reservoir. However, sorbed carbon dioxide stored is much higher than that for methane due to the processes occurring in the linear sorption region of the isotherm. These results provide further evidence for the strong potential for gas shales to store carbon dioxide.

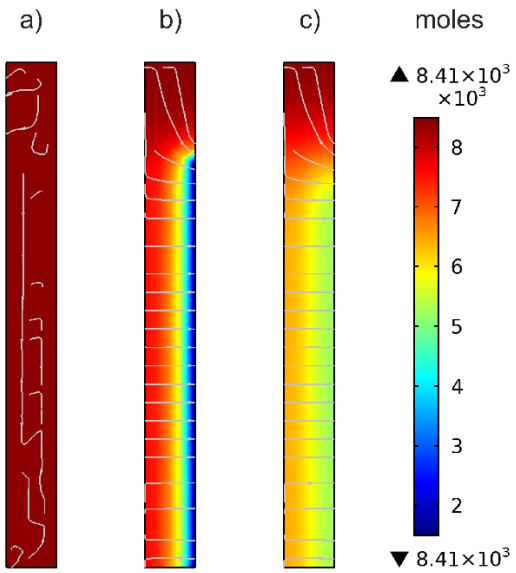

Figure 9-10 Total Methane distribution in the reservoir. Subfigure a plots concentration before methane production. Subfigure b plots concentration after methane production. Subfigure c plots concentration after carbon dioxide injection.

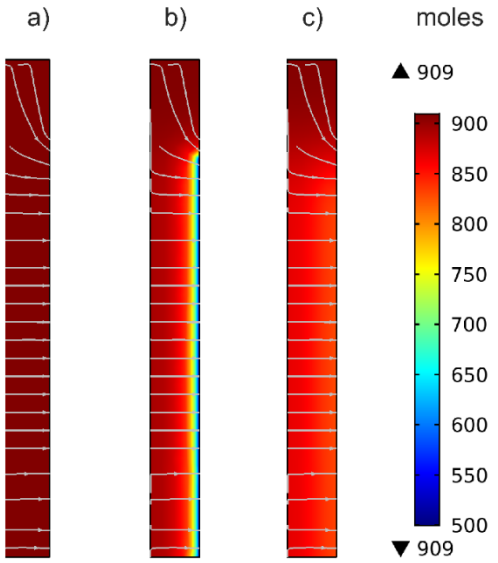

Figure 9-11 Adsorbed Methane distribution in the reservoir. Subfigure a plots concentration before methane production. Subfigure b plots concentration after methane production. Subfigure c plots concentration after carbon dioxide injection.

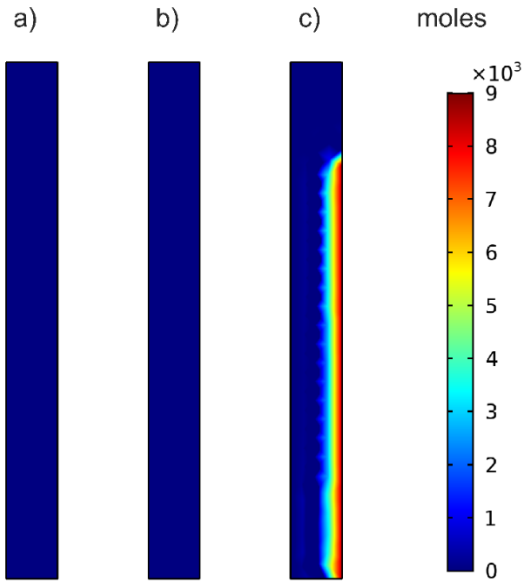

Figure 9-12 Total Carbon dioxide distribution in the reservoir. Subfigure a plots concentration before methane production. Subfigure b plots concentration after methane production. Subfigure c plots concentration after carbon dioxide injection.

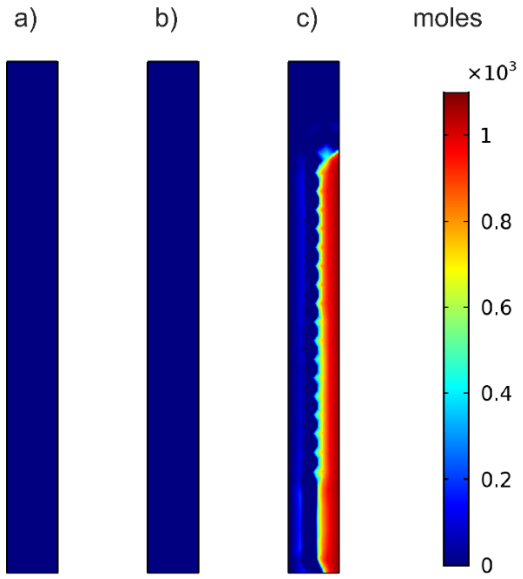

Figure 9-13 Adsorbed carbon dioxide distribution in the reservoir. Subfigure a plots concentration before methane production. Subfigure b plots concentration after methane production. Subfigure c plots concentration after carbon dioxide injection.

9.4 Sensitivity Analysis

A series of simulations were performed for Scenario 1, to assess the sensitivities of adsorption parameters on total and adsorbed methane produced, and on total and adsorbed carbon dioxide sequestered. Results from Figure 9-14a and Figure 9-14b are consistent with those obtained in Chapter 4. Figure 9-14c and Figure 9-14d demonstrate that similar behaviour is observed for carbon dioxide sequestered as compared to methane production. Total production and sequestration are inversely correlated with Langmuir volume. However, adsorbed production and sequestration are positively correlated.

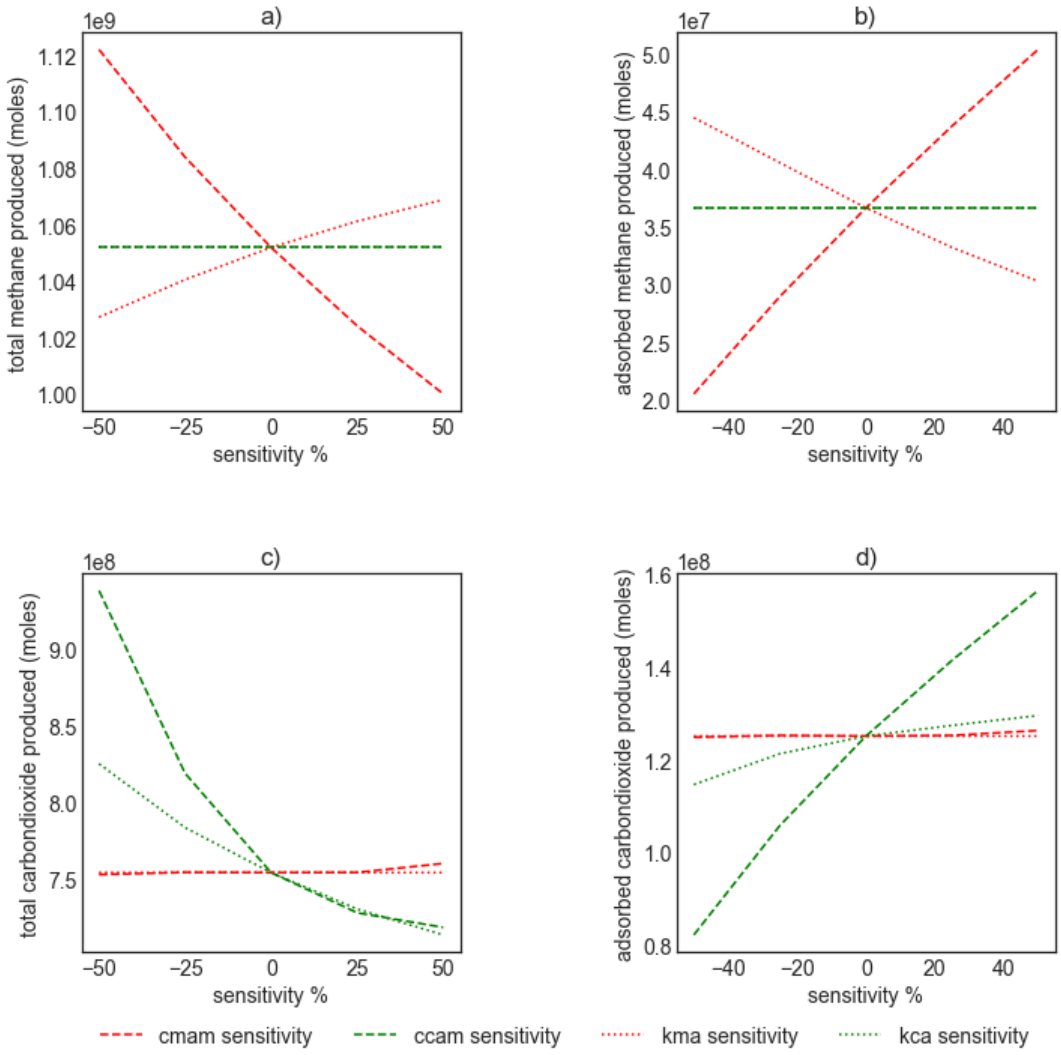

Figure 9-14 Sensitivity of adsorption parameters on methane production and carbon dioxide sequestration

This provides strong evidence that sorption in shales affects methane production and carbon dioxide sequestration phenomena in shales. As with increasing adsorption, the effective diffusion coefficient of the gas in the reservoir decreases, we notice a decrease in methane production and carbon dioxide sequestration with increasing Langmuir adsorption. This phenomenon is reversed for sorbed methane production and sorbed carbon dioxide sequestered. As we previously saw that these sensitivities are dependent on the fracture parameters of the shale besides the permeability, better fracture design could potentially improve these metrics.

9.5 Conclusion

Carbon dioxide sequestration potential of gas shales was analysed using experimental and simulation techniques. It is noted that the experimentally measured adsorption values on a pore scale were used to derive insights on gas behaviour on a field scale using the FEM. Single and multi-component methane and carbon dioxide adsorption isotherms were measured and fitted using Langmuir and IAST theories. Carbon dioxide sorption was significantly larger than methane sorption.

Experimental sorption measurements were integrated with a reservoir simulation. Both adsorption and adsorption uptake parameters strongly influence carbon dioxide sequestration potential of shales. Huff and puff carbon dioxide injection did not increase methane recovery from the reservoir. Longer periods were required for carbon dioxide sequestration as compared to methane production toa achieve a similar mass transfer.

9.6 References

Bell, I.H., Wronski, J., Quoilin, S., Lemort, V., 2014. Pure and Pseudo-pure Fluid Thermophysical Property Evaluation and the Open-Source Thermophysical Property Library CoolProp. Ind. Eng. Chem. Res. 53, 2498–2508. https://doi.org/10.1021/ie4033999

Busch, A., Alles, S., Gensterblum, Y., Prinz, D., Dewhurst, D.N., Raven, M.D., Stanjek, H., Krooss, B.M., 2008. Carbon dioxide storage potential of shales. Int. J. Greenh. Gas Control 2, 297–308.

Celia, M.A., Bachu, S., Nordbotten, J.M., Bandilla, K.W., 2015. Status of CO 2 storage in deep saline aquifers with emphasis on modeling approaches and practical simulations. Water Resour. Res. 51, 6846–6892. https://doi.org/10.1002/2015WR017609

Do, D.D., 1998. Adsorption Analysis: Equilibria And Kinetics: (With CD Containing Computer Matlab Programs).

Do, D.D., Do, H.D., Fan, C., Nicholson, D., 2010. On the existence of negative excess isotherms for argon adsorption on graphite surfaces and in graphitic pores under supercritical conditions at pressures up to 10,000 atm. Langmuir 26, 4796–4806. https://doi.org/10.1021/la903549f

Heller, R., Zoback, M., 2014. Adsorption of methane and carbon dioxide on gas shale and pure mineral samples. J. Unconv. Oil Gas Resour. 8, 14–24.

King, G.E., 2010. Thirty years of gas shale fracturing: What have we learned?, in: SPE Annual Technical Conference and Exhibition. Society of Petroleum Engineers.

Laskar, I.I., Hashisho, Z., 2020. Insights into modeling adsorption equilibria of single and multicomponent systems of organic and water vapors. Sep. Purif. Technol. https://doi.org/10.1016/j.seppur.2020.116681

Lee, A.L., Gonzalez, M.H., Eakin, B.E., 1966. The Viscosity of Natural Gases. J. Pet. Technol. 18, 997–1000. https://doi.org/10.2118/1340-PA

Lillies, A.T., King, S.R., 1982. Sand fracturing with liquid carbon dioxide, in: SPE Production Technology Symposium. Society of Petroleum Engineers.

Liu, F., Ellett, K., Xiao, Y., Rupp, J.A., 2013. Assessing the feasibility of CO 2 storage in the New Albany Shale (Devonian–Mississippian) with potential enhanced gas recovery using reservoir simulation. Int. J. Greenh. Gas Control 17, 111–126. https://doi.org/10.1016/J.IJGGC.2013.04.018

Mathieu, P., 2006. The IPCC special report on carbon dioxide capture and storage, in: ECOS 2006 - Proceedings of the 19th International Conference on Efficiency, Cost, Optimization, Simulation and Environmental Impact of Energy Systems.

Myers, A.L., Prausnitz, J.M., 1965. Thermodynamics of mixed-gas adsorption. AIChE J. 11, 121–127. https://doi.org/10.1002/aic.690110125

Nuttall, B.C., Eble, C.F., Drahovzal, J.A., Bustin, R.M., 2005. Analysis of Devonian black shales in Kentucky for potential carbon dioxide sequestration and enhanced natural gas production.

University Of Kentucky Research Fdn.

Pini, R., 2014. Interpretation of net and excess adsorption isotherms in microporous adsorbents. Microporous Mesoporous Mater. 187, 40–52. https://doi.org/10.1016/j.micromeso.2013.12.005

Profice, S., Lasseux, D., Jannot, Y., Jebara, N., Hamon, G., 2012. Permeability, Porosity and Klinkenberg Coefficient Determination on Crushed Porous Media. Petrophysics 53.

Rouquerol, J., Avnir, D., Fairbridge, C.W., Everett, D.H., Haynes, J.M., Pernicone, N., Ramsay, J.D.F., Sing, K.S.W., Unger, K.K., 1994. Recommendations for the characterization of porous solids (Technical Report). Pure Appl. Chem. 66, 1739–1758.

Rouquerol, J., Rouquerol, F., Llewellyn, P., Denoyel, R., 2016. Surface excess amounts in high-pressure gas adsorption: Issues and benefits. Colloids Surfaces A Physicochem. Eng. Asp. 496, 3–12. https://doi.org/10.1016/j.colsurfa.2015.10.045

Simon, C.M., Smit, B., Haranczyk, M., 2016. pyIAST: Ideal adsorbed solution theory (IAST) Python package. Comput. Phys. Commun. 200, 364–380. https://doi.org/10.1016/J.CPC.2015.11.016

Talu, O., 1998. Needs, status, techniques and problems with binary gas adsorption experiments. Adv. Colloid Interface Sci. 76–77, 227–269. https://doi.org/10.1016/S0001-8686(98)00048-7

Walton, K.S., Sholl, D.S., 2015. Predicting multicomponent adsorption: 50 years of the ideal adsorbed solution theory. AIChE J. 61, 2757–2762. https://doi.org/10.1002/aic.14878

Wang, K., Fu, J., Zheng, Y., 2019. Insights into photocatalytic CO2 reduction on C3N4: Strategy of simultaneous B, K co-doping and enhancement by N vacancies. Appl. Catal. B Environ. 254, 270–282. https://doi.org/10.1016/j.apcatb.2019.05.002

Yu, W., Sepehrnoori, K., 2018. Shale gas and tight oil reservoir simulation.

Yu, W., Sepehrnoori, K., 2014. Simulation of gas desorption and geomechanics effects for unconventional gas reservoirs. Fuel 116, 455–464. https://doi.org/10.1016/j.fuel.2013.08.032

Yu, W., Sepehrnoori, K., Patzek, T.W., 2014. Evaluation of gas adsorption in Marcellus Shale, in: SPE

Annual Technical Conference and Exhibition. Society of Petroleum Engineers.

Zhu, G., Yao, J., Sun, H., Zhang, M., Xie, M., Sun, Z., Lu, T., 2016. The numerical simulation of thermal recovery based on hydraulic fracture heating technology in shale gas reservoir. J. Nat. Gas Sci. Eng. 28, 305–316. https://doi.org/10.1016/J.JNGSE.2015.11.051

10 Thermal Enhanced Recovery for Gas Shales

10.1 Introduction

Reported recover rates for shale gas fields around the world have often been less than 5% (Yu et al., 2014). Given that adsorption in shales is always an exothermic process (Do, 1998), thermal enhanced recovery has been explored as a potential production technology to increase gas recovery from shales. However, there is a gap in the literature for adsorption characterization, which considers sorption as a multi-physical phenomenon with both heat and mass transfer effects (Fianu et al., 2018; Zou et al., 2017), and the reservoir engineering community which considers sorption as a purely mass transfer phenomenon ignoring the heat transfer effects (Wang et al., 2014; Zhu et al., 2016). The implications of this assumption are explored in this chapter, and a correction to the governing equations is proposed.

It is now well understood that there needs to be a modification to the governing equation for mass transfer in gas shales to account for sorbed gas (Fang et al., 2019; Guo, 2015; Teng et al., 2019; Yu and Sepehrnoori, 2014; Zhu et al., 2016). This model has also been used to assess the potential for thermal enhanced recovery to displace sorbed gas in shales (Wang et al., 2014; Zhu et al., 2016). The impact of thermal expansion, thermal fracturing, and thermal volatilization has been explored in the literature (Teng et al., 2016). Different forms of thermal stimulation such as microwave heating and electrical heating have also been explored in the literature (Fianu et al., 2020; Liu et al., 2018; Wang et al., 2017). However, the heat of sorption has been ignored in the literature of gas shale reservoir simulation so far.

This chapter presents an investigation into the potential for thermal enhanced recovery considering the heat of sorption in the governing equation for heat transfer (Seewald et al., 1999). A complete derivation is presented in Chapter 3. The simulated reservoir volume presented in Chapter 3 is considered for this study. Temperature dependence was modelled using a modified version of the Langmuir equation. Sorption and pore characteristics are determined experimentally using a high-pressure manometric rig (Talu, 1998). Adsorption is measured using the Gibbs approach (Rouquerol et al., 2016). Isosteric heats

are measured using the Clausius-Clapeyron equation (Do, 1998). Permeability is measured using the late time technique (Cui et al., 2009). Grain volume is measured using Helium expansion (RP40, 1998). Bulk volume is measured using water immersion (Kuila et al., 2014). A more complete description of the methodology employed is presented in Chapter 3.

10.2 Experimental Characterization

Figure 10-1 shows the experimentally measured sorption values along with their Langmuir fits. Sorption isotherms are Type I up to 60 bar. The purpose of this experiment is to model the temperature dependence of adsorption and to calculate the heat of adsorption using the Clausius-Clapeyron equation. Sorption was also a strong function of temperature with the Langmuir volume decreasing by 25% on increasing the temperature from $60\,^{0}C$ to $80\,^{0}C$. The experimental data are fitted to the modified version of the Langmuir equation shown in Equation (90). The derivation for this equation is presented in Chapter 3.

$$q_a = \frac{\left(a_1 + \frac{a_2}{T}\right) P}{P_{L_\infty} \exp\left(-\frac{H_L}{RT}\right) + P} \tag{90}$$

Where a_1 and a_2 are fitting constants for Langmuir Volume; P_{L_∞} and H_L are fitting constants for Langmuir Pressure; T is temperature, P is pressure, and R is gas constant. Fitting constants are summarised in Table 10-1. Isosteric heats of sorption were calculated using Equation (91).

$$\ln\left(\frac{P_1}{P_2}\right) = -\frac{\mathrm{H_i}}{R}\left(\frac{1}{T_2} - \frac{1}{T_1}\right) \tag{91}$$

Where H_i is isosteric heat.

The isosteric heats are plotted in Figure 10-2. An increase in isosteric heats with increasing surface coverage suggests that strong lateral interactions overpower surface heterogeneities of shales in this case (Sircar et al., 1999). The bulk density of the gas shale was calculated using water immersion: 1.93

g/cc; the grain density from He expansion: 2.14 g/cc; the porosity: 10%. Permeability was calculated from the late-time technique as 4.99×10^{-22} m^2.

Table 10-1 Adsorption fitting constants

Parameter	Value
a_1	-0.51 mol/kg
a_2	231.47 mol K/kg
P_{L_∞}	161749.17 Pa
H_L	-5423.99 J/mol

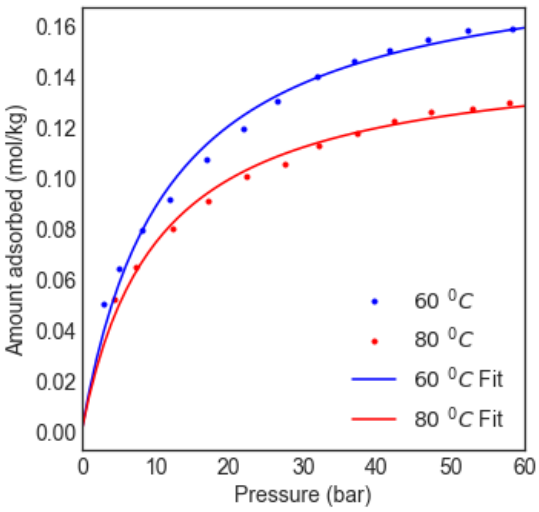

Figure 10-1 Experimental methane adsorption at different temperatures with Langmuir fits

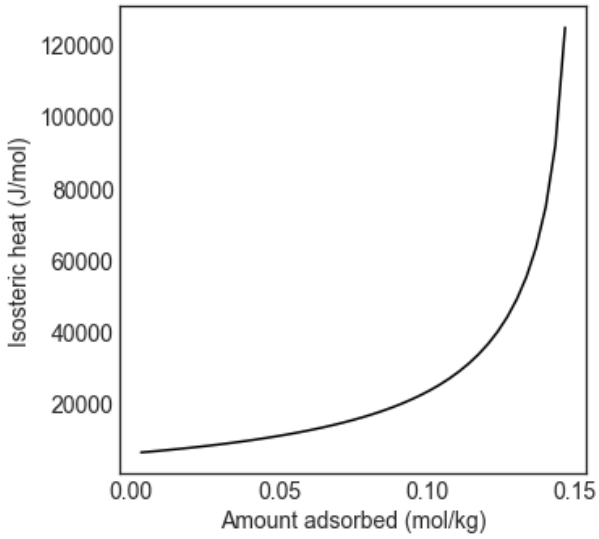

Figure 10-2 Isosteric heat of sorption

10.3 Reservoir Simulation

The Finite Element Meshing for the simulated reservoir volume is presented in Figure 10-3. Model parameters are summarised in Table 10-2. The boundary along the fracture is maintained at a constant temperature and pressure. Boundaries perpendicular to the wellbore were imposed with a no-flow boundary condition due to symmetry. The boundary along the wellbore is also imposed with a no-flow boundary condition, as the produced gas flows from the matrix to the fracture, and further on to the well-bore (Yu et al., 2016). A no-flow boundary condition is also imposed on the boundary opposite to the well-bore. The governing equations are shown in Equations (92) and (93) are solved with the above-mentioned boundary conditions to find out gas flow into the fracture.

$$
\begin{aligned}
&-\left[(1-\phi)\rho_s H_i\left(\frac{\partial \boldsymbol{q_a}}{\partial \boldsymbol{P}}\right)_T\right]\left(\frac{\partial \boldsymbol{P}}{\partial t}\right)\\
&+\left[\phi\rho_g MW\ Cp_g+(1-\phi)\rho_s\left(Cp_s-H_i\left(\frac{\partial \boldsymbol{q_a}}{\partial \boldsymbol{T}}\right)_P\right)\right]\frac{\partial \boldsymbol{T}}{\partial t}\\
&-\nabla\cdot\left(\phi\lambda_g+(1-\phi)\lambda_s\right)\nabla \boldsymbol{T}\\
&+\rho_g MWCp_g\left(\frac{k_m\nabla \boldsymbol{P}}{\mu}\right)\cdot\nabla \boldsymbol{T}\\
&=Q_h
\end{aligned}
\tag{92}
$$

$$
\begin{aligned}
&\left[\phi\rho_g MW\ Cp_g+(1-\phi)\rho_s Cp_s\right]\frac{\partial \boldsymbol{T}}{\partial t}\\
&-\nabla\cdot\left(\phi\lambda_g+(1-\phi)\lambda_s\right)\nabla \boldsymbol{T}\\
&+\rho_g MWCp_g\left(\frac{k_m\nabla \boldsymbol{P}}{\mu}\right)\cdot\nabla \boldsymbol{T}\\
&=Q_h
\end{aligned}
\tag{93}
$$

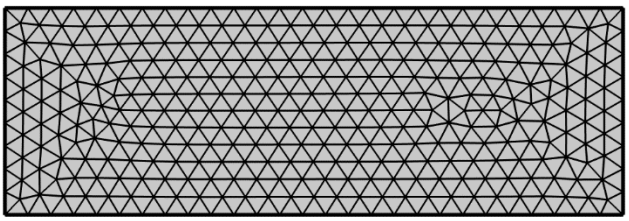

Figure 10-3 Finite Element Meshing of the Simulated Reservoir Volume

The model parameters are summarised in Table 10-2. Shale porosity, density, and permeability were determined in the lab. Initial pressure was assumed to be 100 bars, and flowing well pressure was considered as 30 bars, which are reasonable assumptions. Based on experimental parameters, an initial reservoir temperature of 60°C and a heating temperature of 80°C were assumed. This is within the range

of many shales plays around the world (Zou et al., 2017). Methane viscosity was calculated using Lee's correlation, and the non-ideality factor was calculated using Mahmoud's correlation (Lee et al., 1966; Mahmoud, 2013). A higher fracture spacing was used compared to carbon dioxide sequestration chapter to demonstrate the effectiveness of enhanced recovery. The space differential was solved using the Finite Element Method, whilst the time differential was solved using an implicit method. This was accomplished using the MUMPS solver in COMSOL. Smaller finite element meshing and time steps were also considered for shorter simulations without observing any change in results indicating that convergence was achieved with these parameters.

Table 10-2 Model Summary

Description	Value	Units
Shale porosity	0.1	-
Shale density	2140	kg/m^3
Shale permeability	4.99×10^{-22}	m^2
Shale specific heat capacity [1]	1000	$J/(kg \times K)$
Initial reservoir temperature	333.15	K
Initial reservoir pressure	1x10 [7]	Pa
Reservoir heating temperature	353.15	K
Flowing well pressure	3x10 [6]	Pa
Methane viscosity [2]	12.18×10^{-6}	$Pa\ s$
Methane critical temperature [3]	190.55	K
Methane critical pressure [4]	4599200	Pa

Fracture height	100	m
Reservoir height	150	m
Fracture spacing	100	m
Method employed	Finite Element Method	
Solver used	MUMPS	
Time step	1 day	
References for assumptions: [1] (Robertson, n.d.); [2,3,4] (Bell et al., 2014)		

10.4 Reservoir Model Comparison

Governing equations including and excluding isosteric heats are solved for isothermal and heated conditions. The results are plotted in Figure 10-4, Figure 10-5, and Figure 10-6. The total recovery rate without heating was only 1.5%; total recovery rate with heating was 23.7%. Reservoir heating has been demonstrated to be an excellent production technology to increase sorbed gas recovery from shales. The recovery rate without heating are comparable to those achieved in Chapter 4, considering that only one fracture is considered instead of 10, further validating this model.

It can be seen from Figure 10-5 that the isosteric heat of sorption parameter does not have any effect on reservoir simulation under isothermal conditions. This implies that for normal operating conditions, it is not necessary to account for the heat of sorption. However, the heat of sorption is more significant for thermal enhanced recovery applications; not accounting for the heat effects of sorption significantly overpredicts the potential for thermal enhanced recovery after 20 years of production when the wellbore is maintained at $80\,^{0}$C. Both total gas production and sorbed gas production are significantly overestimated by 15% and 17% respectively. It is therefore important that any study assessing the

potential for thermal stimulation to enhance gas recovery from shales account for both the heat and mass transfer effects of sorption.

Figure 10-4 shows the molar density distribution of total and adsorbed gas in the Simulated Reservoir Volume after 20 years of production. Reservoir heating displaces a significant amount of gas that would otherwise not be produced under isothermal conditions. It can also be seen that when isosteric heat is not considered heating has a bigger effect in displacing sorbed gas. This is expected given that $\Delta H > 0$, for the desorption process that governs gas production from shales.

There seems to be a strong linear relationship between the heating temperature and the total gas production, in the range of reservoir operating parameters considered in this study. It can also be seen from Figure 10-6 that heat injection results in a higher initial production rate, which is central to determining the economic feasibility of a gas shale reservoir (Ahmed and Rezaei-Gomari, 2018). Higher production rates, later in field life, could also potentially allow the operator to delay costly re-fracturing expenses.

Recovery rate has increased significantly due to reservoir heating for 20 years. It was also observed that recovery from sorbed gas after 2 years increased dramatically to 23% with reservoir heating from a base case of 11% without reservoir heating. This suggests that thermal stimulation could bring recovery from sorbed gas forward in the field life cycle. The rest of the study will focus on the potential for reservoir heating to displace sorbed gas from the reservoir.

As seen in Figure 10-9 and Figure 10-10, both sorbed gas production and total recovery rate after 5 years are strongly dependent on heating temperature. Sorbed Gas production increased by a factor of 1.08×10^{6} moles, and total recovery rate (including free gas) increased by a factor of 0.5%, per degree of wellbore temperature increase. Although it might be possible that this linear relationship may not hold for other operating conditions not considered in this study, the thermal simulation of the shale reservoir could be reasonably expected to increase sorbed gas recovery. That said, the heat of sorption needs to be considered when assessing the potential for thermally enhanced recovery production systems for individual shale plays. Ignoring the heat of sorption over predicts the potential for thermal

enhanced recovery to increase sorbed gas recovery by about 0.2×10^{6} moles per degree of heating at wellbore after 5 years of production.

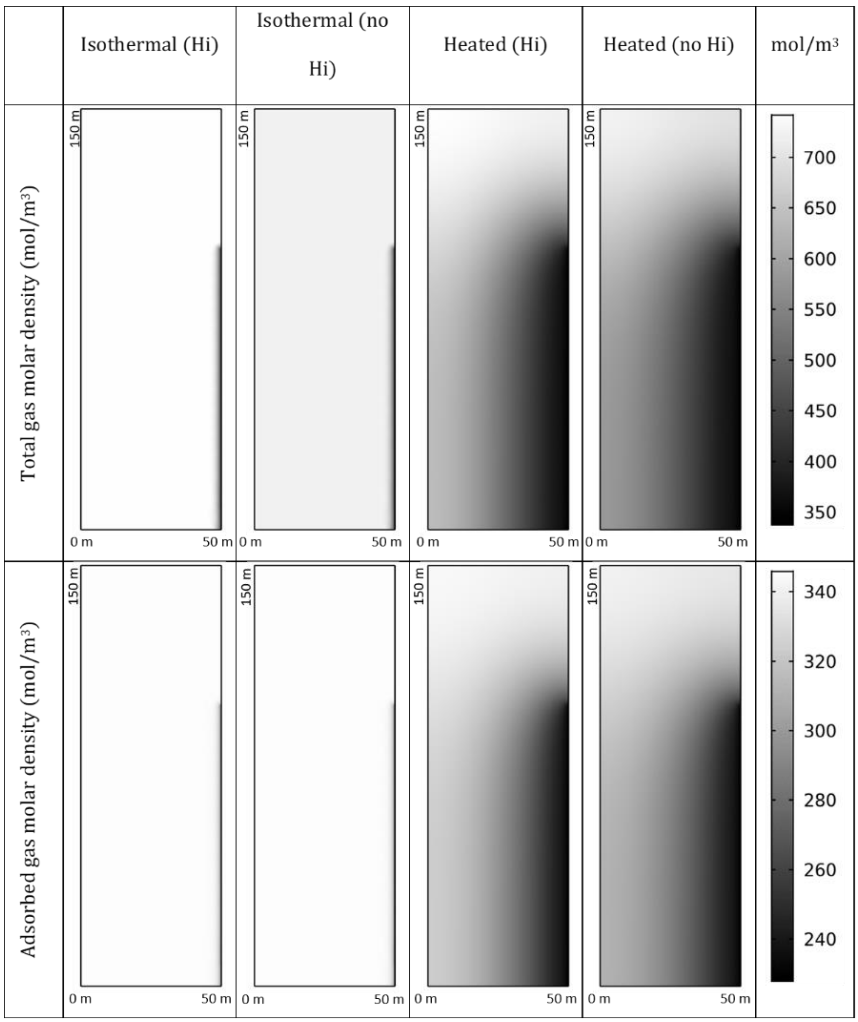

Figure 10-4 Reservoir model comparison

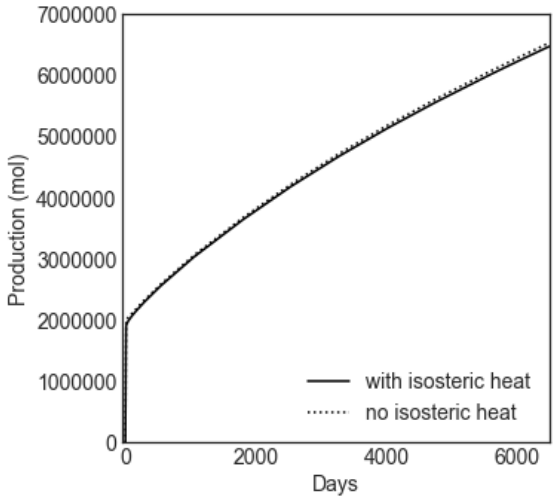

Figure 10-5 Reservoir model comparison at isothermal conditions

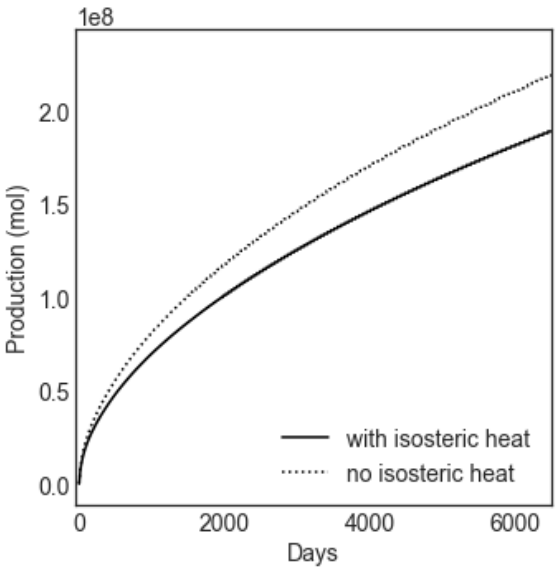

Figure 10-6 Reservoir model comparison at heated conditions

10.5 Thermal Enhanced Gas Recovery

The sensitivity of different parameters on the potential for thermal enhanced recovery is explored through several simulations lasting 5 years. Results are plotted in Figure 10-7, Figure 10-8, Figure 10-9, and Figure 10-10. Gas production increases linearly with increasing temperature. Higher temperature

also results in a higher initial production rate and maintains higher production rates later in the field cycle. Increasing temperature from 60 to 80 ^0C increases recovery rate after 5 years by almost 10%. Sorbed gas produced increased from about 1 mol to 20 million moles.

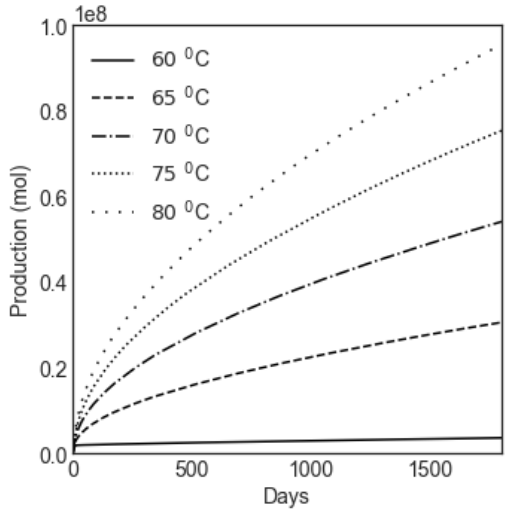

Figure 10-7 Total Production for different temperatures

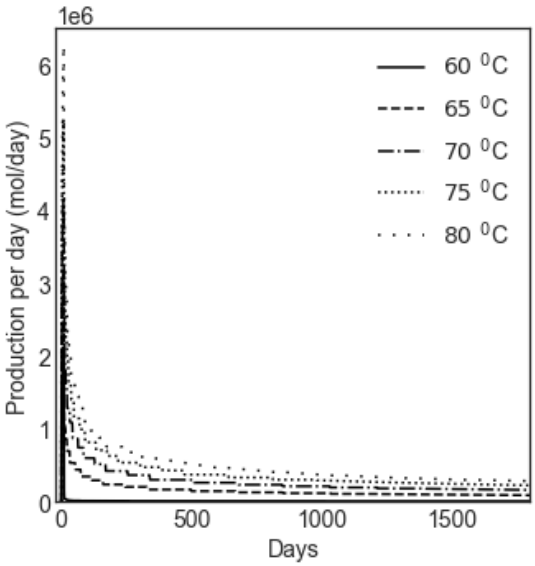

Figure 10-8 Production rates at different heating temperatures

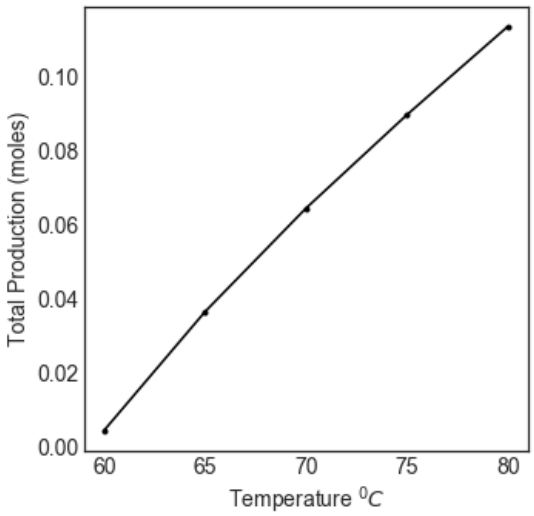

Figure 10-9 Total production against heating temperature

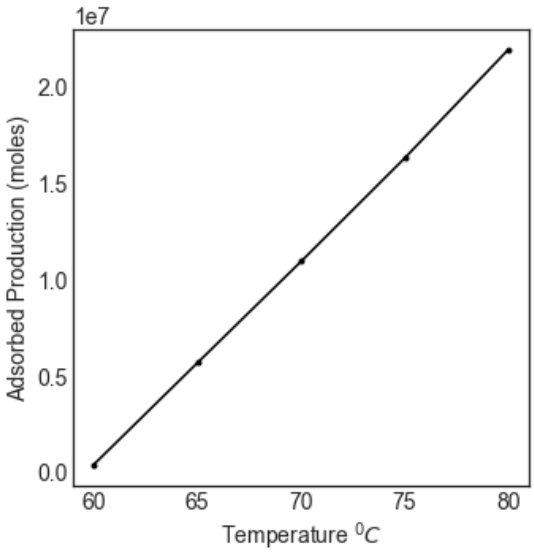

Figure 10-10 Adsorbed production against temperature

At a heating temperature of 80 ^{0}C, sorbed gas production with thermal enhanced recovery is strongly correlated with Langmuir volume and weakly correlated with Langmuir Pressure. Whilst the range of permeabilities considered in this study did not affect sorbed gas production significantly, the amount of sorbed gas displaced under heating has an inverse relation to the isosteric heat of sorption, as with increasing heat of sorption, more energy is required to displace

the same amount of sorbed methane. It was also noted that shales with lower porosity, which are associated with higher initially sorbed gas in bulk shales, displaced more sorbed gas under reservoir heating, This implies that shales with higher amount sorbed, but lower heat of sorption may be better candidates for thermal stimulation to enhance sorbed gas recovery.

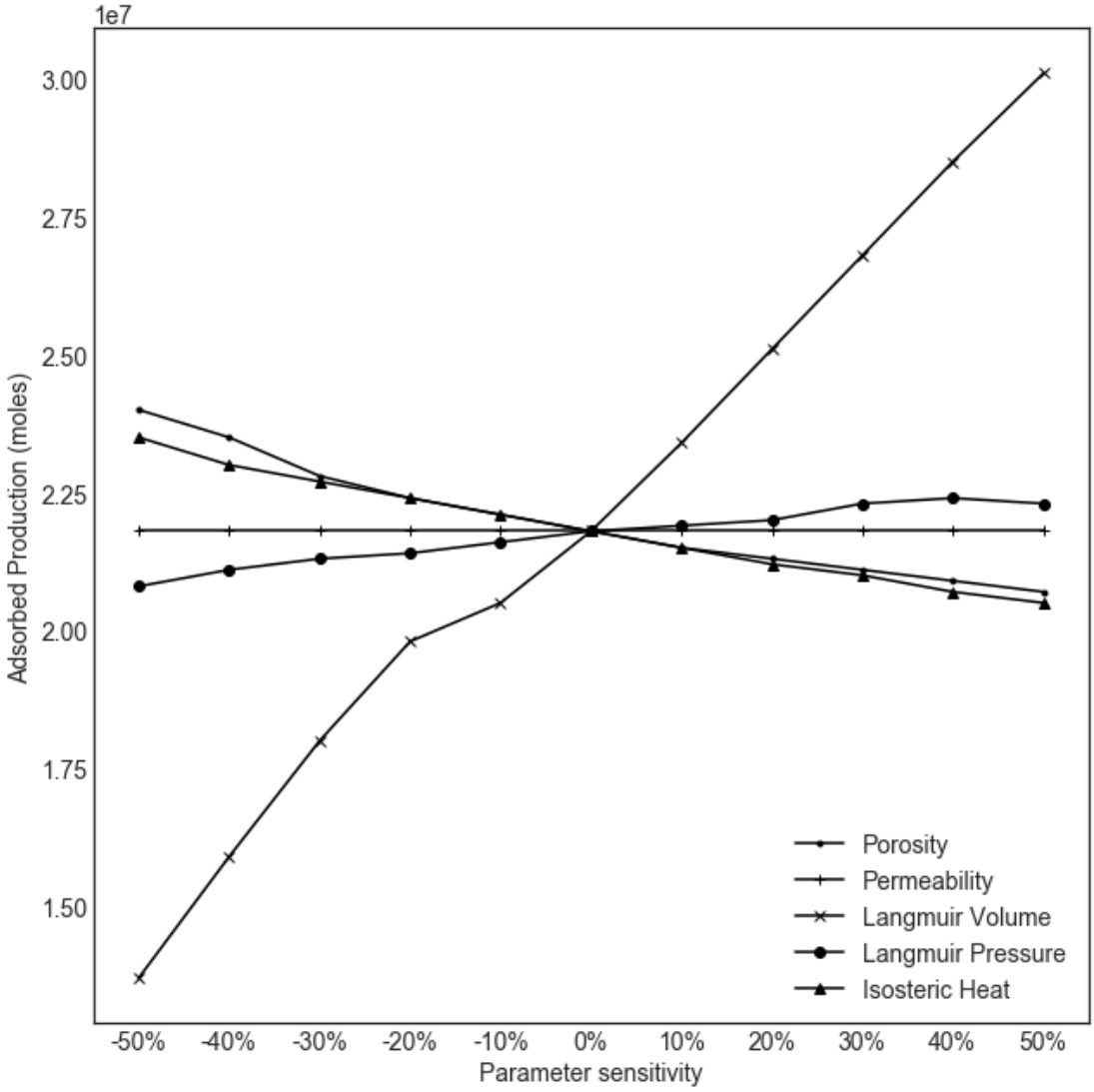

Figure 10-11 Sensitivity of adsorbed production for different model parameters at 80 °C

The above-mentioned trends were in some cases reversed when considering total gas production instead of sorbed gas production after 5 years. This effect is shown in Figure 10-12. Porosity was positively correlated with total gas production as free gas is more readily produced compared to

sorbed gas. The correlation coefficient of Langmuir volume against total gas production was inversely correlated; Langmuir pressure and isosteric heat of sorption also exhibited a weak negative correlation. This was also observed in chapter 4, as increasing amounts of Langmuir volume increases adsorption uptake, which decreases the effective diffusion in shales.

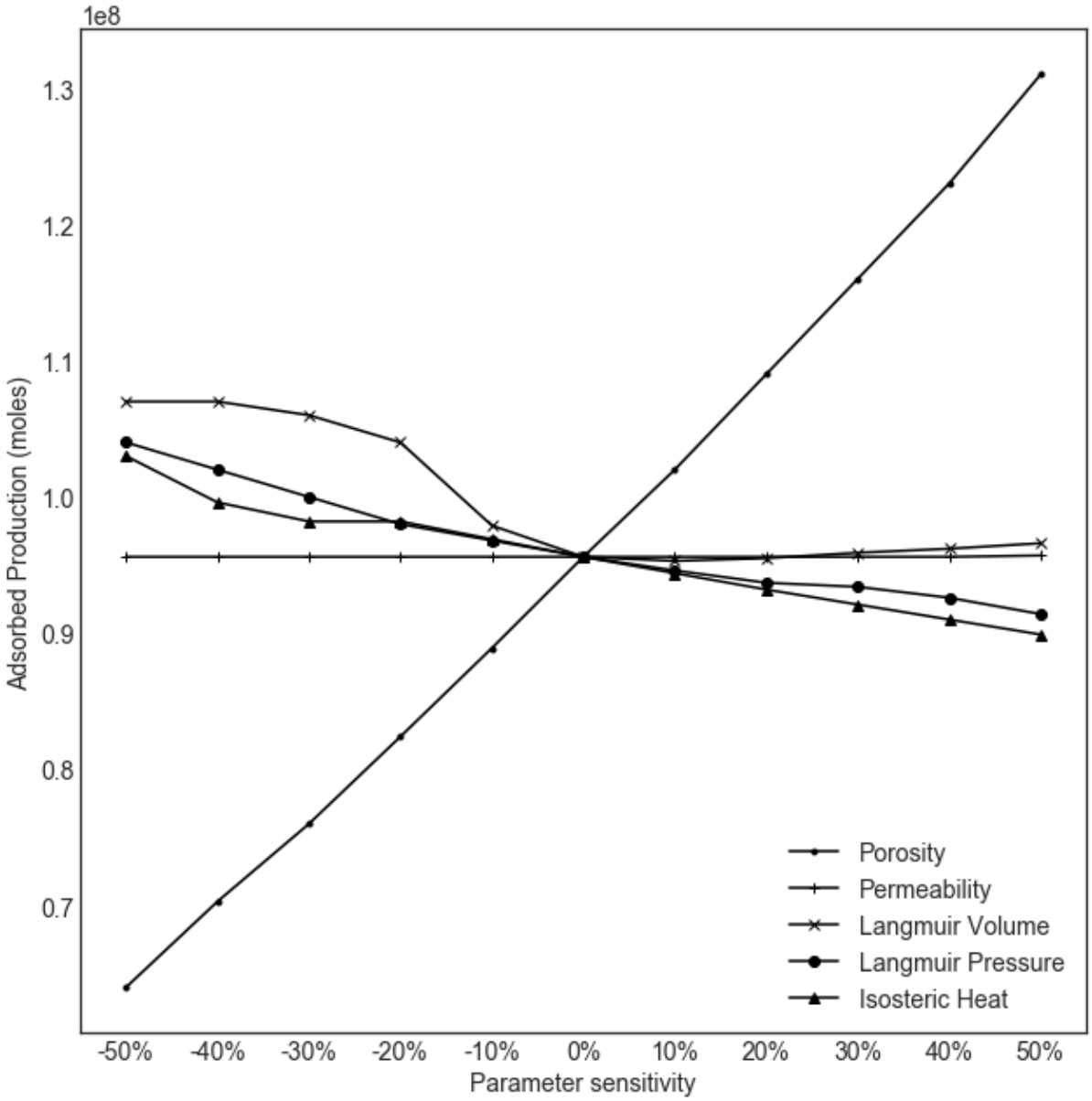

Figure 10-12 Total production sensitivity for the heated reservoir at 80 ^{o}C

It was noted that the reservoir permeability did not have a significant effect of thermal stimulation to enhance sorbed gas recovery in this study. That said we emphasize that the range of permeability considered in this study is in the nano-Darcy range (2.5×10^{-22} to 7.5×10^{-22} m^2). We expect that permeability beyond this range could significantly affect production, but is not considered explicitly in this study.

It is also noted here that this study remains technology agnostic. As further analysis on the economic and energy cost analysis of thermal enhanced recovery is dependent of individual technologies, we are unable to provide that here. Several techniques exist to transfer heat into the reservoir – steam injection, . Of these, steam injection remains to be the most commonly used owing to it being a mature technology (Chaar et al., 2015). Whilst there are other studies that have focused on the energy and financial costs of thermal enhanced recovery for conventional reservoirs (Zekri and Jerbi, 2002), there have been no such studies for gas shales. Further, each of these technologies are also expected to bring forth an individual set of challenges. For example, shales are expected to swell significantly at higher water contents, which may reduce the effective permeability negating any benefit from desorption (Pini et al., 2009). Microwave heating has been demonstrated to be feasible at a conceptual level (Fianu et al., 2020). Therefore further research on the energy and economic costs of thermal enhanced recovery technologies are necessary for shales to reach their full potential. This is left for future researchers in this area.

10.6 Conclusion

Thermal enhanced gas recovery for gas shales is explored as a series of experimental and computational studies. The heat of sorption was demonstrated as an important parameter. A modified version of the Langmuir equation was proposed to account for temperature-dependent sorption. A modified version of the heat transfer governing equation is proposed to include heat of sorption. This is applied to perform a sensitivity analysis on thermal enhanced recovery in gas shales.

Thermal enhanced recovery increased total recovery by almost 10%. This suggests that thermal enhanced recovery could be a good technique to increase recovery from shale reservoirs. Heat of sorption is also an important parameter. Not including this term over-predicts the impact of thermal enhanced recovery significantly. Other terms that affect thermal enhanced recovery include permeability, Langmuir volume, Langmuir pressure, and porosity. Higher Langmuir volume and lower heat of sorption is generally preferred for thermal enhanced recovery from shale reservoirs.

10.7 References

Ahmed, M., Rezaei-Gomari, S., 2018. Economic Feasibility Analysis of Shale Gas Extraction from UK's Carboniferous Bowland-Hodder Shale Unit. Resources 8, 5.

Bell, I.H., Wronski, J., Quoilin, S., Lemort, V., 2014. Pure and Pseudo-pure Fluid Thermophysical Property Evaluation and the Open-Source Thermophysical Property Library CoolProp. Ind. Eng. Chem. Res. 53, 2498–2508.

Chaar, M., Solar, G., Venetos, ; M, Enterprises, W., Dargin, ; J, Palmer, D., 2015. Economics of Steam Generation for Thermal Enhanced Oil Recovery Steam Generation for Thermal EOR.

Cui, X., Bustin, A.M.M., Bustin, R.M., 2009. Measurements of gas permeability and diffusivity of tight reservoir rocks: Different approaches and their applications. Geofluids 9, 208–223.

Do, D.D., 1998. Adsorption Analysis: Equilibria And Kinetics: (With CD Containing Computer Matlab Programs).

Fang, H.-H., Sang, S.-X., Liu, S.-Q., 2019. Numerical simulation of enhancing coalbed methane recovery by injecting CO2 with heat injection. Pet. Sci. 16, 32–43.

Fianu, J., Gholinezhad, J., Hassan, M., 2020. Thermal simulation of shale gas recovery involving the use of microwave heating. J. Pet. Sci. Eng. 186, 106768.

Fianu, J., Gholinezhad, J., Hassan, M., 2018. Comparison of Temperature-Dependent Gas Adsorption Models and Their Application to Shale Gas Reservoirs.

Guo, C., 2015. Flow mechanisms and numerical simulation of gas production from shale reservoirs.

Kuila, U., McCarty, D.K., Derkowski, A., Fischer, T.B., Prasad, M., 2014. Total porosity measurement in gas shales by the water immersion porosimetry (WIP) method. Fuel 117, 1115–1129.

Lee, A.L., Gonzalez, M.H., Eakin, B.E., 1966. The Viscosity of Natural Gases. J. Pet. Technol. 18, 997–1000.

Liu, J., Wang, J., Leung, C., Gao, F., Liu, J., Wang, J., Leung, C., Gao, F., 2018. A Fully Coupled Numerical Model for Microwave Heating Enhanced Shale Gas Recovery. Energies 11, 1608.

Mahmoud, M.A., 2013. Development of a New Correlation of Gas Compressibility Factor (Z-Factor) for High Pressure Gas Reservoir. North Africa Tech. Conf. Exhib.

Pini, R., Ottiger, S., Burlini, L., Storti, G., Mazzotti, M., 2009. Role of adsorption and swelling on the dynamics of gas injection in coal. J. Geophys. Res. Solid Earth 114.

Robertson, E.C., n.d. THERMAL PROPERTIES OF ROCKS.

Rouquerol, J., Rouquerol, F., Llewellyn, P., Denoyel, R., 2016. Surface excess amounts in high-pressure gas adsorption: Issues and benefits. Colloids Surfaces A Physicochem. Eng. Asp. 496, 3–12.

RP40, A., 1998. Recommended practices for core analysis. Feb.

Seewald, F., Pollei, A., Kraume, M., Mittelbach, W., Lang., J., 1999. Numerical Calculation of the Heat Transfer in an Adsorption Energy Storage with KARDOS.

Sircar, S., Mohr, R., Ristic, C., Rao, M.B., 1999. Isosteric Heat of Adsorption: Theory and Experiment. J. Phys. Chem. B 103, 6539–6546.

Talu, O., 1998. Needs, status, techniques and problems with binary gas adsorption experiments. Adv. Colloid Interface Sci. 76–77, 227–269.

Teng, T., Wang, J.G., Gao, F., Ju, Y., 2016. Complex thermal coal-gas interactions in heat injection enhanced CBM recovery. J. Nat. Gas Sci. Eng. 34, 1174–1190.

Teng, T., Xue, Y., Cun, Z., 2019. Modeling and simulation on heat-injection enhanced coal seam gas recovery with experimentally validated non-Darcy gas flow. J. Pet. Sci. Eng.

Wang, H.Y., Ajao, O., Economides, M.J., 2014. Conceptual study of thermal stimulation in shale gas formations. J. Nat. Gas Sci. Eng.

Wang, Y., Wang, X., Xing, Y., Xue, J., Wang, D., 2017. Three-dimensional numerical simulation of enhancing shale gas desorption by electrical heating with horizontal wells. J. Nat. Gas Sci. Eng. 38, 94–106.

Yu, W., Sepehrnoori, K., 2014. Simulation of gas desorption and geomechanics effects for unconventional gas reservoirs. Fuel 116, 455–464.

Yu, W., Sepehrnoori, K., Patzek, T.W., 2016. Modeling gas adsorption in Marcellus shale with Langmuir and bet isotherms. SPE J. 21, 589–600.

Yu, W., Sepehrnoori, K., Patzek, T.W., 2014. Evaluation of gas adsorption in Marcellus Shale, in: SPE Annual Technical Conference and Exhibition. Society of Petroleum Engineers.

Zekri, A.Y., Jerbi, K.K., 2002. Economic Evaluation of Enhanced Oil Recovery, Oil & Gas Science and Technology-Rev. IFP.

Zhu, G., Yao, J., Sun, H., Zhang, M., Xie, M., Sun, Z., Lu, T., 2016. The numerical simulation of thermal recovery based on hydraulic fracture heating technology in shale gas reservoir. J. Nat. Gas Sci. Eng. 28, 305–316.

Zou, J., Rezaee, R., Liu, K., 2017. Effect of Temperature on Methane Adsorption in Shale Gas Reservoirs.

11 Conclusion

11.1 Conclusions

The importance of sorption and diffusion mechanisms on gas shale reservoir characterization was investigated. A complete analysis of experimental parameters was performed. Net sorption contributed to the biggest error in gas shale adsorption characterization. Excesses sorption was also significant although to a lesser extent. For reproducibility, absolute sorption values need to be reported for sorption experiments, along with the method employed to obtain them from the experimentally measured net or excess sorption. Sorption at low pressures could be characterized using a linear isotherm. At higher pressures, a complete analysis of 2 and 3 parameter isotherms that fit Type I data was presented. The Dubinin-Radushkevich isotherm had the best goodness of fit metric, but does not have consistent thermodynamic behaviour in terms of adsorption uptake. The Langmuir adsorption isotherm was the best 2 parameter isotherm with consistent thermodynamic behaviour. The Toth isotherm was the best 3 parameter isotherm. Using numerical experiments and Finite Element simulations, it was demonstrated that sorption significantly decreases the intrinsic permeability of shales and could in some cases lead to decreased production from the reservoir. Because of this, it was also shown that sorption decreases the effective diffusion of shales, thereby decreasing the amount produced during primary recovery. However, it is possible to minimize this effect with better design of fractures.

Many shale samples with different geochemical characteristics from the Bowland formation were analysed using multiple experimental techniques. Using SEM analysis, the pore structure and chemical composition is analysed and compared with the XRD and TOC data. N_2 sorption was used to derive pore size distributions. Pore surface area was heavily concentrated in the organic matter region of the shale. Both surface area and micropore volume were strongly correlated with organic and clay mineral content. The BJH method does not provide accurate pore size estimations for microporous shales. The DFT method is generally preferred. Both adsorption and diffusion were strongly correlated with

kerogen and clay mineral content, although more samples need to be considered to confirm this trend. Sorption was also dependent on the shale's surface area and micropore volume.

With manometric experiments, it is shown that shales have a higher adsorption capacity and a higher adsorption affinity for carbon dioxide as compared to methane with a strong potential for carbon dioxide sequestration. Multi-component isotherms were fit with Extended Langmuir and IAST methods. The shape of the adsorption curve plays a significant role in carbon dioxide sequestration. This was analysed using FEM. Because of low adsorption uptakes at high pressures, carbon dioxide sequestration in shales was more stable compared to other reservoirs with less potential for leakage or overpressure and injection triggered earthquakes. However, carbon dioxide injection did not increase gas recovery. This is because high adsorption uptakes at low 0 carbon dioxide partial pressure (initial reservoir conditions) decreases effective diffusion in shales.

Multiple adsorption isotherms at different temperatures were obtained using manometric techniques to determine the temperature dependence and heat of adsorption. A modified Langmuir model was proposed to fit this data, and integrated into a Finite Element Simulation to find out the potential for thermal enhanced recovery. For this the isosteric heat of sorption included in the governing equations, which is often neglected in the shale gas literature. The heat of sorption was found to be an important parameter in the thermal stimulation of gas shales. Thermal stimulation has the potential to increase recovery from the reservoir by as much as 10% after 10 years.

11.2 Future Work

Although this work addresses many areas of gas shale reservoir characterization, there remains a lot of work that needs to be done. Future work needs to be carried out at supercritical conditions, where the role of the net and excess sorption, and organic matter swelling will be a lot more significant. The impact of moisture also needs to be studied more rigorously. A new experimental technique for sorption characterization is required where experimental moisture concentrations are comparable to those in

reservoir. Sorption in individual shale components needs to be investigated more rigorously through experiments and molecular simulations to better understand the sorbed phase density in individual components. Other phenomena besides sorption that affect carbon dioxide storage in shales such as mineralization need to be investigated more thoroughly.

It would also be very useful to study sorption and pore characteristics in individual shale geochemical components for better understanding on how these contribute to the overall metrics. A much larger sample set needs to be considered to account for shale heterogeneities.

A better model than Extended Langmuir needs to be derived for multi-component adsorption that does not have constant selectivity, but is also differentiable for application in reservoir characterization. Heat of sorption studies need to be considered with calorimetric measurements and integrated into the methodology used in this study.

Geomechanical and geophysical studies are required to investigate the potential for carbon dioxide as a fracturing fluid and as a heat transfer medium. More collaboration is needed between the members of the surface science, fluid flow, and geophysical communities to balance conflicting requirements put forward by gas shale reservoir characterization.